

Exploration of *N*-Ferrocenyl Substituted Thioamides: Synthesis, Properties and Reactivity

Dissertation

Zur Erlangung des Grades

“Doktor der Naturwissenschaften”

Im Promotionsfach Chemie

Am Fachbereich Chemie, Pharmazie und Geowissenschaften

Der Johannes Gutenberg-Universität Mainz

Vorgelegt von

Torben Kienz

Geboren in Worms

Mainz, 2016

Die vorliegende Arbeit wurde unter Betreuung von ___ in der Zeit von Juni 2011 bis Oktober 2016 am Institut für Anorganische Chemie und Analytische Chemie der Johannes Gutenberg-Universität Mainz angefertigt.

Mainz, Oktober 2016

Dekan:

1. Berichterstatter:

2. Berichterstatter:

Tag der mündlichen Prüfung: 11. November 2016

Ich, Torben Kienz, Matrikelnummer 2633374, versichere, dass ich meine Promotionsarbeit selbständig verfasst und keine anderen als die angegebenen schriftlichen und elektronischen Quellen, sowie andere Hilfsmittel benutzt habe. Alle Ausführungen, die anderen Schriften wörtlich oder sinngemäß entnommen wurden, habe ich kenntlich gemacht.

Datum

Unterschrift

Abstract

Electron transfer reactions are fundamental for biological processes. Since the investigation of such processes in vivo are complicated or sometimes impossible, model complexes for biological system have been developed as a valuable tool. The investigation of electron transfer processes via the use of ferrocene derivatives provides insight into the influence of the bridging unit for the rate of electron transfer. Incorporation of asymmetric bridges, such as carboxamides, provides a model for protein environments and have been studied thoroughly. The thioamide as structurally related bridging unit, however, has not yet been explored with respect to electron transfer abilities.

In this study, *N*-Ferrocenyl substituted thioamides are easily prepared from the parent carboxamides by the use of Lawesson's reagent (2,4-bis(*p*-methoxyphenyl)-1,3-dithiaphosphetane-2,4-disulfide). Remarkably, the rotational barrier of the thioamides is high enough to observe *E/Z* isomerism in solution. IR and NMR spectroscopy give insight into the hydrogen bonding motif of the thioamides, as well as the secondary structure. The mixed-valent compounds of dinuclear complexes are investigated by electrochemical measurements, as well as UV/Vis and EPR spectroscopy. The electronic coupling H_{AB} is calculated and compared to the parent carboxamides.

The reaction pathways of ferrocenium compounds in the presence of a non-nucleophilic base are studied by means of spin trapping techniques. The formation of carbon centered ferrocenyl radicals is reported and the location of the unpaired spin in the ferrocenyl radicals could be determined. This study gives insight into the reaction of ferrocenyl radicals and stabilizing effects on them as a plausible mode of action for ferrocene based (pro-)drugs.

Besides the generation of radicals *N*-ferrocenyl substituted thioamides show a second reactivity upon oxidation and deprotonation. A multistep reaction sequence leads to the formation of a novel *N,S*-heterocycle, which initiates oligomerization. Intermediates of this sequence include paramagnetic piano stool like complexes with η^1 -coordinated cyclopentadienyl rings, as well as super electrophilic ferrocenyl ketenimine cations, formed by elimination of hydrogen sulfide. A reaction mechanism is proposed and supported by mass spectrometry, EPR and NMR spectroscopy and DFT calculations. This work is crucial for polymeric materials with CN-backbone and heterocyclic chemistry.

Kurzzusammenfassung

Für biologische Systeme ist Elektronentransfer ein fundamentaler Prozess. Da die Untersuchung solcher Prozesse *in vivo* kompliziert und oft unmöglich ist, wurden Modellkomplexe für biologische Systeme als nützliches Werkzeug zu deren Erforschung entwickelt. Die Untersuchung von Elektronentransfer an Ferrocenderivaten liefert Einsicht über den Einfluss der verbrückenden Gruppen auf die Geschwindigkeit des Elektronentransfers. Asymmetrisch verbrückende Gruppen, wie Carboxamide, welche ein Modell für Proteinumgebungen darstellen, wurden gründlich untersucht. Thioamide hingegen, die in ihrer geometrischen Struktur ähnlich sind, wurden bisher noch nicht im Hinblick auf ihre Elektronentransfereigenschaften erforscht.

In dieser Studie wird eine einfache Synthese *N*-Ferrocenyl substituierte Thioamide durch den Einsatz von Lawessons Reagenz (2,4-Bis(*p*-methoxyphenyl)-1,3-dithiaphosphetan-2,4-disulid) aus den entsprechenden Carboxamiden berichtet. Die Rotationsbarriere von Thioamiden ist bemerkenswerterweise groß genug, um *E/Z*-Isomere in Lösung beobachten zu können. IR und NMR Spektroskopie geben hierbei Aufschluss über das Motiv der Wasserstoff-brückenbindungen in Thioamiden, sowie deren Sekundärstruktur. Die gemischt-valenten Verbindungen der dinuklearen Komplexe werden mittels elektrochemischer Messungen, UV/Vis-Spektroskopie und ESR-Spektroskopie untersucht. Der elektronische Kopplungsparameter H_{AB} wird bestimmt und mit dem der entsprechenden Carboxamide verglichen.

Die Reaktionswege von Ferroceniumverbindungen in Anwesenheit von nicht-nukleophilen Basen werden mittels „Spin-Trapping“ untersucht. Die Bildung von kohlenstoffzentrierten Ferrocenylradikalen wird untersucht und die Position des ungepaarten Elektrons bestimmt. Diese Forschungsarbeit gibt Aufschluss über die Reaktivität und mögliche stabilisierende Effekte von Ferrocenylradikalen. Dies könnte eine mögliche Erklärung für die Wirkungsweise von ferrocenbasierten Medikamenten sein.

Bei Deprotonierung und Oxidation zeigen *N*-ferrocenyl substituierte Thioamide neben der Bildung von Radikalen eine zusätzliche Reaktivität. Durch eine mehrstufige Reaktionsfolge entstehen neuartige *N,S*-Heterocyclen, welche Oligomerisationsreaktionen einleiten können. Zwischenprodukte dieser Reaktionsfolge beinhalten paramagnetische klavierstuhlartige Komplexe mit η^1 -koordinierten Cyclopentadienylringen, sowie ein äußerst elektrophiles Ferrocenylketeniminokation, welches durch die Eliminierung von

Schwefelwasserstoff entsteht. Es wird ein Reaktionsmechanismus postuliert und anhand von Massenspektrometrie, ESR-Spektroskopie, NMR-Spektroskopie und DFT-Rechnungen belegt. Diese Arbeit ist äußerst wichtig im Hinblick auf polymere Materialien und die Chemie von heterocyclischen Verbindungen.

Mein Dank gilt

für die Möglichkeit an diesem komplexen Thema zu arbeiten, die wissenschaftliche Betreuung und fruchtbaren Diskussionen, sowie die Ermutigung dort weiter zu forschen, wo andere längst aufgegeben hätten.

Damit das Mögliche entsteht, muss immer wieder das Unmögliche versucht werden.

Hermann Hesse, Brief an Wilhelm Gundert

Every member in the Brown [Ajah] seeks to produce something lasting. Research or study that will be *meaningful*. Other often accuse us of ignoring the world around us. They think we only look backward. Well, that is inaccurate. If we are distracted, it is because we look forward, toward those who will come. And the information, the knowledge we gather... we leave it for them. The other Ajahs worry about making today better, we yearn to make tomorrow better.

Robert Jordan, The Wheel of Time, The Gathering Storm

Contents

1	Introduction.....	1
1.1	Mixed-Valence and Electron Transfer.....	2
1.1.1	Marcus Theory – Diabatic Approach.....	2
1.1.2	Marcus-Hush Theory – Adiabatic Approach.....	6
1.1.3	Mixed-valent Compounds.....	7
1.1.4	Optical Transitions, Band Shapes and Determination of H_{AB}	10
1.1.5	Half-Wave Potential Splitting in Mixed-valent Systems.....	11
1.1.6	Electron Transfer in Ferrocene Compounds.....	13
1.2	Ferrocene Containing Oligopeptides.....	16
1.2.1	A Structure Comparison of Amides and Thioamides.....	21
1.2.2	Thioamides as Isosteric Replacement.....	24
1.2.3	Thioamide Containing Ferrocene Derivatives.....	26
1.3	EPR Spectroscopy and Spin Trapping of Radicals.....	29
1.4	Ferrocene-Containing (Pro-)Drugs.....	31
1.5	References.....	36
2	Aim of Work.....	47
3	Results and Discussion.....	49
3.1	Impact of O→S Exchange in Ferrocenyl Amides on Structure and Redoxchemistry.....	53
3.1.1	Abstract.....	55
3.1.2	Introduction.....	56
3.1.3	Results and Discussion.....	58
3.1.4	Conclusion.....	72
3.1.5	Experimental Section.....	73
3.1.6	Associated Content.....	77

3.1.7	Acknowledgement	78
3.1.8	References	78
3.2	Spin Trapping of Carbon-Centered Ferrocenyl Radicals with Nitrosobenzene	83
3.2.1	Abstract	85
3.2.2	Introduction	86
3.2.3	Results and Discussion	90
3.2.4	Conclusion	106
3.2.5	Experimental Section	107
3.2.6	Associated Content	108
3.2.7	Acknowledgement	109
3.2.8	Reference	109
3.3	Generation and Oligomerization of <i>N</i> -Ferrocenyl Ketenimines via Open-shell Intermediates	115
3.3.1	Abstract	117
3.3.2	Introduction	118
3.3.3	Results and Discussion	120
3.3.4	Conclusion	136
3.3.5	Experimental Section	137
3.3.6	Associated Content	144
3.3.7	Acknowledgement	144
3.3.8	References	144
4	Summary and Outlook	149
5	Supporting Information	153
5.1	To 3.1: Impact of O→S Exchange in Ferrocenyl Amides on Structure and Redoxchemistry	155

5.2	To 3.2: Spin Trapping of Carbon-Centered Ferrocenyl Radicals with Nitrosobenzene	163
5.3	To 3.3: Generation and Oligomerization of <i>N</i> -Ferrocenyl Ketenimines via Open-shell Intermediates	175
6	Acknowledgements	197
7	List of Publications	201
8	Curriculum Vitae	203

Abbreviations

β	angle between Cp ring plane and substituent bond
δ	chemical shift in NMR spectroscopy
Δ	difference descriptor
ε	Molar extinction coefficient
θ	tilt between two Cp rings
λ	wavelength
λ	Marcus reorganization energy
μ	micro
$\tilde{\nu}$	wavenumber
χ	electronegativity
ω	Angle along the pseudo- C_5 axis in ferrocene
A	hyperfine coupling constant
a.u.	arbitrary units or atomic units
Ac	acetyl
Ala	alanine
Ar	aryl
B	magnetic field
Boc	<i>tert</i> -butyloxycarbonyl
^t Bu	<i>tert</i> -butyl
calcd.	calculated
cat.	catalyst
CD	circular dichroism
Cp	Cyclopentadienyl (C_5H_5)
Cp*	Pentamethyl-cyclopentdienyl (C_5Me_5)
CV	Cyclic voltammetry
CW	Continuous wave
d	doublet
DCM	Dichloromethane
DDQ	2,3-Dichloro-5,6-dicyano-1,4-benzoquinone
DEPMPO	5-(diethoxyphosphoryl)-5-methyl-1-pyrroline-N-oxide
DFT	density functional theory
DIPEA	di- <i>iso</i> -propyl amine

DMF	dimethylformamide
DMSO	dimethylsulfoxide
DPPH	2,2-diphenyl-1-picrylhydrazyl
dq	doublet of quartet
<i>E</i>	energy
<i>E</i> _{1/2}	half wave potential
EPR	electron paramagnetic resonance
ER	estrogen receptor
ES	excited state
Et	ethyl
ET	electron transfer
exp	experimental
F	Farraday constant
Fc	ferrocenyl [Fe (η ⁵ -C ₅ H ₅)(η ⁵ -C ₅ H ₄)]
FD(-MS)	field desorption (mass spectrometry)
Fmoc	fluorenylmethyloxycarbonyl
Fn	[Fe (η ⁵ -C ₅ H ₄)(η ⁵ -C ₅ H ₄)]
<i>g</i>	<i>g</i> -factor
<i>G</i>	free energy
G	Gauss
Gly	glycine
GS	ground state
H	hour
<i>H</i> _{AB}	electronic coupling constant
hfc	hyperfine coupling constant
HOMO	highest occupied molecular orbital
<i>I</i>	nuclear spin
IHB	intramolecular hydrogen bond
IR	infrared
IVCT	intervalence charge transfer
K	kelvin
<i>k</i>	rate of electron transfer
<i>k</i> _B	Boltzmann constant

LUMO	lowest unoccupied molecular orbital
M	molar
m.p.	melting point
Me	methyl
min	minute
MNP	2-methyl-2-nitrosopropane
mT	millitesla
ND	nitrosodurene
NIR	near infrared
nJ	coupling constant (NMR spectroscopy)
NMR	nuclear magnetic resonance
NOB	nitrosobenzene
NOESY	nuclear Overhauser effect spectroscopy
P ₁ 'Bu	<i>tert</i> -butylimino-tris(dimethylamino)phosphorane
PBN	<i>N-tert</i> -butyl nitrone
PCET	proton coupled electron transfer
Ph	Phenyl C ₆ H ₅
PhNO	nitrosobenzene
<i>pKa</i>	decadic logarithm of acid constant
ppm	Parts per million
pt	pseudo triplet
<i>q</i>	charge
R	gas constant
r.t.	room temperature
<i>R</i> _{AB}	distance between A and B
ROS	reactive oxygen species
S	electron spin
S	singlet
SOMO	singly occupied molecular orbital
SWV	square wave voltammetry
TFA	trifluoroacetic acid
THF	tetrahydrofuran
Trp	tryptophan

Abbreviations

TS	transition state
U	potential
UV/vis	ultraviolet-visible
V	volt
Val	valine
X-band	frequency range in EPR spectroscopy ($\nu \approx 9.4$ GHz)

1 Introduction

Iron is believed to make up about 32% of the earth's elemental composition. This high amount is largely attributed to the fact, that the inner core of the earth is believed to consist entirely of an iron-nickel alloy, while the concentration in the crust of the earth is much lower.^[1] Iron is the most used metal with a stock of 2200 kg per capita and therefore essential for human society.^[2] But iron is not only essential for human society, but for life itself. It is found in a variety of bioinorganic compounds, for example in hemoglobin^[3], myoglobin^[4], cytochrome P450^[5-12], in iron-sulfur clusters^[13,14] and ferritin.^[15,16]

The desire to understand biological systems, such as the previously ones mentioned, led to synthesis and analysis of a variety of biomimetic model complexes.^[17-27] In the field of study regarding biological systems a major subject is electron transfer, which is important in many biological processes.^[28-33] While the theoretical foundation has been laid by Marcus and Hush^[28,34-40], for practical studies, mixed-valent compounds, especially ferrocene based compounds, have shown to be a valuable tool for the study of electron transfer. This led to the exploration of symmetrically bridged mixed-valent compounds,^[41-45] while studies of asymmetrically bridged systems are still scarce.^[43,46-49]

Ferrocene has not only proven to be valuable in the study of electron transfer. Since its discovery in 1951^[50] and its structure determination shortly thereafter^[51], ferrocene has been a fertile field of research. This is attributed to its high stability, reversible redox behavior and easy access to derivatives bearing functional groups. Current research focuses amongst others on ferrocenyl containing polymers^[52-54] and pharmaceutical compounds such as anticancer medication,^[55,56] antimalarial medication,^[57-60] vasorelaxants^[61] and antibiotics^[62].

With respect to antibiotic activity a poly thioamide extracted from *Clostridium cellulolyticum* showed remarkable activity against multiresistant staphylococci.^[63] In biological systems, the thioamide linkage is very rare. Only five natural products have been found containing thioamide units and one is believed to be a product of decomposition.^[64-68] This fact is very favorable for the use of thioamide linkage in medication, because it provides greater stability against proteolytic degradation and improved absorption, distribution, metabolism and excretion properties.^[69-71]

All this proves that iron and especially ferrocene is a fascinating field of research, providing new insights and applications, which can only be more exciting by the addition of thioamide units, opening a horn of plenty for future scientists.

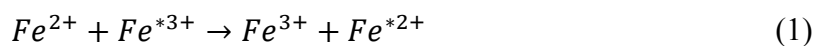
1.1 Mixed-Valence and Electron Transfer

Redox reactions are one of the most fundamental reactions in chemistry. These involve per definition the oxidation of one atom or molecule and therefore the reduction of another atom or molecule, in short an electron is transferred from one to the other. While redox reactions have been commonly used since even before chemistry itself was established, the research and understanding of the electron transfer process in view of mechanism and kinetics only started in the late 1940s.^[37]

Since electron transfer (ET) is such a fundamental process, the knowledge about ET affected a variety of research fields. In the biological field, ET contributed to clarify the nature of intraprotein electron transfer and hence reaction rates of the forward and backward reaction.^[72] Future applications originating from electron transfer considerations are processes which require fast electron transfer (molecular wires)^[73,74] or prevent back electron transfer reaction (molecular diodes, dye sensitized solar cells, photocatalysis).^[75-78]

1.1.1 Marcus Theory – Diabatic Approach

R. A. Marcus made the first approach to quantitative description of electron transfer reactions. While the theory was first developed to describe self-exchange reactions, see Equation (1), it was found, that the theory is applicable to electron transfer reactions in general.^[34,37]



The starting point of the theory is, that redox reactions can be described as a motion of atoms on a potential energy surface (see Figure 1). The atoms included in this motion are the ones of the reactants as well as the atoms of the solvent molecules surrounding them and can be described by the nuclear coordinates.^[34,37] The transition from the reactants to the products passes a saddle point on this energy surface and can only occur if the system

has enough energy. The same is true for all electron transfer reactions, if the electronic interaction between the two reactants is relatively weak.

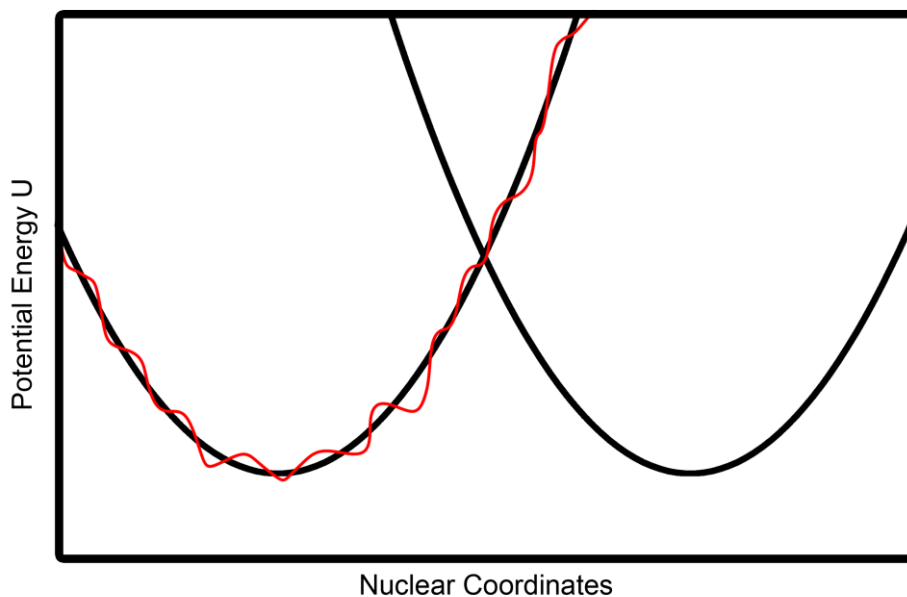


Figure 1. Profile of the real potential energy surface (red) and simplified profiles (black) for a redox reaction.

The basic principle of the theory is, that while thermal electron transfer occurs, the coordinates of the nuclei do not change, as it is for an optical electron transfer (Frank-Condon principle). Because of energy conservation electron transfer can only occur at the saddle point of the energy surface and therefore fluctuations of all coordinates have to occur, to fulfill these criteria.^[34,37]

This rather complex energy diagram, depending on nuclear motion, is simplified by two approximations. One is the assumption that the energy change for motion of the reactant atoms can be approximated by a harmonic oscillator potential. The second one is a “linear response approximation”, which states, that any change in charge of the reactants (through electron transfer) leads to a proportional change in the polarization of the solvent. This results in free energy curves for the reactant G_r and products G_p , shown in Figure 2, which are simple quadratic functions of one general reaction coordinate.^[37] With these simple energy diagrams in mind, the formulas resulting from Marcus theory are easily understood.

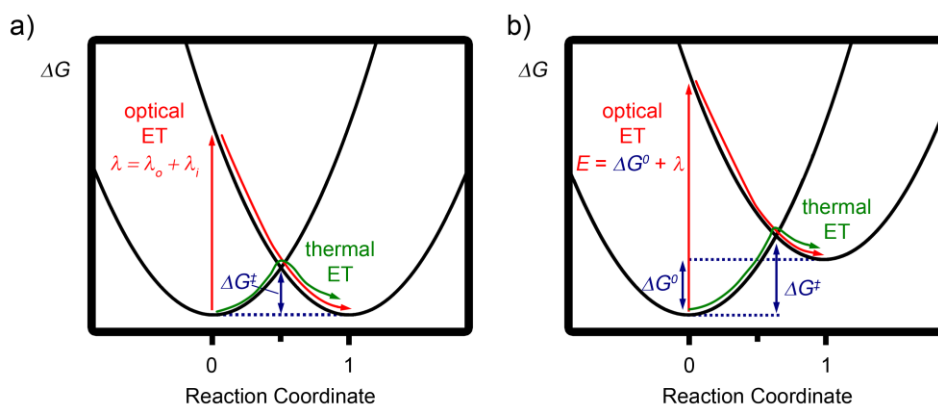


Figure 2. Diabatic free energy surface for electron transfer for a) degenerate states and b) nondegenerate states and the possible pathways for electron transfer (optical and thermal).

The rate constant for thermal electron transfer is given by Equation (2), an Arrhenius-like equation, where ΔG^\ddagger is the activation barrier and A is determined by whether the electron transfer is intramolecular or intermolecular. ΔG^\ddagger itself is given by Equation (3). ΔG^0 is the standard free energy of the reaction and differentiates two cases for electron transfer. The first case for $\Delta G^0 = 0$ and therefore degenerate states and the second case for $\Delta G^0 \neq 0$ resulting in nondegenerate states. λ is the reorganization energy of the system.

$$k = A \exp\left(\frac{-\Delta G^\ddagger}{k_B T}\right) \quad (2)$$

$$\Delta G^\ddagger = \frac{\lambda}{4} \left(\frac{\Delta G^0}{\lambda}\right)^2 \quad (3)$$

As apparent from the free energy surfaces, there are three possible electron transfer pathways. The thermal one, which was explained before, tunneling and the optical electron transfer, which will now be disclosed. For the case of degenerate states, the optical excitation energy equals the reorganization term. This leads to the understanding, that the reorganization energy equals the energy that is liberated by rearrangement of the system

after an optical electron transfer, to yield the new relaxed geometry. This reorganization can be divided into two basic terms. One is the inner reorganization energy λ_i , namely the energy arising from the displacement of the product nuclei and one is the outer reorganization energy λ_o , namely the energy to reorient the solvent molecules surrounding the product.^[37]

In case of non-degenerate states the optical excitation energy equals the sum of reorganization energy and the standard free energy ΔG^0 . The relation of λ and ΔG^0 has a direct effect on ΔG^\ddagger , which can be visualized for three different relations, see Figure 3. For $\Delta G^0 = 0$ the activation barrier ΔG^\ddagger is at its maximum (Marcus-normal region). With decreasing standard enthalpy, the activation barrier decreases until $\Delta G^0 = -\lambda$, where ΔG^\ddagger is zero. For further decreasing standard enthalpy $\Delta G^0 > -\lambda$, the activation barrier rises again. This regime is called the Marcus-inverted region. Combined with Equation (2), this means that the electrons transfer rate first increases for greater values of ΔG^0 , to a point where it reaches a maximum rate and then again becomes slower, if the reaction becomes more exothermic.^[37]

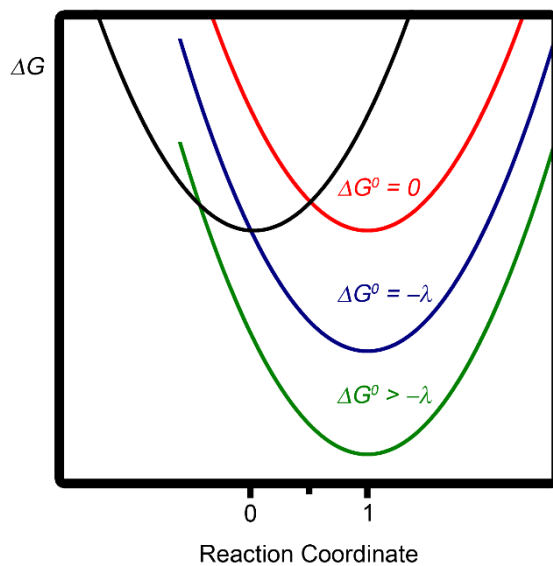


Figure 3. Free energy curves for different values of ΔG^0 .

While Marcus theory in general leads to good quantitative results, a major drawback of this theory is, that it is strictly speaking only applicable to systems with very weak electronic interactions (as stated in the premises of the theory). For systems with a significant

electronic coupling e.g. intramolecular electron transfer reactions, a more sophisticated approach was made by Hush, who extended the Marcus-Theory towards strongly interacting systems.^[37]

1.1.2 Marcus-Hush Theory – Adiabatic Approach

The Marcus-Hush theory applies when electronic communication between two redox sites is greater than the thermal energy $k_B T$. In this adiabatic approach the electronic communication is quantified by the electron coupling H_{AB} . Coupling of the two diabatic free energy curves for the reactants and products known from the previously discussed Marcus-Theory via H_{AB} leads to the curves depicted in Figure 4. The free energy curves show a double minimum in the adiabatic ground state and a single minimum for the excited state. The energy separation between the ground (GS) and excited state (ES) is exactly $2H_{AB}$ for both the degenerate and non-degenerate case.

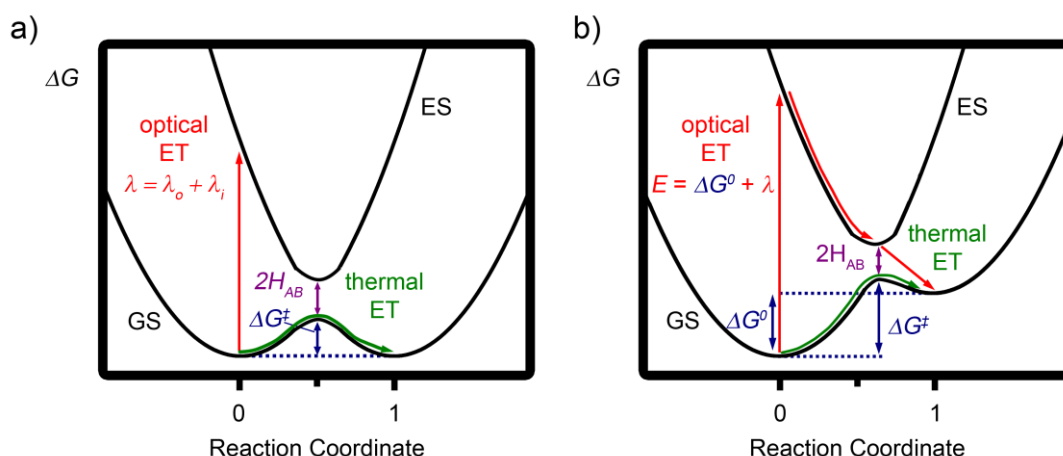


Figure 4. Free energy curves for adiabatic treatment for a) degenerate states and b) non-degenerate states.

In the adiabatic case the term for the activation free energy ΔG^\ddagger is not easy to obtain, because of the fact that the electronic coupling leads to a stabilization of the minima of the curve. What basically is done is formulating a term for free energy of the transition state and the reactant minimum depending on H_{AB} and ΔG^0 (because the terms for the reaction coordinate are as well depending on H_{AB} and ΔG^0). The difference of these two energies

equals the free energy of activation ΔG^\ddagger .^[79] The formula for degenerate states is given in Equation (4), the formula for non-degenerate states in Equation (5).

$$\Delta G^\ddagger = \frac{(\lambda - 2H_{AB})^2}{4\lambda} \quad (4)$$

$$\Delta G^\ddagger = \frac{\lambda}{4} + \frac{\Delta G^0}{2} + \frac{(\Delta G^0)^2}{4(\lambda - 2H_{AB})} - H_{AB} + \frac{H_{AB}^2}{\lambda + \Delta G^0} - \frac{H_{AB}^4 \Delta G^0}{(\lambda + \Delta G^0)^4} \quad (5)$$

1.1.3 Mixed-valent Compounds

The term mixed-valent was for the first time used by Klotz et al. for a $\text{Cu}^{\text{I}}/\text{Cu}^{\text{II}}$ -Komplex.^[80] In general, a mixed-valent system is considered when two or more redox active sites occur in different oxidation states. One of the most famous compounds showing this behavior is the Creutz-Taube-Ion **I**, see Figure 5. It was first reported in 1969 and incorporates two ruthenium redox centers bridged by a pyrazine ligand and saturated by five ammonia ligands per center. The molecule has an overall charge of 5+, leading to either Ru^{II} and Ru^{III} centers or an averaged oxidation state of 2.5.^[31,41] This compound was used to intensively study electron transfer for the next thirty years. At the same time the first ferrocene containing mixed-valent compound was published by Cowan *et al.*, biferrocenium **II** with an overall charge of 1+ and therefore either an Fe^{II} and Fe^{III} center or a formal oxidation state of +2.5 for both centers.^[42,81]

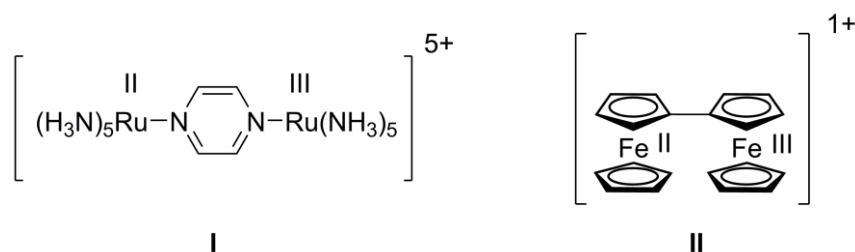


Figure 5. Creutz-Taube-Ion I and biferrocenium II

In the late 1960s, Robin and Day classified mixed-valent compounds and identified three classes of mixed-valent compounds.^[82] Class I, without any electronic coupling. Class II with medium electronic coupling and Class III, with strongly coupled centers. The

difference clarified by comparing the electronic coupling H_{AB} is compared to the Marcus reorganization energy λ as demonstrated in Table 1.^[83]

In Figure 6, the free energy surfaces for class I, II and III are shown. For class I no electronic coupling is observed. The energy diagram shows two distinct curves for the ground states with no crossing point and two strictly separated minima. Therefore the Marcus reorganization energy depicted is merely of theoretical kind. No electron transfer can occur optically or thermally between the two redox centers.

Robin-Day-Class	Electronic Coupling
I	$H_{AB} = 0$
II	$0 < 2H_{AB} < \lambda$
III	$2H_{AB} > \lambda$

Table 1. Electronic coupling for the three Robin Day classes.

Class II, which features an electronic coupling smaller than the Marcus reorganization energy is described by a double minimum in the electronic ground state (if ΔG^0 is significantly smaller than λ , vide supra) and optical and thermal electron transfer is possible for this compounds. With increasing ΔG^0 the energy required for the optical electron transfer and the activation energy for the thermal electron transfer increases as well. If ΔG^0 is on the order of λ the double minimum vanishes and only one minimum persists. A thermal electron transfer is not possible anymore and an optical excitation does not lead to a charge transfer from one center to the other, because the relaxation converges to the same state as before the optical excitation.

Class III features electronic coupling H_{AB} at least as big as λ , the adiabatic ground state shows a single minimum for the degenerate case. The unpaired electron is completely delocalized between the two redox centers. Optical excitations are still possible, but do not lead to charge transfer, because the excited state is delocalized over both redox centers as well, leading to no change in dipole moment. This concludes to the fact, that a description of neither optical nor thermal electron transfer is meaningful.

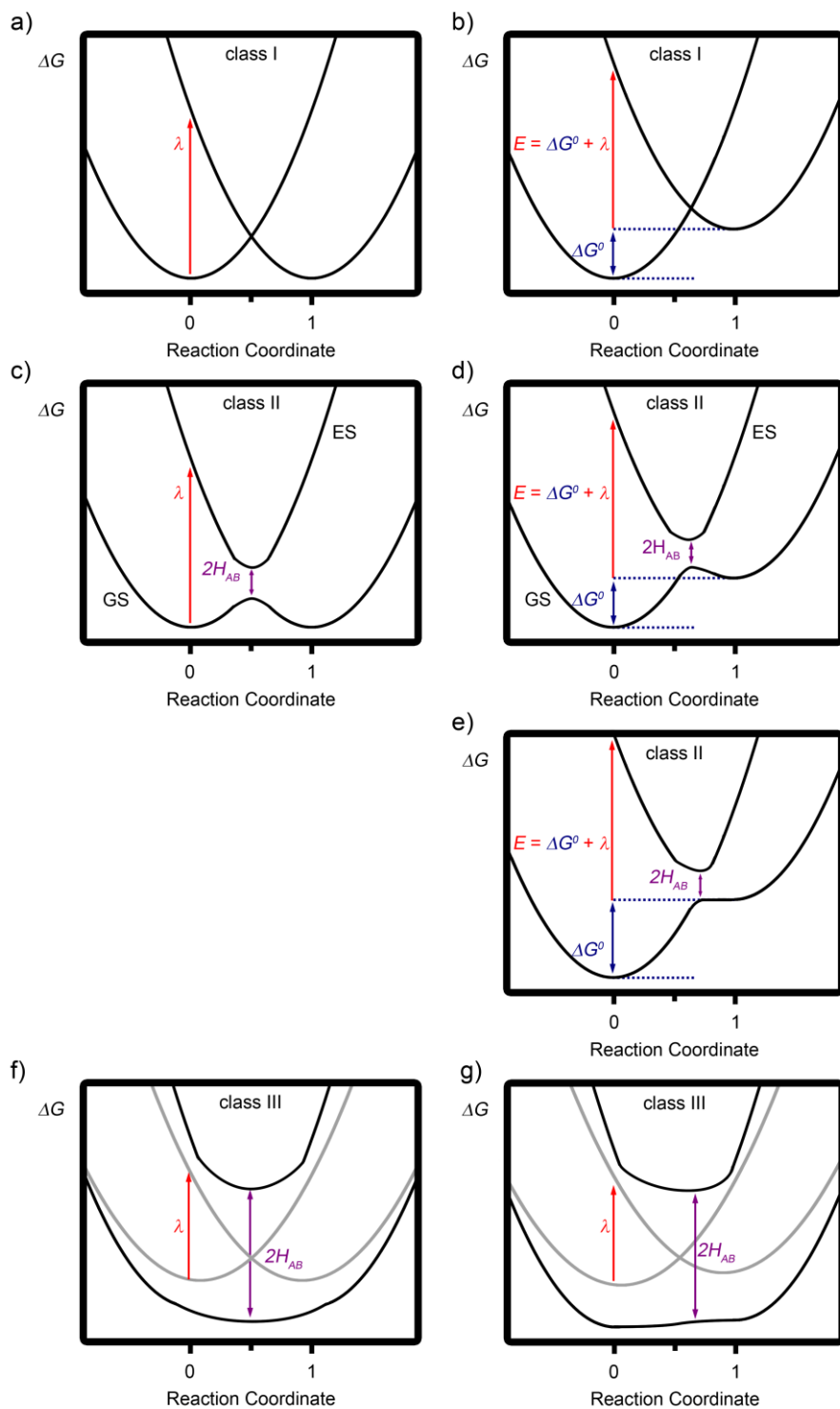


Figure 6. Diabatic and adiabatic free energy curves for class I-III with a), c) and f) degenerate and b), d), e) and g) non-degenerate states.

In the case of non-degenerate states the distinction between Class II and Class III is difficult, because there is still a double minimum in the ground state with a very small thermal activation barrier. This leads to the observation, that the classification of the system is dependent on the time scale applied to the system. This has an effect on the analytical method applied, for each spectroscopic method has its own time scale i.e. 10^{-15} s for optical transitions, $10^{-11} - 10^{-12}$ s for vibrational spectroscopy, 10^{-9} s for Mössbauer spectroscopy, 10^{-8} s for EPR spectroscopy, $10^{-3} - 10^{-8}$ s for NMR spectroscopy. Systems with time scale dependent class assignment to class II or III are therefore often summarized in a “fourth” class, namely class II/III.^[84]

1.1.4 Optical Transitions, Band Shapes and Determination of H_{AB}

The optical transition of class II systems is called intervalence charge transfer band (IVCT). It is often located at small energies, ergo in the near IR in optical spectroscopy. The shape of the band is that of a Gaussian curve, as seen in Figure 25. The shape originates from Boltzmann distributed vibrational states which are occupied for $h\tilde{\nu} \ll k_B T$. The most probable transition in this setup is the one from the lowest vibrational state of the ground state to the excited state with the same coordinates (and therefore a vibrational excited state). The energy of this transition is the Marcus reorganization energy λ plus the standard free energy of the reaction ΔG^0 and therefore directly correlated to the maximum of the IVCT band as shown in Equation (6).

$$\tilde{\nu}_{max} = \lambda + \Delta G^0 \quad (6)$$

The optical transitions of class III systems are also often charge resonance bands (CR) and appear in the same region of the optical spectrum as the IVCT bands of Class II system. The band shape is strongly asymmetric, comparable to a Gaussian band shape with a cutoff at $2H_{AB}$, which is the lowest energy for optical transition. The maximum of the IVCT band is still related to the Marcus reorganization energy λ , but additionally $2H_{AB}$ can directly be received from the cutoff of the spectrum.^[85]

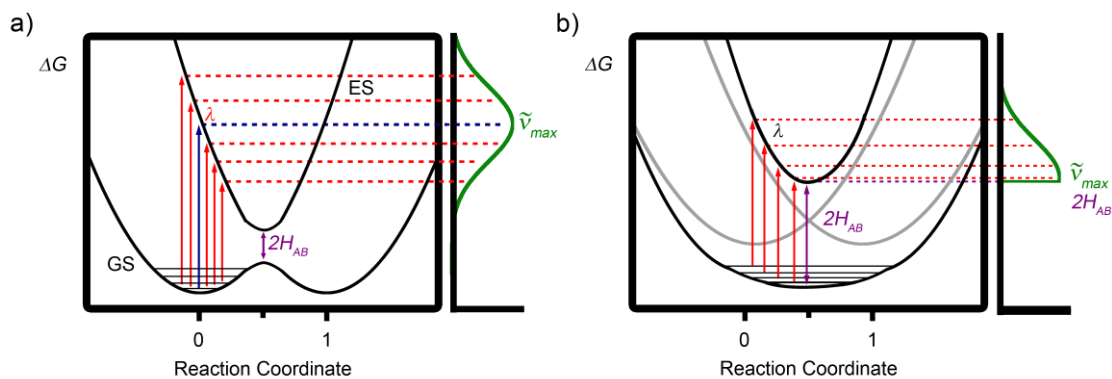


Figure 7. Origin of the band shape for a) class II and b) class III systems.

One of the most important derivations of the Marcus-Hush theory is the possibility to extract the value of H_{AB} through band shape analysis of the IVCT band. For class II systems H_{AB} is given by Equation (7). In this Equation $\tilde{\nu}_{max}$ is the energy of the maximum of the IVCT band in cm^{-1} , ϵ_{max} is the extinction coefficient at the maximum, $\Delta\tilde{\nu}_{0.5}$ equals the bandwidth at half height in cm^{-1} , and R_{AB} is the charge transfer distance in Å.

$$H_{AB} = 0.0206 \frac{(\tilde{\nu}_{max} \epsilon_{max} \Delta\tilde{\nu}_{0.5})^{0.5}}{R_{AB}} \quad (7)$$

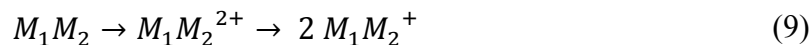
For use of Equation (7) R_{AB} is often set as the distance between the two redox sites, because the actual effective charge transfer distance is very difficult to measure experimentally (e.g. by means of Stark spectroscopy). This in general leads to an overestimation of R_{AB} and an underestimation of H_{AB} .^[86] For strongly coupled systems i.e. class III Equation (8) is valid, where H_{AB} is given by half the energy of the maximum of the transition band.

$$H_{AB} = \frac{\tilde{\nu}_{max}}{2} \quad (8)$$

1.1.5 Half-Wave Potential Splitting in Mixed-valent Systems

The above mentioned thermodynamic stabilization of mixed-valent compounds has a large impact on the electrochemical analysis of these compounds. As apparent from Equation (10) the potential splitting between the first oxidation to the mixed-valent compound and

subsequent oxidation $\Delta E_{1/2}$ is dependent on the comproportionation constant of the compounds. Therefore the half-wave potential splitting is directly correlated to the free energy change of the system $-\Delta G_c$ upon oxidation by Equation (11).



$$K_c = e^{\frac{nF\Delta E_{1/2}}{RT}} \quad (10)$$

$$-\Delta G_c = nF\Delta E_{1/2} \quad (11)$$

The free energy change results from five contributions to the term. The statistical contribution ΔG_{stat} , which accounts for 36 mV and arises from the fact, that the mixed-valent system is statistically favored in comparison to isovalent compounds. The inductive contribution ΔG_{ind} , which arises from the fact, that a change of the oxidation state of one metal center affects the bonding ability of the bridging ligand and therefore alters the redox potential of the second metal center. A magnetic exchange contribution ΔG_{ex} , which is essentially proportional to the antiferromagnetic exchange term. The electrostatic contribution ΔG_{el} , which expresses that adding a second charge to an already charged molecule requires more energy. And last there is the resonance contribution ΔG_{res} , due to the resonance stabilization of the mixed-valent compounds.

While it is obvious, that some contributions to the free energy change, and therefore to the half-wave potential splitting, are rather small and constant, others may contribute significantly for a certain system so that a great half-wave potential splitting may serve as an indicator for electronic coupling in mixed-valent systems, but cannot be used to quantify the electronic coupling by any means.^[86]

$$\Delta G_c = \Delta G_{stat} + \Delta G_{ind} + \Delta G_{ex} + \Delta G_{el} + \Delta G_{res} \quad (12)$$

1.1.6 Electron Transfer in Ferrocene Compounds

Ferrocene compounds have been used since the 1970s to study mixed-valent behavior and electron transfer.^[42,81] These studies have led to interesting results for the value of the electronic coupling depending on the type, length and electron richness of the bridge. While it would be desirable to study any mentioned effect on its own, the nature of chemical bonds prohibits strict separation between above mentioned effects. However, an attempt can be made derive as much information about single effect as possible.

Comparing biferrocene **II**, diferrocenylmethane **III**, 1,2-diferrocenylethene **IV**, and diferrocenylacetylene **V**, it is evident that the type of the bridge with respect to its hybridization has a large impact, see Figure 1. While biferrocenium **II** shows a strong IVCT band with $\lambda_{\max} = 1800$ nm, diferrocenylmethane **III** displays no IVCT band and therefore no electronic communication between the ferrocene units. Compound **IV** has a slightly smaller electronic coupling, derived from an IVCT band at $\lambda_{\max} = 1750$ nm, compared to

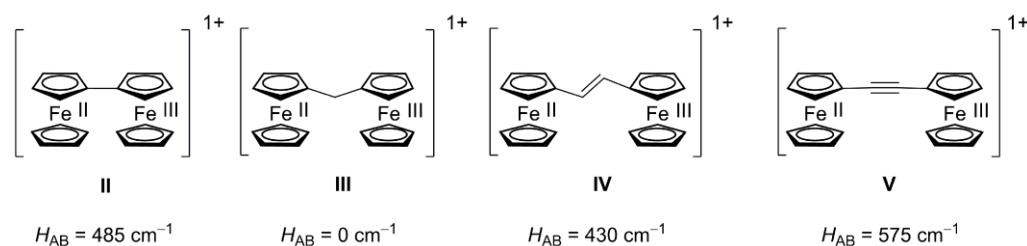


Figure 8. Singly oxidized biferrocene^{1,[43]} II, diferrocenylmethane^{2,[43]} III, 1,2-diferrocenylethene^[44] IV, diferrocenylacetylene^{1,[43]} V and their H_{AB} in CH_2Cl_2 .

biferrocene **II**. Finally, diferrocenylacetylene **V** exhibits the strongest electronic coupling with an IVCT band at $\lambda_{\max} = 1560$ nm. These results are of rather qualitative nature, because biferrocene **II** has a significantly smaller distance between the metal centers than **III**, **IV** and **V** and while the distance in **III**, **IV** and **V** is rather similar, the bridge of **V** is more electron rich than that of **IV**. Therefore, the conclusion is that permitting interaction

¹ Calculated from given values for the interaction parameter α .

² No solvent given in reference

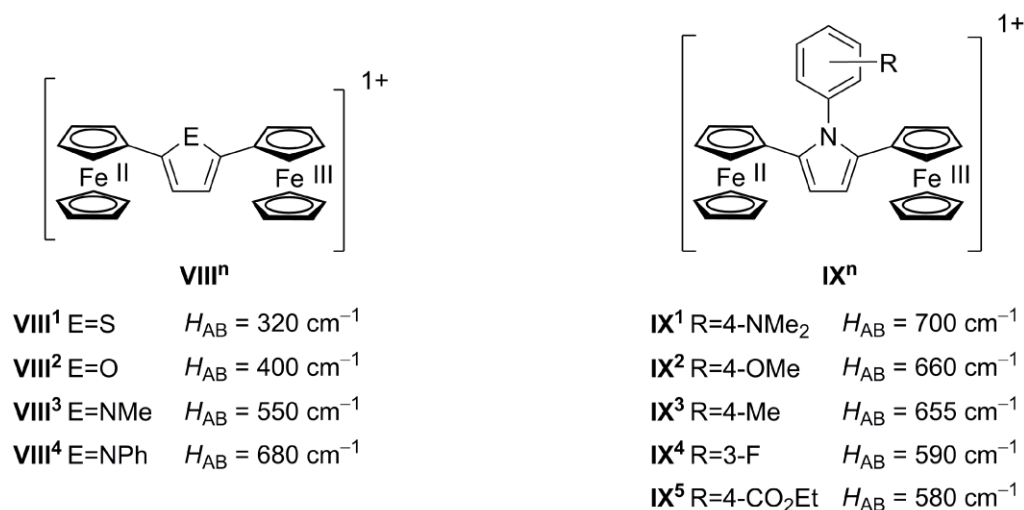


Figure 10. Singly oxidized 2,5-diferrocenyl heterocycles in CH₂Cl₂.^{3[87]}

Electron rich and poor bridges were studied by Lang et al. with heterocyclic five-membered ring systems as a bridge connecting two ferrocenyl substituents, see Figure 10. Changing the bridge from thiophene **VIII¹** over furan **VIII²**, *N*-methylpyrrole **VIII³** to *N*-phenylpyrrole **VIII⁴**, so varying the bridge from electron poor to electron rich heterocycles yields higher electronic coupling H_{AB} . The same is true for changing the substituents on the phenyl ring of *N*-phenylpyrrole derivatives **IXⁿ**. Starting from 4-dimethylaminophenyl substituted pyrrole **IX¹** to 4-ethylcarboxylphenyl substituted pyrrole **IX⁵** H_{AB} decreases with increasing electron deficiency of the bridge. In conclusion, generally higher electronic couplings are achieved with electron rich bridges, rather than with electron poor bridges.

Concerning asymmetrically bridged ferrocene derivatives less data is available. Molina and Veciana et al. studied 1,4-bis(ferrocenyl)-2-aza-1,3-butadiene **X**, see Figure 11. Compared to its all-carbon analogue **VI²** H_{AB} is just half as large. It should be noted, that the comparison is not fair, due to the fact, that with asymmetric bridging the redox potentials of the ferrocenes are no more equivalent. Heinze et al. did an intensive study of amide bridged ferrocenes diminishing the effect of different oxidation potentials by the linkage of two redox similar ferrocene units in derivative **XII**. Comparing the derivative

³ H_{AB} recalculated for $R_{AB} = 7.084 \text{ \AA}$, derived from single crystal X-Ray diffraction of **VIII¹**,^[45] from given H_{AB} values for $R_{AB} = 2.1 \text{ \AA}$ (experimental effective electron transfer distance) for ease of comparison.

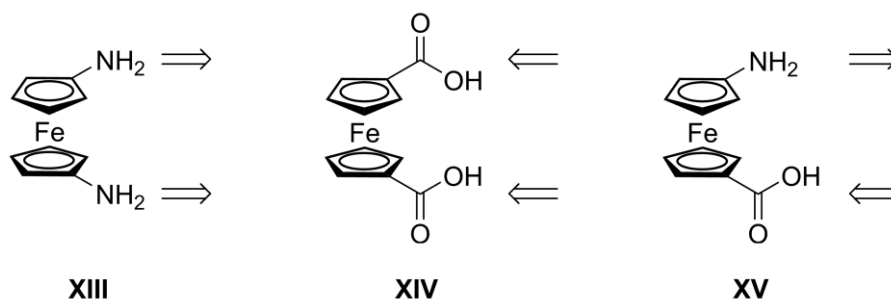


Figure 12. 1,*n*'-diaminoferrocene XIII, 1,*n*'-ferrocenedicarboxylic acid XIV, 1-amino-ferrocene-*n*'-carboxylic acid XV and their peptide strand arrangements.

Rotational freedom along the pseudo- C_5 axis distinguishes five isomers. The 1,1'-isomer with an angle between the two substituents of $-36^\circ < \omega < 36^\circ$, the 1,2' isomer with $36^\circ < \omega < 108^\circ$, the 1,3' isomer with $108^\circ < \omega < 180^\circ$, the 1,4' isomer with $-108^\circ < \omega < -180^\circ$, and the 1,5' isomer with $-36^\circ < \omega < -108^\circ$. The 1,2' isomer and the 1,3' isomer introduce *P*-helical chirality, while the 1,4' isomer and 1,5' isomer introduce *M*-helical chirality. The orientation of the Cp amide bonds is given with an *E/Z* nomenclature, where *Z* isomer denotes that the substituents at the amide with highest priority are facing towards the substituent at the other Cp ring. If the substituent with highest priority is facing the other direction the amide bond is considered the *E* isomer.

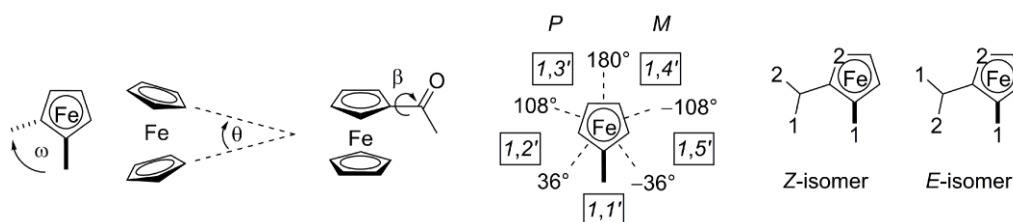


Figure 13. Stereochemical descriptors of ferrocene containing peptides.^[90]

All three ferrocene derivatives mentioned above permit interstrand hydrogen bonding. In peptide chemistry the hydrogen bonding pattern defines the nature of the turn structure. In Figure 14 “normal” and “reverse” turn structures are shown. The turn is called “normal” if the H bond acceptor is located at the N terminus of the peptide, while it is called “reverse” if the hydrogen bond acceptor is located at the C terminus. In case of a normal turn α -helices are featured by 13-membered rings, while β - and γ -turns are featured by ten- and

seven-membered rings. For the “reverse” turn an eleven-membered ring features a reverse α -helix, an eight-membered ring a reverse β -turn and a five-membered ring a reverse γ -turn.

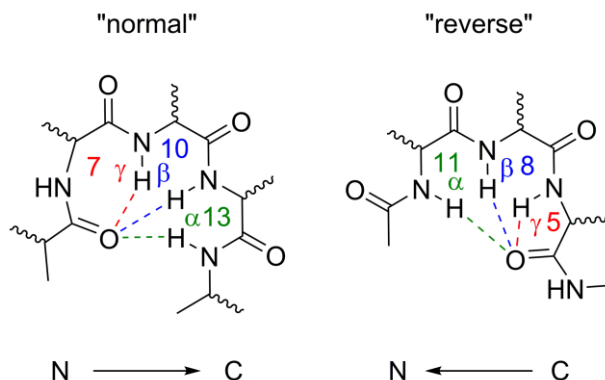


Figure 14. “Normal” and “reverse” turns in peptide chemistry.

The hydrogen bonding motifs of ferrocene peptides feature similar turns, so the same nomenclature can be used. Additionally some structural motifs are named as shown in Figure 15. The “Herrick” conformation^[91] features two ten-membered rings and therefore induces a β -turn. The “van Staveren” conformation^[92] features a seven-membered ring and therefore a γ -turn. Last the open conformation is named “Xu”.^[93]

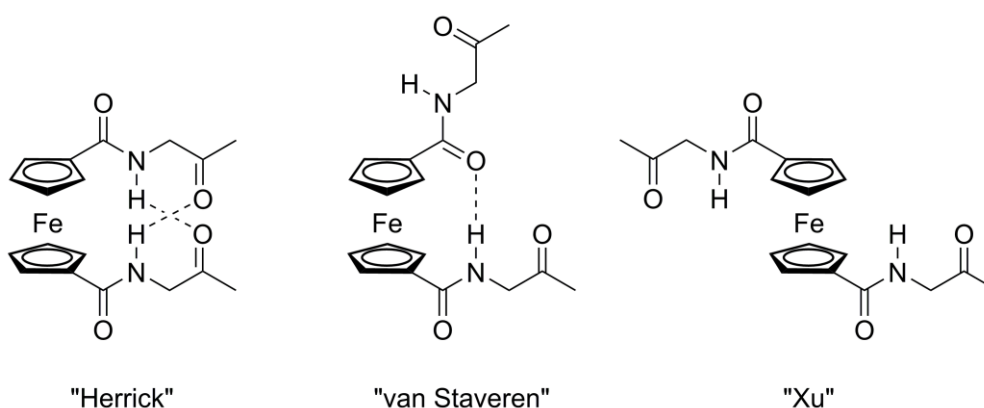


Figure 15. Different H-bonding motifs for 1,n'-ferrocendicarboxylic acid.

Intensive research concerning the properties of amino acid conjugates of ferrocene dicarboxylic acid **XIV** was done by several working groups. The general findings are that the ferrocenyl (Fn) bioconjugates show a ferrocene based positive cotton effect in CD

spectroscopy.^[94] Bioconjugates of L-amino acids show *P*-helicity, while bioconjugates derived from D-amino acids show *M*-helicity.^[90] Various amino acid conjugates are known throughout the literature and their structure in the solid state and solution has been disclosed.^[93,95-99] One of the most interesting findings for this kind of bioconjugates was a tryptophane containing $\text{Fn}[\text{CO-L-Trp-OMe}]_2$, which shows self-assembly to a supramolecular nanofibrillar network. Stimuli responsive (oxidation/reduction, temperature) morphological transformations for this compound were observed, rendering it a good starting point for the development of new redox-active functional biomaterials.^[100]

The first bioconjugates derived from 1,1'-diaminoferrocene **XIII** were reported by Kraatz et al.^[101] A $[\text{Boc-Ala-NH}]_2\text{Fn}$, which shows interstrand hydrogen bonding in two ten-membered rings in the solid state and preserved H bonding in solution. The work was carried on by Heinze and Rapic^[102] with asymmetric conjugates of the type $\text{Boc-AA-NH-Fn-NH-Ac}$ [AA=Gly, Ala, D-Ala, Val). It was found, that a single covalently bonded amino acid is enough to induce chiral organization of the ferrocene central unit and the majority possess *P*-helical conformation for L-amino acids.

Bioconjugates of ferrocene amino acid **XV** (Fca) enable even more diverse H-bonding motifs compared to 1,1'-diaminoferrocene **XIII** and ferrocene dicarboxylic acid **XIV**.^[103] Amongst others they could be realized in form of X-CO-Fca-AA-OMe (X=Me or Boc), with only a single interstrand hydrogen bond due to steric effects. For example, the Me-CO-Fca-Val-OMe derivative exhibits one $\text{NH}_{\text{Fca}} \cdots \text{OC}_{\text{AA}}$ hydrogen bond forming a nine-membered ring.^[104] $\text{X-CO-AA}^1\text{-Fca-AA}^2\text{-OMe}$ derivatives were explored, with two hydrogen bonds forming a 9-membered and eleven-membered ring namely $\text{NH}_{\text{Fca}} \cdots \text{OC}_{\text{AA}2}$ and $\text{NH}_{\text{AA}2} \cdots \text{CO}_{\text{AA}1}$ for the $\text{Me-CO-Ala}^1\text{-Fca-Ala}^2\text{-OMe}$ case.^[104,105,105,106] These rings can even be selectively enlarged by the use of β -amino acids.^[107]

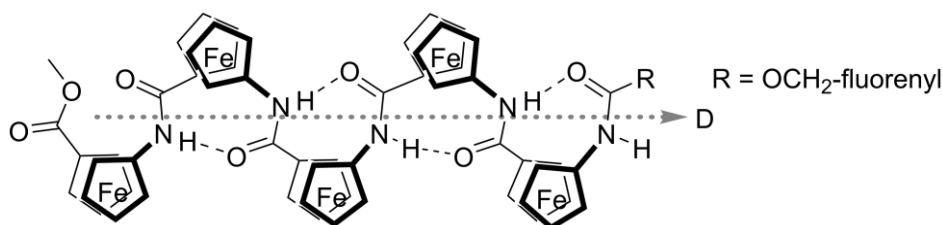


Figure 16. Zig-zag-Conformation of oligoamides of Fca, exemplary for Fmoc-Fca₅-OMe XVI.

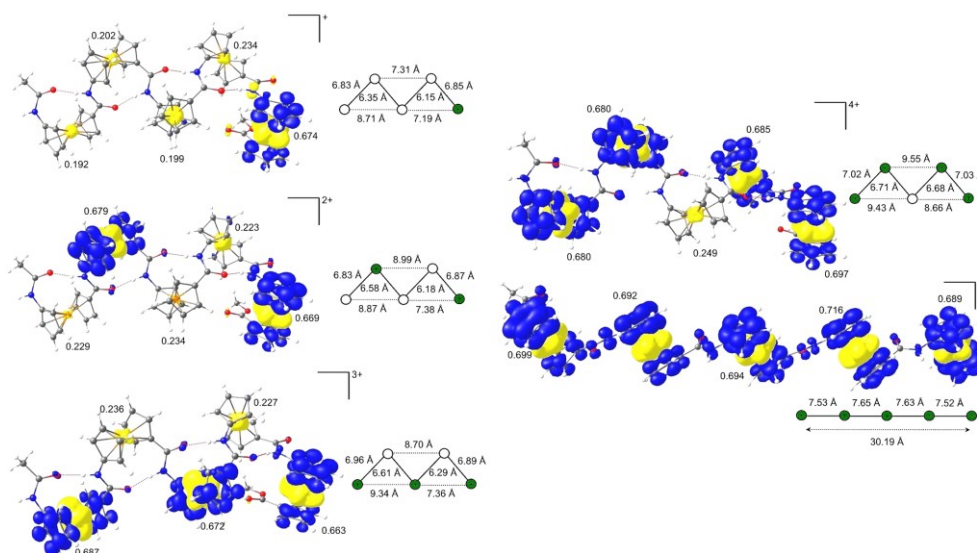


Figure 17 DFT optimized geometries of [Ac-Fca₅-OMe]ⁿ⁺ XVI (n = 1-5); spin density at 0.002 a. u.^{[48]4}

Derivatives with more than one ferrocenyl moiety in the peptide backbone have been studied since 1998. This began with experiments from Nakamura *et al.*^[108] with Me-CO-Fca₂-NHMe and was later continued by Heinze *et al.*^[109] with Me-CO-Fca-NH-Fc. For both compounds only intermolecular hydrogen bonds are observed in the solid state. Thorough investigation of compounds X-CO-Fca_n-NH-Fc (n = 1,2, X= Me, OtBu, OCH₂-fluorenyl) revealed hydrogen bonding in solution. All oligopeptides form an eight-membered ring with a 1,2' (1,5') conformation derived from nuclear Overhauser spectroscopy.^[84] This is conform to DFT calculations of the system showing that one conformer is thermodynamically favored over the others. DFT calculations also suggest, that the hydrogen bonding motif is conserved during oxidation until every single ferrocenyl moiety is oxidized. Then the open conformation becomes the energetically favored one. Experimental evidence for this is currently only obtainable by IR spectroscopy and the absence of hydrogen bonded amide groups, because the strong paramagnetic nature of the fully oxidized compound renders NMR spectroscopy useless. This very stable hydrogen bonding motif is also called zig-zag-conformation and leads to a nearly parallel alignment of the individual amide dipole moments, forming a permanent macrodipole, see Figure 16.

⁴ Adapted from: D. Siebler, Dissertation, Johannes Gutenberg-University, 2010.

DFT calculations for this system suggest mixed-valent states, in which alternating Fe^{II} and Fe^{III} units are present, see Figure 17. The same conformation is seen in oligoamides of the kind Fmoc-Fca_n-OMe (n=2-5).^[47]

1.2.1 A Structure Comparison of Amides and Thioamides

In contrast to amides, which have been extensively studied because of their relation to peptide conformations, thioamides have been essentially neglected. Just as the amide group the thioamide shows a nearly planar arrangement. The bond angles for both groups are essentially identical, as seen in Figure 18. The largest structural difference in structure is the significantly longer C=S bond length of 1.65 Å, exemplarily for *N*-methyl thioacetamide, compared to the C=O bond length of 1.23 Å of its amide analogue.^[110] Another difference is the smaller electronegativity of the sulfur atom ($\chi = 2.58$)^[111] compared to oxygen ($\chi = 3.44$)^[111], which renders the C=S bond ($\Delta\chi = 0.03$) significantly less polar compared to the C=O bond ($\Delta\chi = 0.89$).

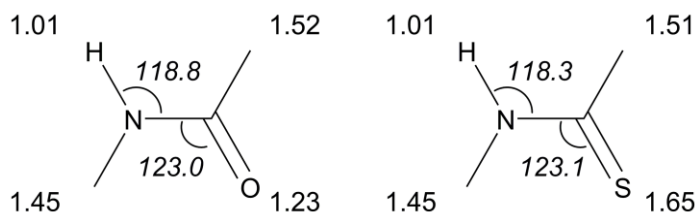


Figure 18. DFT optimized geometries of *N*-methyl acetamide and *N*-methyl thioacetamide with their respective bond lengths in Å and bond angles in deg (*italics*).

In both amides and thioamides an *E* and *Z* configuration is feasible, see Figure 19. In general the rotational barrier around the N-C bond is lower for amides compared to their analogue thioamides.^[112] The origin of the higher rotational barrier for thioamides is the larger stabilization of the ground state. The above mentioned difference in electronegativity for oxygen and sulfur leads to very different polarities for the C=X (X = O, S) bond. The C=O bond is very polar therefore the π orbital of the double bond has a higher coefficient at the oxygen atom and a smaller one at the carbon atom. For the π^* orbital the situation is reversed with larger coefficients at the carbon atom. The electron density in the C=S bond

is evenly distributed between the carbon and sulfur atom and therefore the orbital coefficients of the π and π^* orbital are evenly distributed as well. For both amides and thioamides the nitrogen lone pair donates electrons into the π^* orbital of the C=X (X = O, S) bond, see Figure 20. In amides little stabilization is gained through electron donation from the nitrogen atom to the carbon atom, because the oxygen atom already has a high electron density. In case of thioamides the stabilization is much larger, because the charge is not only donated from the nitrogen to carbon, but is passed on to the sulfur atom, which can easily accommodate higher electron densities through its larger orbitals.^[113]

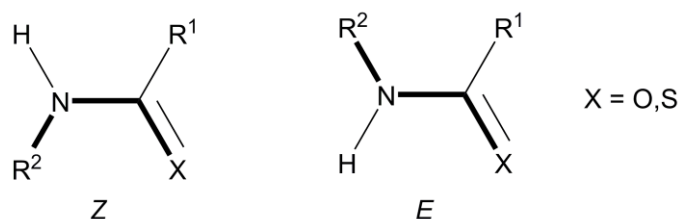


Figure 19. Z and E conformation for amides and thioamides.

For the transition states TS1 and TS2, see Figure 20, Lauvergnat and Hiberty showed via DFT calculations, that a sp^3 hybridization at the nitrogen atom is energetically favored compared to the sp^2 hybridization of the ground state for formamide and thioformamide.^[114] This is applicable to all amides and thioamides. During the rotation from the ground state to the transition state, the orbital overlap between the nitrogen lone pair and the π^* -orbital decreases essentially to zero in the transition state, due to the fact, that the orbitals are orthogonal in the TS. Comparing the ground state and the TS 1 for the amide only small change in C=O bond length is visible, while for the thioamides a significant shortening of the C=S bond length occurs. C-N bond is elongated in the transition state for both amides and thioamides, due to the cleavage of the partial double bond. This is conform to the model of stabilization of the thioamides via electron donation to the sulfur atom, and for amide to a donation to the carbon atom only.

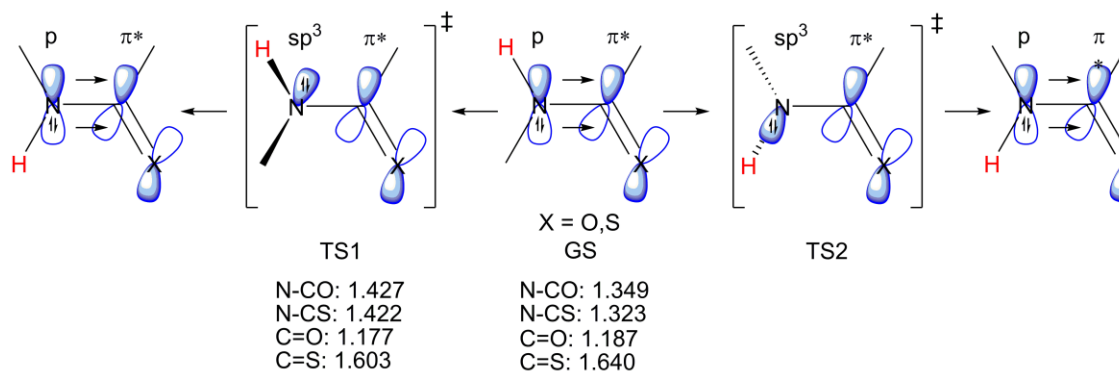


Figure 20. Schematic representation of the orbitals in amides (X=O) and thioamides (X=S) in the ground state (GS) and both transition states (TS), and calculated bond length in Å.

Because of the charge (q) transfer from the nitrogen atom to the sulfur atom and the longer distance (\vec{l}) thioamides display a larger dipole moment (\vec{p}) in the ground state than amides ($\vec{p} = q \cdot \vec{l}$).^[115] This was shown for dimethyl thioacetamide and dimethyl acetamide in their ground state (5.38 vs. 4.37 D), whereas the transition state exhibits essentially the same dipole moment for both (2.45 vs. 2.33 D).^[113] This has great impact for the solvent dependency of the rotational barrier for amides and thioamides. The rotational barrier for both increases with the polarity of the solvent, due to the energy needed for reorganization of the solvent molecules. The greater change in dipole moment during rotation for the thioamides compared to amides, means that the effect of the solvent on the rotational barrier is stronger for thioamides as shown in Table 2. Galabov *et al.* conducted DFT calculations for the effect of electron donating and withdrawing substituents R^2 , see Figure 19. Electron withdrawing substituents lower the rotational barrier significantly, while electron donating substituents lead to higher rotational barriers.^[116] In case of hydrogen bonding, no studies for thioamides have been done yet, but data for amides show, that a hydrogen bond at the NH group with anionic acceptors destabilizes the *E* isomer, while the effect of hydrogen atom donors is negligible. The study also shows, that the effect of hydrogen bonding is not reliably predictable, because chelating effects can occur and reverse the general effect.^[117]

The effect of substitution patterns of secondary thioamides has been thoroughly studied by Rao *et al.* for *N*-monosubstituted thioamides.^[118] In general, the *E/Z* ratio for thioamides is determined by steric effects and therefore the larger sulfur atom compared to oxygen leads to a greater proportion of the *E* isomer. The *E/Z* ratio also increases with the size of

the alkyl substituent R^2 , see Figure 19. Increasing the size of R^1 has the contrary effect, and leads to an increase of the *Z*-isomer.

Medium	ϵ	Dimethylthioacetamide	Dimethylacetamide
gas phase	1.00	74.1	64.1
cyclohexane	1.93	82.0	68.5
dichlormethane	9.0	91.6	75.1
acetonitrile	32.7	92.9	74.3
water	61.0	97.9	79.7

Table 2. Experimental rotational barriers of for *N,N'*-dimethylthioacetamide and *N,N'*-dimethylacetamide at 80°C.^[113,119]

1.2.2 Thioamides as Isosteric Replacement

Thioamides are generally considered to be isosteric replacements for amides in amino acid conjugates (e.g. peptides), but literature shows that this statement is not entirely true. Because of the previously mentioned longer C=S distance compared to the C=O distance in amides the hydrogen bonding of thioamides might introduce changes in protein folding.^[120] The higher acidity of the thioamide NH proton makes it a better proton donor for hydrogen bonding compared to amides ($pK_a = 18.5$ vs. 25.5). The larger sulfur atom on the other hand is a weaker hydrogen bond acceptor than oxygen, leading to weaker hydrogen bonds. Hence the SCN-H \cdots O hydrogen bond is stronger than the OCN-H \cdots O hydrogen bond, while the N-H \cdots SC hydrogen bond is weaker than the N-H \cdots OC hydrogen bond.^[69]

This was tested by Miwa *et al.* by preparation of a thioamide analogue of GCN4, which is a helical peptide consisting of 35 amino acids. Substitution of one amide by a thioamide at the C terminus and in the middle of the strand did not lead to any significant change in structure, as probed by circular dichroism measurements.^[121] Kiefhaber *et al.* found contrary results. Upon substitution of an amide unit by a thioamide unit in Alanine based helical peptides at the N-terminus or in the center a highly helix destabilizing effect was observed. Studies of the incorporation of thioamide units into β -turn hairpin structures lead to the conclusion, that the turn structure is essentially unaffected if the sulfur of the thioamide group is pointing toward the exterior and hydrogen bonding of the NH group is

feasible. But if the thiocarbonyl sulfur is forced to participate in hydrogen bonding a perturbation of the turn structure occurs. This effect is diminished if the thioamide substitution is positioned at the terminal region. In conclusion, the effect of thioamides as isosteric replacement in peptides is highly depending on the position of incorporation, particularly if the thioamide unit participates in hydrogen bonding interactions.^[122]

The weak hydrogen bonding of the thiocarbonyl sulfur can also be put to good use. Beeson *et al.* probed the hydrogen bonding interaction of a ligand to a major histocompatibility complex class II, an antigen presenting peptide, in the main chain. Substitution of the main chain carbonyl function involved in the hydrogen bonding with sulfur lead to a 30-fold increase of ligand dissociation, underlining the crucial role of hydrogen bonding interactions.^[123]

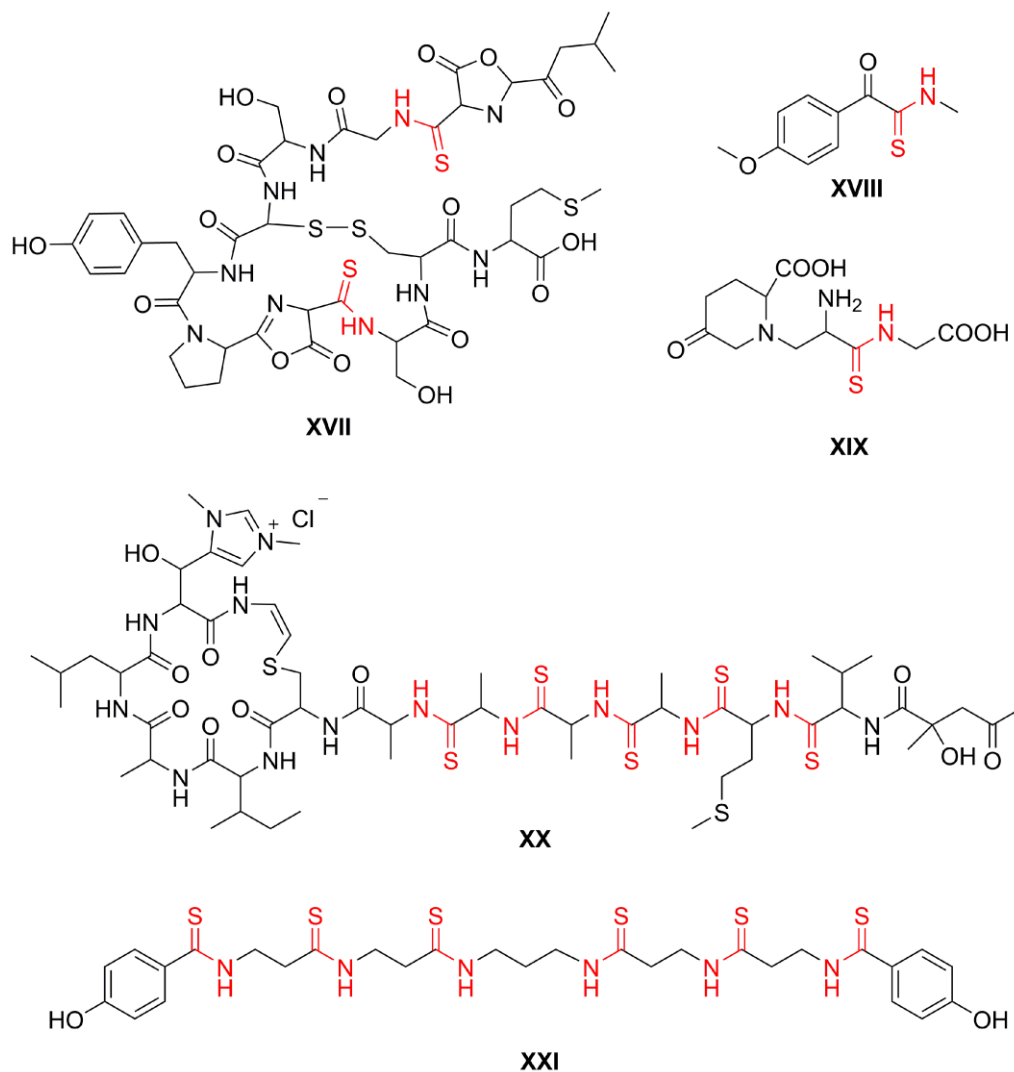


Figure 21. Natural products containing thioamide units.

Only a single naturally occurring protein containing a thioamide group is known today. In the methyl-coenzyme M reductase **XVII**, see Figure 21, a thioglycin residue is incorporated close to the active site.^[65,66,124] Here the thio amino acid is not engaged in hydrogen bonding forming secondary structures like α -helices or β -sheets. It is proposed that the thioamide unit acts as redox mediator in the methane-forming step and maybe undergoes a redox induced *E/Z* conformational facilitating the reaction.

Thioamides as well as carboxamides undergo an *E/Z*-conformational change under irradiation. For amides the $\pi \rightarrow \pi^*$ electronic transition is located at 200 nm and leads to photodecomposition. This decomposition is remarkably reduced in thioamides, where the $\pi \rightarrow \pi^*$ transition is red-shifted to 270 nm. This was put to use in a semisynthetic ribonuclease S containing a thioamide unit. Upon irradiation 30% of the thioamide switched from the *Z*- to the *E*-conformer rendering the enzyme inactive. More widespread application of this method could disclose important structural influences on enzyme reactivity.^[125]

Thioamides compared to amides exhibit greater stability against proteolytic degradation and improved absorption, distribution, metabolism and excretion properties.^[69–71] That biological systems are unfamiliar to thioamides is also represented by the fact, that besides the *apo*-methanobactin **XVII** in the methyl-coenzyme M reductase only four other natural products containing thioamide groups are known. The oxothioacetamide derivative^[67] **XVIII**, which is believed to be a decomposition product of more complex molecules, cychthioamide^[68] **XIX**, which is a non proteinogenic amino acid isolated from plants, thioviridiamide^[64] **XX**, an apoptosis inducer of bacterial origin, and clostioamide^[63,126] **XXI**. The latter shows remarkable antibiotic activity and was isolated from the anaerobic bacterium *Clostridium cellulolyticum* as a secondary metabolite, see Figure 21. It was shown, that the thioamide groups are of fundamental importance in this compound, because tests with the all carboxamide compound closamide showed no significant antibacterial activity.

1.2.3 Thioamide Containing Ferrocene Derivatives

All thioamide containing ferrocene derivatives known before this thesis are formally derived from ferrocene carboxylic acid. The first thioamide bearing ferrocenyl derivative was *N,N*-dimethyl ferrocene carbothioamide **XXII** and was reported by Nonoyama *et*

al.^[127], see Figure 22. This derivative was used to form cyclopalladated compounds. This work was later expanded using *N,N,N',N'*-tetramethylferrocene-1,1'-dicarbothioamide **XXIII**.^[128]

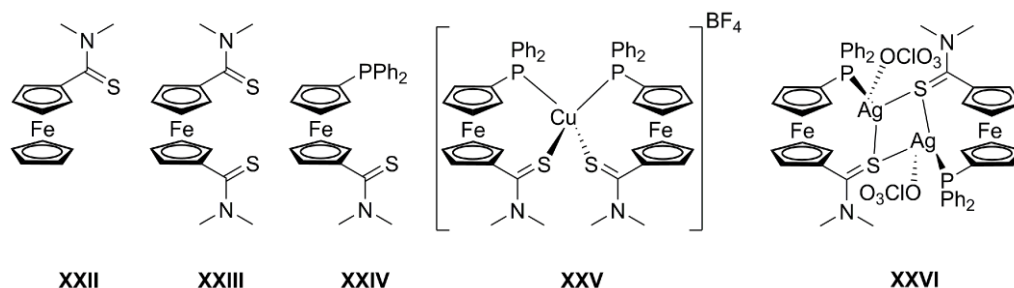
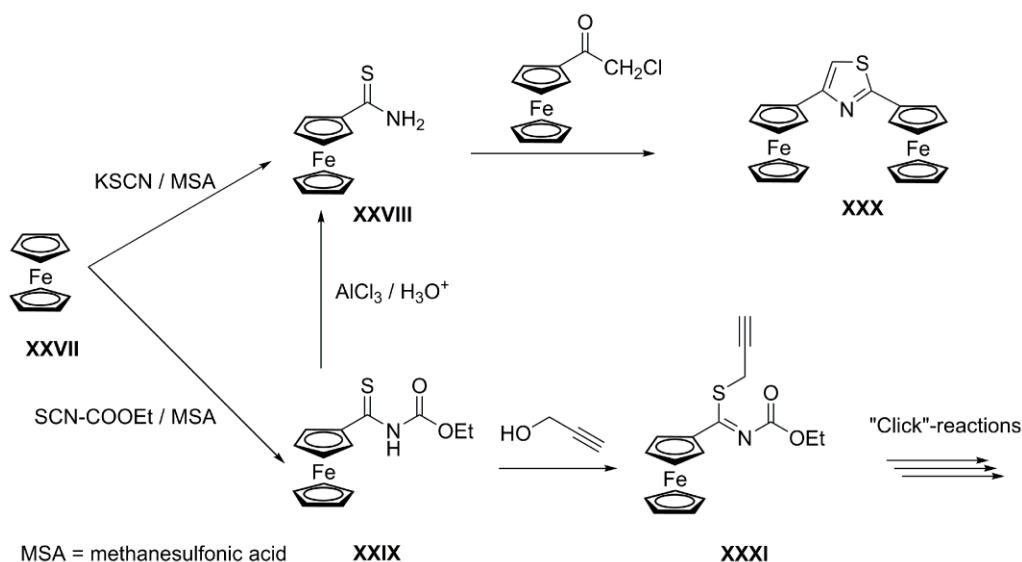


Figure 22. Various ferrocenyl thioamide containing ligand system and metal complexes derived from them.

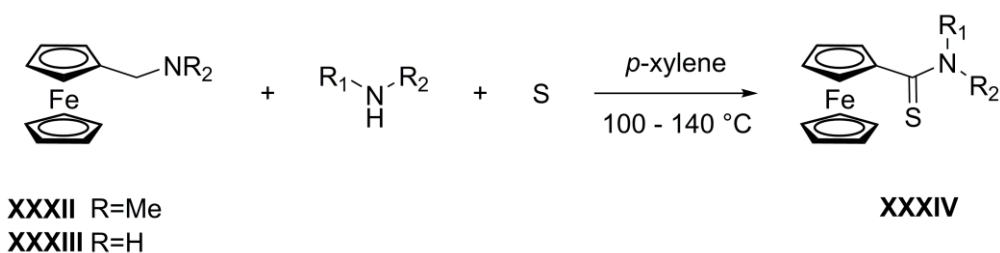
The essence of ferrocenyl substituted thioamides as a ligand was later picked up by Štěpnička *et al.*^[129] who prepared 1'-(diphenylphosphino)-1-[(dimethylamino)-thio-carbonyl]-ferrocene **XXIV** and it was found that this compound can act as a very flexible ligand, which allows perfect preorganization via rotation of the ferrocenyl moiety and twisting of the thioamide unit around the C-C bond. The redox behavior of compound **XXIV** is much more complex than that of the oxo analogue, showing only irreversible oxidations, which is probably attributed to the fact that the HOMO of the thioamide compound encompasses the ferrocenyl and thioamide moiety. The coordination properties of compound **XXIV** was probed by reaction with copper(I) and silver(I) resulting in complexes of the type $[\text{Cu}(\kappa P, \kappa S\text{-XXIV})_2][\text{BF}_4]$ **XXV** and the dimeric complex $[\text{Ag}_2(\text{ClO}_4)(\kappa P, \kappa S\text{-}\mu S\text{-XXIV})_2]$ **XXVI**.

Zakrzewski *et al.* used ferrocenecarbothioamide **XXVIII** and its *N*-ethoxycarbonyl derivative **XXIX** as precursors for the synthesis of 2,4-diferrocenylthiazole **XXX**.^[130] A proof of concept for the synthesis of ferrocene containing heterocycles, which are of interest as redox active markers^[131,132] and for their potential biological activity.^[57,59,60,133] This work was continued by the use of **XXXI** as a precursor for “click”-chemistry compounds containing a ferrocenyl moiety, see Scheme 1.



Scheme 1. Synthesis of ferrocenyl substituted heterocycles and “click” precursors.

The use of thioamides as anion receptors was disclosed by Beer *et al.*. They synthesized ((butylamino)-thiocarbonyl)ferrocene from the oxo analogue by reaction with Lawesson's reagent. The comparison of the two ferrocene derivatives showed, that the thioamide binds halogen anions more effectively than the carboxamide, because of its higher acidity and therefore better hydrogen bonding ability, providing a better NMR antenna for anion detection^[134].



Scheme 2. Condensation of (dimethylaminomethyl)ferrocene XXXII and aminomethylferrocene XXXIII with aliphatic and aromatic amines.

A big step for the widespread application of ferrocenyl thioamides **XXXIV** was done by Gasser *et al.*^[135], see Scheme 2. A new synthetic route was developed starting from (dimethylaminomethyl)ferrocene **XXXII** or aminomethylferrocene **XXXIII**, elemental sulfur and primary alky- or arylamines or in case of morpholine a secondary amine with

good tolerance of functional groups (Ether-, Ester-, Nitro-, Amino- and hydroxylgroups as well as halogens). This makes it one of the most straightforward synthetic routes to C-ferrocenyl thioamides.

1.3 EPR Spectroscopy and Spin Trapping of Radicals

EPR spectroscopy is the analytical method of choice for detection of unpaired electrons. When applying an external electromagnetic field to a paramagnetic compound, the Zeeman effect occurs, just like in NMR spectroscopy. The parallel and antiparallel orientations of the spin are separated in energy and transition between the two states is possible by absorption of irradiation. The shift of this absorption (g -value) depends mainly on the spin-orbit interaction, which itself generally depends on the mass of the nucleus, and gives a rough estimation about the location of the spin (i.e. different elements can be distinguished). The main source of information about the environment of the spin is derived from hyperfine coupling interactions. The interactions of the electron spin with nuclear spins, leads to a distinct coupling pattern, which can allow determination of the spin location, see Figure 23. Due to the high reactivity of some radicals, especially organic radicals, and the mostly applied slow sweep technique to measure EPR spectra a detection of these intermediate species is impossible. For detection of short-lived species spin trapping is a valuable tool.

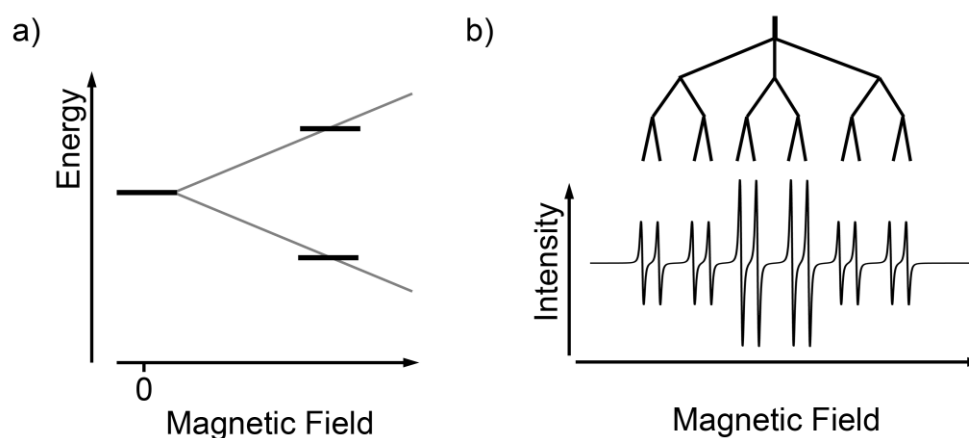
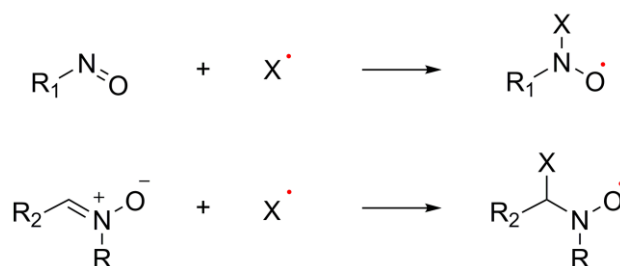


Figure 23. a) Schematic representation of the Zeeman effect b) Hyperfine coupling pattern.

Spin trapping means that the radical species of interest undergoes an addition reaction to a diamagnetic compound (spin trap) forming a relatively long-lived spin adduct.^[136] Despite the fact, that over 100 different compounds have been found to be suitable spin trapping agents, the most widespread used spin trapping agents are nitrones and nitroso compounds.^[137] Both form stable nitroxide radicals, however, the nitroso spin traps can provide more information, because the radical adds directly to the nitroso nitrogen and is therefore more likely to engage in hyperfine coupling interactions with the trapped spin, see Scheme 3.



Scheme 3. Spin trapping reaction of nitroso and nitron compounds.

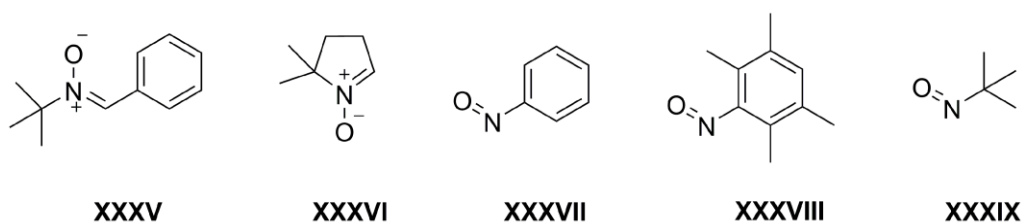


Figure 24. Most commonly used spin trapping agents. *N*-tert-butyl nitron (PBN) XXXV, 5,5-dimethyl-1-pyrrolidine-N-oxide (DMPO) XXXVI, nitrosobenzene (NOB) XXXVII, nitrosodurene (ND) XXXVIII and 2-methyl-2-nitrosopropane (MNP) XXXIX.

The most commonly used spin trapping agents are *N*-tert-butyl nitron (PBN) XXXV, 5,5-dimethyl-1-pyrrolidine-N-oxide (DMPO) XXXVI, nitrosobenzene (NOB) XXXVII, nitrosodurene (ND) XXXVIII and 2-methyl-2-nitrosopropane (MNP) XXXIX, see Figure 24. The spin trapping of organic radicals has been intensively studied and extended tables with parameters for different spin adducts exist.^[136,138,139] Even inorganic radicals can be trapped for some fragments that are isolobal to organic radicals and are expected to behave accordingly, trapping a metal centered radical in a spin adduct.^[137,140–143] EPR spectra

derived from a purely organic radical and a manganese centered radical trapped with nitrosodurene **XXXVIII** are shown in Figure 25.

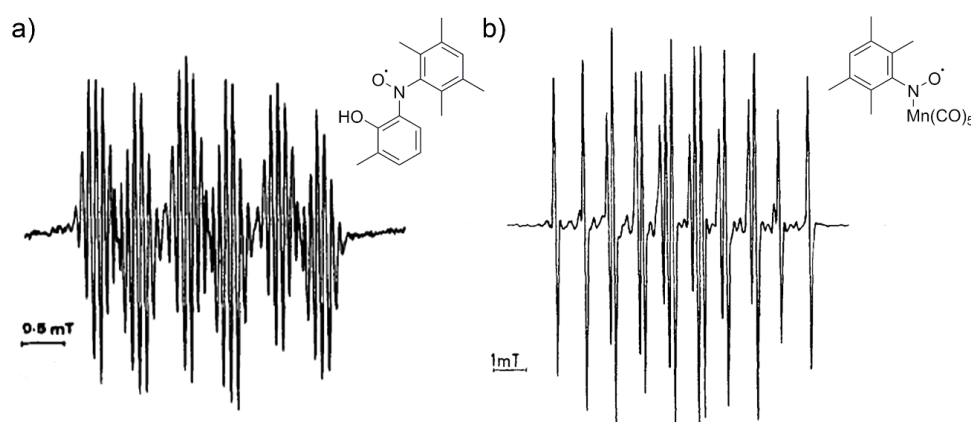


Figure 25. Examples of a) an organic^{[139]5} and b) a manganese^{[140]6} centered radical trapped with nitrosodurene.

1.4 Ferrocene-Containing (Pro-)Drugs

The exploration of ferrocene containing drugs started as early as 1978, when Brynes and coworkers found, that ferrocenyl polyamines exhibit a low but significant antitumor activity against lymphocytic leukemia P-388.^[144] Since then the medicinal applications for ferrocenyl derivatives have become a widespread research field.^[145]

In 2000 a fluconazole **XL** analogue bearing a ferrocenyl moiety **XLI** with antifungal activity has been reported by Biot *et al.*, see Figure 26. It showed remarkable growth inhibition for some strains of yeasts of the genus *Candida*. Antibacterial activity was reported for ferrocenyl-thiazoleacylhydrazones **XLII** against *Staphylococcus aureus*, *Escherichia coli* and *Pseudomonas aeruginosa*.^[146] Even studies for ferrocenyl containing vasorelaxants for the treatment of hypertension showed promising results.^[147] The

⁵ EPR spectrum adapted from L. Omelka, J. Kováčová, *Magn. Reson. Chem.* **1994**, 32, 525–531 with permission of John Wiley and Sons. Copyright © 1994 John Wiley and Sons.

⁶ EPR spectrum adapted from A. Hudson, M. F. Lappert, P. W. Lednor und B. K. Nicholson, *J. Chem. Soc., Chem. Commun.*, **1974**, 966 with permission of the Royal Society of Chemistry. Copyright © 1969, Royal Society of Chemistry

ferrocenyl-pyrido[2,3-d]pyrimidines **XLIII** studied were even more effective than the control drug rolipram **XLIV**. Recently a Ferrocenylquinoline **XLV** was tested as potential agent against leishmanial disease, which is a major problem in developing countries.^[61]

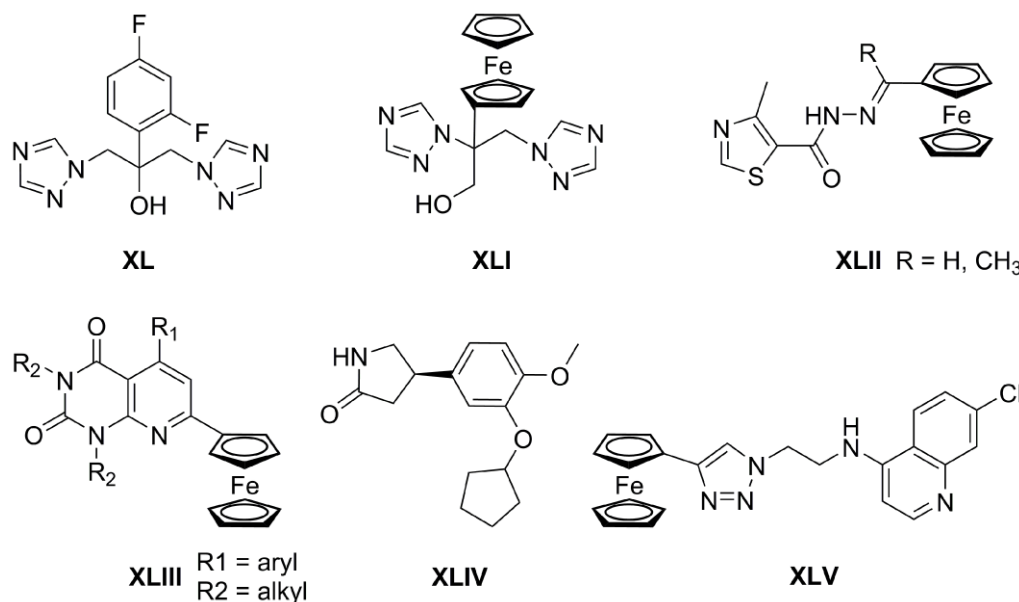


Figure 26. Fluconazole XL, ferrocenyl-fluconazole analogue XLI, ferrocenyl-thiazoleacylhydrazones XLII, ferrocenyl-pyrido[2,3-d]pyrimidines XLIII, rolipram XLIV and ferrocenylquinoline XLV.

One of the most exciting research centers around ferroquine **XLVII**, a structural analogue of chloroquine **XLVI** and potent antimalarial drug, see Figure 27. The research on incorporation of ferrocenyl moieties into antimalarial drugs began in the mid 1990s^[148], but it took until 2006 for the development of ferroquine **XLVII**. This compound shows greater antimalarial activity than its parent analogue chloroquine **XLVI** and even targets chloroquine resistant malarial strains.^[149] It was shown that the intramolecular hydrogen bond of ferroquine **XLVII**, which is absent in chloroquine **XLVI** has a significant effect on the biological activity, most probably due to the fact that it helps to maintain the conformation of the molecule and allows better interaction with the receptor.^[150] The mechanism of action of ferroquine **XLVII** is proposed to be a dual one. On the one hand it targets the hemozoin formation, a crystalline form of β -hematin, in which the cytotoxic α -hematin is converted and therefore rendered harmless.^[151] On the other hand it is able to form reactive oxygen species (ROS) upon oxidation. This causes lipid peroxidation,

eventually leading to death of the malarial parasites.^[152] Most recently ferroquine **XLII** has entered phase 2 of clinical research and shows promising results as a standalone drug and even in combination with other antimalarial drugs.^[153]

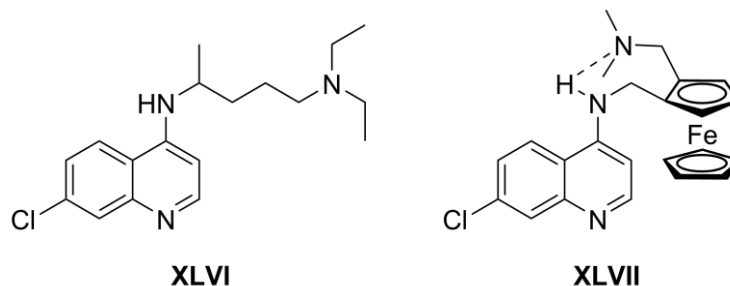


Figure 27. Chloroquine XLVI and ferroquine XLVII.

The generation of ROS was also proposed as the mechanism of action for the antitumor activity of ferrocenium derivatives as was disclosed more than 20 years after the first report of anticancer activity for this derivatives.^[154] This thesis was proven to be highly probable by studies, where the oxidative damage to DNA in MCF-7, a type of breast cancer cells, was monitored, under the addition of different ferrocenium compounds. It was also possible to spin trap reactive oxygen species via the use of DEPMPO a derivative of DMPO bearing a diethylester phosphonic acid substituent (*vide supra*).^[155]

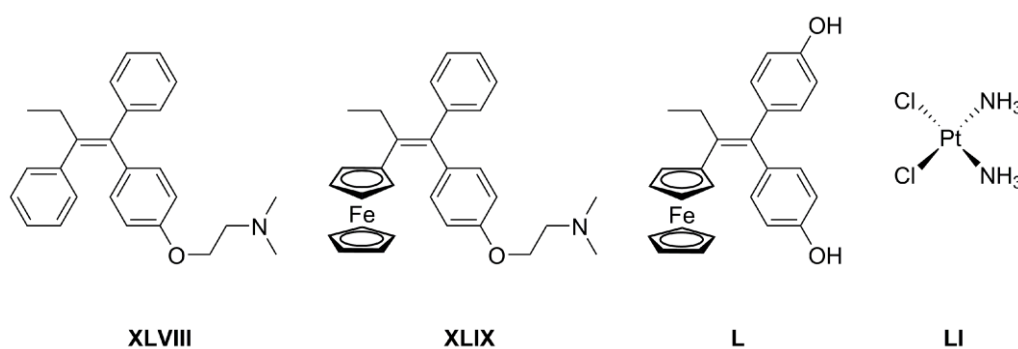


Figure 28. Antitumor agents.

The most promising ferrocene derivative in anticancer studies is ferrocifen **XLIX**, a derivative of tamoxifen **XLVIII**, which is widely used to treat ER-responsive breast cancer, see Figure 29.^[156] Tamoxifen **XLVIII** is a Selective Estrogen Receptor Modulator and therefore blocks this receptor. Without the estrogen stimulus the proliferation of the ER-

responsive breast cancer cells is inhibited. One major drawback of tamoxifen **XLVIII** is, that it is only effective against ER+ types of cancer cells, which excludes about 40% of breast cancer tumors from treatment. Ferrocifen **XLIX** on the other hand shows powerful anti-proliferative effects on both ER+ and ER- cancer cell lines.

Ferrocifen **XLIX** and a second derivative ferrociphenol **L** show even cytotoxic effects against various types of melanoma cells.^[157] These compounds even showed higher activity than *cis*-platin **LI** for mesothelioma cells.^[56] The research of ferrocifen has recently become more widespread. New derivatives bearing two aminoalkyl chains^[158] have been found to show strong antiproliferative effects on breast cancer cells. Other ferrocifen derivatives have found to induce senescence in cancer cells, an irreversible arrest in the cell-cycle prohibiting proliferation.^[159] Remarkably, it was found that the anticancer activity of ferrocifen is not attributed to the generation of reactive oxygen species (ROS), as reported for ferrocenium derivatives.^[157,160] The mode of action for this compounds is still yet to be disclosed.

Mokhir *et al.* synthesized a series of amino- and diaminoferrocene based prodrugs for the treatment of leukemia, see Figure 29. The Concept of the prodrugs **LII**, **LIII** and **LIV** is based on the cleavage of the B-C bond under oxidizing conditions, as found in cancer cells. A phenolate **LVI** is formed, which releases a *p*-quinone methide **LVII**, which can affect cancer cells, as well as an unstable ferrocenyl derivative **LVIII**, which quickly undergoes decarboxylation to the aminoferrocene derivative **LIX**. The aminoferrocene is either oxidized under the predominant condition and acts as ROS generator or decomposes by nucleophilic attack to Fe²⁺/Fe³⁺ ions, which can then generate ROS species leading to cell death, see Scheme 4.^[161] It was found, that for the most compounds the cytotoxicity correlates with the release of iron ions, except for the most active compound **LIIe**, which only generates ferrocenium ions. Therefore it was concluded, that ferrocenium ions are more cytotoxic, than mere iron ions, probably due to the retarded metabolism of such compounds. The diaminoferrocene based prodrugs **LIII** exhibited a slightly greater antitumor effect than the parent aminoferrocene compound **LII**. This is most likely attributed to the formation of a second *p*-quinone methide **LVII** rather than a direct effect of the substitution pattern of ferrocene.^[162]

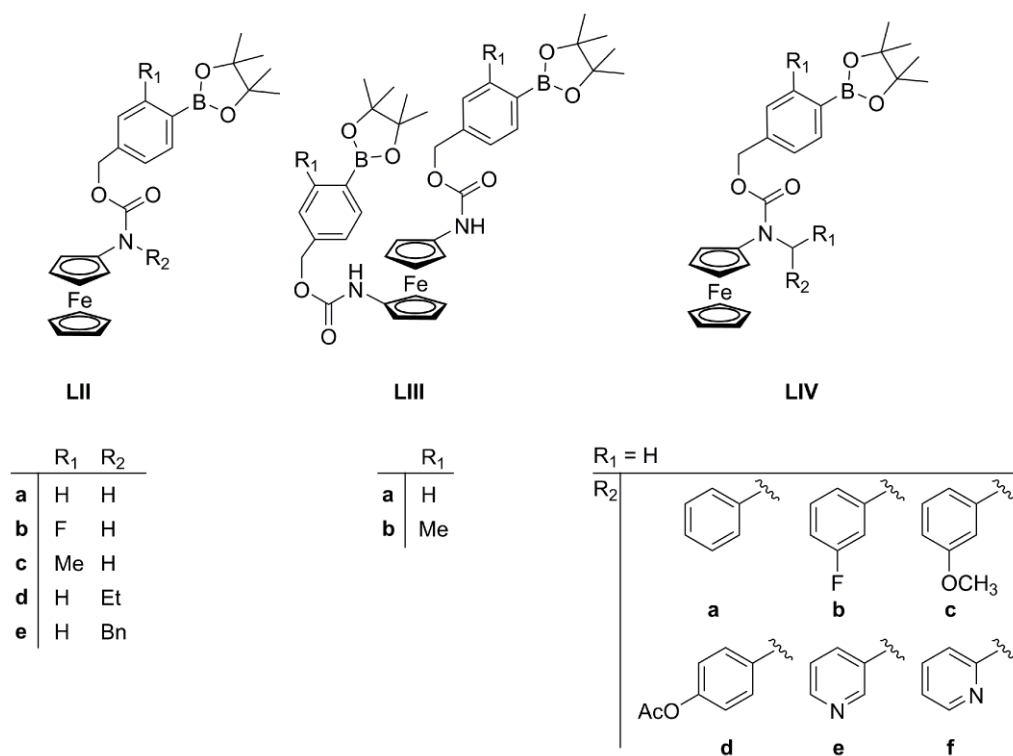
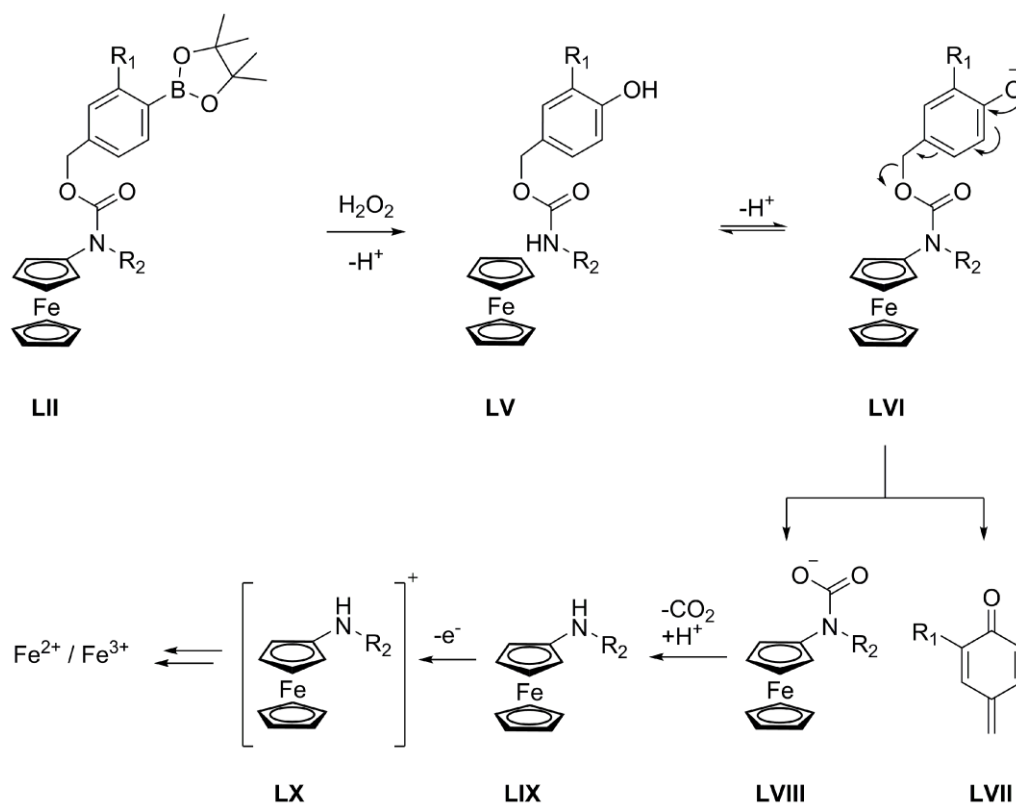


Figure 29. Amino- and Diamonoferrocene based Prodrugs.

A variation of the substituent at the amide nitrogen led to dramatic changes in activity. While compounds **LIVa** – **LIVd** exhibit a rather similar activity, **LIVe** and **LIVf** show decreased activity for at least one cell line type.^[163] This sort of compound does not only show high activity, but also high selectivity for cancer cells, as it was found that mononuclear cells are almost unaffected when treated with the prodrugs.^[161] Finally mice, which carry Leukemia, treated with **LIIe**, had a prolonged life span, even if the applied doses, were much lower than the determined safe maximum dose of the compounds.^[163]

From the facts reported above it is apparent, that ferrocenyl derivatives are valuable compounds for pharmaceutical applications. The potential of ferrocene as biologically active moiety has just started to be explored and might lead to novel drugs and prodrugs in the near future.



Scheme 4. Reaction mode for aminoferrocene based prodrugs LII.

1.5 References

- [1] Morgan, J. W.; Anders, E. *Proc. Natl. Acad. Sci. U.S.A.* **1980**, 77, 6973–6977.
- [2] *Metal stocks in society*; T. E. Graedel, Nairobi **2010**.
- [3] Perutz, M. F.; Rossmann, M. G.; Cullis, A. F.; Muirhead, H.; Will, G.; North, A. C. T. *Nature* **1960**, 185, 416–422.
- [4] Kendrew, J. C.; Dickerson, R. E.; Strandberg, B. E.; Hart, R. G.; Davies, D. R.; Phillips, D. C.; Shore, V. C. *Nature* **1960**, 185, 422–427.
- [5] Haines, D. C.; Tomchick, D. R.; Machius, M.; Peterson, J. A. *Biochemistry* **2001**, 40, 13456–13465.
- [6] Li, H.; Poulos, T. L. *Nat. Struct. Biol.* **1997**, 4, 140–146.
- [7] Li, H.; Poulos, T. L. *Curr. Top. Med. Chem.* **2004**, 4, 1789–1802.
- [8] Poulos, T. L.; Finzel, B. C.; Howard, A. J. *J. Mol. Biol.* **1987**, 195, 687–700.
- [9] Rowland, P.; Blaney, F. E.; Smyth, M. G.; Jones, Jo J.; Leydon, Vaughan R.; Oxbrow, Amanda K.; Lewis, Ceri J.; Tennant, Mike G.; Modi, Sandeep;

- Eggleston, Drake S.; Chenery, Richard J.; Bridges, Angela M. *J. Biol. Chem.* **2006**, 281, 7614–7622.
- [10] Schlichting, I.; Berendzen, J.; Chu, K.; Stock, A. M.; Maves, S. A.; Benson, D. E.; Sweet, R. M.; Ringe, D.; Petsko, G. A.; Sligar, S. G. *Science* **2000**, 287, 1615–1622.
- [11] Schoch, G. A.; Yano, J. K.; Wester, M. R.; Griffin, Keith J.; Stout, C. David; Johnson, Eric F. *J. Biol. Chem.* **2004**, 279, 9497–9503.
- [12] Scott, E. E.; White, M. A.; He, Y. A.; Johnson, Eric F.; Stout, C. David; Halpert, James R. *J. Biol. Chem.* **2004**, 279, 27294–27301.
- [13] Venkateswara Rao, P.; Holm, R. H. *Chem. Rev.* **2004**, 104, 527–559.
- [14] Beinert, H.; Holm, R. H.; Munck, E. *Science* **1997**, 277, 653–659.
- [15] Lawson, D. M.; Artymiuk, P. J.; Yewdall, S. J.; Smith, J. M.; Livingstone, J. C.; Treffry, A.; Luzzago, A.; Levi, S.; Arosio, P.; Cesareni, G. *Nature* **1991**, 349, 541–544.
- [16] Quintana, C.; Bonnet, N.; Jeantet, A. Y.; Chemelle, P. *Biology of the Cell* **1987**, 59, 247–254.
- [17] Schrock, R. R. *Acc. Chem. Res.* **2005**, 38, 955–962.
- [18] Schrock, R. R. *Angew. Chem.* **2008**, 120, 5594–5605.
- [19] Schrock, R. R. *Nat. Chem.* **2011**, 3, 95–96.
- [20] Weare, W. W.; Dai, X.; Byrnes, M. J.; Chin, Jia Min; Schrock, Richard R.; Muller, Peter *Proc. Natl. Acad. Sci. U.S.A.* **2006**, 103, 17099–17106.
- [21] Kliegman, S.; McNeill, K. *Dalton. Trans.* **2008**, 4191–4201.
- [22] MacKay, B. A.; Fryzuk, M. D. *Chem. Rev.* **2004**, 104, 385–401.
- [23] Leppin, J.; Forster, C.; Heinze, K. *Inorg. Chem.* **2014**, 53, 12416–12427.
- [24] Berg, J. M.; Holm, R. H. *J. Am. Chem. Soc.* **1985**, 107, 917–925.
- [25] Tsao, Y.-Y. P.; Fritchie, C. J.; Levy, H. A. *J. Am. Chem. Soc.* **1978**, 100, 4089–4095.
- [26] Wünsche von Leupoldt, A.; Förster, C.; Fiedler, T. J.; Bings, Nicolas H.; Heinze, Katja *Eur. J. Inorg. Chem.* **2013**, 2013, 6079–6090.
- [27] Visser, S. P. de; Quesne, M. G.; Martin, B.; Comba, Peter; Ryde, Ulf *Chem. Commun.* **2014**, 50, 262–282.
- [28] Marcus, R. A.; Sutin, N. *BBA-Bioenergetics* **1985**, 811, 265–322.

- [29] Closs, G. L.; Miller, J. R. *Science* **1988**, 240, 440–447.
- [30] Gray, H. B.; Winkler, J. R. *Annu Rev Biochem* **1996**, 65, 537–561.
- [31] Creutz, C.; Taube, H. *J. Am. Chem. Soc.* **1969**, 91, 3988–3989.
- [32] Neidlinger, A.; Ksenofontov, V.; Heinze, K. *Organometallics* **2013**, 32, 5955–5965.
- [33] Gagliardi, C. J.; Vannucci, A. K.; Concepcion, J. J.; Chen, Zuofeng; Meyer, Thomas J. *Energy Environ. Sci.* **2012**, 5, 7704.
- [34] Marcus, R. A. *J. Chem. Phys.* **1956**, 24, 966.
- [35] Marcus, R. A. *Discuss. Faraday Soc.* **1960**, 29, 21–31.
- [36] Marcus, R. A. *J. Chem. Phys.* **1965**, 43, 679.
- [37] Marcus, R. A. *Angew. Chem. Int. Ed. Engl.* **1993**, 32, 1111–1121.
- [38] Day, P.; Hush, N. S.; Clark, R. J. *Philos. Trans. A Math. Phys. Eng. Sci.* **2008**, 366, 5–14.
- [39] Hush, N. S. *Electrochim. Acta* **1968**, 13, 1005–1023.
- [40] Hush, N. S. *Coord. Chem. Rev.* **1985**, 64, 135–157.
- [41] Creutz, C.; Taube, H. *J. Am. Chem. Soc.* **1973**, 95, 1086–1094.
- [42] Cowan, D. O.; LeVanda, C.; Park, J.; Kaufman, Frank *Acc. Chem. Res.* **1973**, 6, 1–7.
- [43] Delgado-Pena, F.; Talham, D. R.; Cowan, D. O. *J. Organomet. Chem.* **1983**, 253, C43-C46.
- [44] Ribou, A.-C.; Launay, J.-P.; Sachtleben, M. L.; Li, Hu; Spangler, Charles W. *Inorg. Chem.* **1996**, 35, 3735–3740.
- [45] Mathur, P.; Singh, A. K.; Singh, V. K.; Singh, Priti; Rahul; Mobin, Shaikh M.; Thöne, Carsten *Organometallics* **2005**, 24, 4793–4798.
- [46] Lloveras, V.; Caballero, A.; Tárraga, A.; Velasco, M. Desamparados; Espinosa, Arturo; Wurst, Klaus; Evans, David J.; Vidal-Gancedo, José; Rovira, Concepció; Molina, Pedro; Veciana, Jaume *Eur. J. Inorg. Chem.* **2005**, 2005, 2436–2450.
- [47] Siebler, D.; Forster, C.; Heinze, K. *Dalton Trans.* **2011**, 40, 3558–3575.
- [48] Siebler, D., Dissertation, Johannes Gutenberg-University **2010**.
- [49] Heinze, K.; Siebler, D. *Z. Anorg. Allg. Chem.* **2007**, 633, 2223–2233.
- [50] Kealy, T. J.; Pauson, P. L. *Nature* **1951**, 168, 1039–1040.
- [51] Fischer, E. O.; Pfab, W. *Z. Naturforsch. B Chem. Sci.* **1952**, 7, 377–379.

- [52] Casado, C. M.; Cuadrado, I.; Moran, M.; Alonso, B.; Garcia, B.; Gonzalez, B.; Losada, J. *Coord. Chem. Rev.* **1999**, 185-6, 53–79.
- [53] Huo, J.; Wang, L.; Yu, H.; Deng, Libo; Ding, Jianhua; Tan, Qiaohua; Liu, Qingquan; Xiao, Anguo; Ren, Guoqing *J. Phys. Chem. B* **2008**, 112, 11490–11497.
- [54] V. Mittal „Polymer Brushes“, Auflage, *CRC Press* **2012**.
- [55] Plazuk, D.; Vessières, A.; Hillard, E. A.; Buriez, Olivier; Labbé, Eric; Pigeon, Pascal; Plamont, Marie-Aude; Amatore, Christian; Zakrzewski, Janusz; Jaouen, Gérard *J. Med. Chem.* **2009**, 52, 4964–4967.
- [56] Zanellato, I.; Heldt, J.-M.; Vessières, A.; Jaouen, Gérard; Osella, Domenico *Inorg. Chim. Acta* **2009**, 362, 4037–4042.
- [57] Biot, C.; Delhaes, L.; N'Diaye, C. M.; Maciejewski, L. A.; Camus, D.; Dive, D.; Brocard, J. S. *Bioorg. Med. Chem.* **1999**, 7, 2843–2847.
- [58] Biot, C.; Delhaes, L.; Abessolo, H.; Domarle, O.; Maciejewski, L.A; Mortuaire, M.; Delcourt, P.; Deloron, P.; Camus, D.; Dive, D.; Brocard, J.S *J. Organomet. Chem.* **1999**, 589, 59–65.
- [59] Biot, C.; Glorian, G.; Maciejewski, L. A.; Brocard, J. S. *J. Med. Chem.* **1997**, 40, 3715–3718.
- [60] Biot, C.; Nosten, F.; Fraisse, L.; Ter-Minassian, D.; Khalife, J.; Dive, D. *Parasite* **2011**, 18, 207–214.
- [61] Yousuf, M.; Mukherjee, D.; Pal, A.; Dey, Somaditya; Mandal, Supratim; Pal, Chiranjib; Adhikari, Susanta *ChemMedChem.* **2015**, 10, 546–554.
- [62] Chantson, J. T.; Verga Falzacappa, M. V.; Crovella, S.; Metzler-Nolte, Nils *ChemMedChem.* **2006**, 1, 1268–1274.
- [63] Lincke, T.; Behnken, S.; Ishida, K.; Roth, Martin; Hertweck, Christian *Angew. Chem.* **2010**, 122, 2055–2057.
- [64] Hayakawa, Y.; Sasaki, K.; Nagai, K.; Shin-ya, Kazuo; Furihata, Kazuo *J. Antibiot.* **2006**, 59, 6–10.
- [65] Ermler, U. *Science* **1997**, 278, 1457–1462.
- [66] Shima, S.; Krueger, M.; Weinert, T.; Demmer, Ulrike; Kahnt, Jorg; Thauer, Rudolf K.; Ermler, Ulrich *Nature* **2012**, 481, 98–101.

- [67] Abas, S. A.; Hossain, M. B.; van der Helm, D.; Schmitz, Francis J.; Laney, Maureen; Cabuslay, Ronnel; Schatzman, Randall C. *J. Org. Chem.* **1996**, 61, 2709–2712.
- [68] Pan, M.; Mabry, T. J.; Beale, J. M.; Mamiya, Blain M. *Phytochemistry* **1997**, 45, 517–519.
- [69] Lee, H.-J.; Choi, Y.-S.; Lee, K.-B.; Park, Jeunghee; Yoon, Chang-Ju *J. Phys. Chem. A* **2002**, 106, 7010–7017.
- [70] Banala, S.; Sussmuth, R. D. *Chembiochem.* **2010**, 11, 1335–1337.
- [71] Reiner, A.; Wildemann, D.; Fischer, G.; Kiefhaber, Thomas *J. Am. Chem. Soc.* **2008**, 130, 8079–8084.
- [72] Moser, C. C.; Keske, J. M.; Warncke, K.; Farid, R. S.; Dutton, P. L. *Nature* **1992**, 355, 796–802.
- [73] MacDiarmid, A. G. *Synth. Met.* **2001**, 125, 11–22.
- [74] Flores-Torres, S.; Hutchison, G. R.; Soltzberg, L. J.; Abruna, Hector D. *J. Am. Chem. Soc.* **2006**, 128, 1513–1522.
- [75] Capozzi, B.; Xia, J.; Adak, O.; Dell, Emma J.; Liu, Zhen-Fei; Taylor, Jeffrey C.; Neaton, Jeffrey B.; Campos, Luis M.; Venkataraman, Latha *Nat. Nanotechnol.* **2015**, 10, 522–527.
- [76] Hoffmann, N. *ChemSusChem* **2012**, 5, 352–371.
- [77] Yao, C.-J.; Zheng, R.-H.; Shi, Q.; Zhong, Yu-Wu; Yao, Jiannian *Chem. Commun.* **2012**, 48, 5680–5682.
- [78] Hu, K.; Robson, K. C.; Johansson, P. G.; Berlinguette, Curtis P.; Meyer, Gerald J. *J. Am. Chem. Soc.* **2012**, 134, 8352–8355.
- [79] Brunschwig, B. S.; Sutin, N. *Coord. Chem. Rev.* **1999**, 187, 233–254.
- [80] Klotz, I. M.; Czerlinski, G. H.; Fiess, H. A. *J. Am. Chem. Soc.* **1958**, 80, 2920–2923.
- [81] Cowan, D. O.; Kaufman, F. *J. Am. Chem. Soc.* **1970**, 92, 219–220.
- [82] Robin, M. B.; Day, P. *Adv. Inorg. Chem. Radiochem.*, 1968, 247–442.
- [83] Heckmann, A.; Lambert, C. *Angew. Chem. Int. Ed. Engl.* **2012**, 51, 326–392.
- [84] Siebler, D.; Linseis, M.; Gasi, T.; Carrella, Luca M.; Winter, Rainer F.; Förster, Christoph; Heinze, Katja *Chem. Eur. J.* **2011**, 17, 4540–4551.
- [85] Brunschwig, B. S.; Creutz, C.; Sutin, N. *Chem. Soc. Rev.* **2002**, 31, 168–184.

- [86] Winter, R. F. *Organometallics* **2014**, 33, 4517–4536.
- [87] Hildebrandt, A.; Lang, H. *Organometallics* **2013**, 32, 5640–5653.
- [88] Kraatz, H.-B.; Bediako-Amoa, I.; Gyepi-Garbrah, S. H.; Sutherland, Todd C. *J. Phys. Chem. B* **2004**, 108, 20164–20172.
- [89] Long, Y.-T.; Abu-Irhayem, E.; Kraatz, H.-B. *Chemistry* **2005**, 11, 5186–5194.
- [90] Kirin, S. I.; Kraatz, H.-B.; Metzler-Nolte, N. *Chem. Soc. Rev.* **2006**, 35, 348–354.
- [91] Herrick, R. S.; Jarret, R. M.; Curran, T. P.; Dragoli, Dean R.; Flaherty, Maryellen B.; Lindyberg, Susan E.; Slate, Rebecca A.; Thornton, Lisa C. *Tetrahedron Lett.* **1996**, 37, 5289–5292.
- [92] van Staveren, D. R.; Weyhermüller, T.; Metzler-Nolte, N. *Dalton Trans.* **2003**, 210.
- [93] Xu, Y.; Saweczko, P.; Kraatz, H.-B. *J. Organomet. Chem.* **2001**, 637-639, 335–342.
- [94] Kirin, S. I.; Wissenbach, D.; Metzler-Nolte, N. *New J. Chem.* **2005**, 29, 1168.
- [95] Nomoto, A.; Moriuchi, T.; Yamazaki, S.; Ogawa, Akiya; Hirao, Toshikazu *Chem. Commun.* **1998**, 1963–1964.
- [96] Moriuchi, T.; Nomoto, A.; Yoshida, K.; Ogawa, Akiya; Hirao, Toshikazu *J. Am. Chem. Soc.* **2001**, 123, 68–75.
- [97] Moriuchi, T.; Nomoto, A.; Yoshida, K.; Hirao, Toshikazu *J. Organomet. Chem.* **1999**, 589, 50–58.
- [98] Appoh, F. E.; Sutherland, T. C.; Kraatz, H.-B. *J. Organomet. Chem.* **2004**, 689, 4669–4677.
- [99] Hatten, X. d.; Weyhermüller, T.; Metzler-Nolte, N. *J. Organomet. Chem.* **2004**, 689, 4856–4867.
- [100] Adhikari, B.; Afrasiabi, R.; Kraatz, H.-B. *Organometallics* **2013**, 32, 5899–5905.
- [101] Chowdhury, S.; Mahmoud, K. A.; Schatte, G.; Kraatz, Heinz-Bernhard *Org. Biomol. Chem.* **2005**, 3, 3018–3023.
- [102] Djaković, S.; Siebler, D.; Semenčić, M. Č.; Heinze, Katja; Rapić, Vladimir *Organometallics* **2008**, 27, 1447–1453.
- [103] *Modeling of Molecular Properties*; P. Comba, Weinheim, Germany **2011**.
- [104] Semenčić, M. Č.; Siebler, D.; Heinze, K.; Rapić, Vladimir *Organometallics* **2009**, 28, 2028–2037.

- [105] Barisic, L.; Dropucic, M.; Rapić, V.; Pritzkow, Hans; Kirin, Srečko I.; Metzler-Nolte, Nils *Chem. Commun.* **2004**, 2004–2005.
- [106] Heinze, K.; Wild, U.; Beckmann, M. *Eur. J. Inorg. Chem.* **2007**, 2007, 617–623.
- [107] Semenčić, M. Č.; Heinze, K.; Förster, C.; Rapić, Vladimir *Eur. J. Inorg. Chem.* **2010**, 2010, 1089–1097.
- [108] Okamura, T.-a.; Sakauye, K.; Doi, M.; Yamamoto, Hitoshi; Ueyama, Norikazu; Nakamura, Akira *Bull. Chem. Soc. Jpn.* **2005**, 78, 1270–1278.
- [109] Heinze, K.; Schlenker, M. *Eur. J. Inorg. Chem.* **2004**, 2004, 2974–2988.
- [110] Alemán, C. *J. Phys. Chem. A* **2001**, 105, 6717–6723.
- [111] *Handbook of chemistry and physics on CD-ROM*; D. R. Lide, Boca Raton Fla. **2003**.
- [112] Wiberg, K. B.; Rush, D. J. *J. Org. Chem.* **2002**, 67, 826–830.
- [113] Wiberg, K. B.; Rush, D. J. *J. Am. Chem. Soc.* **2001**, 123, 2038–2046.
- [114] Lauvergnat, D.; Hiberty, P. C. *J. Am. Chem. Soc.* **1997**, 119, 9478–9482.
- [115] Wiberg, K. B.; Rablen, P. R. *J. Am. Chem. Soc.* **1995**, 117, 2201–2209.
- [116] Galabov, B.; Ilieva, S.; Hadjieva, B.; Dinchova, Eli *J. Phys. Chem. A* **2003**, 107, 5854–5861.
- [117] Deetz, M. J.; Fahey, J. E.; Smith, B. D. *J. Phys. Org. Chem.* **2001**, 14, 463–467.
- [118] Rao, C. N.; Rao, K. G.; Goel, A.; Balasubramanian, D. *J. Chem. Soc. A* **1971**, 3077–3083.
- [119] Wiberg, K. B.; Rablen, P. R.; Rush, D. J.; Keith, T. A. *J. Am. Chem. Soc.* **1995**, 117, 4261–4270.
- [120] Artis, D. R.; Lipton, M. A. *J. Am. Chem. Soc.* **1998**, 120, 12200–12206.
- [121] Miwa, J. H.; Pallivathucal, L.; Gowda, S.; Lee, Katherine E. *Org. Lett.* **2002**, 4, 4655–4657.
- [122] Petersson, E. J.; Goldberg, J. M.; Wissner, R. F. *Phys. Chem. Chem. Phys.* **2014**, 16, 6827–6837.
- [123] McFarland, B. J.; Katz, J. F.; Sant, A. J.; Beeson, Craig *J. Mol. Biol.* **2005**, 350, 170–183.
- [124] Behling, L. A.; Hartsel, S. C.; Lewis, D. E.; DiSpirito, Alan A.; Choi, Dong W.; Masterson, Larry R.; Veglia, Gianluigi; Gallagher, Warren H. *J. Am. Chem. Soc.* **2008**, 130, 12604–12605.

- [125] Wildemann, D.; Schiene-Fischer, C.; Aumuller, T.; Bachmann, Annett; Kiefhaber, Thomas; Lucke, Christian; Fischer, Gunter *J. Am. Chem. Soc.* **2007**, 129, 4910–4918.
- [126] Lincke, T.; Behnken, S.; Ishida, K.; Roth, Martin; Hertweck, Christian *Angew. Chem. Int. Ed. Engl.* **2010**, 49, 2011–2013.
- [127] Nonoyama, M.; Hamamura, K. *J. Organomet. Chem.* **1991**, 407, 271–277.
- [128] Hamamura, K.; Kita, M.; Nonoyama, M.; Fujita, Junnosuke *J. Organomet. Chem.* **1993**, 463, 169–177.
- [129] Fernandes, T. A.; Solarova, H.; Cisarova, I.; Uhlik, Filip; Sticha, Martin; Stepnicka, Petr *Dalton. Trans.* **2015**, 44, 3092–3108.
- [130] Damian Plazuk; Janusz Zakrzewski; Agnieszka Rybarczyk-Pirek; Slawomir Domagala *J. Organomet. Chem.* **2005**, 690, 4302–4308.
- [131] van Staveren, D. R.; Metzler-Nolte, N. *Chem. Rev.* **2004**, 104, 5931–5985.
- [132] Forrow, N. J.; Foulds, N. C.; Frew, J. E.; Law, John T. *Bioconjug. Chem.* **2004**, 15, 137–144.
- [133] Marco-Contelles, J.; León, R.; Morales, E.; Villarroya, Mercedes; García, Antonio G. *Tetrahedron Lett.* **2004**, 45, 5203–5205.
- [134] Beer, P. D.; Graydon, A. R.; Johnson, A. O.; Smith, David K. *Inorg. Chem.* **1997**, 36, 2112–2118.
- [135] Patra, M.; Hess, J.; Konatschnig, S.; Spingler, Bernhard; Gasser, Gilles *Organometallics* **2013**, 32, 6098–6105.
- [136] Buettner, G. R. *Free Radical Biol. Med.* **1987**, 3, 259–303.
- [137] Rehorek, D.; Hennig, H.; Dubose, C. M.; Kemp, Terence J.; Janzen, Edward G. *Free Radical Res.* **2009**, 10, 75–84.
- [138] Klauschenz, E.; Haseloff, R. F.; Volodarskii, L. B.; Blasig, Ingolf E. *Free Radical Res.* **2009**, 20, 103–111.
- [139] Omelka, L.; Kováčová, J. *Magn. Reson. Chem.* **1994**, 32, 525–531.
- [140] Hudson, A.; Lappert, M. F.; Lednor, P. W.; Nicholson, Brian K. *J. Chem. Soc., Chem. Commun.* **1974**, 966.
- [141] Huffadine, A. S.; Peake, B. M.; Robinson, B. H.; Simpson, Jim; Dawson, Pete A. *J. Organomet. Chem.* **1976**, 121, 391–403.
- [142] Benner, L. S.; Balch, A. L. *J. Organomet. Chem.* **1977**, 134, 121–130.

- [143] Hudson, A.; Lappert, M. F.; Nicholson, B. K. *J. Chem. Soc., Dalton Trans.* **1977**, 551.
- [144] Fiorina, V. J.; Dubois, R. J.; Brynes, S. *J. Med. Chem.* **1978**, 21, 393–395.
- [145] Ornelas, C. *New J. Chem.* **2011**, 35, 1973.
- [146] Zhang, J. *Appl. Organometal. Chem.* **2008**, 22, 6–11.
- [147] Arellano, I.; Rodríguez-Ramos, F.; González-Andrade, M.; Navarrete, Andrés; Sharma, Manju; Rosas, Noé; Sharma, Pankaj *J. Heterocyclic Chem.* **2016**, 53, 1147–1154.
- [148] Wani, W. A.; Jameel, E.; Baig, U.; Mumtazuddin, Syed; Hun, Lee Ting *Eur. J. Med. Chem.* **2015**, 101, 534–551.
- [149] Biot, C.; Daher, W.; Ndiaye, C. M.; Melnyk, Patricia; Pradines, Bruno; Chavain, Natascha; Pellet, Alain; Fraisse, Laurent; Pelinski, Lydie; Jarry, Christian; Brocard, Jacques; Khalife, Jamal; Forfar-Bares, Isabelle; Dive, Daniel *J. Med. Chem.* **2006**, 49, 4707–4714.
- [150] Biot, C.; Chavain, N.; Dubar, F.; Pradines, Bruno; Trivelli, Xavier; Brocard, Jacques; Forfar, Isabelle; Dive, Daniel *J. Organomet. Chem.* **2009**, 694, 845–854.
- [151] Pisciotta, J. M.; Sullivan, D. *Parasitol. Int.* **2008**, 57, 89–96.
- [152] Chavain, N.; Vezin, H.; Dive, D.; Touati, Nadia; Paul, Jean-Francois; Buisine, Eric; Biot, Christophe *Mol. Pharm.* **2008**, 5, 710–716.
- [153] Held, J.; Supan, C.; Salazar, C. L.; Tinto, Halidou; Bonkian, Léa N.; Nahum, Alain; Moulero, Bancole; Sié, Ali; Coulibaly, Boubacar; Sirima, Sodiomon B.; Siribie, Mohamadou; Otsyula, Nekoye; Otieno, Lucas; Abdallah, Ahmed M.; Kimutai, Robert; Bouyou-Akotet, Marielle; Kombila, Maryvonne; Koiwai, Kimiko; Cantalloube, Cathy; Din-Bell, Chantal; Djeriou, Elhadj; Waitumbi, John; Mordmüller, Benjamin; Ter-Minassian, Daniel; Lell, Bertrand; Kremsner, Peter G. *Lancet Infect. Dis.* **2015**, 15, 1409–1419.
- [154] Osella, D.; Ferrali, M.; Zanello, P.; Laschi, Franco; Fontani, Marco; Nervi, Carlo; Cavigliolo, Giorgio *Inorg. Chim. Acta* **2000**, 306, 42–48.
- [155] Tabbi, G.; Cassino, C.; Cavigliolo, G.; Colangelo, Donato; Ghiglia, Annalisa; Viano, Ilario; Osella, Domenico *J. Med. Chem.* **2002**, 45, 5786–5796.
- [156] Jaouen, G.; Top, S.; Vessières, A.; Leclercq, G.; McGlinchey, Michael J. *Curr. Med. Chem.* **2004**, 11, 2505–2517.

- [157] Michard, Q.; Jaouen, G.; Vessieres, A.; Bernard, B. A. *J. Inorg. Biochem.* **2008**, 102, 1980–1985.
- [158] Pigeon, P.; Top, S.; Vessières, A.; Huché, Michel; Görmen, Meral; El Arbi, Mehdi; Plamont, Marie-Aude; McGlinchey, Michael J.; Jaouen, Gérard *New J. Chem.* **2011**, 35, 2212.
- [159] Bruyère, C.; Mathieu, V.; Vessières, A.; Pigeon, Pascal; Top, Siden; Jaouen, Gérard; Kiss, Robert *J. Inorg. Biochem.* **2014**, 141, 144–151.
- [160] Osella, D.; Mahboobi, H.; Colangelo, D.; Cavigiolo, Giorgio; Vessières, Anne; Jaouen, Gerard *Inorg. Chim. Acta* **2005**, 358, 1993–1998.
- [161] Hagen, H.; Marzenell, P.; Jentsch, E.; Wenz, Frederik; Veldwijk, Marlon R.; Mokhir, Andriy *J. Med. Chem.* **2012**, 55, 924–934.
- [162] Marzenell, P.; Hagen, H.; Sellner, L.; Zenz, Thorsten; Grinyte, Ruta; Pavlov, Valeri; Daum, Steffen; Mokhir, Andriy *J. Med. Chem.* **2013**, 56, 6935–6944.
- [163] Daum, S.; Chekhun, V. F.; Todor, I. N.; Lukianova, Natalia Yu; Shvets, Yulia V.; Sellner, Leopold; Putzker, Kerstin; Lewis, Joe; Zenz, Thorsten; de Graaf, Inge A M; Groothuis, Geny M M; Casini, Angela; Zozulia, Oleksii; Hampel, Frank; Mokhir, Andriy *J. Med. Chem.* **2015**, 58, 2015–2024.

2 Aim of Work

The first part of this work focuses on *N*-ferrocenyl substituted thioamides in comparison to their parent carboxamide compounds to understand the effect of the oxygen to sulfur exchange in respect to the use of thioamides as isosteric replacements for carboxamides and asymmetric bridging units for redox centers in general. The facile synthesis of *N*-ferrocenyl substituted thioamides by means of oxygen to sulfur exchange by the use of Lawesson's reagent (2,4-bis-(4-methoxyphenyl)-1,3,2,4-dithiadiphosphetane-2,4-disulfide) is chosen to benefit from the well-established chemistry of carboxamide bridged ferrocenes to vary substitution patterns and redox potentials. The influence of the oxygen to sulfur exchange on the *E/Z* or respectively *cis/trans* conformation of the synthesized mono- and dinuclear thioamides and their secondary structure is elucidated by NMR spectroscopy in order to determine the rotational barriers and favored structural motifs of this kind of compounds. A comparison to DFT calculations for this systems is used to validate the results and vice versa validate the DFT methods applied for future investigations. Oxidation of the dinuclear compounds to the mixed-valent species and probing by UV/Vis/NIR, EPR and NMR spectroscopy as well as electrochemical methods allows to determine the site of oxidation and the electronic coupling. This promises new insights into electron transfer reactions via asymmetrically bridged e.g. facilitated or hindered electron transfer compared to parent carboxamides.

The second part of this work centers on the ability of ferrocenium compounds to generate radicals under alkaline, non-nucleophilic conditions. These ferrocenyl radicals can be envisaged to play a major role in the mode of action for ferrocenyl containing drugs and prodrugs like ferrocifen by Jaouen et al., ferroquine by Biot et al. and the aminoferrocene based prodrugs by Mokhir et al.. These short lived radicals are investigated by means of spin-trapping technique for EPR spectroscopy providing insight in the localization of the unpaired electron. Quantitative EPR measurements are performed to elucidate the reactivity of the radicals.

The last part explores a specific reactivity of *N*-ferrocenylthioamide under oxidizing and alkaline conditions, leading to EPR signals that cannot be explained by mere oxidation and deprotonation of the compounds. This study gives insight into the process of formation of

this open shell intermediates, as well as the follow up reactions under elimination of hydrogensulfide. Influences of ligand properties of the thioamide unit are disclosed as well. The complex mechanism proposed is supported by NMR spectroscopy, mass spectrometry, single crystal X-Ray diffraction and interpreted with the aid of DFT calculations. These study is valuable with respect to of synthesis of novel ferrocenyl containing polymers as well as ferrocenyl containing (pro)drugs.

3 Results and Discussion

In this chapter the results are presented in the form of two publications and a submitted manuscript.

The first section contains the publication “Impact of O→S Exchange in Ferrocenyl Amides on Structure and Redoxchemistry”. The single crystal X-Ray diffraction analysis reported were done by Christoph Förster. The publication, which was published in *Organometallics*, was written by Torben Kienz (50%) and Katja Heinze (50%). All synthetic work and analytical investigations, as well as DFT calculations were performed by Torben Kienz. An easy route to *N*-ferrocenyl substituted thioamides using Lawesson’s reagent is reported. The synthesized mono- and dinuclear ferrocene compounds are analyzed by means of IR-, NMR-, EPR-, UV/Vis/NIR-spectroscopy and mass spectrometry. The rotational barrier of *N*-ferrocenyl substituted thioamides is disclosed. The dinuclear complexes exhibit hydrogen bonding leading to a distinct secondary structure. Upon oxidation the dinuclear compounds are mixed-valent species of Robin-Day class II with an electron coupling parameter $H_{AB} = 190$ and 230 cm^{-1} .

In the second section, the publication “Spin Trapping of Carbon-Centered Ferrocenyl Radicals with Nitrosobenzene” is presented. EPR spectra of the compounds were performed by Andreas Neidlinger, except for the thioamide containing starting material, which was performed by Torben Kienz. The simulation of EPR spectra was done by both authors: Andreas Neidlinger (40 %) and Torben Kienz (60%). Electrochemical measurements were performed by Andreas Neidlinger. DFT calculations of the thioamide containing products were performed by Torben Kienz, while the remaining calculations were performed by Andreas Neidlinger. The publication, which was published in *Organometallics*, was written by Andreas Neidlinger (40 %), Torben Kienz (40%), and Katja Heinze (20 %). The generation of highly reactive carbon centered ferrocenyl radicals is reported. These radicals may provide an additional mode of action for ferrocenyl containing (pro-)drugs.

The last section consists of the manuscript “Generation and Oligomerization of *N*-ferrocenyl Ketenimines via Open-shell Intermediates”. The single crystal X-Ray diffraction analysis reported were done by Christoph Förster. The preparative work and analyses, as well as DFT calculations were performed by Torben Kienz. The manuscript was written by Torben Kienz (60%) and Katja Heinze (40 %) and submitted to *Organometallics*. A specific reaction of *N*-ferrocenyl thioamide is reported. The mechanistical investigation reveals, that upon oxidation and deprotonation reactive open shell intermediates are generated, which eliminate hydrogen sulfide, generating a *N*-ferrocenyl ketenimine and initiating an oligomerization reaction. Furthermore the influence of the ligand properties of thioamide containing ferrocene derivatives is disclosed. To complete the work DFT calculations for the reactive open shell intermediates of the novel *N*-ferrocenyl ketenimine were performed.

Contents

3.1 Impact of O→S Exchange in Ferrocenyl Amides on Structure and Redoxchemistry

Torben Kienz, Christoph Förster and Katja Heinze

Published in: *Organometallics* **2014**, *33*, 4803–4812.

[DOI: 10.1021/om500052k]

<http://pubs.acs.org/doi/abs/10.1021/om500052k>

“Adapted with permission from T. Kienz, C. Förster, K. Heinze,
Organometallics **2014**, *33*, 4803–4812.

Copyright 2014 American Chemical Society.”

3.2 Spin Trapping of Carbon-Centered Ferrocenyl Radicals with Nitrosobenzene

Andreas Neidlinger, Torben Kienz, Katja Heinze

Published in: *Organometallics* **2015**, *34*, 5310–5320.

[DOI: 10.1021/acs.organomet.5b00778]

<http://pubs.acs.org/doi/10.1021/acs.organomet.5b00778>

“This is an unofficial adaptation of an article that appeared in an ACS publication.
ACS has not endorsed the content of this adaptation or the context of its use.

Copyright 2015 American Chemical Society.”

3.3 Generation and Oligomerization of N-Ferrocenyl Ketenimines via Open-shell Intermediates

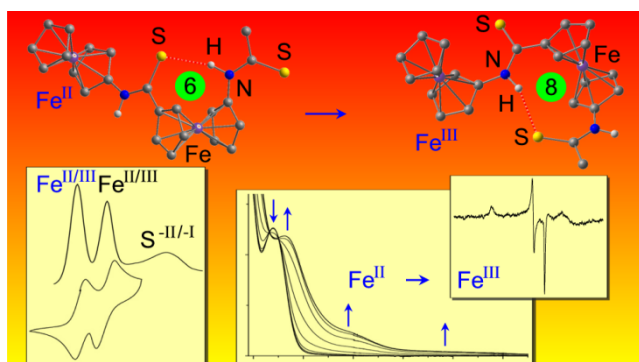
Torben Kienz, Christoph Förster, Katja Heinze

Submitted to: *Organometallics*

3.1 Impact of O→S Exchange in Ferrocenyl Amides on Structure and Redoxchemistry

Torben Kienz, Christoph Förster, and Katja Heinze

Organometallics **2014**, 33, 4803–4812.



Supporting information for this article (without Cartesian coordinates from DFT calculations) is found at pp. 155. For full supporting information refer to:

<http://pubs.acs.org/doi/suppl/10.1021/om500052k>

Adapted with permission from T. Kienz, C. Förster, K. Heinze,
Organometallics **2014**, 33, 4803-4812.
Copyright 2014 American Chemical Society.

3.1.1 Abstract

The conformations and redox chemistry of ferrocenyl amides have been investigated in considerable depth in the last few years, while ferrocenyl thioamides have attracted less interest so far, although distinctly different conformations and reactivity patterns are expected. Monoferrocenyl amides Fc-NHC(O)CH₃ (**1**) and 1,1'-CH₃O(O)C-Fn-NHC(O)CH₃ (**2**) and diferrocenyl amides Fc-NHC(O)-Fc (**5**) and Fc-NHC(O)-Fn-NHC(O)CH₃ (**6**) are easily transformed into the corresponding thioamides (**3**, **4**, **7**, **8**) by treatment with Lawesson's reagent (2,4-bis(*p*-methoxyphenyl)-1,3-dithiaphosphetane-2,4-disulfide) (Fc = Fe(C₅H₄)(C₅H₅), Fn = Fe(C₅H₄)₂). The thioamide conformations (*cis/trans*) in **3**, **4**, **7**, and **8** and the hydrogen bond determined secondary structure of dithioamide **8** are elucidated by IR and NMR spectroscopy as well as by DFT calculations (B3LYP, LANL2DZ, PCM CH₂Cl₂) and contrasted with the corresponding amides **1**, **2**, **5**, and **6**. The electronic communication via the thioamide bridge in **7**⁺ and **8**⁺ in comparison to the interaction in the parent mixed-valent amides **5**⁺ and **6**⁺ has been probed by cyclic voltammetry, square wave voltammetry, UV/Vis spectroelectrochemistry, EPR spectroscopy, and paramagnetic NMR spectroscopy. Additional chemical reactivity of the thioamide unit has been detected by electrochemical analysis.

3.1.2 Introduction

Although oxygen-to-sulfur isosteric substitutions have been successfully employed in organic peptide and protein chemistry, it is generally accepted that organic thioamides $R-C(S)NH-R'$ differ considerably from their oxo counterparts $R-C(O)NH-R'$ and the concept of true isosteric replacement might be too simplified. Thioamides are more acidic than amides: e.g. $pK_a(X=S) = 14.7$ and $pK_a(X = O) = 21.5$ for $Me-C(X)NH-Ph$.¹ In line with this higher acidity thioamides are better hydrogen atom donors than amides in $NH\cdots X$ hydrogen bonds.² On the other hand, due to the reduced electronegativity of sulfur vs. oxygen, thioamides are weaker hydrogen acceptors in $XH\cdots S$ hydrogen bonds.² The better hydrogen atom donor capability of thioamides has been exploited by Beer et al. in ferrocenyl thioamide anion receptors (Chart 1, **A**, $R = nBu$).³ The macrocyclic derivative **B**

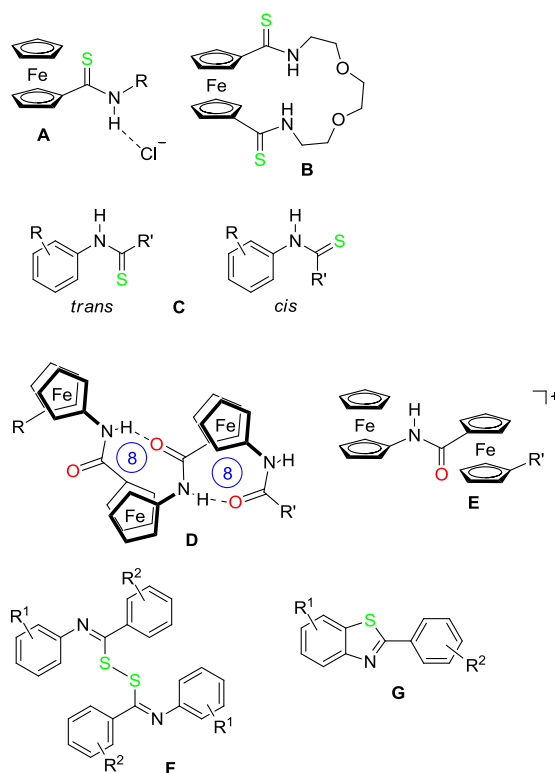


Chart 1. Ferrocenyl thioamides as anion (A) or cation receptors (B), *cis/trans* isomerism in *N*-aryl Thioamides (C), secondary structure of oligoferrocenyl oligopeptides (D), and mixed-valent oligoferrocenyl amides (E), disulfides (F), and benzothiazoles (G) derived from thioamides.

had been tested by Hall et al. as receptor for hard metal cations such as Ca^{2+} or Dy^{3+} . Not too unexpectedly, these metal cations do not bind to **B**.⁴ On the other hand, nature seems to employ thio amino acids for binding of the softer metal cation Cu^+ .⁵ Thioamides are more stable towards hydrolysis by natural enzymes: e.g. by the Zn^{2+} containing enzyme carboxypeptidase A. Replacing the hard Zn^{2+} ion in the enzyme's active site by the softer Cd^{2+} yields an active enzyme capable of cleaving thioamides.⁶ Furthermore, a fine tuning of the secondary and tertiary structure of enzymes can be achieved by replacing amides with thioamides.⁷

All ferrocene-containing thioamides such as **A** (Fc-C(S)NHR) and dithioamides such as **B** ($1,1'\text{-Fc}(\text{C(S)NHR})_2$) reported to date are formally derived from ferrocenecarboxylic acid or 1,1'-ferrocenedicarboxylic acid.^{3,4,8} To the best of our knowledge, R-C(S)NH-Fc thioamides derived from aminoferrocenes have not yet been reported. Interestingly, organic *N*-aryl substituted thioamides **C** are typically obtained as mixtures of *cis* and *trans* isomers (Chart 1) while *N*-alkyl thioamides are exclusively formed as *trans* isomers similarly to amides.⁹ The thioamide conformation of *N*-ferrocenyl thioamides remains to be elucidated.

Oligoferrocenyl complexes with amide bridges (Chart 1, **D**) have been shown to form distinct secondary structures with intramolecular hydrogen bonds characterized by eight-membered rings.¹⁰ Mixed-valence cations of such oligoferrocenyl amides **E** feature intervalence charge transfer bands around $\lambda_{\text{IVCT}} = 1030 - 1055 \text{ nm}$ with electronic couplings $H_{\text{AB}} = 140 - 190 \text{ cm}^{-1}$, placing these mixed-valent species **E** in the Robin-Day class II¹¹ with moderate electronic interaction.¹⁰ Hence, these oligoamides are molecular wires equipped with a distinct secondary structure. As multiple positive charges are opponents to the intramolecular hydrogen bonds, full oxidation should disrupt the hydrogen bonds, giving an extended conformation¹⁰ and rendering these amide-based foldamers responsive to redox stimuli.

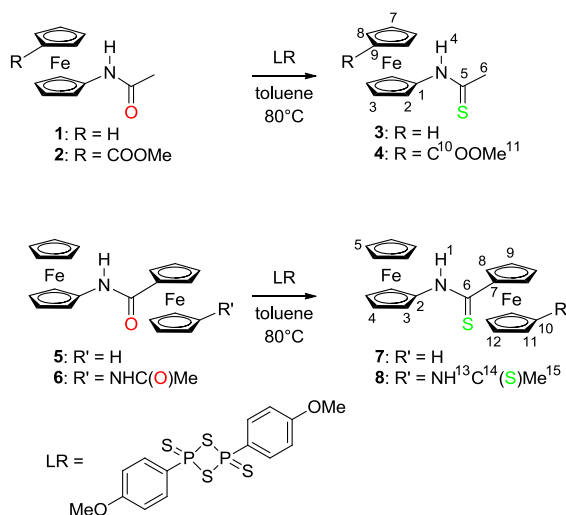
With the special features of thioamides in mind, we were interested in the effects of the $\text{O} \rightarrow \text{S}$ substitution in *N*-ferrocenyl (thio)amides with respect to (thio)amide conformation (*cis/trans* isomers?), secondary structure (occurrence of intramolecular hydrogen bonds?), electronic communication in mixed-valent systems (facilitated or hampered electron transfer?), and redox stability of the ferrocenyl thioamide unit. In the last case especially the oxidation/deprotonation of the thioamide to the corresponding disulfide $\text{RC}(\text{NR}')\text{-S-S-(NR}')\text{CR}$ (Chart 1, **F**)¹² or benzothiazole **G** (Chart 1)^{12a} is of particular interest, as this

reactivity is obviously impossible for the parent amides. The diferrocenoyl disulfide Fc-C(O)-S-S-C(O)-Fc has been reported previously.¹³

3.1.3 Results and Discussion

Synthesis and Characterization.

The mono- and diferrocenyl thioamides **3**, **4**, **7**, and **8** shown in Scheme 1 were conveniently prepared by thionation of the corresponding amides **1**, **2**, **5**, and **6**^{10,14} with Lawesson's reagent (2,4-bis(*p*-methoxyphenyl)-1,3-dithiaphosphetane-2,4-disulfide).¹⁵ After column chromatography the products were obtained as orange (**3**, **4**) to red powders (**7**, **8**) in 40–90% isolated yield. All complexes were characterized by FD or ESI mass spectrometry, NMR spectroscopy, and elemental analyses proving the desired composition and purity.



Scheme 1. Synthesis of thioamides **3**, **4**, **7**, and **8** from the corresponding amides **1**, **2**, **5**, and **6** (atom numbering for NMR assignment).

In the UV/vis spectra of the thioamides **3**, **4**, **7**, and **8** the characteristic ferrocene absorption band in CH₂Cl₂ is consistently shifted to lower energy in comparison to that of the corresponding amides **1**, **2**, **5**, and **6** ($\lambda_{\max} = 441, 441, 445, 446 \text{ nm}^{10,14} \rightarrow \lambda_{\max} = 446, 444, 470, 480 \text{ nm}$). These shifts already indicate some electronic influence of the O \rightarrow S substitution and some admixed charge-transfer character of the Fc band (see Supporting Information, Figures S1 – S4).

The IR spectra obtained as KBr disks show characteristic NH and CS(I) and CS(II) absorption bands. The CO band of the ester group in **4** at 1686 cm^{-1} confirms that the ester carbonyl oxygen atom is not exchanged by sulfur using Lawesson's reagent and furthermore that the CO_{ester} group acts as a hydrogen atom acceptor in the solid state. The NH stretching frequencies around $3230\text{--}3310\text{ cm}^{-1}$ are indicative of the presence of hydrogen bonds in the solid state. An analogous observation has also been made for the corresponding amides.^{10,14} **4** shows two absorptions for the NH group at 3462 (br) cm^{-1} and 3288 (m) cm^{-1} , suggesting free and hydrogen-bonded NH groups, respectively (NH \cdots O_{ester}). The dithioamide **8** features NH absorptions at 3375 and 3233 cm^{-1} corresponding to free NH groups and hydrogen-bonded (NH \cdots S) groups, respectively.

In CH₂Cl₂ solution the hydrogen bonds of **3** and **7** are essentially disrupted, as the NH stretching vibrations are observed around $3380\text{--}3400\text{ cm}^{-1}$. This clearly proves the intermolecular nature of the hydrogen bonds in **3** and **7** in the solid state. Ester **4** shows two NH absorption bands at 3379 and 3281 cm^{-1} in solution. The CO_{ester} vibration of **4** is shifted to 1713 cm^{-1} , indicative of essentially free CO groups, in addition to some hydrogen-bonded CO groups (shoulder at 1695 cm^{-1}). Hence, ester **4** features some (intramolecular) NH \cdots O_{ester} hydrogen bonds also in CH₂Cl₂ solution resulting in a six-membered ring (vide infra). Dithioamide **8** also shows the signatures of hydrogen-bonded and free NH groups at 3165 and 3384 cm^{-1} in solution, suggesting the presence of an intramolecular NH \cdots S hydrogen bond in addition to a free NH group. The diamides of 1,1'-disubstituted ferrocenes have been shown to possess intramolecular hydrogen bonds as well.^{10,14} The detailed conformations (*cis/trans*) and especially the intramolecular hydrogen bond of **8** will be disclosed in the next section by NMR and DFT methods.

Conformational Analysis.

N-Ferrocenyl thioamides **3** and **4** display a double set of resonances in their ¹H and ¹³C NMR spectra, indicative of the presence of *cis* and *trans* isomers which do not interconvert at room temperature on the NMR time scale (Figure 1, Experimental Section). This finding is congruent to reported organic *N*-aryl thioamides.⁹ From NOE spectra resonances are assigned to *cis* and *trans* isomers by the decisive contact of the methyl protons H⁶ to the thioamide proton NH⁴ in the *trans* isomer (see Supporting Information, Figure S5). In addition to significantly different chemical shifts of the methyl protons H⁶, the methyl

carbon atom C⁶, and the C=S carbon atom C⁵ the cyclopentadienyl H² resonances of *trans*-**3** and *trans*-**4** are shifted to lower field by 0.47 and 0.36 ppm in comparison to the respective *cis* counterparts, respectively, due to the vicinity of the sulfur atom to the H² proton in the *trans* isomers. Conversely, the NH⁴ resonance is shifted to lower field by 0.73 and 0.37 ppm, respectively, in the *cis* isomers as compared to the *trans* isomers due to the neighboring sulfur atom. The *cis:trans* ratio obtained by integration of corresponding proton resonances is approximately 1 : 1 for **3** and 1 : 2.7 for **4**. Heating a toluene solution of **3** to 110 °C allows observation of the coalescence of the methyl proton resonances H⁶ at around $T_c = 373$ K (Figure 2). From T_c and the chemical shifts of the CH₃ proton resonances (H⁶) an activation barrier of $\Delta G^\ddagger = 75$ kJ mol⁻¹ can hence be estimated for the *cis/trans* isomerization of **3**, similar to the barriers determined for *N,N'*-dimethylthioformamide and *N,N'*-dimethylthioacetamide.¹⁶

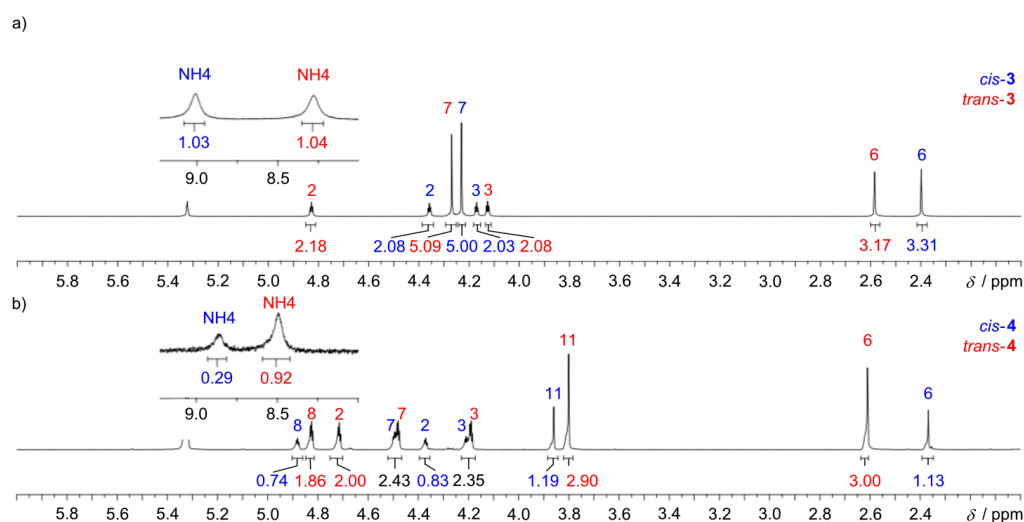


Figure 1. ¹H NMR spectra of (a) **3** and (b) **4** in CD₂Cl₂ at room temperature (atom numbering see Scheme 1).

DFT calculations (B3LYP, LANL2DZ, PCM CH₂Cl₂) yield somewhat higher activation barriers of 101 and 110 kJ mol⁻¹ for **3** and **4**, respectively (Figure 3). The calculations show a slight preference of the *trans* isomers, especially for **4** which matches the experimental results. *trans*-**4** might form an intramolecular NH⁺⋯O_{ester} hydrogen bond slightly more stable than that of *cis*-**4** (*trans*-**4**: NH⁺⋯O 1.94 Å; *cis*-**4**: NH⁺⋯O 2.00 Å). Such intramolecular

NH \cdots O hydrogen bonds giving a six-membered ring (Figure 3b) are likely present to some extent in the ensemble in solution, as already suggested by the IR data.

On the other hand, intermolecular hydrogen bonds as suggested by the solid-state IR spectra might stabilize the *cis* isomer. Indeed, thioamide **3** crystallizes in the monoclinic space group $P2_1/c$ as centrosymmetric hydrogen-bonded dimers of *cis* isomers (Figure 4). In contrast, its amide analogue **1** crystallizes with NH \cdots O hydrogen-bonded chains of *trans*-**1** in the solid state.^[14a,17] The N \cdots S distance in *cis*-**3** amounts to 3.39 Å. The *cis* thioamide unit is nearly planar but twisted relative to the Cp plane with a C¹⁰-C⁶-N¹-C¹¹ angle of 51°. This twist is also seen in the DFT calculation of *cis*-**3** (44°) and of the hydrogen bonded dimer (*cis*-**3**)₂ (39.0°, see Supporting Information, Figure S6).

In contrast to the case for *N*-ferrocenyl amides **1** and **2** *cis/trans* isomers with high rotation barriers are found in *N*-ferrocenyl *C*-methyl thioamides **3** and **4**. The *N*-ferrocenyl *C*-ferrocenyl thioamide **7**, however, displays only single sets of proton and carbon resonances in the respective NMR spectra suggesting the presence of a single isomer only. DFT calculations favor the *trans* isomer *trans*-**7** by 9.8 kJ mol⁻¹ with a rather planar Cp-NHC(S)-Cp bridge, while the *cis* isomer *cis*-**7** is severely distorted (see Supporting Information, Figure S7). The NOE spectrum of **7** in CD₂Cl₂ (see Supporting Information, Figure S8) reveals NOE contacts of the NH¹ proton to H⁸ (strong) and H³ (medium) fully consistent with the *trans* configuration (DFT distances of *trans*-**7**: H¹ \cdots H⁸ 2.05 Å, H¹ \cdots H³ 2.47 Å; DFT distances of *cis*-**7**: H¹ \cdots H⁸ 3.97 Å, H¹ \cdots H³ 3.06 Å, Supporting Information, Figure S7).

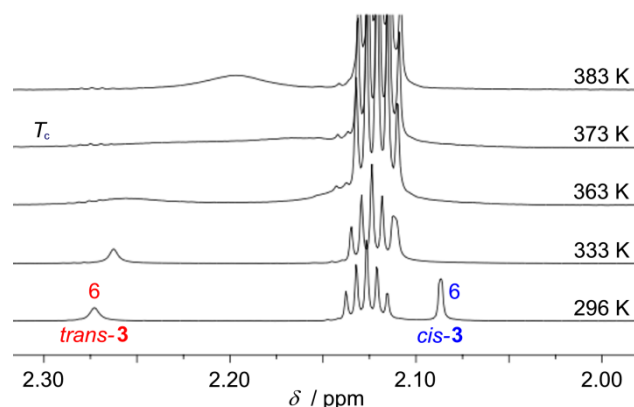


Figure 2. Variable temperature ¹H NMR spectra of **3** in d₈-toluene.

For diferrocene dithioamide **8** several further conformational possibilities are conceivable (Figure 5). A double signal set is observed in the integral ratio 1 : 6.4 in the ^1H NMR spectrum of **8**. The major isomer is assigned to the *trans,trans* isomer (*trans,trans-8*) on the basis of an NOE cross peak between the methyl group H^{15} and the thioamide proton NH^{13} (*trans*-Cp-NHC(S)Me moiety) and two NOE contacts between thioamide NH^1 and H^8 (strong) and H^3 (medium) similar to the *trans-7* case. These data are consistent with the DFT calculated metrics of the *trans,trans-8* isomer ($\text{H}^1\cdots\text{H}^8$ 2.22 Å, $\text{H}^1\cdots\text{H}^3$ 2.48 Å; $\text{H}^{13}\cdots\text{H}^{15}$ 2.15 Å). The minor isomer in solution is likely the *trans,cis* isomer with a terminal *cis*-Cp-NHC(S)Me moiety (*trans,cis-8*) similar to **3** and **4**.

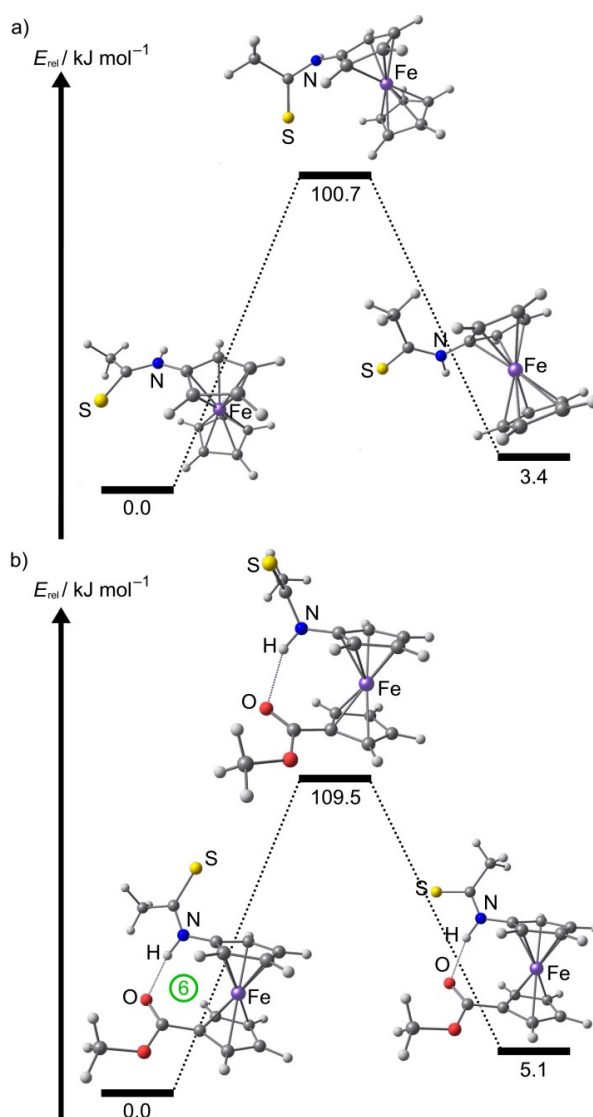


Figure 3. DFT (B3LYP, LANL2DZ, PCM CH_2Cl_2) calculated cis/trans isomerization of a) **3** and b) **4**.

As dithioamide **8** features two hydrogen atom donors and two hydrogen atom acceptors, intramolecular NH \cdots S hydrogen bonds are feasible similar to the all-amide complex **6**. Indeed, amide **6** folds into a secondary structure in solution with eight-membered NH \cdots O hydrogen-bonded rings (cf. Chart 1, **D**). The IR spectra of **8** suggest an intramolecular hydrogen bond in CH₂Cl₂ solution as well (vide supra). DFT calculations of *trans,trans*-**8** in different folding arrangements show that – in contrast to **6** – the six-membered NH \cdots S hydrogen-bonded rings are more favorable (Figure 5). The most stable arrangement of **8** comprises the six-membered ring and a 1,2'-conformation of the Cp rings of the disubstituted ferrocene.

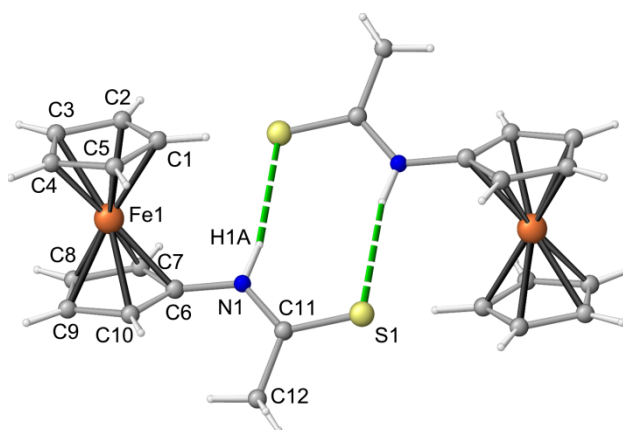


Figure 4. Hydrogen bonding motif of *cis*-**3** in the solid state.

In the ¹H¹H NOE spectrum (Figure 6) the terminal thioamide proton NH¹³ of **8** displays three contacts to neighboring protons, namely one to the methyl group (H¹⁵), a second one to the adjacent Cp proton H¹¹, and –decisively– a third contact to a Cp proton adjacent to the bridging C(S) substituent H⁸. The latter contact is only feasible in the 1,2'-conformation with the six-membered ring (NH¹³ \cdots H⁸ = 3.00 Å) while for all other conformations (Figure 5) this distance is larger than 3.88 Å according to DFT calculations. The preference of the smaller six-membered ring in the dithioamide **8** as opposed to the eight-membered ring in the diamide **6** can be ascribed to the larger atomic radius of sulfur as compared to oxygen and the concomitantly longer bonds. To conclude this section, Me-C(S)NH-Fc thioamides can form *cis* and *trans* isomers while the *trans* isomer is preferred in Fc-C(S)NH-Fc

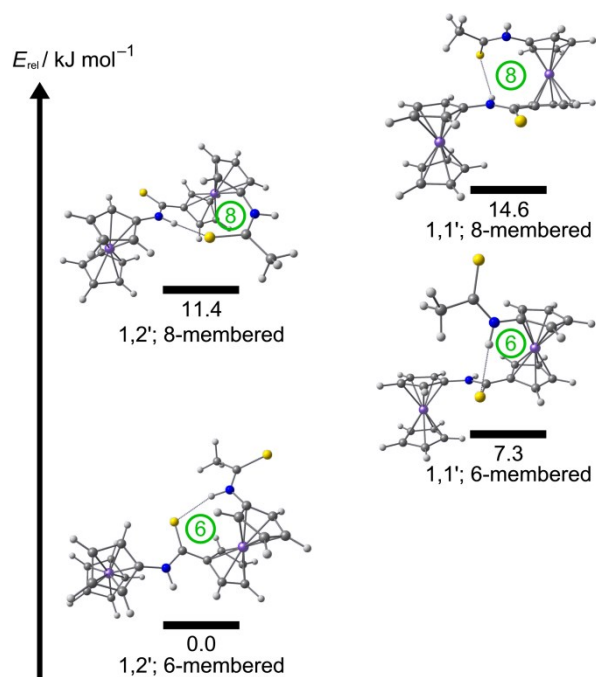


Figure 5. DFT (B3LYP, LANL2DZ, PCM CH₂Cl₂) calculated hydrogen-bonded isomers of *trans,trans*-8.

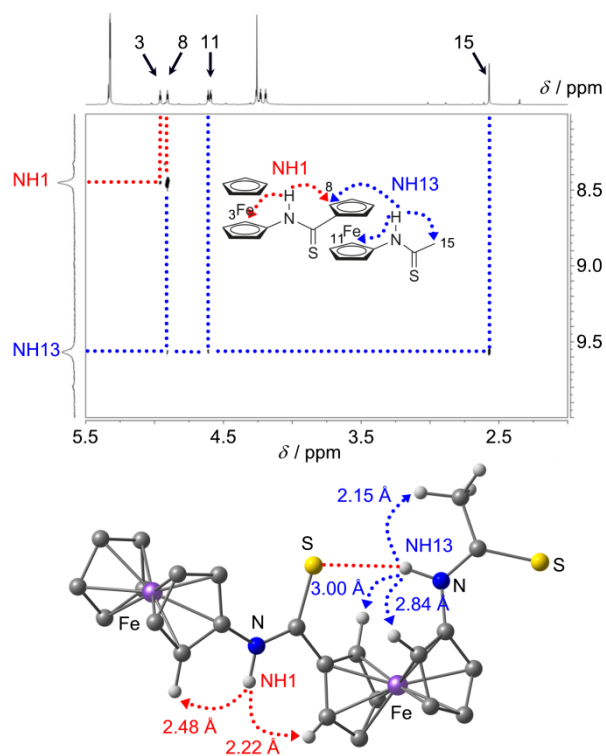


Figure 6. ¹H¹H NOESY of 8 in CD₂Cl₂ at room temperature (top) and selected NOE relevant metric data of the lowest energy conformation of 8 (bottom, only relevant protons are shown).

thioamides. In addition the disubstituted ferrocene Me-C(S)NH-Fn-C(S)NH-Fc (**8**) preferably arranges in a six-membered ring with an intramolecular NH...S hydrogen bond.

Electrochemistry.

The monoferrocenyl derivatives **3** and **4** are oxidized in CH₂Cl₂ to the respective ferrocenium cation radicals **3**⁺ and **4**⁺ at $E_{1/2} = -0.020$ V and $E_{1/2} = 0.205$ V (vs. FcH/FcH⁺), respectively (Figure 7). The higher potential of the **4**/**4**⁺ couple is due to the presence of the electron withdrawing ester substituent, as expected.^{10a,18} In comparison to the respective amides **1/2** the potentials of **3/4** are shifted to higher values by 85 – 100 mV (Figure 7). Obviously, the NHC(S)Me group is more electron withdrawing than the NHC(O)Me substituent. At higher potentials an irreversible wave is observed ($E_p = 0.345$ V and $E_p = 0.510$ V for **3** and **4**, respectively). This oxidation (corresponding to only 0.5 electrons) can be ascribed to oxidation of the sulfur in **3**⁺ or **4**⁺ to give transient ferrocenium sulfuryl diradicals **3**²⁺ or **4**²⁺. These doubly charged ferrocenium thioamide radical cations should be highly acidic and should easily lose a proton to give the diradicals [**3-H**]⁺ or [**4-H**]⁺, respectively (Scheme 2). In full agreement DFT calculations on *trans*-**3**ⁿ⁺ (n = 0–2) assign the first oxidation to the Fc/Fc⁺ couple and the second oxidation to the sulfur atom, as judged from Fe...Cp(centroid) distances and spin densities (see the Supporting Information, Figure S9). In agreement with the proposed increased acidity the NH bond lengths increase as the positive charge becomes greater, from 1.018, 1.019 to 1.022 Å (see Supporting Information, Figure S9). The sulfur-based radicals should be prone to disulfide formation. Hence, we propose an intermolecular radical coupling of [**3-H**]⁺ with **3**⁺ and [**4-H**]⁺ with **4**⁺, respectively. This suggestion fits the observed transfer of only 0.5e in the second oxidation step (Figure 7). A further proton loss might stabilize the resulting mixed-valence disulfides [**3-H**]₂⁺ and [**4-H**]₂⁺ (Scheme 2). A ferrocenyl-containing disulfide Fc-C(O)-SS-C(O)-Fc had been prepared before by iodine oxidation and deprotonation of Fc-C(O)SH or by thionation of Fc-C(O)-im (im = *N*-imidazolidine) with Lawesson's reagent.¹³ Oxidation of organic thioamides by iodine, Cu²⁺ or quinones has been reported to yield disulfides with concomitant deprotonation.¹² Hence, the proposed EEC pathway (Scheme 2) is a viable mechanism.

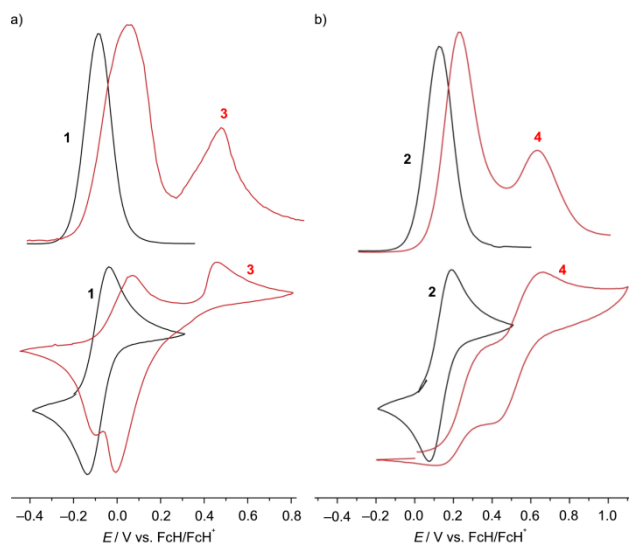
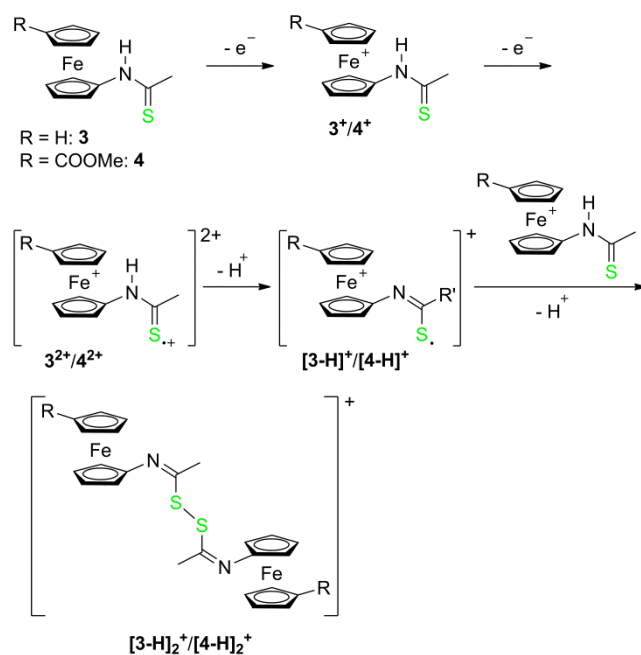


Figure 7. Cyclic (bottom) and square-wave voltammograms (top) of a) 1/3 and b) 2/4 in CH_2Cl_2 /[nBu_4N][PF_6].



Scheme 2. Suggested EEC mechanism and intermolecular disulfide formation of 3 and 4 (postulated species in brackets).

The observed redox processes are basically similar for the diferrocenes **7** and **8** with the first oxidation potential of the ferrocene units shifted to higher values in comparison to the corresponding amides **5** and **6** (Figure 8). We ascribe the first two oxidation waves to the oxidations of the ferrocene units to give the mixed-valent species $7^+/8^+$ and the all- Fe^{III}

complexes $7^{2+}/8^{2+}$, respectively. At somewhat higher potentials the irreversible sulfur oxidations are observed, yielding the reactive trications $7^{3+}/8^{3+}$ (Figure 8). Similar to **3/4**, deprotonation and disulfide formation might be the dominating pathway after 3-fold oxidation of **7** and **8**. For dithioamide 8^{3+} intramolecular disulfide formation might be feasible in addition to intermolecular S-S coupling. A possible reaction pathway yielding a mixed-valent disulfide *ansa*-ferrocene $[8-2H]^+$ is depicted in Scheme 3. According to DFT calculations the proposed disulfide $[8-2H]^+$ is shown to be an unstrained [5]ferrocenophane with an appended ferrocenium ion (Figure 9).²⁰

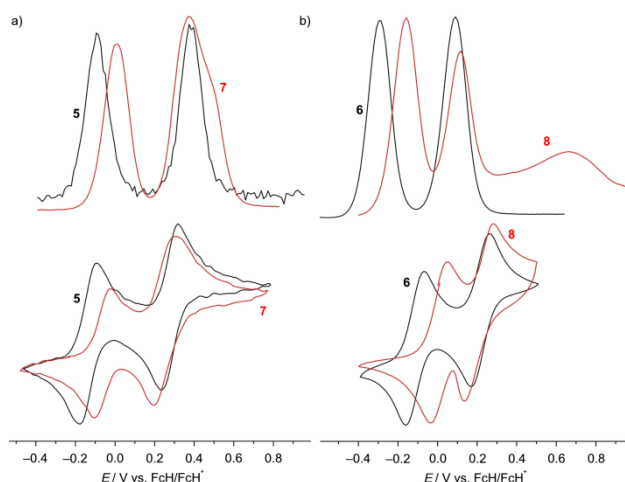
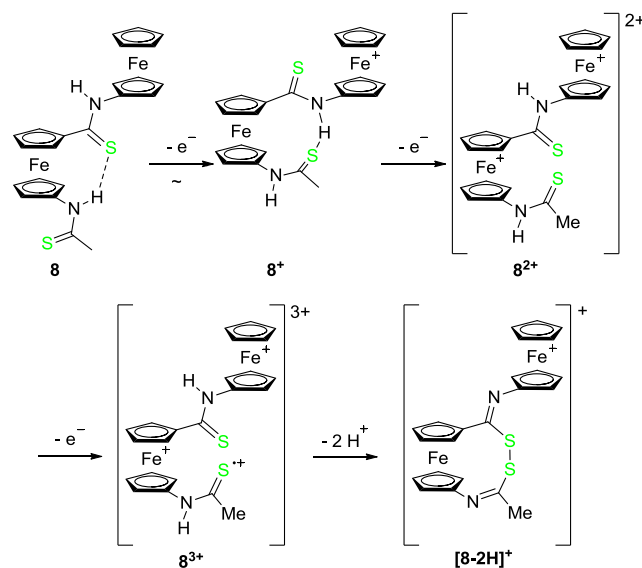


Figure 8. Cyclic (bottom) and square-wave voltammograms (top) of a) 5/7 and b) 6/8 in $CH_2Cl_2/[nBu_4N][PF_6]$.

The monocations 1^+ , 2^+ , 5^+ , and 6^+ as well as 3^+ , 4^+ , 7^+ , and 8^+ were prepared electrochemically in an optically transparent thin-layer electrode cell and the UV/vis spectra were recorded. As an example, the spectroelectrochemical oxidation of **8** to 8^+ is depicted in Figure 10. A clean oxidation of the ferrocene **8** (480 nm) to the mixed-valent cation 8^+ (527, 751, 1170 nm) is observed with isosbestic points at 464 and 500 nm. The typical ferrocenium absorption bands of the amides are observed at 756, 799, 759 and 799 nm (1^+ , 2^+ , 5^+ , and 6^+ ; from Gaussian band shape analysis) while those of the thioamides are found at 799, 797, 800 and 751 nm (3^+ , 4^+ , 7^+ , and 8^+ ; from Gaussian band shape analysis, Supporting Information, Figures S10 and S11). In addition, the mixed-valent complexes 5^+ , 6^+ , 7^+ , and 8^+ show intervalence charge transfer bands at 1075, 961, 1150, and 1170 nm from Gaussian band shape analysis ($E_{op} = 9300, 10400, 8695, 8547 \text{ cm}^{-1}$).



Scheme 3. Suggested EEEC mechanism and intramolecular disulfide formation of **8 (postulated species in brackets).**

These values show that in the thioamides the optical electron transfer occurs at lower energy. From the Hush formula, the band shape parameters of the IVCT bands (see Supporting Information, Figures S10 and S11) and an estimated $Fe\cdots Fe$ distance of 7.2 Å the electronic couplings are calculated as $H_{AB} = 200, 260, 190,$ and 230 cm^{-1} ($\pm 10\text{ cm}^{-1}$) for **5⁺**, **6⁺**, **7⁺**, and **8⁺**, respectively. These moderate values assign class II to **7⁺** and **8⁺** according to the Robin–Day classification.¹¹ The similar electronic coupling in amides and their corresponding thioamides suggests that the electron transfer is not significantly mediated by the (thio)amide bridge but rather occurs through space.

Activation barriers for the thermal electron transfer in the mixed-valent cations are estimated from $\Delta G^{\ddagger}_{ET} = \lambda/4 + \Delta G^0/2 + (\Delta G^0)^2/(4(\lambda - 2H_{AB}) - H_{AB} + H_{AB}^2/(\lambda + \Delta G^0))$ with $\lambda = E_{op} - \Delta G^0$ as 0.43, 0.40, 0.36, and 0.34 eV for **5⁺**, **6⁺**, **7⁺**, and **8⁺**, respectively (42, 39, 35, 33 kJ mol⁻¹).^{11b} The significantly lower barriers in the thioamides Fc-NHC(S)-FnR (**7⁺**, **8⁺**) are largely based on the smaller electronic differences of the ferrocene/ferrocenium redox sites in thioamides. The oxidation potential of Fc-NHC(S)R is more similar to that of Fc-C(S)NHR in comparison to the very different potentials of Fc-NHC(O)R and Fc-C(O)NHR. Facilitated electron transfer in thioamides **7⁺** and **8⁺** is hence based on a more pronounced redox similarity of the redox sites (smaller ΔG^0) as opposed to a stronger electronic interaction via the C(X)NH bridge (similar H_{AB}).

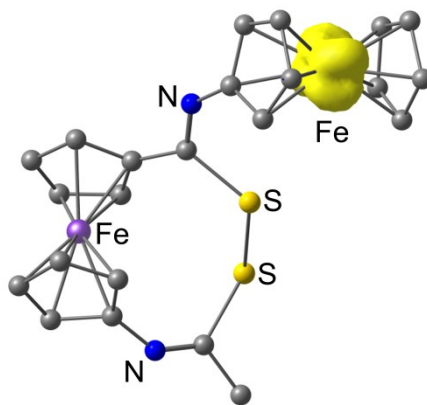


Figure 9. DFT calculated structure of $[8-2H]^+$ (CH hydrogen atoms omitted for clarity) including spin density distribution (isosurface value 0.01 a.u.).

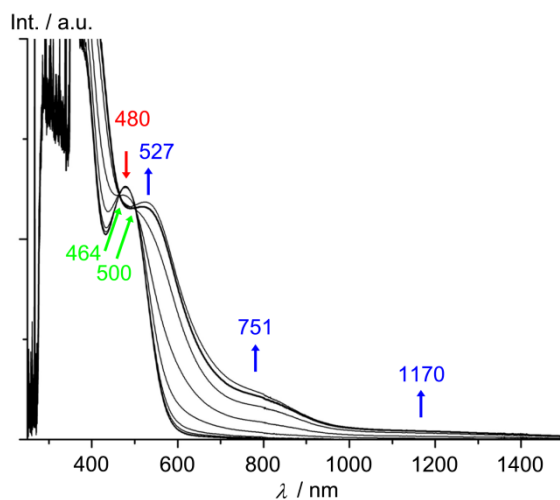


Figure 10. Spectroelectrochemical oxidation of **8** to 8^+ in $\text{CH}_2\text{Cl}_2/[\text{nBu}_4\text{N}][\text{B}(\text{C}_6\text{F}_5)_4]$.

To experimentally corroborate the preferred site of oxidation the diferrocenes **7** and **8** were titrated with iodine ($E_{1/2} = -0.14$ V vs. ferrocene in CH_3CN)¹⁹ and paramagnetic ^1H NMR spectra were recorded.^{10b,20a} As an example, the ^1H NMR spectra of **7** and increasing substoichiometric amounts of iodine are displayed in Figure 11 (see Supporting information, Figure S12 for titration of **8** with I_2). Due to the typically fast intermolecular self-exchange reaction of the Fc/Fc^+ couple, averaged NMR resonances are observed. Clearly, the resonances of the NH-substituted ferrocene (H^3 , H^4 , H^5) are more affected (paramagnetic shift, paramagnetic broadening) than the resonances of the CS-substituted ferrocene (H^8 , H^9 , H^{10}) demonstrating that the NH-substituted ferrocene is the site of

primary oxidation, similar to the amide case **5/5**⁺.^{10b} Fully analogously, the site of first oxidation in **8/8**⁺ is the monosubstituted ferrocene, as shown by iodine titrations (see Supporting Information, Figure S12) and DFT calculations.

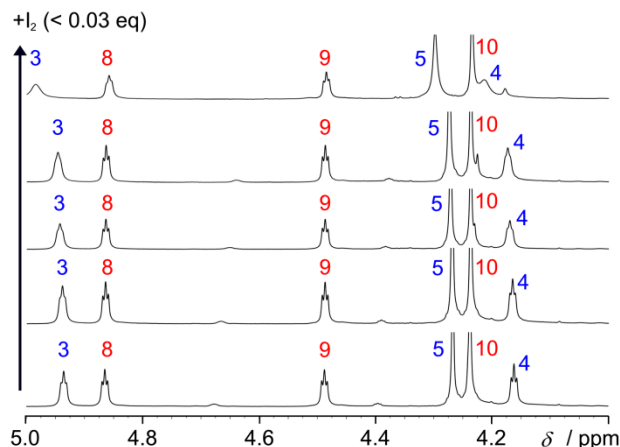


Figure 11. ¹H NMR spectra of **7 upon titration with iodine in CD₂Cl₂ (atom numbering according to Scheme 1).**

The monocations **3**⁺, **4**⁺, **7**⁺, and **8**⁺ were additionally prepared by chemical oxidation using one equiv of AgSbF₆ in a mixture of CH₂Cl₂ and THF (4/1). After rapid freezing to 77 K EPR spectra of the ferrocenium cation radicals were recorded.²¹ Nearly axial EPR spectra were obtained with $g_z = 3.400$, $g_{x,y} = 1.860$ (**3**⁺, $\Delta g = 1.54$), $g_z = 3.300$, $g_{x,y} = 1.852$ (**4**⁺, $\Delta g = 1.45$) (see Supporting Information, Figures S13 and S14) and $g_z = 3.300$, $g_y = 1.881$, $g_x = 1.845$ (**7**⁺, $\Delta g = 1.46$, Figure 12a). Comparable resonances have been observed previously for [Fc-NHCOR]⁺ radicals in CH₂Cl₂ and assigned to contact ion pairs with the [SbF₆]⁻ ion attached via NH \cdots F hydrogen bonds.^{21b} In THF solvent separated ion pairs are additionally present which feature NH \cdots O hydrogen bonds to the THF oxygen atom. These solvated [Fc-NHCOR]⁺ radicals possess a smaller g anisotropy and sharper resonance lines.^{21b} Notably, **8**⁺ shows two signal sets with a broad resonance at $g_z = \text{n.o.}$, $g_y = 1.889$, $g_x = 1.849$ (50%) suggestive of a contact ion pair and a sharp prominent resonance at $g_z = 2.340$, $g_y = 2.067$, $g_x = 2.001$ ($\Delta g = 0.34$, 50%) with a small g anisotropy (Figure 12b). The latter resonance suggests that the spin-carrying terminal [Fc-NHCSR]⁺ unit is not hydrogen-bonded to [SbF₆]⁻ but rather to a different acceptor (oxygen of THF or sulfur of bridging C=S). In contrast to **3**⁺, **4**⁺, and **7**⁺ a bridging C=S unit is available in **8**⁺ as an internal hydrogen atom acceptor. This results in an eight-membered-ring system in **8**⁺ (Figure 12b).

A hexafluoroantimonate counterion that might be additionally attached to the terminal NHCSCH₃ group does not dramatically influence the terminal Fc⁺ radical (Figure 12b and Supporting Information). The terminal Fc⁺ seems to be influenced mainly by the donor atom coordinated to its proximal NH group (THF, counter ion, sulfur atom).

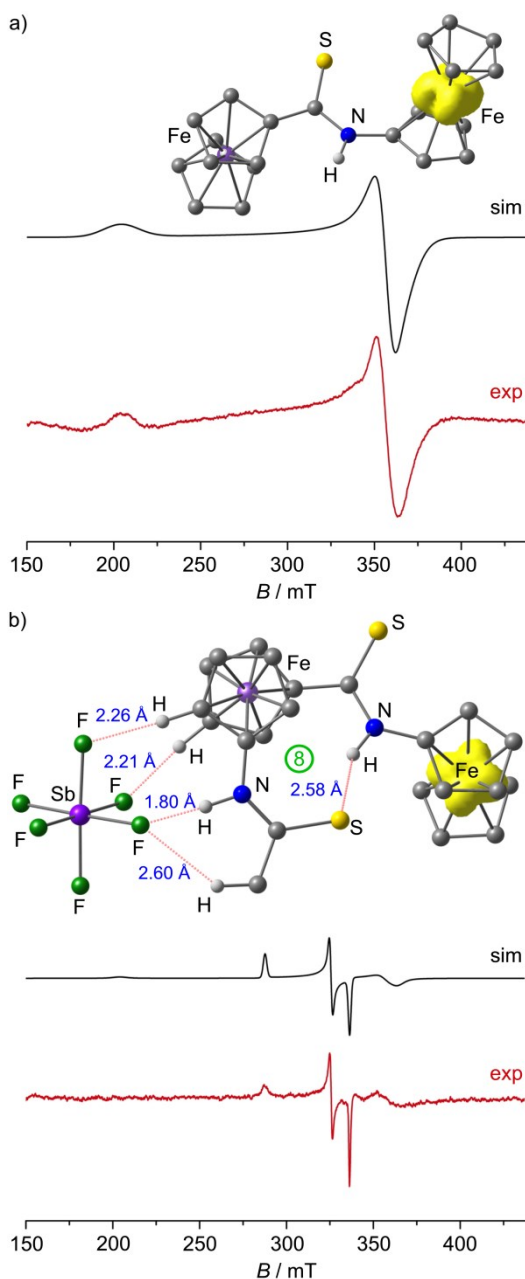


Figure 12. X-band EPR spectra in CH₂Cl₂ and THF (4:1) at 77 K, simulations and DFT calculated spin density distributions (isosurface value 0.01 a.u.) of a) 7⁺ and b) 8⁺×[SbF₆]⁻ (bottom). Only relevant hydrogen atoms are shown.

Interestingly, the DFT optimized lowest energy conformation of **8**⁺ features an eight-membered ring, confirming the EPR results. This conformation of **8**⁺ (eight-membered ring, 1,2'-conformation) is calculated to be more stable than the six-membered ring (1,2'-conformation) by 8 kJ mol⁻¹ (see Supporting Information). Hence, the intramolecular NH...S hydrogen bond of the acidic terminal Fc⁺-NH group favors the eight-membered ring in **8**⁺ as opposed to neutral **8** with a six-membered ring (Figure 5). The DFT calculations do not reveal a significant spin density on sulfur atoms in **3**⁺, **4**⁺, **7**⁺, and **8**⁺, respectively, ruling out a significant contribution of sulfur radical character in the singly oxidized complexes.

In summary, the mixed-valent cation **8**⁺ likely features a different secondary structure (eight-membered ring) different from that of its parent neutral thioamide **8** (six-membered ring) due to a changed preference of intramolecular hydrogen bonds (Scheme 3). This contrasts to the secondary structure of ferrocenyl amides which is preserved upon a single electron transfer (eight-membered ring).

3.1.4 Conclusion

Oxygen to sulfur exchange in ferrocenyl amides results in distinct consequences concerning preferred conformations of neutral complexes, electronic communication in mixed-valence systems, and reactivity of oxidized species. Amides Fc-NHC(O)Me (e.g. **1**, **2**) prefer *trans* conformations of the amide, while for thioamides Fc-NHC(S)Me (**3**, **4**) both *cis* and *trans* isomers are equally accessible. The barrier of *cis/trans* isomerization has been measured as 75 kJ mol⁻¹ for **3** by variable-temperature NMR spectroscopy. The *trans* configuration of the central thioamide is again favored for diferrocenyl thioamides of the type Fc-NHC(S)-Fn^R (**7**, **8**). Dithioamide **8** features a well-defined secondary structure in solution comprising an intramolecular NH...S hydrogen bond giving a six-membered ring in contrast to the oxo analogue **6** featuring an eight-membered ring with an intramolecular NH...O hydrogen bond.

In the thioamides the Fc/Fc⁺ redox couples are typically shifted to higher potentials in comparison to the corresponding amides. In addition irreversible oxidations follow at even higher potential which can be ascribed to disulfide formations. In the triply charged dithioamide **8**³⁺ the disulfide formation may even occur intramolecularly and the possible

formation of an *ansa*-ferrocene **[8-2H]⁺** is proposed. This proposed oxidatively induced cyclization reaction will be investigated in more detail in the future. Furthermore, the preferred secondary structure (1,2'; six-membered ring) of the dithioamide **8** transforms into an eight-membered ring with an inverted NH...S hydrogen bond motif upon oxidation to **8⁺**. This perception will be exploited in the near future for redox stimulated conformational changes in oligothiopeptides.

The mixed-valence cations **7⁺** and **8⁺** belong to the Robin-Day class II with electronic coupling similar to that of the corresponding mixed-valent amides **5⁺** and **6⁺** ($H_{AB} \approx 220 \text{ cm}^{-1}$). However, electron transfer is more rapid in thioamides **7⁺** and **8⁺**, due to the diminished redox asymmetry of the C(S)NH bridge as compared to the C(O)NH bridge. In any event, the most easily oxidized site is still the monosubstituted Fc-NHCX subunit irrespective of the chalcogen atom X of the bridge.

3.1.5 Experimental Section

General Procedures:

All reactions were performed under an argon atmosphere unless otherwise noted. Dichloromethane was dried with CaH₂ and distilled prior to use. All reagents were used as received from commercial suppliers (Acros, Sigma-Aldrich, ABCR). **1**, **2**, **5**, and **6** were prepared according to literature procedures.^{10,14} NMR spectra were recorded on a Bruker DRX 400 spectrometer at 400.31 MHz (¹H) and 100.07 MHz (¹³C{¹H}). All resonances are reported in ppm vs. the solvent signal as internal standard. CD₂Cl₂ (¹H: δ 5.32 ppm; ¹³C: δ 54.0 ppm). *d*₈-Toluene (¹H: δ 2.30, 7.19 ppm). IR spectra were recorded with a BioRad Excalibur FTS 3100 spectrometer as KBr disks or by using KBr cells in CH₂Cl₂. Electrochemical experiments were carried out on a BioLogic SP-50 voltammetric analyzer by using a platinum working electrode, a platinum wire counter electrode and a 0.01 M Ag/AgNO₃ reference electrode. The measurements were carried out at a scan rate of 100 mV s⁻¹ for cyclic voltammetry experiments and at 50 mV s⁻¹ for square wave voltammetry experiments in 0.1 M [ⁿBu₄N][PF₆] as supporting electrolyte in CH₂Cl₂. Potentials are referenced against the decamethylferrocene/decamethylferrocenium couple ($E_{1/2} = 550 \pm 5 \text{ mV}$ vs ferrocene/ferrocenium under our experimental conditions) and are given relative to the ferrocene/ferrocenium couple. UV/vis/near-IR spectra were recorded on a Varian Cary 5000 spectrometer by using 1.0 cm cells (Hellma, suprasil). Spectroelectrochemical

experiments were performed using a thin layer quartz glass (path length 1 mm) cell kit (GAMEC Analysentechnik, Illingen, Germany) equipped with a Pt gauze working electrode, a Pt counter electrode and a Ag/AgNO₃ reference electrode (0.01 M solutions in CH₂Cl₂ containing 0.1 M [¹Bu₄N][B(C₆F₅)₄]). CW EPR spectra (X-band; ca. 9.4 GHz; ca. 20 mM) were measured on a Miniscope MS 300 at 77 K cooled by liquid nitrogen in a finger dewar (Magnettech GmbH, Berlin, Germany). Settings were as follows: center field: 2499.01 G; modulation amplitude: 3000 mG; receiver gain: 5.0; microwave attenuation: 3 dB; sweep time: 120 s. *g*-values are referenced to external Mn²⁺ in ZnS (*g* = 2.118, 2.066, 2.027, 1.986, 1.946, 1.906). Simulations of EPR spectra were performed with EasySpin (v 4.0.0)²² for MatLab (R2007b). FD mass spectra were recorded on a FD Finnigan MAT95 spectrometer. ESI mass spectra were recorded on a Micromass Q-TOF-Ultima spectrometer. Melting points were determined by using a Gallenkamp MFB 595 010 capillary melting point apparatus and were not corrected. Elemental analyses were performed by the microanalytical laboratory of the chemical institutes of the University of Mainz.

Density Functional Calculations.

Density functional calculations were carried out with the Gaussian09/DFT series²³ of programs. The B3LYP formulation of density functional theory was used employing the LANL2DZ basis set. No symmetry constraints were imposed on the molecules. The presence of energy minima of the ground states and first order saddle points was checked by analytical frequency calculations. Solvent modeling was done employing the integral equation formalism polarizable continuum model (IEFPCM, dichloromethane). The approximate free energies at 298 K were obtained through thermochemical analysis of the frequency calculation, using the thermal correction to Gibbs free energy as reported by Gaussian09.

Crystal Structure Determination.

Intensity data were collected with a Bruker AXS Smart1000 CCD diffractometer with an APEX II detector and an Oxford cooling system and corrected for absorption and other effects using Mo K α radiation (λ = 0.71073 Å). The diffraction frames were integrated using the SAINT package and most were corrected for absorption with MULABS.^{24,25} The structures were solved by direct methods and refined by the full-matrix method based on F^2 using the SHELXTL software package.^{26,27} All non-hydrogen atoms were refined

anisotropically while the positions of all hydrogen atoms were generated with appropriate geometric constraints and allowed to ride on their respective parent carbon/nitrogen atoms with fixed isotropic thermal parameters. Crystal data: C₁₂H₁₃FeNS (259.15); *T* = 173 K; yellow plate; 0.21 × 0.17 × 0.02 mm; monoclinic; P2₁/c; *a* = 14.2351(8) Å; *b* = 9.4951(6) Å; *c* = 8.4156(5) Å; β = 105.437(2)°; *V* = 1096.45(11) Å³; *Z* = 4; F(000) = 536.0; ζ = 1.570 g cm⁻³; μ = 1.528 mm⁻¹; 2 θ range = 5.22° – 55.76°; index ranges -18 ≤ *h* ≤ 18; -12 ≤ *k* ≤ 11; -11 ≤ *l* ≤ 10; reflections collected 15617; 2615 independent reflections; 136 parameters; maximum/minimum transmission = 0.9701/0.7397; goodness of fit on *F*² 0.957; largest difference peak and hole = 0.468/-0.381 e Å⁻³; R1(*I* > 2σ) = 0.0305; R1(all data) = 0.0465; R_w(*I* > 2σ) = 0.0709; R_w(all data) = 0.0741. CCDC-978126 contains supplementary crystallographic data for this paper. These data can be obtained free of charge from The Cambridge Crystallographic Data Centre via www.ccdc.cam.ac.uk/data_request/cif.

Synthesis of 3.

Amide **1** (298 mg, 1.23 mmol) and Lawesson's reagent (248 mg, 0.61 mmol) were suspended in toluene (250 mL) and heated to 80 °C for 3 h. The solvent was removed under reduced pressure. After column chromatography (SiO₂, 3 × 12 cm, CH₂Cl₂) **3** was obtained as orange solid (286 mg, 1.10 mmol, 90%). *R_f*(SiO₂, CH₂Cl₂) = 0.26. M.p. 130 °C dec. ¹H NMR (400 MHz, CD₂Cl₂, 298 K): [*cis*-**3**] δ = 9.01 (s, 1H, NH⁴), 4.36 (pt, 2H, ³*J*_{HH} = 1.83 Hz, H²), 4.23 (s, 5H, H⁷), 4.17 (pt, 2H, ³*J*_{HH} = 1.83 Hz, H³), 2.40 ppm (s, 3H, H⁶); [*trans*-**3**] δ = 8.28 (s, 1H, NH⁴), 4.83 (pt, 2H, ³*J*_{HH} = 1.80 Hz, H²), 4.27 (s, 5H, H⁷), 4.13 (pt, 2H, ³*J*_{HH} = 1.80 Hz, H³), 2.59 ppm (s, 3H, H⁶). ¹³C{¹H} NMR (100 MHz, CD₂Cl₂, 298 K): [*cis*-**3**] δ = 205.9 (C⁵), 94.9 (C¹), 69.9 (C⁷), 67.1 (C³), 66.0 (C²), 30.3 ppm (C⁶); [*trans*-**3**] δ = 200.4 (C⁵), 95.8 (C¹), 70.2 (C⁷), 66.0 (C³), 64.8 (C²), 36.2 ppm (C⁶). MS(FD): *m/z* (%) = 259.9 (100) [M]⁺. IR(KBr): $\tilde{\nu}$ = 3261 (w, NH), 1548 (b, CS(I)), 1378 (b, CS(II)) cm⁻¹. IR(CH₂Cl₂): $\tilde{\nu}$ = 3383 (m, NH), 1502 (m, CS(I)), 1367 (m, CS(II)) cm⁻¹. UV/vis (CH₂Cl₂): λ_{max}(ε) = 348 (1890), 446 nm (365 M⁻¹ cm⁻¹). CV (CH₂Cl₂, vs. FcH/FcH⁺): *E*_{1/2} = -0.020 V (rev.), *E*_p = 0.345 V (irrev.). Anal. calcd for C₁₂H₁₃FeNS (259.1): C 55.62, H 5.06, N 5.40, S 12.37; Found: C 55.29, H 4.79, N 5.38, S 12.37.

Synthesis of 4.

Amide ester **2** (100 mg, 0.33 mmol) and Lawesson's reagent (66 mg, 0.17 mmol) were suspended in toluene (70 mL) and heated to 80 °C for 2.5 h. The organic phase was washed with water, saturated aqueous sodium bicarbonate solution, and brine. The organic phase

was dried over MgSO₄ and the solvent was removed under reduced pressure. After column chromatography (SiO₂, 3 × 12 cm, ethylacetate / petroleum ether (b.p. 40 – 60 °C), (1:1)) **4** was obtained as orange-red solid (56 mg, 0.18 mmol, 53%). *R_f*(SiO₂, ethylacetate / petroleum ether (b.p. 40 – 60 °C) 1:1) = 0.68. M.p. 105.5 °C. ¹H-NMR (400 MHz, CD₂Cl₂, 298 K): [*cis*-**4**] δ = 8.86 (s, 1H, NH⁴), 4.88 (pt, 2H, ³*J*_{HH} = 1.97 Hz, H⁸), 4.49 (pt, 2H, ³*J*_{HH} = 1.97 Hz, H⁷), 4.37 (pt, 2H, ³*J*_{HH} = 1.96 Hz, H²), 4.21 (pt, 2H, ³*J*_{HH} = 1.96 Hz, H³), 3.86 (s, 3H, H¹¹), 2.36 ppm (s, 3H, H⁶); [*trans*-**4**] δ = 8.49 (s, 1H, NH⁴), 4.82 (pt, 2H, ³*J*_{HH} = 1.95 Hz, H⁸), 4.73 (pt, 2H, ³*J*_{HH} = 1.98, H²), 4.48 (pt, 2H, ³*J*_{HH} = 1.95 Hz, H⁷), 4.19 (pt, 2H, ³*J*_{HH} = 1.98, H³), 3.80 (s, 3H, H¹¹), 2.61 ppm (s, 3H, H⁶). ¹³C{¹H} NMR (100 MHz, CD₂Cl₂, 298 K): [*cis*-**4**] δ = 206.1 (C⁵), 170.7 (C¹⁰), 94.7 (C^{1/9}), 73.3 (C⁷), 72.1 (C⁸), 68.7 (C³), 67.5 (C²), 52.4 (C¹¹), 30.3 ppm (C⁶); [*trans*-**4**] δ = 202.4 (C⁵), 171.6 (C¹⁰), 94.8 (C^{1/9}), 73.3 (C⁷), 71.9 (C⁸), 68.0 (C³), 67.4 (C²), 52.4 (C¹¹), 35.5 ppm (C⁶). MS(ESI): *m/z* (%) = 340.0 (100) [M + Na]⁺. IR(KBr): $\tilde{\nu}$ = 3462 (br, NH), 3288 (m, NH), 1686 (s, CO), 1578 (b, CS(I)), 1475 (b, CS(II)), 1467 (b, CS(II)) cm⁻¹. IR(CH₂Cl₂): $\tilde{\nu}$ = 3379, 3281 (m, NH), 1713 (s, CO), 1695 (sh, CO), 1523 (m, CS(I)), 1508 (m, CS(II)), 1370 (m, CS(II)) cm⁻¹. UV/vis (CH₂Cl₂): λ_{max}(ε) = 359 (sh, 3065), 444 nm (680 M⁻¹ cm⁻¹). CV (CH₂Cl₂, vs. FcH/FcH⁺): *E*_{1/2} = 0.205 V (rev.), *E*_p = 0.510 V (irrev.). Anal. calcd for C₁₄H₁₅FeNO₂S (317.2): C 53.01, H 4.77, N 4.42, S 10.11; Found: C 52.83, H 4.62, N 4.35, S 10.10.

Synthesis of 7.

Diferrocene **5** (300 mg, 0.73 mmol) and Lawesson's reagent (147 mg, 0.36 mmol) were suspended in toluene (300 mL) and heated to 80 °C for 16 h. The solvent was removed under reduced pressure. After column chromatography (SiO₂, 5 × 30 cm] with ethylacetate / petroleum ether (b.p. 40 – 60 °C) (1:9) **7** was isolated as a red solid (185 mg, 0.43 mmol, 59%). *R_f*(SiO₂, ethylacetate / petroleum ether (b.p. 40 – 60 °C) 1:9) = 0.18. M.p. 230 °C (decomp). ¹H-NMR (400 MHz, CD₂Cl₂, 298 K): δ = 8.29 (s, 1H, NH¹), 4.94 (pt, 2H, ³*J*_{HH} = 1.94, H³), 4.87 (pt, 2H, ³*J*_{HH} = 1.92, H⁸), 4.49 (pt, 2H, ³*J*_{HH} = 1.92, H⁹), 4.27 (s, 5H, H⁵), 4.24 (s, 5H, H¹⁰), 4.16 ppm (pt, 2H, ³*J*_{HH} = 1.94, H⁴) ¹³C{¹H} NMR (100 MHz, CD₂Cl₂, 298 K): δ = 198.2 (C⁶), 96.4 (C²), 85.8 (C⁷), 71.9 (C⁹), 71.3 (C¹⁰), 69.9 (C⁵), 69.1 (C⁸), 65.9 (C⁴), 64.8 ppm (C³). MS(FD): *m/z* (%) = 429.3 (100) [M]⁺. IR(KBr): $\tilde{\nu}$ = 3270 (w, NH), 1542 (m, CS(I)), 1367 (b, CS(II)) cm⁻¹. IR(CH₂Cl₂): $\tilde{\nu}$ = 3397 (m, NH), 1537 (m, CS(I)), 1363 (m, CS(II)) cm⁻¹. UV/vis (CH₂Cl₂): λ_{max}(ε) = 375 (2560), 470 nm (1560 M⁻¹ cm⁻¹). CV (CH₂Cl₂, vs. FcH/FcH⁺): *E*_{1/2} = -0.065 (rev.), 0.240 (rev.) V, *E*_p = 0.345 V (irrev) Anal.

calcd for C₂₁H₁₉Fe₂NS (429.1): C 58.77, H 4.46, N 3.26, S 7.47; Found: C 57.90, H 4.33, N 2.98, S 7.53.

Synthesis of **8**.

Diamide **6** (250 mg, 0.53 mmol) and Lawesson's reagent (258 mg, 0.64 mmol) were suspended in toluene (300 mL) and heated to 80 °C for 1.5 h. The solvent was removed reduced pressure. After column chromatography (SiO₂, 3 × 15 cm) with CH₂Cl₂ / petroleum ether (b.p. 40 – 60 °C) (8/2 to pure CH₂Cl₂) **8** was obtained as a red solid (108 mg, 0.22 mmol, 40%). *R_f*(SiO₂, CH₂Cl₂) = 0.21. M.p. 175°C dec. ¹H-NMR (400 MHz, CD₂Cl₂, 298 K). δ = 9.57 (s, 1H, NH¹³), 8.45 (s, 1H, NH¹), 4.96 (pt, 2H, ³J_{HH} = 1.96, H³), 4.90 (pt, 2H, ³J_{HH} = 1.98, H⁸), 4.61 (pt, 2H, ³J_{HH} = 1.98, H¹¹), 4.59 (pt, 2H, ³J_{HH} = 1.98, H⁹), 4.26 (s, 5H, H⁵), 4.23 (pt, 2H, ³J_{HH} = 1.98, H¹²), 4.19 (pt, 2H, ³J_{HH} = 1.96, H⁴), 2.57 ppm (3H, H¹⁵) ¹³C{¹H} NMR (100 MHz, CD₂Cl₂, 298 K): δ = 202.6 (C¹⁴), 196.1 (C⁶), 95.7 (C²), 93.6 (C¹⁰), 87.0 (C⁷), 73.1 (C⁹), 70.1 (C⁸), 69.9 (C⁵), 68.8 (C¹¹), 68.1 (C¹²), 66.1 (C⁴), 64.8 (C³), 34.4 ppm (C¹⁵). MS(FD): *m/z* (%) = 502.3 (100) [M]⁺. IR(KBr): $\tilde{\nu}$ = 3375, 3233 (w, NH), 1552 (b, CS(I)), 1364 (b, CS(II)), 1350 (b, CS(II)) cm⁻¹. IR(CH₂Cl₂): $\tilde{\nu}$ = 3384, 3165 (m, NH), , 1537 (m, CS(I)), 1504 (m, CS(I)), 1367 (m, CS(II)) cm⁻¹. UV/vis (CH₂Cl₂): λ_{max}(ε) = 384 (3336), 480 nm (2141 M⁻¹ cm⁻¹); CV (CH₂Cl₂, vs. FcH/FcH⁺): *E*_{1/2} = -0.035, +0.205 V (rev.), *E*_p = 0.655 V (irrev.); Anal. calcd for C₂₃H₂₂Fe₂N₂S₂ (502.3): C 55.00, H 4.41, N 5.58, S 12.77; Found: C 54.20, H 4.14, N 5.03, S 12.41.

3.1.6 Associated Content

Supporting Information

Figures, tables, CIF and .xyz files giving UV/vis spectra of **1** and **3** in CH₂Cl₂, UV/vis spectra of **2** and **4** in CH₂Cl₂; UV/vis spectra of **5** and **7** in CH₂Cl₂; UV/vis spectra of **6** and **8** in CH₂Cl₂; ¹H¹H NOESY of **3** in CD₂Cl₂ at room temperature, DFT (B3LYP, LANL2DZ, PCM CH₂Cl₂) calculated (*cis-3*)₂, DFT (B3LYP, LANL2DZ, PCM CH₂Cl₂) calculated *cis-7* and *trans-7*, ¹H¹H NOESY of **7** in CD₂Cl₂ at room temperature, DFT (B3LYP, LANLDZ, PCM CH₂Cl₂) calculated *trans-3*ⁿ⁺ (n = 0–2), Gaussian band shape analysis of IVCT bands of **7**⁺, Gaussian band shape analysis of IVCT bands of **8**⁺, ¹H NMR spectra of **8** upon titration with iodine in CD₂Cl₂; EPR spectrum of **3** in THF/CH₂Cl₂ (1/4) and simulation,

EPR spectrum of **4** in THF/CH₂Cl₂ (1/4) and simulation, Cartesian coordinates of optimized geometries. This material is available free of charge via the Internet at <http://pubs.acs.org>.

Author Information

Corresponding Author.

*E-mail: katja.heinze@uni-mainz.de

Notes

The authors declare no competing financial interest.

3.1.7 Acknowledgement

We are grateful to Dipl.-Chem. Andreas Neidlinger and Dipl.-Chem. Anica Wünsche von Leupoldt for helpful discussions of the EPR spectra, and Nathalie Pilger and Katharina Welter for preparative assistance.

3.1.8 References

- [1] a) Huang, Y.; Jahreis, G.; Fischer, G.; Lücke, C. *Chem. Eur. J.* **2012**, *18*, 9841–9848; b) Bordwell, F. G. *Acc. Chem. Res.* **1988**, *21*, 456–463.
- [2] a) Lee, H.-J.; Choi, Y.-S.; Lee, K.-B.; Park, J.; Yoon, C.-J. *J. Phys. Chem. A* **2002**, *106*, 7010–7017; b) Alemán, C. *J. Phys. Chem. A* **2001**, *105*, 6717–6723; c) Artis, D. R.; Lipton, M. A. *J. Am. Chem. Soc.* **1998**, *120*, 12200–12206.
- [3] Beer, P. D.; Graydon, A. R.; Johnson, A. O. M.; Smith, D. K. *Inorg. Chem.* **1997**, *36*, 2112–2118.
- [4] Hall, C. D.; Danks, I. P.; Sharpe, N. W. *J. Organomet. Chem.* **1990**, *390*, 227–235.
- [5] a) Kloss, F.; Pidot, S.; Goerls, H.; Friedrich, T.; Hertweck, C. *Angew. Chem.* **2013**, *125*, 10945–10948; *Angew. Chem. Int. Ed.* **2013**, *52*, 10745–10748; b) Behling, L. A.; Hartsel, S. C.; Lewis, D. E.; DiSpirito, A. A.; Choi, D. W.; Masterson, L. R.; Veglia, G.; Gallagher, W. H. *J. Am. Chem. Soc.* **2008**, *130*, 12604–12605.

- [6] Mock, W. L.; Chen, J.-T.; Trang, J. W. *Biochem. Biophys. Res. Commun.* **1981**, *102*, 389–396.
- [7] a) Miwa, H. J.; Patel, A. K.; Vivatrat, N.; Popek, S. M.; Meyer, A. M. *Org. Lett.* **2001**, *3*, 3373–3375; b) Grabarse, W.; Mahlert, F.; Shima, S.; Thauer, R. K.; Ermler, U. *J. Mol. Biol.* **2000**, *303*, 329–344.
- [8] a) Patra, M.; Hess, J.; Konatschnig, S.; Spingler, B.; Gasser, G. *Organometallics* **2013**, *32*, 6098–6105; b) Sandoval-Chávez, C.; López-Cortéz, J.; Gutiérrez-Hernández, A. I.; Ortega-Alfaro, M. C.; Toscano, A.; Alvarez-Toledano, C. *J. Organomet. Chem.* **2009**, *694*, 3692–3700; c) Plažuk, D.; Zakrzewski, J.; Rybarczyk-Pirek, A.; Domogała, S. *J. Organomet. Chem.* **2005**, *690*, 4302–4308.
- [9] Katritzky, A. R.; Moutou, J.-L.; Yang, Z. *Synthesis* **1995**, 1497–1505.
- [10] a) Heinze, K.; Siebler, D. *Z. Anorg. Allg. Chem.* **2007**, *633*, 2223–2233; b) Siebler, D.; Linseis, M.; Gasi, T.; Carrella, L. M.; Winter, R. F.; Förster, C.; Heinze, K. *Chem. Eur. J.* **2011**, *17*, 4540–4551; c) Siebler, D.; Förster, C.; Heinze, K. *Dalton Trans.* **2011**, *40*, 3558–3575; d) Heinze, K.; Hüttinger, K.; Siebler, D. In *Modeling of Molecular Properties*; Comba, P., Ed.; Wiley-VCH Weinheim, Germany, 2011; pp. 325–346.
- [11] a) Robin, M. B.; Day, P. *Adv. Inorg. Chem. Radiochem.* **1967**, *10*, 247–422; b) Brunschwig, B. S.; Sutin, N. *Coord. Chem. Rev.* **1999**, *187*, 233–254.
- [12] a) Lo, W.-S.; Hu, W.-P.; Lo, H.-P.; Chen, C.-Y.; Kao, C.-L.; Vandavasi, J. K.; Wang, J.-J. *Org. Lett.* **2010**, *12*, 5570–5572; b) Mollin, J.; Kasperek, F.; Odlerova, Z.; Sindelar, Z. *Chem. Papers* **1986**, *40*, 239–246.
- [13] a) Imrie, C.; Cook, L.; Levendis, D. C. *J. Organomet. Chem.* **2001**, *637–639*, 266–275; b) Katada, T.; Nishida, M.; Kato, S.; Mizuta, M. *J. Organomet. Chem.* **1977**, *129*, 189–196.
- [14] a) Heinze, K.; Schlenker, M. *Eur. J. Inorg. Chem.* **2004**, 2974–2988; b) Okamura, T.; Sakauye, K.; Ueyama, N.; Nakamura, A. *Inorg. Chem.* **1998**, *37*, 6731–6736; c) Barišić, L.; Rapić, V.; Kovač, V. *Croat. Chem. Acta* **2002**, *75*, 199–210.
- [15] a) Jesberger, M.; Davis, T. P.; Baner, L. *Synthesis* **2003**, 1929–1958; b) Murai, T. *Top. Curr. Chem.* **2005**, *251*, 247–272.
- [16] Wiberg, K. B.; Rush, D. J. *J. Am. Chem. Soc.* **2001**, *123*, 2038–2046.

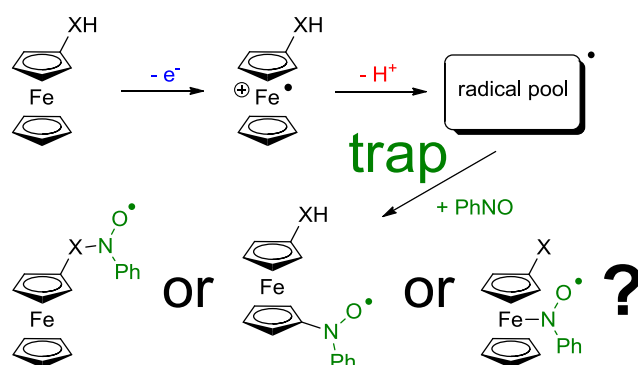
- [17] Okamura, T.-a.; Sakauye, K.; Doi, M.; Yamamoto, H.; Ueyama, N.; Nakamura, A. *Bull. Chem. Soc. Jpn.* **2005**, *78*, 1270–1278.
- [18] Lu, S.; Strelets, V. V.; Ryan, M. F.; Pietro, W. J.; Lever, A. B. P. *Inorg. Chem.* **1996**, *35*, 1013–1023.
- [19] Connelly, N. G.; Geiger, W. E. *Chem. Rev.* **1996**, *96*, 877–910.
- [20] a) Adams, J. J.; Curnow, O. W.; Huttner, G.; Smail, S. J.; Turnbull, M. M. *J. Organomet. Chem.* **1999**, *577*, 44–57; b) Musgrave, R. A.; Russell, A. D.; Manners, I. *Organometallics* **2013**, *32*, 5654–5667.
- [21] a) Siebler, D.; Förster, C.; Gasi, T.; Heinze, K. *Organometallics* **2011**, *30*, 313–327; b) Neidlinger, A.; Ksenofontov, V.; Heinze, K. *Organometallics* **2013**, *32*, 5955–5965.
- [22] Stoll, S.; Schweiger, A. *J. Magn. Reson.* **2006**, *178*, 42–55.
- [23] Frisch, M. J.; Trucks, G. W.; Schlegel, H. B.; Scuseria, G. E.; Robb, M. A.; Cheeseman, J. R.; Scalmani, G.; Barone, V.; Mennucci, B.; Petersson, G. A.; Nakatsuji, H.; Caricato, M.; Li, X.; Hratchian, H. P.; Izmaylov, A. F.; Bloino, J.; Zheng, G.; Sonnenberg, J. L.; Hada, M.; Ehara, M.; Toyota, K.; Fukuda, R.; Hasegawa, J.; Ishida, M.; Nakajima, T.; Honda, Y.; Kitao, O.; Nakai, H.; Vreven, T.; Montgomery, Jr., J. A.; Peralta, J. E.; Ogliaro, F.; Bearpark, M.; Heyd, J. J.; Brothers, E.; Kudin, K. N.; Staroverov, V. N.; Kobayashi, R.; Normand, J.; Raghavachari, K.; Rendell, A.; Burant, J. C.; Iyengar, S. S.; Tomasi, J.; Cossi, M.; Rega, N.; Millam, J. M.; Klene, M.; Knox, J. E.; Cross, J. B.; Bakken, V.; Adamo, C.; Jaramillo, J.; Gomperts, R.; Stratmann, R. E.; Yazyev, O.; Austin, A. J.; Cammi, R.; Pomelli, C.; Ochterski, J. W.; Martin, R. L.; Morokuma, K.; Zakrzewski, V. G.; Voth, G. A.; Salvador, P.; Dannenberg, J. J.; Dapprich, S.; Daniels, A. D.; Farkas, Ö.; Foresman, J. B.; Ortiz, J. V.; Cioslowski, J.; Fox, D. J. *Gaussian 09*, 2009, Revision A.02; Gaussian, Inc., Wallingford, CT.
- [24] *SMART Data Collection and SAINT-Plus Data Processing Software for the SMART System (various versions)*; Bruker Analytical X-Ray Instruments, Inc.: Madison, WI, 2000.
- [25] Blessing, B. *Acta Cryst.* **1995**, *A51*, 33–38.
- [26] Sheldrick, G. Ma. *SHELXTL*, Version 5.1; Bruker AXS: Madison, WI, 1998.

- [27] Sheldrick, G. M. *SHELXL-97*; University of Göttingen, Göttingen, Germany, 1997.

3.2 Spin Trapping of Carbon-Centered Ferrocenyl Radicals with Nitrosobenzene

Andreas Neidlinger,[‡] Torben Kienz,[‡] and Katja Heinze^{*}

Organometallics **2015**, *34*, 5310–5320.



Supporting information for this article (without Cartesian coordinates from DFT calculations) is found at pp. 163. For full supporting information refer to:

<http://pubs.acs.org/doi/suppl/10.1021/om500052k>

Adapted with permission from A. Neidlinger, T. Kienz, K. Heinze,
Organometallics **2015**, *34*, 5310–5320.

“This is an unofficial adaptation of an article that appeared in an ACS publication. ACS has not endorsed the content of this adaptation or the context of its use. Copyright. 2015 American Chemical Society.”

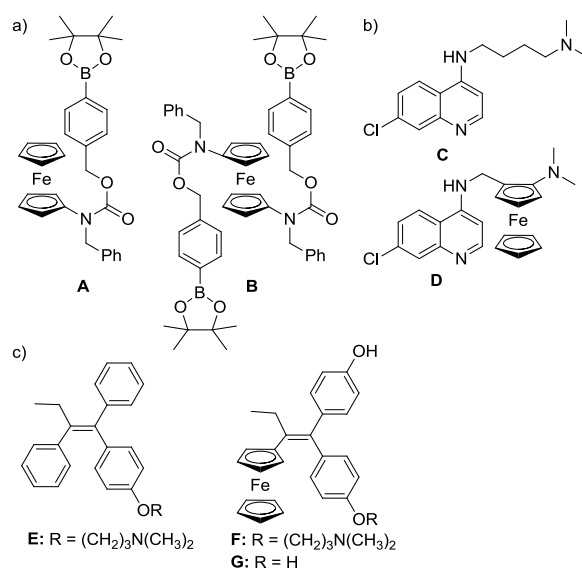
3.2.1 Abstract

In contrast to metal centered 17 valence electron radicals, such as $[\text{Mn}(\text{CO})_5]^{\bullet}$, ferrocenium ions $[\text{Fe}(\text{C}_5\text{H}_5)_2]^+$ (**1**⁺), $[\text{Fe}(\text{C}_5\text{Me}_5)_2]^+$ (**2**⁺), $[\text{Fe}(\text{C}_5\text{H}_5)(\text{C}_5\text{H}_4\text{Et})]^+$ (**3**⁺), $[\text{Fe}(\text{C}_5\text{H}_5)(\text{C}_5\text{H}_4\text{NHC}(\text{O})\text{Me})]^+$ (**4**⁺) and $[\text{Fe}(\text{C}_5\text{H}_5)(\text{C}_5\text{H}_4\text{NHC}(\text{S})\text{Me})]^+$ (**5**⁺) do not add to nitrosobenzene PhNO to give metal-coordinated stable nitroxyl radicals. In the presence of the strong and oxidatively stable phosphazene base *tert*-butylimino-tris(dimethylamino)-phosphorane the quite acidic ferrocenium ions **1**⁺ – **5**⁺ are deprotonated to give a pool of transient and persistent radicals with different deprotonation sites **[1–H^x][•]** – **[5–H^x][•]**. One rather persistent iron-centered radical **[4–H^N][•]**, deprotonated at the nitrogen atom, has been detected by rapid-freeze EPR spectroscopy at 77 K. This iron-centered radical **[4–H^N][•]** is also inert toward PhNO. The transient carbon-centered radicals **[1–H^x][•]** – **[5–H^x][•]** appear to rapidly abstract hydrogen atoms from the adjacent base or the solvent to regenerate the corresponding ferrocenes **1** – **5**. These transient radicals are only present in trace amounts (< 1%). However, some of the transient carbon-centered radicals in the radical pool can be trapped by 1 – 1.2 equiv of PhNO, even at room temperature. The corresponding resulting stable nitroxyl radicals **[6][•]** – **[10][•]** were studied by EPR spectroscopy at room temperature and at 77 K. The hyperfine coupling pattern to protons close to the spin center allows to assign the site of PhNO attack in radicals **[6][•]** – **[10][•]**, namely at the C₅H₅ ring in **[6][•]**, **[9^{Cp}][•]** and **[10^{Cp}][•]**, at a methyl group in **[7][•]** and at the methylene group in **[8¹][•]**. These studies give a deeper insight into the stability and reactivity of radicals derived from ferrocene derivatives which might also be relevant for the biological activity of high-potent antitumor and antimalaria ferrocene-based drugs and prodrugs such as ferrocifen or ferroquine.

3.2.2 Introduction

Ferrocene and its derivatives have been found useful for a variety of applications in fundamental research, especially electron transfer, in biology and catalysis, as well as in material and pharmaceutical science.¹⁻⁵ While many of these applications rely on the reversible oxidation chemistry of the ferrocenyl moiety, investigation of the reactivity and possible degradation pathways of the resulting ferrocenium cations is worthwhile.

For instance, ferrocene itself displays no antitumor activity, while ferrocenium derivatives show *in vitro* cytotoxicity due to oxidative damage of DNA.⁶ This has been further exploited using amino ferrocene based selective prodrugs **A** by Mohkir et al. (Scheme 1). In tumor cells, ferrocenes **A** are oxidized to the corresponding ferrocenium ions **A⁺**. The ferrocenium cations **A⁺**, as well as their degradation products, iron(II) ions, appear to catalyze the generation of reactive oxygen species. This increases the oxidative stress in cancer cells and finally leads to apoptosis.^{7,8} This concept has been further explored with a variety of amino ferrocene and diamino ferrocene based prodrugs (**B**; Scheme 1a). The degradation products of **B/B⁺** again act as catalysts for generating reactive oxygen species.⁹ In fact, first *in vivo* experiments show promising results for further pharmaceutical applications.¹⁰



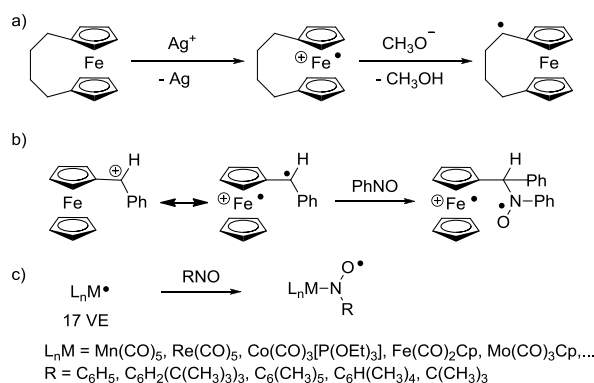
Scheme 1. a) Aminoferrocene based prodrugs A, B; b) chloroquine C and ferroquine D; c) tamoxifen E, ferrocifen F and ferrociphenol G.

The effectiveness of the antimalarial drug chloroquine **C** has been drastically improved by incorporation of a ferrocenyl moiety giving the potent drug ferroquine **D** (Scheme 1b). This adds the generation of reactive oxygen species as a further mode of action to the drug and takes effect in all stages of the live cycle of the parasites, thus inhibiting merozoites reinvasion.¹¹⁻¹³

While the generation of reactive oxygen species is a valuable mechanism for amino ferrocene based prodrugs **A** and **B** and ferroquine **D**, other antitumor agents appear to follow a different mode of action. The ferrocene derivatives of tamoxifen **E**, ferrocifen **F** and ferrociphenol **G** (Scheme 1c) show high levels of cytotoxicity against breast cancer cells. Ferrocifen **F** is even more cytotoxic than *cis*-platin.¹⁴⁻¹⁸ Both ferrocifen **F** and hydroxyferrocifen **G** cause less oxidative stress compared to tamoxifen **E**.^{19,20} Yet, in cells treated with ferrocifen derivatives a higher rate of senescence has been found. As this is unlikely to be related to oxidative stress a further mode of action is assumed showing the versatility of ferrocenium ions. Indeed, carbon-centered radicals have been proposed to be generated after oxidation and deprotonation of ferrocifens **F**.¹⁶

Various experiments have been reported which focus on the ability of ferrocene to form radicals itself. First hints to the existence of ferrocenyl radicals were obtained by photo- and thermolysis of ferrocenyl azide by Sutherland *et al.*²¹ γ -Irradiation of methylferrocene lead to the ferrocenyl methylradical.²² Later, it was found that ferrocenyl substituted radicals are stabilized due to spin delocalization to the iron atom.²³ This can even be exploited to generate polymetallocenylenes²⁴ or in stereoselective pinacol coupling reactions.²⁵

The radical reactivity of ferrocenium ions has been demonstrated by the oxidation of ferrocenophanes with silver salts in the presence of sodium methoxide. As reported by Hisatome *et al.*, this procedure results in the intermediate formation of a carbon-centered radical in the aliphatic bridge (Scheme 2a). Ferrocenylmethyl cations, as shown by Ashkenazi and Cais, react as biradicals with nitrosobenzene PhNO as spin trap (Scheme 2b).²⁶

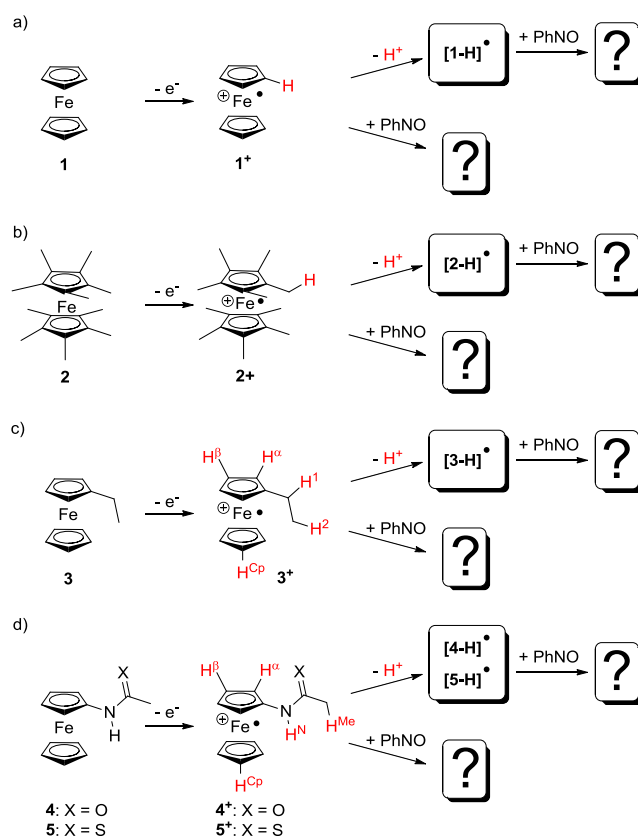


Scheme 2. a) Oxidation and deprotonation of a [4]ferrocenophane; b) spin trapping of a ferrocenylmethyl cation with nitrosobenzene and c) spin trapping of metal centered 17 valence electron radicals.

Obviously, spin trapping is a valuable tool for the investigation of transient radicals. Indeed, various manganese centered 17 valence electron radicals prepared by homolysis of carbonyl complexes could be spin trapped with nitrosodurene as spin trapping agent by Hudson and Lappert²⁷ as well as with 2,4,6-tri(*tert*-butyl)nitrosobenzene by Simpson et al.²⁸ and with the aid of nitroso-*tert*-butane by Benner and Balch.²⁹ Later on, Re, Co, Fe, and Mo centered 17 valence electron radicals could be trapped with 2,3,5,6-tetramethyl-1-nitrosobenzene as spin trapping agent and identified by EPR spectroscopy (Scheme 2c).³⁰

With the versatile and not yet fully understood reaction pathways of ferrocenium ions in mind, we were interested to generate and trap radical species of different ferrocenium ions under neutral and strongly basic conditions using the spin trapping technique. The starting iron(III) complexes ferrocenium (**1**⁺), decamethylferrocenium (**2**⁺), ethylferrocenium (**3**⁺), *N*-acetylaminoferrocenium (**4**⁺), and *N*-thioacetylaminoferrocenium (**5**⁺) were prepared by oxidation of the corresponding ferrocenes **1** – **5** with silver hexafluoroantimonate. Spin trapping of radicals was attempted with nitrosobenzene (PhNO) in the absence and presence of the strong non-nucleophilic, non-coordinating, and oxidatively stable phosphazene base P₁^tBu (*tert*-butylimino-tris(dimethylamino)-phosphorane (Scheme 3). In the presence of P₁^tBu, **1**⁺ – **5**⁺ are expected to yield the corresponding radicals or radical pools [**1**–**H**][•] – [**5**–**H**][•]. In order to address the question as to whether radicals are formed at all and to identify the site of the generated radicals (carbon, iron, nitrogen centered), the conceivable spin trapped nitroxide radical adducts of **1**⁺ – **5**⁺ and [**1**–**H**][•] – [**5**–**H**][•] were probed by EPR spectroscopy (Scheme 3).

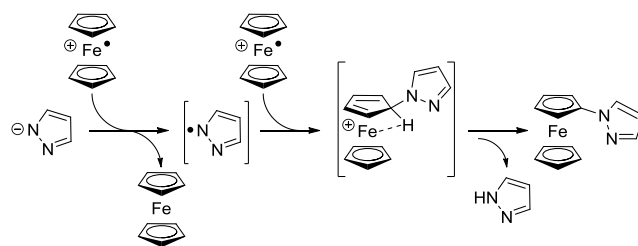
While ferrocenyl nitroxide radicals have been prepared via autoxidation of ferrocenyl hydrazine and investigated by EPR spectroscopy by Forrester and Hepburn, the present approach offers a different and more general access to ferrocenyl nitroxyl radicals.^{31a} Elschenbroich has reported the electrochemical generation and EPR spectroscopic study of isoelectronic radical anions of ferrocenyl arylketones.^{31b} Similarly, ferrocenyloxy silanes have been reduced to the corresponding radical anions by Grignard reagents.^{31c}



Scheme 3. Spin trapping reactions of ferrocenium derivatives in the absence and presence of P^tBu for a) 1⁺, b) 2⁺, c) 3⁺, and d) 4⁺ and 5⁺ investigated in this study. Relevant atom numbering is given. Possible acidic hydrogen atoms are marked in red.

Reactions of ferrocenium 1⁺ with nitrogen bases (pyrazolide, 3,5-dimethyl pyrazolide, imidazolide, and benzotriazolide) have been reported in the literature.³² Yet, these bases are oxidized by the ferrocenium cation 1⁺ to the corresponding azolide radicals while 1⁺ is reduced to 1. The azolide radicals are suggested to attack 1⁺ to give *N*-ferrocenyl azoles

after proton loss (Scheme 4). No ferrocenyl radicals were reported. Clearly, such a reactivity is not expected with the base P_1^tBu employed in this study.



Scheme 4. Suggested mechanism of the formation of *N*-ferrocenylpyrazole from ferrocenium radical cations and pyrazolide anions.³²

3.2.3 Results and Discussion

Spin Trapping of Ferrocenium Ions.

The oxidations of ferrocenes **1** – **5** to their respective cations 1^+ – 5^+ (Scheme 3) are performed in CH_2Cl_2 under inert conditions using one equivalent of silver hexafluoroantimonate $AgSbF_6$ as oxidant as its oxidation potential [$E_{1/2}(CH_2Cl_2) = 650$ mV vs. FcH/FcH^+]^{33a} is sufficient for this purpose [$E_{1/2}(CH_2Cl_2) = 0, -480, -55, -50, -20$ mV for **1** – **5**, respectively]³³. Furthermore, the coproduct silver is easily removed by filtration.

The presence of 1 – 1.2 equivalents of PhNO does not influence the EPR spectra of the ferrocenium ions. Indeed, 1^+ is EPR silent both at 298 K and at 77 K as its EPR spectrum has been observed only below 20 K due to fast spin-lattice relaxation.³⁴ No EPR resonances are observed in the presence of PhNO as well. Obviously, the iron-centered 17 valence electron radical 1^+ does not add to PhNO to give the conceivable nitroxide adduct $[1-PhNO]^+$, in contrast to what has been reported for $[Mn(CO)_5]^•$ radicals for example (Scheme 2c). DFT calculations for 1^+ , PhNO, and $[1-PhNO]^+$ account for this lack of reactivity as the formation of $[1-PhNO]^+$ is endergonic by 49 kJ mol⁻¹ (Supporting Information, Figure S1).

Similarly, 4^+ gives a nearly axial EPR resonance at 77 K in frozen solution³⁵ which remains unchanged in the presence of PhNO. At room temperature 4^+ and the 4^+ /PhNO mixture are EPR-silent. Obviously, iron-centered ferrocenium radical ions are unable to

react with PhNO to give the nitroxyl radicals. This behavior contrasts the reactivity of other organometallic 17 valence electron complexes (Scheme 2c).^{27–30}

Spin Trapping of Ferrocenium Ions in the Presence of a Base.

The ferrocenium ions $1^+ - 5^+$ were treated with one equivalent of the non-nucleophilic and noncoordinating phosphazene base P_1^tBu (*tert*-butylimino-tris(dimethylamino)-phosphorane, (pK_a (MeCN) = 26.98)³⁶ as a proton acceptor. To ensure that the ferrocenium salts $1^+ - 5^+$ are unable to oxidize the employed P_1^tBu base, its redox potential has been determined by cyclic voltammetry. Indeed, P_1^tBu is irreversibly oxidized at $E_p = 400$ mV vs. FcH/FcH⁺ ($[^nBu_4N][B(C_6F_5)_4]/CH_2Cl_2$), significantly higher than the redox potentials of the $1/1^+ - 5/5^+$ redox couples (Supporting Information, Figure S2). A mechanistic scenario as shown in Scheme 4 for heterocyclic nitrogen bases is possible in principle due to the irreversible nature of the $P_1^tBu / P_1^tBu^+$ oxidation, although it is not very likely. Hence, a simple deprotonation of $1^+ - 5^+$ to give the radicals and radical pools $[1-H]^{\bullet} - [5-H]^{\bullet}$ should be achieved (Scheme 3). As illustrated in Scheme 3, deprotonation of 1^+ and 2^+ should yield the radicals $[1-H]^{\bullet}$ and $[2-H]^{\bullet}$, respectively. As 3^+ , 4^+ and 5^+ possess five chemically different protons, which might be abstracted, radical pools consisting of up to five radical species might be present. The different radicals will be designated by the location of the abstracted proton as $[3-H^{Cp}]^{\bullet}$, $[3-H^{\alpha}]^{\bullet}$, $[3-H^{\beta}]^{\bullet}$, $[3-H^1]^{\bullet}$ and $[3-H^2]^{\bullet}$ for the radical pool $[3-H]^{\bullet}$, $[4-H^{Cp}]^{\bullet}$, $[4-H^{\alpha}]^{\bullet}$, $[4-H^{\beta}]^{\bullet}$, $[4-H^N]^{\bullet}$ and $[4-H^{Me}]^{\bullet}$ for the radical pool $[4-H]^{\bullet}$ and $[5-H^{Cp}]^{\bullet}$, $[5-H^{\alpha}]^{\bullet}$, $[5-H^{\beta}]^{\bullet}$, $[5-H^N]^{\bullet}$ and $[5-H^{Me}]^{\bullet}$ for the radical pool $[5-H]^{\bullet}$ (Scheme 3). Trapping of these radicals or some of these radicals by the spin trapping technique using nitrosobenzene PhNO is attempted. We will start with the simple ferrocene and decamethylferrocene derivatives $[1-H]^{\bullet}$ and $[2-H]^{\bullet}$ and then describe the more diverse reactivity of $[3-H]^{\bullet} - [5-H]^{\bullet}$. DFT calculations were employed both for the radical species $[1-H]^{\bullet} - [5-H]^{\bullet}$ as well as for the conceivable corresponding PhNO adducts $[6]^{\bullet} - [10]^{\bullet}$.

For the $1^+/PhNO/P_1^tBu$ mixture an EPR triplet resonance at $g_{iso} = 2.0063$ with nitrogen hyperfine coupling (hfc) $A(^{14}N) = 11.1$ G was recorded (Figure 1), similar to typical nitroxyl radicals.^{37–40} Furthermore, hyperfine couplings to hydrogen nuclei of the phenyl moiety and the substituted cyclopentadienyl ring are extracted from the simulation of the EPR resonance (Table 1). H^o , H^m , and H^p denote the *ortho*, *meta*, and *para* protons of the phenyl substituent, respectively, while H^{α} and H^{β} are the *alpha* and *beta* protons of the substituted Cp ring. The observed coupling pattern allows a clear assignment to the

ferrocenyl phenyl nitroxide radical **[6]**[•] (*N*-oxyl-*N*-phenyl-ferrocenylamine). The hfc to ¹⁴N in **[6]**[•] is close to the observed hfc in the reported nitroxide radical [Fc-N(O)-tBu][•] [$A(^{14}\text{N}) = 11.75 \text{ G}$].^{31a} Some phenyl hydrogen hfc's of **[6]**[•] are similar to those obtained for the isoelectronic radical anion [Fc-C(O)-Ph]^{•-}.^{31b} At 77 K a slightly anisotropic signal at $g_{\text{av}} \approx 2.0071$ with a large nitrogen hyperfine coupling of $A(^{14}\text{N}) = 26 \text{ G}$ in the high field region is recorded (Table 2; Supporting Information, Figure S4a). Hyperfine couplings to hydrogen atoms are not resolved in the frozen solution spectrum, and hence a larger linewidth was applied in the simulation instead.

Obviously, the increased acidity of the positively charged ferrocenium ion **1**⁺^{35,41} allows C-H deprotonation by P₁'Bu. The initially formed C-deprotonated zwitterionic ferrocenium species corresponds to an electronically excited state and relaxes to the carbon centered radical **[1-H]**[•] by internal electron transfer (Supporting Information, Figure S3a; Mulliken spin density at C 0.787; Mulliken spin density at Fe 0.212). The C-centered radical **[1-H]**[•] attacks the nitrogen atom of PhNO leading to the spin trapped nitroxyl radical *N*-oxyl-*N*-phenyl-ferrocenylamine **[6]**[•] (Figure 2a). DFT calculations revealed that the nitroxyl radical **[6]**[•] is lower in energy than the starting materials **[1-H]**[•] and PhNO by 208 kJ mol⁻¹ (Supporting Information, Figure S3a), explaining the facile formation of **[6]**[•].

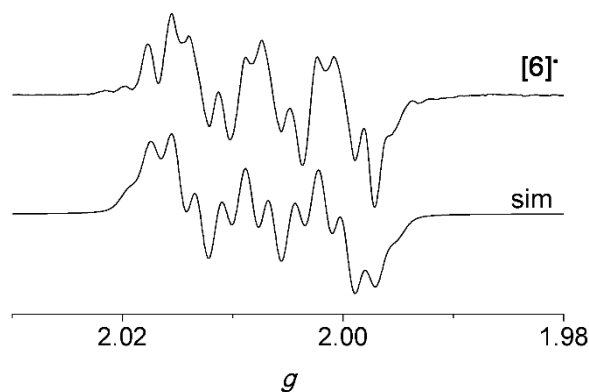


Figure 1. X-band EPR spectrum (top) and simulated spectrum (bottom) of **[6][•] (20 mM **1** in CH₂Cl₂) at the following experimental parameters: temperature = 298 K, field = 3358.98 G, sweep = 298.72 G, sweep time = 120 s, modulation = 1000 mG, MW attenuation = 9 db.**

Table 1. EPR parameters obtained by simulation of experimental spectra (298 K).

radical	g_{iso}	$A(^{14}\text{N})$ / G	$A(^1\text{H}^{\alpha}) /$ G (2 ×)	$A(^1\text{H}^{\beta}) /$ G (2 ×)	$A(^1\text{H}^{\gamma}) /$ G	$A(^1\text{H}^{\delta}) /$ G	$A(^1\text{H}^{\epsilon}) /$ G	$A(^1\text{H}^{\zeta}) /$ G	Gauss pp linewidth / MHz	Lorentz pp linewidth / MHz
[6]•	2.0063	11.10	2.90	0.80	2.70	3.80 (2 ×)	0.60 (2 ×)		0.15	0.08
[7]•	2.0068	11.07	2.77	0.95	2.64			8.64 (2 ×)	0.02	0.015
[8 ¹]•	2.0072	11.16	2.77	1.00	2.65			2.10	0.035	0.065
[9 ^{Cp}]•	2.0072	10.90	2.77	0.90	2.64	1.20 / 1.10	0.70 (2 ×)		0.06	0.02
[10 ^{Cp}]•	2.0068	11.09	2.77	0.91	2.64	2.55 / 2.10	1.82 / 1.08		0.085	0.005

Table 2. EPR parameters obtained by simulation of experimental spectra (77 K).

radical (mixture)	$g_{1,2,3}$	$A(^{14}\text{N}) /$ G	fraction / %	Gauss pp linewidth / MHz	Lorentz pp linewidth / MHz
[6]•	2.0104, 2.0068, 2.0040	4.0, 4.0, 26.0		0.90	0.30
[7]•	2.0094, 2.0067, 2.0048	4.0, 4.0, 26.0		1.50	0.60
[8 ¹]•	2.0095, 2.0073, 2.0045	3.0, 3.0, 27.5		0.90	0.40
[9 ^{Cp}]•	2.0105, 2.0060, 2.0045	3.5, 3.5, 28.0	17	0.30	0.40
[4-H ^N]•	N/A ^a , 1.9620, 1.9450	N/A	83	0.50	0.20
[4-H ^N]• (x = $\alpha, \beta, \text{Cp}, \text{Me}$)	2.0095, 2.0065, 2.0030		0.8	0.30	0.2
[4-H ^N]•	N/A ^a , 1.9650, 1.9400		99.2	0.1	0.1
[10 ^{Cp}]•	2.0105, 2.0060, 2.0020	3.5, 3.5, 28.0	5	0.60	0.60
[11a]•	2.3100, 2.0695, 1.9990		48	0.50	0.50
[11b]•	2.2250, 2.0565, 2.0095		47	0.50	0.50

a) Too broad to be observed.

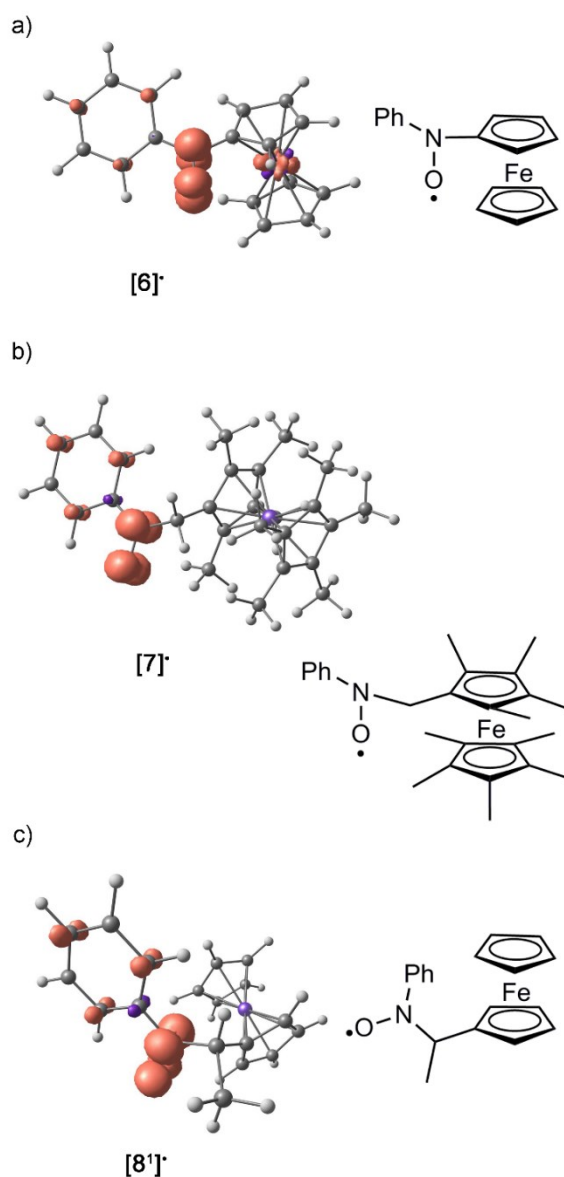


Figure 2. DFT optimized geometries with spin densities (0.01 a.u. isosurface value) in CH_2Cl_2 continuum solvent as well as Lewis structures of nitroxide radicals a) $[\mathbf{6}]^\bullet$, b) $[\mathbf{7}]^\bullet$, and c) $[\mathbf{8}]^\bullet$.

Successful deprotonation of $\mathbf{1}^+$ with P_1^tBu was further evidenced by cyclic voltammetry of $\mathbf{1}$ in the absence and presence of the base using tetra(*n*-butyl)ammonium tetrakis(pentafluorophenyl)borate ($[\text{nBu}_4\text{N}][\text{B}(\text{C}_6\text{F}_5)_4]$) as weakly coordinating electrolyte.^{42,43} Expectedly, ferrocene $\mathbf{1}$ shows a reversible one-electron redox process at a potential of $E_{1/2} = 0$ V vs. FcH/FcH^+ per definition (Supporting Information, Figure S5a). Addition of a stoichiometric amount of P_1^tBu renders this oxidation irreversible, due to the

deprotonation of $\mathbf{1}^+$ to $[\mathbf{1-H}]^\bullet$ and follow up reactions of the highly reactive C-centered radical $[\mathbf{1-H}]^\bullet$ (Supporting Information, Figure S5b). As the oxidation process occurs at essentially the same potential (against the Ag/AgNO₃ reference electrode) in the presence of P₁^tBu, deprotonation of $\mathbf{1}$ to $[\mathbf{1-H}]^-$ by P₁^tBu prior to oxidation is unlikely. Deprotonation of ferrocene $\mathbf{1}$, however, is achieved using alkyl lithium bases as a well-known starting point for the rich ferrocene substitution chemistry.^{44–47}

Despite the lack of aromatic C-H atoms, decamethylferrocenium $\mathbf{2}^+$ reacts with PhNO as well in the presence of P₁^tBu (Scheme 3b). Obviously, the methyl groups become sufficiently acidic upon oxidation of $\mathbf{2}$ to $\mathbf{2}^+$ due to the increased electron deficiency. Hence, the C-centered radical $[\mathbf{2-H}]^\bullet$ is generated from $\mathbf{2}^+$ by deprotonation of a CH₃ group (Supporting Information, Figure S3b, Mulliken spin density at C 0.650; Mulliken spin density at Fe 0.513). Similar to $[\mathbf{1-H}]^\bullet$, $[\mathbf{2-H}]^\bullet$ is trapped by PhNO resulting in the formation of the nitroxide radical $[\mathbf{7}]^\bullet$ 1-[(N-oxy-N-phenylamino)methyl]-1',2,2',3,3',4,4',5,5'-nonamethylferrocene (Figure 2b). The driving force for the formation of $[\mathbf{7}]^\bullet$ from the starting materials $[\mathbf{2-H}]^\bullet$ and PhNO (Supporting Information, Figure S3b) is calculated as 80 kJ mol⁻¹ by DFT methods. At 298 K $[\mathbf{7}]^\bullet$ gives an EPR resonance with parameters summarized in Table 1 (Figure 3). The nitrogen and hydrogen hyperfine couplings for the PhNO moiety of $[\mathbf{7}]^\bullet$ are very similar to those of $[\mathbf{6}]^\bullet$. The two large hydrogen hyperfine couplings of $[\mathbf{7}]^\bullet$ ($A(^1\text{H}) = 8.64$ G), obtained by simulation, are assigned to the protons of the methylene group. The large hfc's nicely fit to the reported hfc's for the ferrocenylmethyl radical prepared from methylferrocene by γ -irradiation ($A(^1\text{H}) = 14.71$ G).²² At 77 K in frozen solution the nitroxide radical $[\mathbf{7}]^\bullet$ displays a slightly anisotropic resonance similar to $[\mathbf{6}]^\bullet$ (Supporting Information, Figure S4b) with one large nitrogen hyperfine coupling component (Table 2). Again, hydrogen hyperfine couplings are not resolved under these conditions.

In contrast to $\mathbf{1}$ and $\mathbf{2}$, ethylferrocene $\mathbf{3}$ has five chemically different protons resulting in five conceivable C-centered radicals $[\mathbf{3-H}^{\text{Cp}}]^\bullet$, $[\mathbf{3-H}^\alpha]^\bullet$, $[\mathbf{3-H}^\beta]^\bullet$, $[\mathbf{3-H}^1]^\bullet$, and $[\mathbf{3-H}^2]^\bullet$ (Scheme 3c). Consequently, five distinct nitroxyl radicals can in principle be obtained from this radical pool by reaction with PhNO, namely $[\mathbf{8}^{\text{Cp}}]^\bullet$, $[\mathbf{8}^\alpha]^\bullet$, $[\mathbf{8}^\beta]^\bullet$, $[\mathbf{8}^1]^\bullet$, and $[\mathbf{8}^2]^\bullet$. Despite the possible mixture of products, the room temperature EPR spectrum of $[\mathbf{8}]^\bullet$ is well resolved suggesting the presence of only a single nitroxide radical. The EPR pattern of $[\mathbf{8}]^\bullet$ is well reproduced by assuming the typical ¹⁴N and ¹H hfc's of the PhNO unit in addition

to a further hfc to a single hydrogen atom (Table 1). This perfectly fits to the $[8^1]^\bullet$ nitroxide radical with the PhNO substituent attached to the C^1 atom of the ethyl substituent. For all other nitroxide radicals $[8^{Cp}]^\bullet$, $[8^\alpha]^\bullet$, $[8^\beta]^\bullet$, and $[8^2]^\bullet$ more than one chemically different hydrogen atom would have been expected to display hfc's. At 77 K a similar spectrum as for $[6]^\bullet$ is recorded for $[8^1]^\bullet$ (Table 2; Supporting Information, Figure S4c).

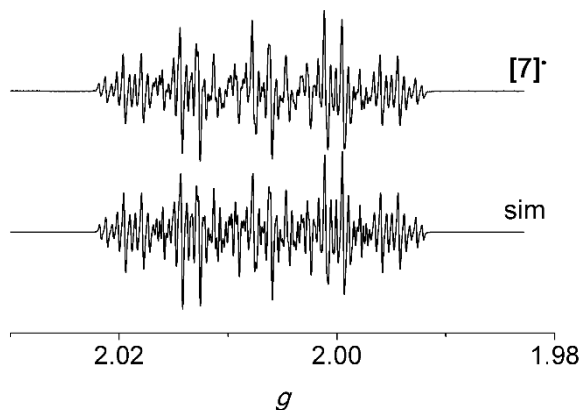


Figure 3. X-band EPR spectrum (top) and simulated spectrum (bottom) of $[7]^\bullet$ (25 mM **2 in CH_2Cl_2) at the following experimental parameters: temperature = 298 K, field = 3346.20 G, sweep = 94.79 G, sweep time = 90 s, modulation = 250 mG, MW attenuation = 5 db.**

The presence of only a single product $[8^1]^\bullet$ derived from $[3-H^1]^\bullet$ is straightforwardly explained by the pronounced stability of the secondary C -centered radical $[3-H^1]^\bullet$ by more than 60 kJ mol^{-1} with respect to all other radicals $[3-H^{Cp}]^\bullet$, $[3-H^\alpha]^\bullet$, $[3-H^\beta]^\bullet$, and $[3-H^2]^\bullet$ according to DFT calculations (Supporting Information, Figure S6, Mulliken spin density at C^1 0.757; Mulliken spin density at Fe 0.341). However, all five conceivable nitroxide radicals $[8^{Cp}]^\bullet$, $[8^\alpha]^\bullet$, $[8^\beta]^\bullet$, $[8^1]^\bullet$, and $[8^2]^\bullet$ are quite similar in energy (Supporting Information, Figure S7). The driving force for the formation of $[8^1]^\bullet$ from $[3-H^1]^\bullet$ and PhNO amounts to 81 kJ mol^{-1} (Supporting Information, Figure S7). Hence, the product distribution is controlled by the relative stability of the C -centered radical $[3-H^1]^\bullet$ but not by the relative stability of the product nitroxide radical $[8^1]^\bullet$.

In order to gain insight into the reactivity of NH-containing ferrocenyl compounds, which are substructures of cytotoxic prodrugs **A** and **B** and antimalarial drugs **D** (Scheme 1),^{7,9-13} we investigated the reactivity of the simple oxo- and thioamides, namely N -

acetylaminoferrocenium 4^+ (Scheme 3d), and *N*-thioacetylaminoferrocenium 5^+ in the presence of the P_1^tBu base.

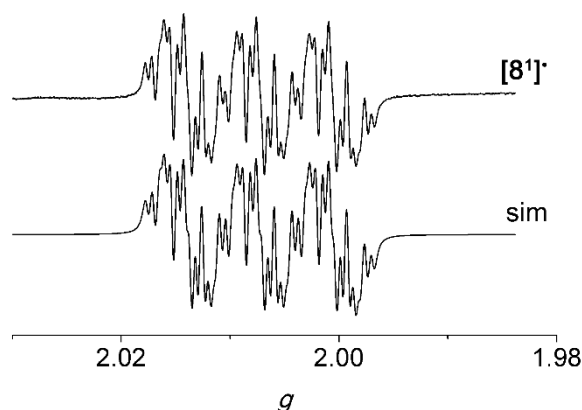


Figure 4. X-band EPR spectrum (top) and simulated spectrum (bottom) of $[8^1]^\bullet$ (25 mM **3 in CH_2Cl_2) at the following experimental parameters: temperature = 298 K, field = 3346.20 G, sweep = 94.79 G, sweep time = 90 s, modulation = 250 mG, MW attenuation = 0 db.**

Because of the presence of five chemically different protons in **4**, five distinct radicals $[4-H^{Cp}]^\bullet$, $[4-H^\alpha]^\bullet$, $[4-H^\beta]^\bullet$, $[4-H^N]^\bullet$ and $[4-H^{Me}]^\bullet$ can be conceived in the radical pool $[4-H]^\bullet$ (Scheme 3d). The same holds analogously for **5**. This translates to the corresponding nitroxide radicals $[9^{Cp}]^\bullet$, $[9^\alpha]^\bullet$, $[9^\beta]^\bullet$, $[9^N]^\bullet$, and $[9^{Me}]^\bullet$ derived from 4^+ and PhNO and $[10^{Cp}]^\bullet$, $[10^\alpha]^\bullet$, $[10^\beta]^\bullet$, $[10^N]^\bullet$, and $[10^{Me}]^\bullet$ derived from the thioanalogue 5^+ and PhNO. Similar to the situation observed for $[8^1]^\bullet$, the room temperature EPR spectrum of $[9]^\bullet$ is rather well resolved, suggesting that only one or two nitroxide radical species are present (Figure 5). The main features of the experimental EPR resonance of $[9]^\bullet$ can be simulated by the expected hfc's to the PhNO moiety (^{14}N , H^o , H^m , H^p , Table 1) and coupling to four protons of 1.2 G (1H), 1.1 G (1H) and 0.70 G (2H). Further, small differences between the simulated and the experimental spectrum are associated to the presence of a second nitroxide radical with rather similar parameters. However, simulation of a full second parameter set would lead to severe over-parametrization of the simulation. Hence, we note, that the hfc's to ferrocene protons are less well defined for $[9]^\bullet$ than for $[6]^\bullet$, $[7]^\bullet$, and $[8^1]^\bullet$. The presence of four protons close to the radical center suggest the $[9^{Cp}]^\bullet$ nitroxide radical derived from $[4-H^{Cp}]^\bullet$ as the major trapped species (Figure 6). In $[9^{Cp}]^\bullet$ the hfc to H^α is smaller than that in $[6]^\bullet$ and furthermore, two slightly different hfc's to chemically different H^α atoms are

found for $[9^{CP}]^{\bullet}$ (Table 1). The larger hfc to H^{α} in $[6]^{\bullet}$ is easily traced back to the favorable coplanar orientation of the NO unit with the C_5H_4 ring ($O-N-C^{ipso}-C^{\alpha} = -23.0^{\circ}$) as compared to the corresponding torsion angle in $[9^{CP}]^{\bullet}$ ($O-N-C^{ipso}-C^{\alpha} = -31.4^{\circ}$). The larger twist in $[9^{CP}]^{\bullet}$ arises from an intramolecular $NH(\text{amide})\cdots O(\text{nitroxyl})$ hydrogen bond (Figure 6). Similar intramolecular hydrogen bonds have been amply observed in ferrocenyl polyamides.^{49–51} This hydrogen bond furthermore provides a straightforward explanation for the chemically different $H^{\alpha}/H^{\alpha'}$ protons.

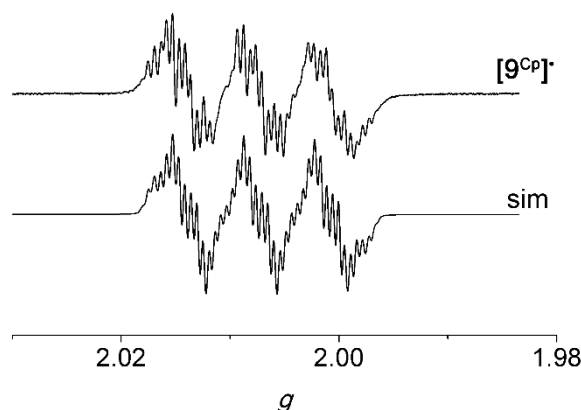


Figure 5. X-band EPR spectrum (top) and simulated spectrum (bottom) of $[9^{CP}]^{\bullet}$ (25 mM **4 in CH_2Cl_2) at the following experimental parameters: temperature = 298 K, field = 3346.20 G, sweep = 94.79 G, sweep time = 90 s, modulation = 1000 mG, MW attenuation = 10 db.**

Expectedly, in the radical pool $[4-H]^{\bullet}$ the nitrogen-deprotonated radical $[4-H^N]^{\bullet}$ is the most stable one (Supporting Information, Figure S9). However, this radical is essentially iron-centered with a Mulliken spin density at iron of 1.248 with some small contribution of the nitrogen atom (Mulliken spin density at N 0.016). Attack of PhNO at iron is excluded based on the general lack of reactivity of ferrocenium ions towards PhNO. Attack of PhNO at the nitrogen atom of $[4-H^N]^{\bullet}$ to give $[9^N]^{\bullet}$ is calculated to be disfavored by 37 kJ mol^{-1} relative to the starting materials $[4-H^N]^{\bullet}$ and PhNO (Figure 6). A ring-slipped isomer $[4-H^{N'}]^{\bullet}$ has been calculated as well, yet its spin density is also localized at the iron atom (Mulliken spin density at Fe 1.268), precluding the reaction of $[4-H^{N'}]^{\bullet}$ with PhNO (Figure S9). The calculated ring-slipped structure of $[4-H^{N'}]^{\bullet}$ suggests a viable decomposition

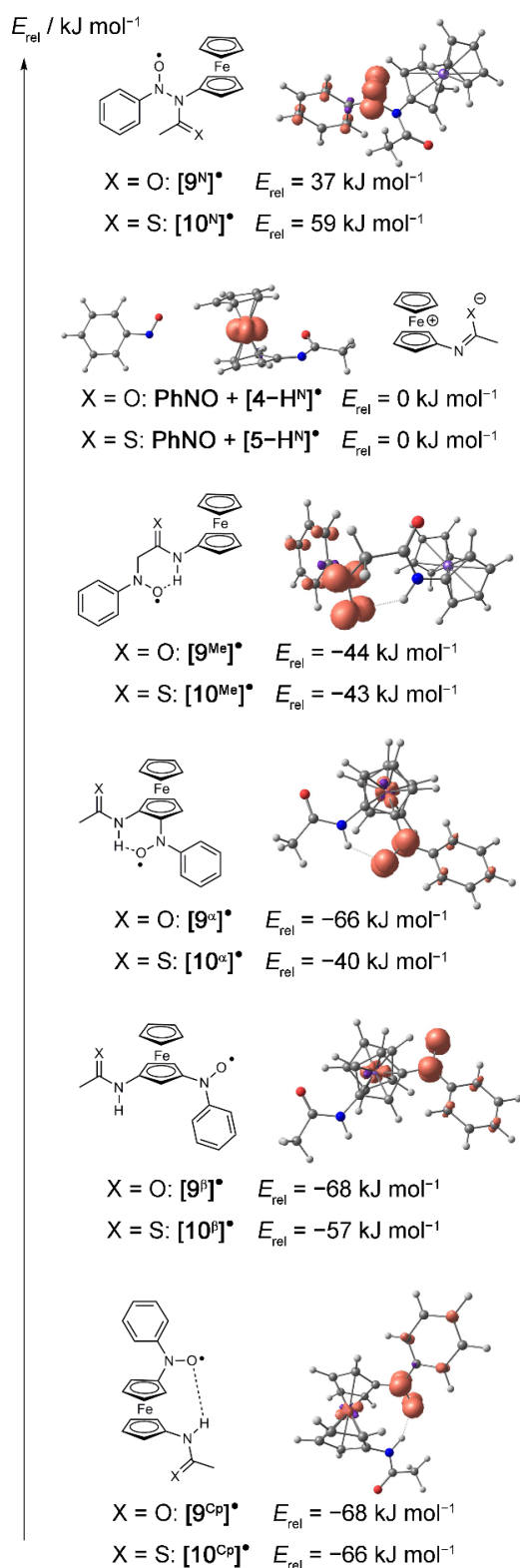


Figure 6. DFT optimized geometries with spin densities for $[9^{\text{x}}]^*$ ($\text{x} = \alpha, \beta, \text{Cp}, \text{N}, \text{Me}$) (0.01 a.u. isosurface value) and energies in CH_2Cl_2 continuum solvent for $[9^{\text{x}}]^*$ and $[10^{\text{x}}]^*$ ($\text{x} = \alpha, \beta, \text{Cp}, \text{N}, \text{Me}$) as well as Lewis structures.

pathway of radicals $[4-H]^{\bullet}$ releasing the substituted cyclopentadienyl ligand as *N*-acetyl-2,4-cyclopentadien-1-imine. Indeed, the formation of di(cyclopentadiene) and di(aminocyclopentadiene) has been observed in the reaction of prodrugs **A** with H_2O_2 (Scheme 1).⁷

In addition to these PhNO-resistant iron-centered radicals $[4-H^N]^{\bullet}$ and $[4-H^{N'}]^{\bullet}$ the radicals $[4-H^{Cp}]^{\bullet}$, $[4-H^{\alpha}]^{\bullet}$, $[4-H^{\beta}]^{\bullet}$, and $[4-H^{Me}]^{\bullet}$ deprotonated at carbon atoms were calculated by DFT (Figure S9). The reactions of $[4-H^{Cp}]^{\bullet}$, $[4-H^{\alpha}]^{\bullet}$, $[4-H^{\beta}]^{\bullet}$, and $[4-H^{Me}]^{\bullet}$ and PhNO to $[9^{Cp}]^{\bullet}$, $[9^{\alpha}]^{\bullet}$, $[9^{\beta}]^{\bullet}$, and $[9^{Me}]^{\bullet}$, respectively, are thermodynamically feasible (Figure 6). Interestingly, $[4-H^{\alpha}]^{\bullet}$ mainly features spin density at the iron center (Mulliken spin density at Fe 1.251) and is hence considered unreactive towards PhNO, so $[9^{\alpha}]^{\bullet}$ should not be observed. In $[4-H^{Me}]^{\bullet}$ the spin density is smeared over the nitrogen, oxygen, and CH_2 units of the substituent. This spin delocalization reduces the probability of PhNO attack and hence $[9^{Me}]^{\bullet}$ is not particularly favored as well. The remaining two highly reactive radicals $[4-H^{Cp}]^{\bullet}$ and $[4-H^{\beta}]^{\bullet}$, although high in energy, might account for the observed EPR pattern with $[9^{Cp}]^{\bullet}$ derived from $[4-H^{Cp}]^{\bullet}$ being the major and $[9^{\beta}]^{\bullet}$ derived from $[4-H^{\beta}]^{\bullet}$ being the minor species based on simple statistical arguments. This interpretation agrees with the EPR spectral data. While the radicals $[4-H^{Cp}]^{\bullet}$ and $[4-H^{\beta}]^{\bullet}$ of the radical pool can be trapped by PhNO, $[4-H^N]^{\bullet}$ and $[4-H^{N'}]^{\bullet}$ are inert towards PhNO. In order to possibly detect the rather persistent and PhNO-resistant Fe-centered radical $[4-H^N]^{\bullet}$ rapid-freeze EPR techniques have been employed.

The EPR spectrum recorded at 77 K rapidly after deprotonation of 4^+ in the presence of PhNO shows a characteristic broad ferrocenium-based resonance (83 %) in addition to the slightly anisotropic nitrogen-split triplet resonance of a nitroxide radical with one large hfc to ^{14}N (17 %) (Figure 7, Table 2). The latter EPR resonance is very similar to the corresponding resonance of **[6]**[•] and is hence safely assigned to already formed nitroxide radicals $[9^{Cp/\beta}]^{\bullet}$. The broad ferrocenium resonance ($g_{1,2,3} = N/A$, 1.9650, 1.9400, Table 2), however, clearly differs from the EPR resonance of the ferrocenium ion 4^+ ($g_{1,2,3} = 3.3500$, 1.8750, 1.7870).³⁵ Hence, the resonance is assigned to $[4-H^N]^{\bullet}$. This iron-centered radical is unable to react with PhNO itself, but equilibrates with radical species deprotonated at carbon atoms $[4-H^x]^{\bullet}$ ($x = \alpha, \beta, Cp, Me$). After annealing the sample to room temperature for 5 min and refreezing to 77 K, the ferrocenium resonance of $[4-H^N]^{\bullet}$ has vanished, and only the resonance of the nitroxide radicals $[9^{Cp/\beta}]^{\bullet}$ remained.

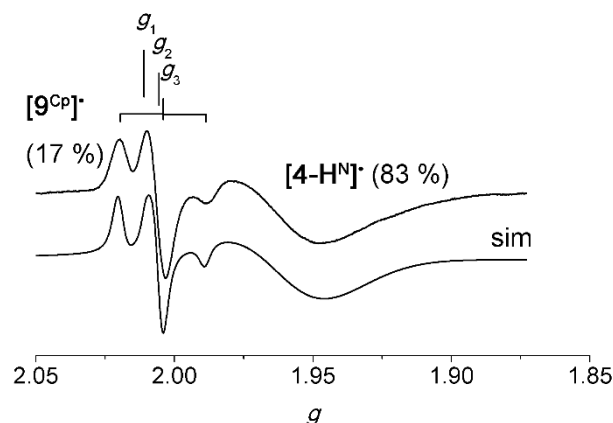
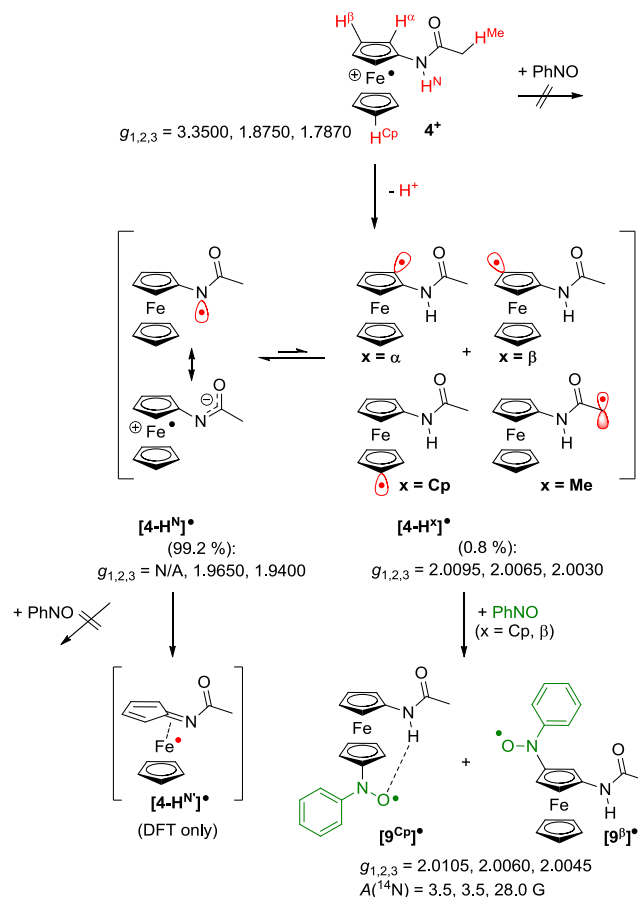


Figure 7. X-band EPR spectrum (top) and simulated spectrum (bottom) of $[9^{Cp}]^{\bullet}$ / $[4-H^N]^{\bullet}$ (25 mM 4 in CH_2Cl_2) at the following experimental parameters: temperature = 77 K, field = 3346.20 G, sweep = 499.77 G, sweep time = 90 s, modulation = 5000 mG, MW attenuation = 10 db.

In the absence of PhNO, rapid-freeze EPR spectroscopy of the 4^+ / P_1^tBu mixture yields an EPR spectrum displaying the resonance assigned to $[4-H^N]^{\bullet}$ (99.2 %) (Figure S8a). This finding supports the above assignment. Furthermore, a weak, but significant slightly anisotropic resonance at $g = 2.0$ without resolved hyperfine couplings is detected (0.8 %) (Table 2, Figure S8a). This resonance is assigned to traces of the carbon-centered radicals $[4-H^x]^{\bullet}$ ($x = \alpha, \beta, Cp, Me$) of the radical pool $[4-H]^{\bullet}$ (Table 2). At room temperature, this sample exhibits a transient EPR resonance without discernible hfc's at $g_{iso} = 2.0078$ (Supporting Information, Figure S8b) which is assigned to the C-centered radicals $[4-H^x]^{\bullet}$ ($x = \alpha, \beta, Cp, Me$) as well. The proposed reactivity of 4^+ in the presence of a base is summarized in Scheme 5. Deprotonation of 4^+ gives the radical pool $[4-H]^{\bullet}$ with $[4-H^N]^{\bullet}$ being the most stable and abundant radical (99.2 %). Neither 4^+ nor $[4-H^N]^{\bullet}$ react with PhNO. Less than one percent of the observed radicals are carbon-centered radicals $[4-H^x]^{\bullet}$ ($x = \alpha, \beta, Cp, Me$). However, two of these, namely $[4-H^{Cp}]^{\bullet}$ and $[4-H^{\beta}]^{\bullet}$, can be trapped by PhNO to give the respective nitroxide radicals $[9^{Cp}]^{\bullet}$ and $[9^{\beta}]^{\bullet}$. Quantification⁵² of the nitroxide radical species $[9^{Cp}]^{\bullet}$ and $[9^{\beta}]^{\bullet}$ with respect to external calibration with DPPH reveals that indeed less than 1 % of the original ferrocenium radical 4^+ is transformed into the nitroxides $[9^{Cp}]^{\bullet}$ and $[9^{\beta}]^{\bullet}$. One possible decomposition pathway of the radicals via the ring-slipped isomer $[4-H^N]^{\bullet}$ is proposed on the basis of DFT calculations of $[4-H^N]^{\bullet}$.



Scheme 5. Suggested radical reactivity of 4^+ in the presence of a base and PhNO; EPR data (77 K) of identified intermediates given.

Further radical reactivity might be hydrogen atom abstraction from the solvent or the base to give the starting material **4**. Indeed, quenching the radical pool $[4-H]^{\bullet}$ by hydrazine hydrate essentially quantitatively recovers ferrocene **4** as shown by ^1H NMR spectroscopy.

The successful deprotonation of 4^+ to the radical pool $[4-H]^{\bullet}$ is furthermore evidenced by cyclic voltammetry. At 298 K in $\text{CH}_2\text{Cl}_2/[\text{nBu}_4\text{N}][\text{B}(\text{C}_6\text{F}_5)_4]$ a reversible one-electron process is observed at $E_{1/2} = -50$ mV vs. FcH/FcH^+ and assigned to the $4/4^+$ couple (S10a). After addition of stoichiometric amounts of P_1^tBu , this process is replaced by an irreversible oxidation at $E_p = -175$ mV vs. FcH/FcH^+ (Figure S10b). The lower potential of the $4/4^+$ couple in the presence of P_1^tBu is ascribed to coordination of the base to the amide unit of **4** via a hydrogen bond. Oxidation to 4^+ acidifies this NH proton, and the proton is transferred to the base giving the radicals $[4-H]^{\bullet}$, with $[4-H^{\text{N}}]^{\bullet}$ being the major product. Reduction of the rather persistent radical $[4-H^{\text{N}}]^{\bullet}$ occurs at $E_p' = -890$ mV vs. FcH/FcH^+

(Figure S10b). These results reflect the intimate coupling of proton transfer and electron transfer reactions in ferrocenium amides as reported in the literature.^{35,49–51}

In order to investigate the effect of O → S exchange in the amide for the spin trapping experiments in the presence of P₁'Bu, we employed thioamide **5** as sulfur analogue of **4**.⁵¹ Similar to **4**⁺, a radical pool [**5**-H^{Cp}][•], [**5**-H^α][•], [**5**-H^β][•], [**5**-H^N][•] and [**5**-H^{Me}][•] is established after deprotonation of **5**⁺. (Scheme 5) Fully paralleling the energies of the corresponding radicals [**4**-H][•], the most stable one is the iron-centered radical [**5**-H^N][•] (Figure S9) while the ring and side chain radicals [**5**-H^{Cp}][•], [**5**-H^α][•], [**5**-H^β][•] and [**5**-H^{Me}][•] are higher in energy.

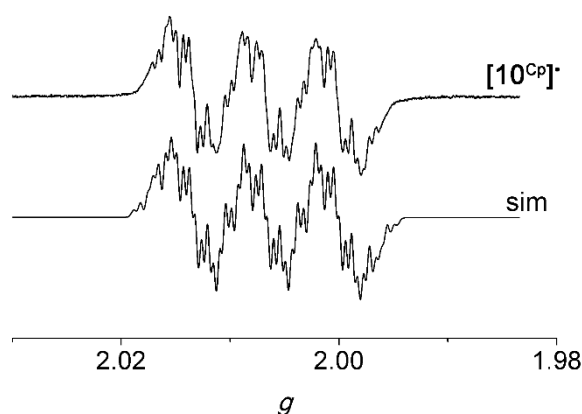


Figure 8. X-band EPR spectrum (top) and simulated spectrum (bottom) of [10^{Cp}][•] (25 mM **5 in CH₂Cl₂) at the following experimental parameters: temperature = 298 K, field = 3346.20 G, sweep = 94.79 G, sweep time = 90 s, modulation = 1000 mG, MW attenuation = 10 db.**

The EPR spectrum obtained from the **5**⁺/PhNO/P₁'Bu mixture at room temperature is very well simulated by a single set of parameters (Figure 8, Table 1). The hfc's are consistent with the nitroxide radical [10^{Cp}][•]. Similar to [9^{Cp}][•], hyperfine coupling to the H^α atoms is split due to the chemical dissimilarity of H^α and H^{α'} in [10^{Cp}][•] featuring an intramolecular NH(thioamide)⋯O(nitroxide) hydrogen bond (Figure 6). According to the DFT calculations this hydrogen bond is shorter in [10^{Cp}][•] (NH⋯O 1.885 Å) than in [9^{Cp}][•] (NH⋯O 1.984 Å), suggesting a stronger bond in [10^{Cp}][•] in agreement with the increased acidity of thioamides.⁵¹ The stronger intramolecular hydrogen bond might also lead to a more

pronounced differentiation between H^α and $H^{\alpha'}$. In fact, even the β -hydrogen atoms become chemically inequivalent and yield different hfc's in $[10^{Cp}]^\bullet$ (Table 1). The larger hfc to $H^\alpha/H^{\alpha'}$ in $[10^{Cp}]^\bullet$ than in $[9^{Cp}]^\bullet$ might be associated with the smaller torsion angle $O-N-C^{ipso}-C^\alpha = -25.1^\circ$ in $[10^{Cp}]^\bullet$.

In order to observe iron-centered radicals, the 5^+ /PhNO/ P_1^t Bu reaction mixture was subjected to EPR spectroscopy at 77 K (Figure 9). The EPR spectrum displays three discernible resonances. One resonance originates from the spin trapped product $[10^{Cp}]^\bullet$ (5 %) bearing close resemblance to the resonance of the amide nitroxide radical $[9^{Cp}]^\bullet$ (Table 2). The other two rhombic resonances, present in nearly equal intensities (48 %; 47 %; Table 2), appear to correlate to follow-up products $[11a]^\bullet$ and $[11b]^\bullet$ of the initially formed radicals $[5-H]^\bullet$. The identity of these follow-up products is as yet unknown. In the absence of PhNO, the resonances of these follow-up products $[11a]^\bullet$ and $[11b]^\bullet$ are observed as well (Figure 10). This finding eliminates a reaction with PhNO as being responsible for the formation of $[11a]^\bullet$ and $[11b]^\bullet$. In the absence of PhNO, the resonance of the 5^+ cation⁵¹ is observed additionally (Table 2, Figure 10). Hence, $[11a]^\bullet$ and $[11b]^\bullet$ seem to be associated to follow-up products of the sulfur substituent $[5-H]^\bullet$, independent of the presence of PhNO.

While it has been reported previously that the chemical reactivity and properties of ferrocenyl thioamides can differ from the chemistry of the corresponding amides,⁵¹ C -radical reactivity in the presented spin trapping reaction results in the analogous product(s) $[9^{Cp/\beta}]^\bullet$ and $[10^{Cp}]^\bullet$. Yet, the sulfur atom appears to open further reaction pathways yielding radicals $[11a]^\bullet$ and $[11b]^\bullet$. Their investigation is beyond the scope of the present study and will be reported elsewhere.

Obviously, oxidized ferrocenyl amides and thioamides 4^+ and 5^+ can be easily deprotonated at their respective nitrogen atoms yielding the metal centered radicals $[4-H^N]^\bullet$ (observed by rapid-freeze EPR) and $[5-H^N]^\bullet$. These iron-centered radicals are even resistant towards reaction with PhNO. Yet, the N -deprotonated tautomers $[4-H^N]^\bullet$ and $[5-H^N]^\bullet$ can isomerize to reactive C -deprotonated species $[4-H^x]^\bullet$ and $[5-H^x]^\bullet$ to a small extent ($x = \alpha, \beta, Cp, Me$). Some of these C -centered radicals $[4-H^x]^\bullet$ and $[5-H^x]^\bullet$ can be trapped by PhNO (<1%) to give the stable nitroxyl radicals $[9^{Cp/\beta}]^\bullet$ and $[10^{Cp}]^\bullet$. In the presence of a base even two more radical species $[11a]^\bullet$ and $[11b]^\bullet$ are detected for the sulfur derivative 5^+ by EPR in the reaction mixture. $[11a]^\bullet$ and $[11b]^\bullet$ are inert towards

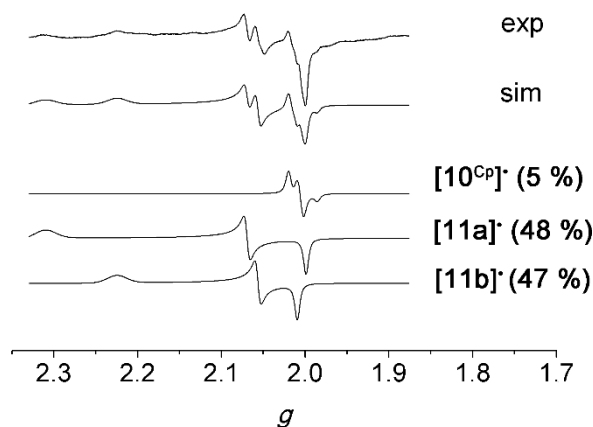


Figure 9. X-band EPR spectrum (exp) and simulated spectrum (sim) of [10^{Cp}][•] consisting of three components [10^{Cp}][•], [11a][•], and [11b][•]; (5 mM 5 in CH₂Cl₂) at the following experimental parameters: temperature = 77 K, field = 3245.45 G, sweep = 697.96 G, sweep time = 90 s, modulation = 5000 mG, MW attenuation = 10 db.

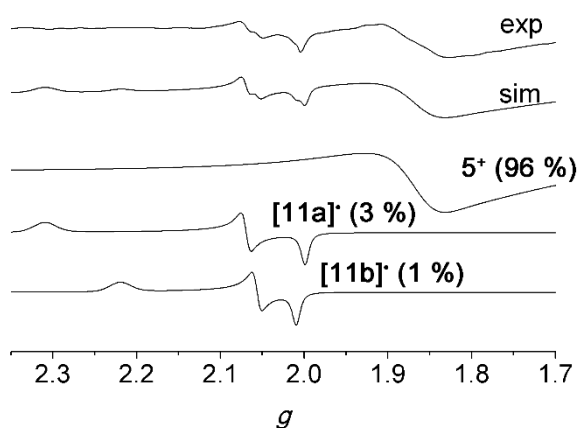


Figure 10. X-band EPR spectrum (exp) and simulated spectrum (sim) of 5⁺/P1^tBu consisting of three components 5⁺, [11a][•], and [11b][•]; (5 mM 5 in CH₂Cl₂) at the following experimental parameters: temperature = 77 K, field = 2499.01 G, sweep = 3989.53 G, sweep time = 120 s, modulation = 3000 mG, MW attenuation = 10 db.

PhNO, similar to other ferrocenium radicals $1^+–5^+$. It appears that Fc-NHC(X)R can be oxidized to the rather stable conjugate acid/base pair $[\text{Fc-NHC(X)R}]^+ / [\text{Fc-NC(X)R}]^\bullet$ (X = O, S). C-centered reactive radicals are then slowly formed via intramolecular proton-coupled electron transfer (PCET) or hydrogen atom transfer (Scheme 5).^{53–64}

In the PCET reaction, a proton is transferred from a cyclopentadienyl carbon atom to the nitrogen atom, while an electron from the original CH bond is transferred to the iron(III) center. Hence, $4^+ / [4-\text{H}^\text{N}]^\bullet$ and $5^+ / [5-\text{H}^\text{N}]^\bullet$ might act as a reservoir for reactive C-centered radicals (maybe even under physiological conditions). This might also explain some of the enhanced biological reactivity patterns observed for amino ferrocene based drugs and prodrugs such as **A**, **B**, or **D** (Scheme 1). C-centered radicals have also been proposed for the active species derived from ferrocifen **F** (Scheme 1). Hence, a common feature of such biologically active ferrocene/ferrocenium species might be the presence of some ionizable NH/OH group close to the ferrocenium site, suggesting an intimate coupling of electron and proton transfer to generate metastable iron-centered radicals. Highly reactive carbon-centered radicals might then be formed from these species in small amounts via intramolecular proton-coupled electron transfer reactions. These might account for further biological effects.

3.2.4 Conclusion

In contrast to other 17 valence electron metal centered radicals, such as $[\text{Mn}(\text{CO})_5]^\bullet$, ferrocenium ions are inert towards the reaction with the spin trapping agent nitrosobenzene. However, in the presence of a suitable base, small amounts of carbon-centered radicals are generated. Some of these reactive radicals add to nitrosobenzene giving the respective stable nitroxide radicals. EPR spectra of the corresponding stable ferrocenyl phenyl nitroxide radicals clearly reveal the position of the original radical site, namely C_5H_5 for ferrocene, CH_3 for decamethylferrocene, and CH_2 for ethylferrocene. The most acidic site in NHC(X) CH_3 substituted ferrocene/ferrocenium couples (X = O, S) is the NH group and iron-centered radicals are formed according to EPR studies. Again, these iron-centered radicals do not add to nitrosobenzene. Yet, small amounts of C-deprotonated tautomers generated from the N-deprotonated, iron-centered radicals are trapped by attack of nitrosobenzene at the Cp rings. Hence, these stable and inert NHC(X) CH_3 substituted ferrocene/ferrocenium couples slowly release reactive C-centered radicals and can thus be

considered as a reservoir for reactive radicals. This reactivity might also be of importance in the biological mode of action of OH/NH-substituted ferrocene-based drugs and prodrugs, such as ferrocifen, ferroquine and related compounds.

3.2.5 Experimental Section

General Considerations.

All reactions were performed under argon atmosphere unless otherwise noted. Dichloromethane was dried over CaH_2 and distilled prior to use. Ferrocene (**1**) was commercially available from Acros. Decamethylferrocene (**2**) was used as received from ABCR. Ethylferrocene (**3**), P^tBu , 2,2-diphenyl-1-picrylhydrazyl (DPPH), and nitrosobenzene (PhNO) were commercially available from Sigma-Aldrich. *N*-Acetylaminoferrocene (**4**),⁶⁵ *N*-thioacetylaminoferrocene (**5**),⁵¹ and $[\text{Bu}_4\text{N}][\text{B}(\text{C}_6\text{F}_5)_4]$ ^{42,43} were prepared according to literature procedures. Filtrations from precipitated silver after oxidation were performed with syringe filters (Rotilabo-Spritzenfilter, $\varnothing = 15$ mm, pore size = 0.20 μm ; Carl Roth GmbH + Co. KG, Germany). Electrochemical experiments were carried out on a BioLogic SP-50 voltammetric analyzer using a platinum working electrode, a platinum wire as counter electrode, and a 0.01 M Ag/AgNO₃ electrode as reference electrode. The measurements were carried out at a scan rate of 100 mV s^{-1} for cyclic voltammetry experiments and for square wave voltammetry experiments unless noted otherwise using 0.1 M $[\text{Bu}_4\text{N}][\text{B}(\text{C}_6\text{F}_5)_4]$ as supporting electrolyte and 0.001 M solution of the sample in CH_2Cl_2 . Potentials are given relative to the ferrocene/ferrocenium couple. Referencing was achieved by addition of ferrocene or decamethylcobaltocene ($E_{1/2} = -2.04$ V vs. FcH/FcH^+ (CH_2Cl_2 ; $[\text{Bu}_4\text{N}][\text{B}(\text{C}_6\text{F}_5)_4]$)) to the sample.^{42,43} CW EPR spectra (X-band; ca. 9.4 GHz) were measured on a Miniscope MS 300 at 298 K and at 77 K cooled by liquid nitrogen in a finger dewar (Magnettech GmbH, Berlin, Germany). Settings are given at the respective displayed spectra. *g*-Values are referenced to external Mn^{2+} in ZnS ($g = 2.118, 2.066, 2.027, 1.986, 1.946, 1.906$). Simulations of EPR spectra were performed with EasySpin (v 5.0.0)⁶⁶ for MatLab (R2015a). For quantification measurements, EPR tubes with an internal diameter of 2.0 mm were used. The calibration curve was determined using commercially available 2,2-diphenyl-1-picrylhydrazyl (DPPH) as standard. The samples were prepared in a glove box under argon, and the EPR tubes were filled with 400 μl of the solution and sealed with Critoseal®. They were inserted

10.4 cm (measured at the Teflon holder) into the EPR spectrometer. Three concentrations (0.03, 0.01, and 0.005 mM) in CH₂Cl₂ were used for the calibration. The settings for the calibration curve and the sample EPR spectra were as follows: temperature = 298 K, field = 3346.20 G, sweep = 94.79 G, sweep time = 90 s, modulation = 5000 mG, MW attenuation = 10 db, number of passes = 3. For an estimation of the error at the insertion of the EPR tube into the spectrometer cavity, the sample with 0.03 mM concentration was inserted, measured, reinserted, and measured three times. For the $c = 0.03$ mM sample a variation of 13 % between highest and lowest value of the three measurements after double integration is obtained. Baseline correction was achieved with EasySpin⁶⁶ for MatLab with normalization turned off. The obtained spectra were integrated twice with Origin Pro 8.0, and the double integral values were plotted against the concentration (Figures S11 and S12).

Density Functional Calculations.

These were carried out with the ORCA 3.0.2 / DFT series⁶⁷ of programs. For geometry optimizations and energy calculations, the B3LYP formulation of density functional theory was used employing the SV(P)^{68,69} basis set, the RIJCOSX approximation, approximate Second Order SCF (SOSCF),^{70,71} the zeroth order regular approximation (ZORA),⁷²⁻⁷⁴ the KDIIS algorithm, at GRIDX4. No symmetry constraints were imposed on the molecules. The presence of energy minima of the ground states was checked by numerical frequency calculations. Solvent modeling was done employing the conductor like screening model (COSMO, CH₂Cl₂).⁷⁵ The approximate free energies at 298 K were obtained through thermochemical analysis of the frequency calculation, using the thermal correction to Gibbs free energy as reported by ORCA 3.0.2.

3.2.6 Associated Content

Supporting Information.

The Supporting Information is available free of charge on the ACS Publications website at DOI: 10.1021/acs.organomet.5b00778.

Square wave and cyclic voltammograms of P₁^tBu, **1**, 1/P₁^tBu, **4**, and 4/P₁^tBu in CH₂Cl₂/[^mBu₄N][B(C₆F₅)₄] at 298 K, DFT optimized geometry and spin density in CH₂Cl₂ for [1-PhNO]⁺, [1-H][•], [2-H][•], [3-H^x][•] (x = α , β , Cp, 1, 2), [8^x][•] (x = α , β , Cp, 1, 2),

[4-H^x][•] and [5-H^x][•] (x = α , β , Cp, N, Me), and [4-H^N][•], EPR spectra and simulations in CH₂Cl₂ at 77 K of [6][•], [7][•], [8¹][•], [4-H^N][•] and [4-H^x][•] (x = α , β , Cp, Me), and at 298 K of [4-H^x][•] (x = α , β , Cp, Me), EPR spectra of quantification experiments in CH₂Cl₂ at 298 K of [6][•], [7][•], [8¹][•], [9^{Cp/ β][•], [10^{Cp}][•], and DPPH in 0.03 mM, 0.01 mM, and 0.005 mM concentration, and Cartesian coordinates of optimized structures (PDF)}

Cartesian Coordinates of all DFT optimized structures in .xyz format (XYZ)

Authors Information

Corresponding Author

*E-mail: katja.heinze@uni-mainz.de.

Notes

‡Authors contributed equally to the manuscript. The authors declare no competing financial interest.

3.2.7 Acknowledgement

We are grateful to Dipl.-Chem. Christoph Kreitner for his helpful remarks concerning DFT calculations. Parts of this research were conducted using the supercomputer Mogon and advisory services offered by Johannes Gutenberg University Mainz (www.hpc.uni-mainz.de), which is a member of the AHRP and the Gauss Alliance e.V.

3.2.8 Reference

- [1] Special issue on ferrocene chemistry: Heinze, K.; Lang, H. *Organometallics* **2013**, *32*, 5623–5625.
- [2] Special issue on ferrocene chemistry: Adams, R. D. *J. Organomet. Chem.* **2001**, 637-639, 1.
- [3] a) Togni, A.; Hayashi, T. *Ferrocenes*; Togni, A., Hayashi, T., Eds.; VCH: Weinheim, 1995; b) Stepnicka, P., Ed., *Ferrocenes: Ligands, Materials and Biomolecules*, VCH Weinheim, 2008.
- [4] Ornelas, C. *New J. Chem.* **2011**, *35*, 1973–1985.
- [5] Gasser, G.; Ott, I.; Metzler-Nolte, N. *J. Med. Chem.* **2011**, *54*, 3–25.

- [6] Tabbi, G.; Cassino, C.; Cavigiolio, G.; Colangelo, D.; Ghiglia, A.; Viano, I.; Osella, D. *J. Med. Chem.* **2002**, *45*, 5786–5796.
- [7] Hagen, H.; Marzenell, P.; Jentsch, E.; Wenz, F.; Veldwijk, M. R.; Mokhir, A. *J. Med. Chem.* **2012**, *55*, 924–934.
- [8] Osella, D.; Ferrali, M.; Zanello, P.; Laschi, F.; Fontani, M.; Nervi, C.; Cavigiolio, G. *Inorg. Chim. Acta* **2000**, *306*, 42–48.
- [9] Marzenell, P.; Hagen, H.; Sellner, L.; Zenz, T.; Grinyte, R.; Pavlov, V.; Daum, S.; Mokhir, A. *J. Med. Chem.* **2013**, *56*, 6935–6944.
- [10] Daum, S.; Chekhun, V. F.; Todor, I. N.; Lukianova, N. Y.; Shvets, Y. V.; Sellner, L.; Putzker, K.; Lewis, J.; Zenz, T.; de Graaf, I. A. M.; Groothuis, G. M. M.; Casini, A.; Zozulia, O.; Hampel, F.; Mokhir, A. *J. Med. Chem.* **2015**, *58*, 2015–2024.
- [11] Dubar, F.; Slomianny, C.; Khalife, J.; Dive, D.; Kalamou, H.; Guérardel, Y.; Grellier, P.; Biot, C. *Angew. Chem.* **2013**, *125*, 7844–7847; *Angew. Chem. Int. Ed.* **2013**, *52*, 7690–7693.
- [12] Biot, C.; Nosten, F.; Fraisse, L.; Ter-Minassian, D.; Khalife, J.; Dive, D. *Parasite* **2011**, *18*, 207–214.
- [13] Biot, C.; Glorian, G.; Maciejewski, L. A.; Brocard, J. S.; Domaire, O.; Blampain, G.; Millet, P.; Georges, A. J.; Abessolo, H.; Dive, D.; Lebibi, J. *J. Med. Chem.* **1997**, *40*, 3715–3718.
- [14] Zanellato, I.; Heldt, J.-M.; Vessières, A.; Jaouen, G.; Osella, D. *Inorg. Chim. Acta* **2009**, *362*, 4037–4042.
- [15] Hamels, D.; Dansette, P. M.; Hillard, E. A.; Top, S.; Vessières, A.; Herson, P.; Jaouen, G.; Mansuy, D. *Angew. Chem.* **2009**, *121*, 9288–9290; *Angew. Chem. Int. Ed.* **2009**, *48*, 9124–9126.
- [16] Hillard, E.; Vessières, A.; Thouin, L.; Jaouen, G.; Amatore, C. *Angew. Chem.* **2006**, *118*, 291–296; *Angew. Chem. Int. Ed.* **2006**, *45*, 285–290.
- [17] Jaouen, G.; Top, S.; Vessieres, A.; Leclercq, G.; McGlinchey, M. *Curr. Med. Chem.* **2004**, *11*, 2505–2517.
- [18] Nguyen, A.; Top, S.; Pigeon, P.; Vessières, A.; Hillard, E. a.; Plamont, M. A.; Huché, M.; Rigamonti, C.; Jaouen, G. *Chem. Eur. J.* **2009**, *15*, 684–696.

- [19] Michard, Q.; Jaouen, G.; Vessieres, A.; Bernard, B. A. *J. Inorg. Biochem.* **2008**, *102*, 1980–1985.
- [20] Osella, D.; Mahboobi, H.; Colangelo, D.; Cavigliolo, G.; Vessières, A.; Jaouen, G. *Inorg. Chim. Acta* **2005**, *358*, 1993–1998.
- [21] Abramovitch, R. A.; Azogu, C. I.; Sutherland, R. G. *J. Chem. Soc., Chem. Commun.* **1971**, 134–135.
- [22] Jackson, R. A.; Scarmoutsos, M.; Zarkadis, A. K. *J. Chem. Soc. Perkin Trans.* **1991**, *2*, 809–810.
- [23] a) Cais, M.; Ashkenazi, P.; Dane, S.; Gottlieb, J. *J. Organomet. Chem.* **1976**, *122*, 403–411; b) Creary, X. *Org. Lett.* **2000**, *2*, 2069–2072.
- [24] Neuse, E. W. *J. Macromol. Sci. Part A - Chem.* **1981**, *16*, 3–72.
- [25] Taniguchi, N.; Uemura, M. *Tetrahedron Lett.* **1998**, *39*, 5385–5388.
- [26] Ashkenazi, P.; Cais, M. *Angew. Chem.* **1972**, *84*, 1106–1107; *Angew. Chem. Int. Ed.* **1972**, *11*, 1027–1028.
- [27] Hudson, A.; Lappert, M. F.; Lednor, P. W.; Nicholson, B. K. *J. Chem. Soc. D Chem. Commun.* **1974**, 966–967.
- [28] Huffadine, A. S.; Dawson, P. A.; Peake, B. M.; Robinson, B. H.; Simpson, J. *J. Organomet. Chem.* **1976**, *121*, 391–403.
- [29] Bennar, L. S.; Balch, A. L. *J. Organomet. Chem.* **1977**, *134*, 121–130.
- [30] Hudson, A.; Lappert, M. F.; Nicholson, B. K. *J. Chem. Soc. Dalton Trans.* **1977**, 551–554.
- [31] a) Forrester, A. R.; Hepburn, P.; Dunlop, R. S.; Mills, H. H. *J. Chem. Soc., Chem. Commun.* **1969**, 698–699; b) Elschenbroich, C.; Cais, M. *J. Organomet. Chem.* **1969**, *18*, 135–143; c) Alberti, A.; Benaglia, M.; Bonini, B. F.; Fochi, M.; Macciantelli, D.; Marcaccio, Paolucci, F.; Roffia, S. *J. Phys. Org. Chem.* **2004**, *17*, 1084–1090.
- [32] Babin, V. N.; Belousov, Y. A.; Belousova, T. A.; Borisov, Y. A.; Gumenyuk, V. V.; Nekrasov, Y. S. *Russ. Chem. Bull. Int. Ed.* **2011**, *60*, 2081–2087.
- [33] a) Connelly, N. G.; Geiger, W. E. *Chem. Rev.* **1996**, *96*, 877–910; b) Fujita, E.; Gordon, B.; Hillman, M.; Nagy, A. G. *J. Organomet. Chem.* **1981**, *218*, 105–114.
- [34] Prins, R. *Mol. Phys.* **1970**, *19*, 603–620.

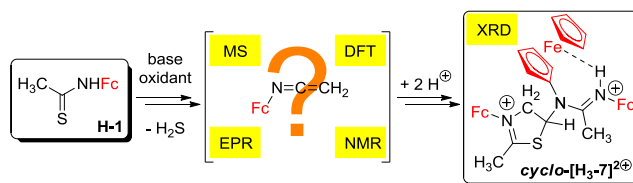
- [35] Neidlinger, A.; Ksenofontov, V.; Heinze, K. *Organometallics* **2013**, *32*, 5955–5965.
- [36] Kondo, Y. In *Superbases for Organic Synthesis*; Ishikawa, T., Ed.; John Wiley & Sons, Ltd: Chichester, UK, 2009; pp 145–185.
- [37] Barclay, L. R. C.; Dust, J. M. *Can. J. Chem.* **1982**, *60*, 607–615.
- [38] Omelka, L.; Kováčová, J. *Magn. Reson. Chem.* **1994**, *32*, 525–531.
- [39] Cais, M.; Ashkenazi, P.; Dani, S.; Gottlieb, J. *J. Organomet. Chem.* **1977**, *124*, 49–58.
- [40] Buettner, G. R. *Free Radic. Biol. Med.* **1987**, *3*, 259–303.
- [41] Huesmann, H.; Förster, C.; Siebler, D.; Gasi, T.; Heinze, K. *Organometallics* **2012**, *31*, 413–427.
- [42] LeSuer, R. J.; Buttolph, C.; Geiger, W. E. *J. Organomet. Chem.* **2004**, *76*, 6395–6401.
- [43] Camire, N.; Mueller-Westerhoff, U. T.; Geiger, W. E. *J. Organomet. Chem.* **2001**, *639*, 823–826.
- [44] Bildstein, B.; Malaun, M.; Kopacka, H.; Wurst, K.; Ongania, K.-H.; Opromolla, G. *Organometallics* **1999**, *18*, 4325–4336.
- [45] Sanders, R.; Mueller-Westerhoff, U. T. *J. Organomet. Chem.* **1996**, *512*, 219–224.
- [46] Guillaneux, D.; Kagan, H. B. *J. Org. Chem.* **1995**, *60*, 2502–2505.
- [47] Förster, C.; Heinze, K. *Z. Anorg. Allg. Chem.* **2015**, *641*, 517–520.
- [48] Plazuk, D.; Vessières, A.; Hillard, E. A.; Buriez, O.; Labbé, E.; Pigeon, P.; Plamont, M. A.; Amatore, C.; Zakrzewski, J.; Jaouen, G. *J. Med. Chem.* **2009**, *52*, 4964–4967.
- [49] a) Heinze, K.; Siebler, D. *Z. Anorg. Allg. Chem.* **2007**, *633*, 2223–2233; b) Siebler, D.; Linseis, M.; Gasi, T.; Carrella, L. M.; Winter, R. F.; Förster, C.; Heinze, K. *Chem. Eur. J.* **2011**, *17*, 4540–4551; c) Siebler, D.; Förster, C.; Heinze, K. *Dalton Trans.* **2011**, *40*, 3558–3575.
- [50] Heinze, K.; Hüttinger, K.; Siebler, D. in *Modeling of Molecular Properties* (Ed. P. Comba), Wiley-VCH, 2011.
- [51] Kienz, T.; Förster, C.; Heinze, K. *Organometallics* **2014**, *33*, 4803–4812.
- [52] Eaton, G. R.; Eaton, S. S.; Barr, D. P.; Weber, Ralph, T. *Quantitative EPR*; Springer Wien, New York, 2010.

- [53] Dempsey, J. L.; Winkler, J. R.; Gray, H. B. *Chem. Rev.* **2010**, *110*, 7024–7039.
- [54] Hammes-Schiffer, S. *Chem. Rev.* **2010**, *110*, 6937–6938.
- [55] Hammes-Schiffer, S.; Stuchebrukhov, A. *Chem. Rev.* **2010**, *110*, 6939–6960.
- [56] Wenger, O. S. *Chem. Eur. J.* **2011**, *17*, 11692–11702.
- [57] Herzog, W.; Bronner, C.; Löffler, S.; He, B.; Kratzert, D.; Stalke, D.; Hauser, A.; Wenger, O. S. *ChemPhysChem* **2013**, *14*, 1168–1176.
- [58] Warren, J. J.; Tronic, T. A.; Mayer, J. M. *Chem. Rev.* **2010**, *110*, 6961–7001.
- [59] Weinberg, D. R.; Gagliardi, C. J.; Hull, J. F.; Murphy, C. F.; Kent, C. A.; Westlake, B. C.; Paul, A.; Ess, D. H.; Mccafferty, D. G.; Meyer, T. J. *Chem. Rev.* **2012**, *112*, 4016–4093.
- [60] Bonin, J.; Robert, M. *Photochem. Photobiol.* **2011**, *87*, 1190–1203.
- [61] Savéant, J.-M. *Energy Environ. Sci.* **2012**, *5*, 7718–7731.
- [62] Gagliardi, C. J.; Vannucci, A. K.; Concepcion, J. J.; Chen, Z.; Meyer, T. J. *Energy Environ. Sci.* **2012**, *5*, 7704–7717.
- [63] Hammarström, L.; Styring, S. *Energy Environ. Sci.* **2011**, *4*, 2379–2388.
- [64] Costentin, C.; Robert, M.; Savéant, J.-M. *Phys. Chem. Chem. Phys.* **2010**, *12*, 11179–11190.
- [65] Heinze, K.; Schlenker, M. *Eur. J. Inorg. Chem.* **2004**, 2974–2988.
- [66] Stoll, S.; Schweiger, A. *J. Magn. Reson.* **2006**, *178*, 42–55.
- [67] Neese, F. *Wiley Interdiscip. Rev. Comput. Mol. Sci.* **2012**, *2*, 73–78.
- [68] Schäfer, A.; Horn, H.; Ahlrichs, R. *J. Chem. Phys.* **1992**, *97*, 2571–2577.
- [69] Weigend, F.; Ahlrichs, R. *Phys. Chem. Chem. Phys.* **2005**, *7*, 3297–3305.
- [70] Neese, F. *Chem. Phys. Lett.* **2000**, *325*, 93–98.
- [71] Fischer, T. H.; Almlof, J. *J. Phys. Chem.* **1992**, *96*, 9768–9774.
- [72] Lenthe, E. van; Baerends, E. J.; Snijders, J. G. *J. Chem. Phys.* **1993**, *99*, 4597–4610.
- [73] Van Wüllen, C. *J. Chem. Phys.* **1998**, *109*, 392.
- [74] Pantazis, D. A.; Chen, X. Y.; Landis, C. R.; Neese, F. *J. Chem. Theory Comput.* **2008**, *4*, 908–919.
- [75] Sinnecker, S.; Rajendran, A.; Klamt, A.; Diedenhofen, M.; Neese, F. *J. Phys. Chem. A* **2006**, *110*, 2235–2245.

3.3 Generation and Oligomerization of N-Ferrocenyl Ketenimines via Open-shell Intermediates

Torben Kienz, Christoph Förster, and Katja Heinze

Submitted



Supporting information for this article (without Cartesian coordinates from DFT calculations) is found at pp.175.

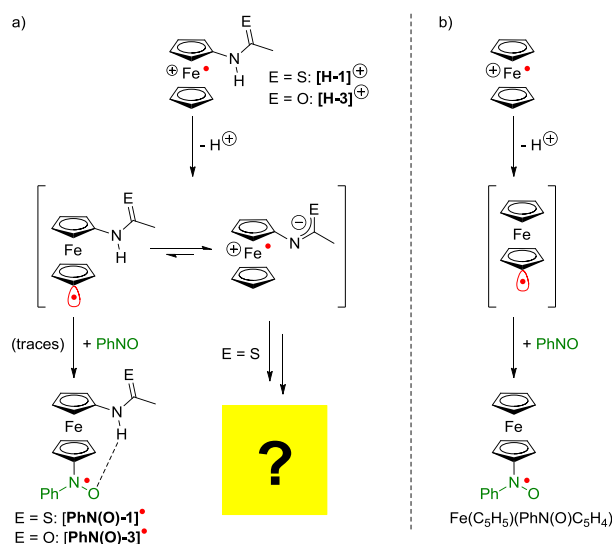
Adapted with permission from T. Kienz, C. Förster, K. Heinze.

3.3.1 Abstract

In the presence of oxidant ($\text{Ag}[\text{SbF}_6]$) and base, *N*-ferrocenyl thioamide Fc-NHC(S)CH_3 (**H-1**; $\text{Fc} = \text{Fe}(\eta^5\text{-C}_5\text{H}_5)(\eta^5\text{-C}_5\text{H}_4)$) converts in an unexpected multistep reaction sequence to a novel N,S-heterocyclic ring which initiates an oligomerization reaction. Key intermediates towards the resulting complicated material are $\text{Ag}_6(\mathbf{1})_6$ silver clusters of the anionic N,S-chelating ligand $\mathbf{1}^-$, EPR-active piano stool complexes resulting from ring-slipped cyclopentadienyl ligands as well as electrophilic *N*-ferrocenyl ketenimine Fc-N=C=CH_2 (**2**) and its ferrocenium cation $\mathbf{2}^{\bullet+}$ formed by hydrosulfide elimination. Mechanistic insight is achieved using XRD, mass spectrometric as well as EPR and NMR spectroscopic studies combined with DFT calculations. In addition to the fundamental mechanistic insight, the results could have impact for smart oligo-mers/polymers, heterocycle synthesis and controlled-release materials.

3.3.2 Introduction

N-Ferrocenyl amides Fc-NHC(O)R (Fc = Fe(η^5 -C₅H₅)(η^5 -C₅H₄); R = CH₃: **Z-[H-3]**) and thioamides Fc-NHC(S)R (R = CH₃: **E/Z-[H-1]**) become acidic upon oxidation to the corresponding ferrocenium ions due to the increased positive charge close to the nitrogen atom.¹⁻⁸ Vice versa, deprotonation of the amide lowers the oxidation potential of the ferrocene/ferrocenium redox couple due to the negative charge adjacent to ferrocene.⁷⁻⁹ In addition to the expected acidity of the NH group of ferrocenyl amides and thioamides, CH activation can also occur in the presence of a non-nucleophilic base (P₁-^tBu) and an oxidant (Ag[SbF₆]), leading to ferrocenyl radicals (P₁-^tBu = *tert*-butylimino-tris(dimethylamino)phosphorane). These carbon-centered radicals have been trapped by nitrosobenzene (PhNO) and unambiguously identified by EPR spectroscopy as their characteristic nitroxide radicals **[PhN(O)-1]•** and **[PhN(O)-3]•**, respectively (Scheme 1a).⁷ Even ferrocene Fe(C₅H₅)₂ and decamethylferrocene Fe(C₅Me₅)₂ display such radical reactivity giving the respective ferrocenyl phenyl nitroxide radicals Fe(C₅H₅)(PhN•(O))C₅H₄ (Scheme 1b) and Fe(C₅Me₅)(PhN•(O)CH₂)C₅Me₄, respectively.⁷



Scheme 1. Established and unexplained radical reactivity of a) *N*-thioacetyl amino ferrocene H-1 and *N*-acetyl aminoferrocene H-3 and b) ferrocene Fe(C₅H₅)₂ in the presence of oxidant and base followed by trapping with PhNO.⁷

Sulfur derivatives such as *E/Z*-[H-1]⁶ exhibit a further, as yet undisclosed reactivity in the presence of both base and oxidant, based on electrochemical data as well as on EPR spectroscopic findings (Figure 1).^{6,7} Unusual rhombic EPR resonances are observed at 77 K in frozen solution (Figure 1b). These EPR patterns differ significantly from the typical axial resonances of ferrocenium ions, such as *E*-[H-3]^{•+} or *E/Z*-[H-1]^{•+} (Figure 1a).⁶⁻¹¹ In addition to the rhombic symmetry, the *g* anisotropy (Δg) is dramatically reduced. Yet, Δg is still much larger than expected for EPR resonances of light-atom radicals, suggesting a strong participation of the iron center. The occurrence of such resonances is specific for ferrocenyl thioamides but not for ferrocenyl amides or unsubstituted ferrocene. Obviously, the sulfur atom in place of the oxygen atom plays a major role. Furthermore, the 1:1 mixture of *E/Z* iso-mers *E/Z*-[H-1] gives rise to two different rhombic EPR resonances in CH₂Cl₂ in a 4:1 ratio suggesting an effect of the original configuration for these two open-shell species (Figure 1b). In the presence of PhNO, the ratio of the two species changes to 1:1 pointing to subtle differences in solubility or reactivity of the radicals or precursors to the radicals derived from *E*-[H-1] and *Z*-[H-1].⁷

In the present mechanistic study, we will disclose the unexpected reactivity of ferrocenyl thioamide *E/Z*-[H-1] under oxidative and alkaline conditions. The proposed pathway encompasses reactive open-shell intermediates and finally leads to diamagnetic ferrocenyl containing oligomers with [CN]_n backbone and N,S-heterocyclic head groups. Details of the suggested multistep reaction mechanism are supported by EPR and NMR spectroscopic and mass spectrometric data, by single crystal XRD analyses of intermediates and products as well as by density functional theory (DFT) calculations. Apart from the fundamental mechanistic insight, the obtained results could be relevant for smart redox-active polymers with ferrocene in the side chain¹²⁻¹⁵, for heterocycle synthesis and for ferrocene-containing pro-drugs for controlled release.¹⁶

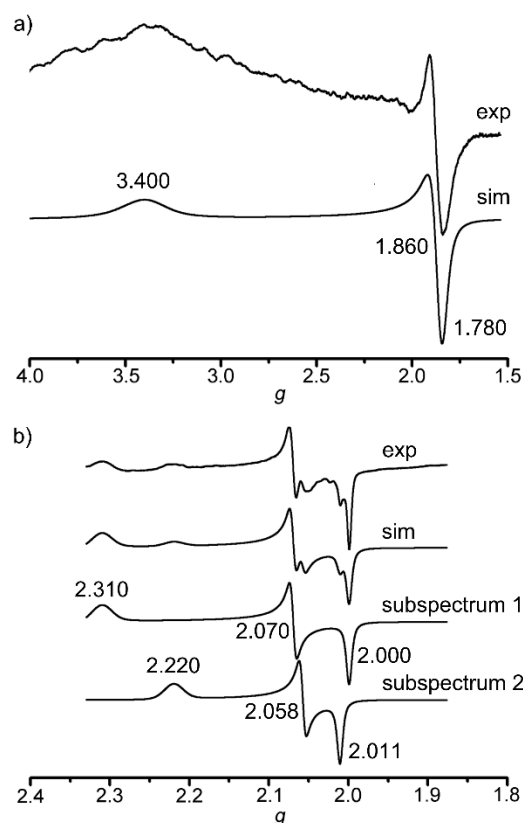


Figure 1. a) EPR spectrum of E/Z -[H-1] $^{\bullet+}$ in CH_2Cl_2 at 77 K and simulated spectrum [B_0 2499.81 G; sweep 3791.34 G; modulation 3000 mG; MW attenuation 3 dB; gain 5.0; sweep time 120 s; $c = 20$ mM] and b) EPR spectrum of E/Z -[H-1] treated with $\text{Ag}[\text{SbF}_6]$ and P_1 - t -Bu in CH_2Cl_2 at 77 K [B_0 3245.45 G; sweep 697.96 G; modulation 5000 mG; MW attenuation 15 dB; gain 5.0; sweep time 90 s; $c = 19$ mM]; simulated EPR spectrum of the radical mixture (ratio 4:1) and the corresponding subspectra.

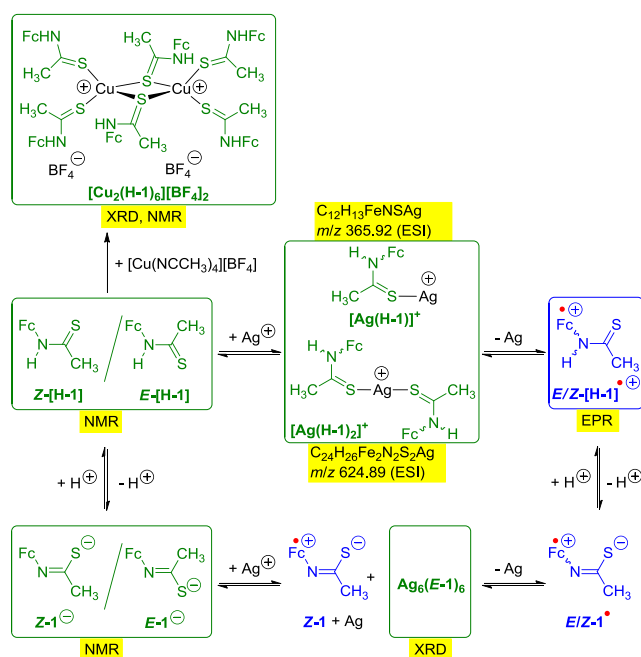
3.3.3 Results and Discussion

The multifaceted interactions of E/Z -[H-1] i) with $\text{Ag}[\text{SbF}_6]$, ii) with bases and iii) with both agents will be examined and discussed in the following.

Reaction of E/Z -[H-1] and $\text{Ag}[\text{SbF}_6]$.

In CH_2Cl_2 solution, thioamide E/Z -[H-1] exists as a 1:1 mixture of E/Z isomers.⁶ E/Z -[H-1] is conveniently oxidized to the ferrocenium cations E/Z -[H-1] $^{\bullet+}$ by $\text{Ag}[\text{SbF}_6]$ in CH_2Cl_2 according to their respective redox potentials.^{6,17} The presence of ferrocenium ions is

confirmed by EPR spectroscopy with E -[H-1] $^{\bullet+}$ and Z -[H-1] $^{\bullet+}$ delivering indistinguishable essentially axial EPR resonances (Figure 1a; $g = 3.400, 1.860, 1.780$).⁶ In CH_3CN , the oxidation potential of Ag^+ is insufficient for oxidation of the ferrocenyl unit in E/Z -[H-1].¹⁷ The ESI $^+$ mass spectrum of this mixture in CH_3CN displays peak clusters at $m/z = 365.92$ and $m/z = 624.89$ fitting to the mono- and diligated silver complex cations $[\text{Ag}(\text{H-1})]^+$ and $[\text{Ag}(\text{H-1})_2]^+$ with expected isotopic patterns of $^{107/109}\text{Ag}$, respectively (Scheme 2; Supporting, Information, Figure S1).



Scheme 2. Initial steps in the reaction sequence of E/Z -[H-1] in the presence of base and oxidant (compounds in boxes are identified by spectroscopic/analytical techniques highlighted in yellow).

As the oxidative power of silver cations depends on their coordination environment (solvent, potential ligands)¹⁷, the redox reaction between Ag^+ and sulfur-containing **H-1** and the competing κS coordination reaction to give $[\text{Ag}(\text{H-1})_2]^+$ is probably a delicate equilibrium (Scheme 2). Indeed, attempts to grow crystals of silver complexes of **H-1** failed. However, a copper(I) complex has been successfully prepared from E/Z -[H-1] and tetrakis(acetonitrile)copper(I) tetrafluoroborate (Scheme 2). The copper(I) complex crystallizes with a $[\text{Cu}_2(\text{H-1})_6][\text{BF}_4]_2$ stoichiometry featuring hydrogen bonded counterions (Figure 2a). A detailed discussion of the solidstate structure and comparison with

similar compounds¹⁸⁻²¹ can be found in the Supporting Information (Supporting Information, Table S1). NMR, IR, and conductivity studies²² in solution confirm that the $[\text{Cu}_2(\text{H-1})_6]^{2+}$ structural motif and the hydrogen bonded counter ions ($[\text{Cu}_2(\text{H-1})_6][\text{BF}_4]_2$ 1:2 contact ion pairs) is retained in CH_2Cl_2 solution as discussed in more detail in the Supporting Information.

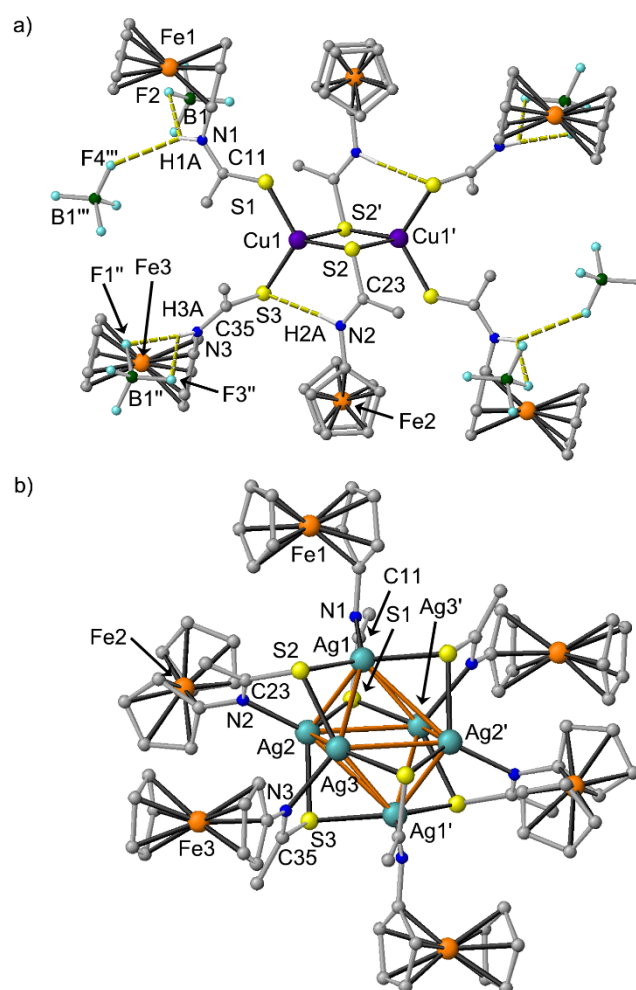


Figure 2. a) Molecular structure of $[\text{Cu}_2(\text{H-1})_6][\text{BF}_4]_2$ derived from single crystal XRD analysis (CH protons omitted for clarity; four additional $[\text{BF}_4]^-$ ions are shown to illustrate the hydrogen bonding pattern). b) Molecular structure of $\text{Ag}_6[\mu_3-(\text{E-1})]_6$ derived from single crystal XRD analysis (CH protons omitted for clarity).

These contact ion pairs are oxidized at $E_{1/2} = 0.16 \text{ V}$ ($\approx 2 e^-$), 0.36 V ($\approx 4 e^-$) and 0.73 V ($\approx 2 e^-$), suggesting that the ferrocene units are reversibly oxidized to ferrocenium cations in two

electrochemical steps. Finally, the copper(I) centers are oxidized quasireversibly as often observed for copper(I) complexes (Supporting Information, Figures S13 and S14). The high positive charge of the terminal ferrocenium ions might be compensated for by counter ions, yet the $\text{Cu}^{\text{I/II}}$ oxidation is not reversible on the electrochemical timescale. The UV/vis absorption bands of the ferrocenyl moieties of $[\text{Cu}_2(\text{H-1})_6][\text{BF}_4]_2$ in CH_2Cl_2 are shifted to lower energy from 348/446 nm (**H-1**) to 378/456 nm (Supporting Information, Figure S15).

Although silver(I) complexes of thioamides **H-1** could not be crystallized and NMR spectroscopic analyses of $\text{Ag}[\text{SbF}_6]/\text{H-1}$ mixtures are hampered due to the concomitant formation of open-shell species by oxidation processes, we assume, that, based on ESI mass spectroscopic evidence (vide supra, Supporting Information, Figure S1) and the formed copper(I) complex $[\text{Cu}_2(\text{H-1})_6][\text{BF}_4]_2$, contact ion pairs of the type $[\text{Ag}_n(\text{H-1})_m][\text{SbF}_6]_n$ should be present in CH_2Cl_2 solution as well. Indeed, silver(I) complexes of the redoxinert HpyS ligand display polymeric structures $[\text{Ag}_n(\text{HpyS-}\kappa\text{S})_{2n}][\text{X}]_n$ in the solid state.²³ Hence, **E/Z-H-1** can simply coordinate to $\text{Ag}[\text{SbF}_6]$ to give $[\text{Ag}_n(\text{E/Z-H-1})_m][\text{SbF}_6]_n$ ion pairs or can be oxidized by $\text{Ag}[\text{SbF}_6]$ to give **E/Z-H-1** $^+$ $[\text{SbF}_6]^-$ ferrocenium salts, depending on the environment, e.g. the solvent (Scheme 2).

Reaction of and **E/Z-H-1** and bases.

Deprotonation of thioamide **E/Z-H-1** is facile with *n*-butyl lithium $n\text{-BuLi}$, lithium dimethyl amide $\text{Li}(\text{NMe}_2)$ or phosphazene base²⁴ $\text{P}_1\text{-}^t\text{Bu}$ (Scheme 2). In all cases, the resulting ^1H NMR spectra confirm the NH deprotonation based on the disappearance of the NH proton resonances at 8.96 and 8.25 ppm of **E-H-1** and **Z-H-1**, respectively (Supporting Information, Figure S16). Furthermore, all resonances of **[E-1]** $^-$ are significantly broadened and display lower intensity, while the resonances of **[Z-1]** $^-$ remain sharp. Indeed, a precipitate is observed. This precipitate might well consist of less soluble $[\text{cation}]^+[\text{E-1}]^-$ salts, while $[\text{cation}]^+[\text{Z-1}]^-$ is obviously better soluble in CD_2Cl_2 (cation = $[\text{Li}(\text{THF})_n]^+$; $[\text{H-P}_1\text{-}^t\text{Bu}]^+$; Supporting Information, Figure S16). This different solubility could be due to the different coordinating ability of **[E-1]** $^-$ and **[Z-1]** $^-$. Hence, **E/Z-H-1** can be deprotonated by bases to give salts $[\text{cation}][\text{E-1}]$ and $[\text{cation}][\text{Z-1}]$, respectively, with different solubility (Scheme 2).

Deprotonation and Oxidation of *E/Z*-[**H-1**].

Preparative scale deprotonation of *E/Z*-[**H-1**] and subsequent oxidation with Ag^+ is achieved i) by one equivalent of $n\text{BuLi}$ in THF, removal of the solvent, oxidation with $\text{Ag}[\text{SbF}_6]$ in CH_2Cl_2 ($E_{1/2} = 0.65$ V in CH_2Cl_2 vs. $\text{FcH}/\text{FcH}^{\bullet+}$)¹⁷ (method A) and purification by column chromatography over silica, ii) by one equivalent of $\text{Li}(\text{NMe}_2)$ in THF, removal of the solvent, oxidation with $\text{Ag}[\text{SbF}_6]$ in CH_2Cl_2 (method B) and purification by column chromatography over aluminium oxide or iii) by one equivalent of $\text{P}_1\text{-}^t\text{Bu}$ in CH_2Cl_2 followed by oxidation with $\text{Ag}[\text{SbF}_6]$ and filtration through a syringe filter (method C). Before chromatographic workup, the samples of these mixtures were subjected to mass spectrometric analyses (ESI^+ , FD^+). EPR samples were prepared by oxidation with $\text{Ag}[\text{SbF}_6]$ and deprotonation with $\text{P}_1\text{-}^t\text{Bu}$ in CH_2Cl_2 , followed by filtration (method C).

From a sample prepared by method C, a few orange-red crystals separated which were analyzed by single crystal XRD analysis (Figure 2b; Supporting Information, Table S2, Figure S17). A hexameric, centrosymmetric neutral cluster $\text{Ag}_6[\mu_3\text{-}(\text{E-1})]_6$ consisting of a distorted Ag_6 octahedron ($\text{Ag}\cdots\text{Ag}$ distances 2.886 – 3.552 Å) with six edges bridged by sulfur atoms of the six *E-1*⁻ ligands is present (Supporting Information, Table S2). The E configuration further allows for a $\kappa\text{N}, \kappa\text{S}$ bridging mode of the deprotonated thioamide *E-1*⁻. A similar assembly has been observed in Ag_6L_6 clusters with L = anion of 1-R-imidazoline-2-thione (R = Pr, ^{*i*}Pr),²⁵ 2-hydroxynaphthalene-1-carboxaldehyde thiosemicarbazone,²⁶ ferrocenyl thiosemicarbazone,²⁷ and 2-benzimidazolethiolate.²⁸ The C=S distances in $\text{Ag}_6[\mu_3\text{-}(\text{E-1})]_6$ (1.767(9) Å) are significantly larger than that in **H-1** (1.671(2) Å)⁶ suggesting a dominant thioiminolate character of the coordinated ligand. All Fe-C distances support neutral ferrocenes without ferrocenium character, i.e. no electron transfer from ferrocene to Ag^+ has occurred (Scheme 2, Table S2).

The poor solubility of $\text{Ag}_6(\text{E-1})_6$ removes *E-1*⁻ from the reaction mixture, i.e. enriches the solution in *Z-1*⁻ and furthermore represses the oxidation of *E-1*⁻ to the neutral radical *E-1*[•] (Scheme 2). Yet, the cluster $\text{Ag}_6(\text{E-1})_6$ can act as reservoir of *E-1*⁻ and *E-1*[•], respectively. These events are further probed by EPR spectroscopy in solution.

The EPR spectrum of a sample rapidly frozen after addition of $\text{P}_1\text{-}^t\text{Bu}$ to a solution of *E/Z*-[**H-1**]^{•+} in CH_2Cl_2 (from a 1:1 *E/Z*-[**H-1**] mixture) merely shows the axial resonance of the ferrocenium ions *E/Z*-[**H-1**]^{•+} ($g = 3.400, 1.860, 1.780$; Figure 1a). Upon warming to room temperature for 2 minutes, the rhombic resonances at $g = 2.310, 2.070, 2.000$

(subspectrum 1) and $g = 2.220, 2.058, 2.011$ (subspectrum 2) appear in a 4:1 ratio (Figure 1b), while the axial resonance of $E/Z\text{-[H-1]}^{\bullet+}$ vanished. Interestingly, no comparable rhombic EPR resonances appear in the reaction of ferrocenium amide $[\mathbf{H-3}]^{\bullet+}$ and $P_1\text{-}^i\text{Bu}$, so this reactivity is associated with the sulfur of $E/Z\text{-[H-1]}^{\bullet+}$.

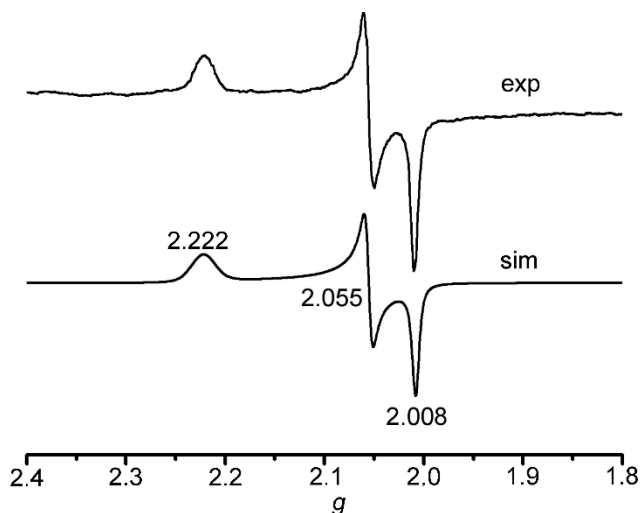
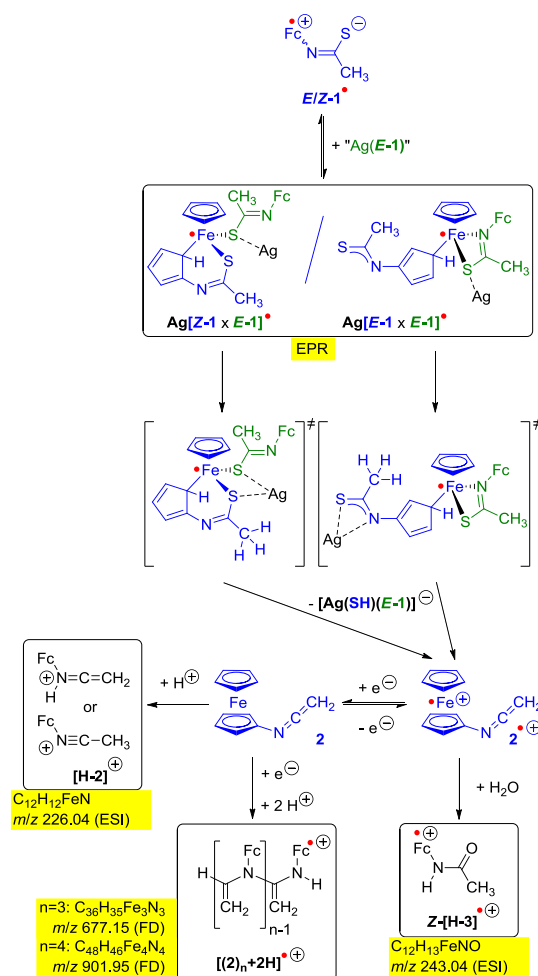


Figure 3. (Top) Experimental EPR spectrum of $Z\text{-[H-1]}/\text{DDQ}$ at 77 K prepared by method D in CH_3CN (black) [B_0 2499.14 G; sweep 3989.53 G; modulation 3000 mG; MW attenuation 7 dB; gain 5.0; sweep time 120 s; $c = 19$ mM]. (Bottom) simulated EPR spectrum.

In CH_2Cl_2 , thioamide $\mathbf{H-1}$ is present as 1:1 E/Z mixture, while in CH_3CN the Z isomer $Z\text{-[H-1]}$ is preferred. This opens the opportunity to monitor the fate of a single isomer. However, as $\text{Ag}[\text{SbF}_6]$ is incompetent to oxidize $\mathbf{H-1}$ in CH_3CN , 2,3-dichloro-5,6-dicyano-1,4-benzoquinone (DDQ) is employed both as oxidant and base in CH_3CN , both for EPR and mass spectrometric experiments (method D). The EPR spectrum obtained by method D in CH_3CN ($g = 2.222, 2.055, 2.008$; Z isomer; Figure 3) coincides with subspectrum 2 obtained by method C in CH_2Cl_2 (Figure 1b). Accordingly, the EPR subspectrum 1 obtained by method C is assigned to species arising from the E isomer (Figure 1b).

This EPR-active open-shell species derived from $Z\text{-[H-1]}$ decays within 30 min at room temperature in CH_3CN to EPR-silent products (Scheme 3, Figure 4a; half-life $\tau_{1/2} = 13$ min in CH_3CN). EPR experiments with a 1:1 mixture of both isomers $E\text{-[H-1]}$ and $Z\text{-[H-1]}$ in CH_2Cl_2 (method C), monitoring both radicals over time show that the EPR resonance

derived from **Z-[H-1]** ($g = 2.220, 2.058, 2.011$; $\tau_{1/2} = 3$ min) decays faster than the EPR resonance derived from **E-[H-1]** ($g = 2.310, 2.070, 2.000$; $\tau_{1/2} = 84$ min) (Figure 4b, 4c).



Having assigned the subspectra 1 and 2 (Figure 1b) to radicals derived from **E-[H-1]** and **Z-[H-1]**, respectively, their composition and structures are not yet clear (Schemes 2 and 3). The rhombic symmetry of the EPR resonances is incompatible with simple axial ferrocenium ions such as **E/Z-1•** (Scheme 3). Hence, a reduction of symmetry has to be taken into account, e.g. by coordination of a nucleophile to the Fe^{III} center in the zwitterions **E-1•** and **Z-1•**. Notably, the rhombic resonances (Figures 1b, 3, 4) closely resemble those obtained for “half-open” ferrocenium ions, e.g. Fe^{III}(η^5 -Cp)(η^5 -2,4-Me₂C₅H₇)²⁹ or pseudo-

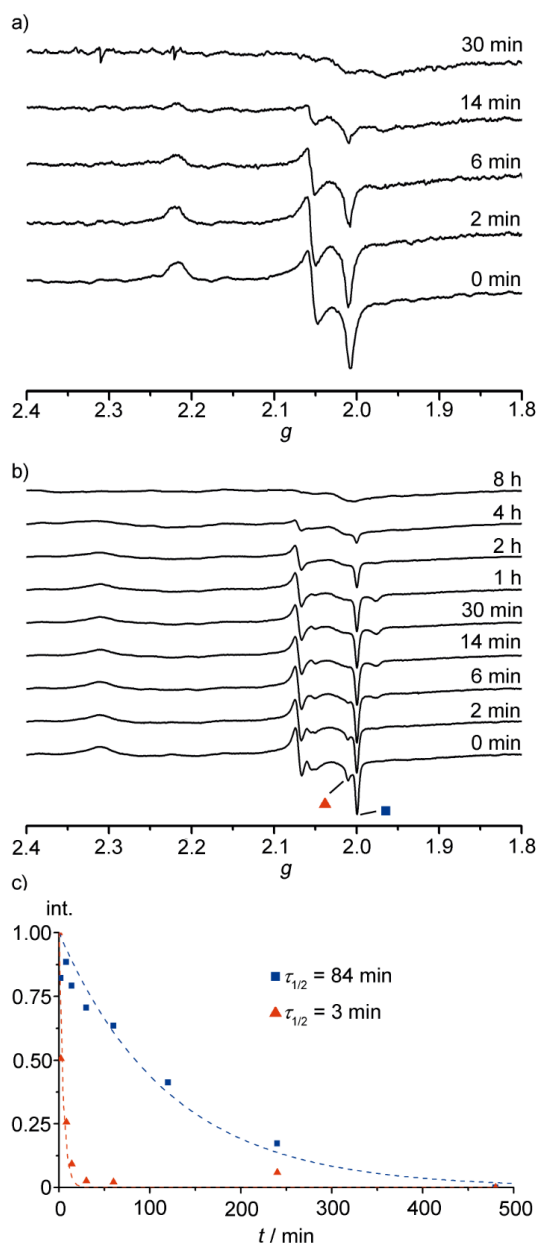


Figure 4. a) Experimental EPR spectra of Z-[H-1] at 77 K treated with DDQ in CH₃CN (method D) after different time intervals at room temperature [B_0 2499.01 G; sweep 3989.53 G; modulation 3000 mG; MW attenuation 7 dB; gain 5.0; sweep time 120 s; $c = 13$ mM], b) experimental EPR spectra of E-[H-1]/Z-[H-1] at 77 K treated with Ag[SbF₆] and P₁-t-Bu in CH₂Cl₂ (method C) after different time intervals at room temperature [B_0 3266.74 G; sweep 999.54 G; modulation 5000 mG; MW attenuation 7 dB; gain 5.0; sweep time 120 s; $c = 30$ mM] and c) time traces of the relative EPR resonance intensities in CH₂Cl₂ including exponential fits.

octahedral d^5 low-spin $[\text{Fe}^{\text{III}}(\eta^5\text{-Cp}^*)(\text{dppe})(\text{C}\equiv\text{CR})]^+$ cations [dppe = 1,2-bis(diphenylphosphano)ethane], i.e. complexes with a $[\text{Fe}^{\text{III}}(\eta^5\text{-Cp})\text{LL}'\text{L}'']^{2+}$ piano stool symmetry.^{30,31}

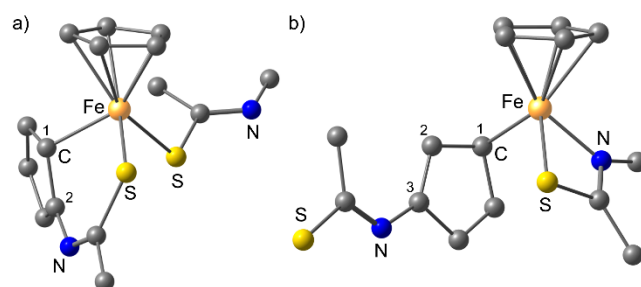


Figure 5. DFT calculated molecular structures of model piano stool open-shell species a) $[(Z-1)\times(E\text{-CH}_3\text{C}(\text{S})=\text{N-CH}_3)\text{-}\kappa\text{S}]^{\bullet-}$ and b) $[(E-1)\times(E\text{-CH}_3\text{C}(\text{S})=\text{N-CH}_3)\text{-}\kappa\text{N}\kappa\text{S}]^{\bullet-}$ (protons omitted for clarity).

Such piano stool species can be envisaged by nucleophilic attack of anions $[E/Z-1]^-$ to the zwitterions $E-1^\bullet$ and $Z-1^\bullet$ (Scheme 3). DFT calculations indeed suggest the formation of species with slipped Cp rings. According to the calculations, coordination of a model nucleophile $[E\text{-CH}_3\text{C}(\text{S})=\text{N-CH}_3]^-$ to zwitterions $E-1^\bullet$ or $Z-1^\bullet$ induces a ring slippage of the substituted $\text{C}_5\text{H}_4\text{-NC}(\text{S})\text{CH}_3$ rings from η^5 to η^1 . With zwitterion $Z-1^\bullet$, the sulfur atom of the substituent of the η^1 -Cp ring binds to iron(III) in a chelating fashion, in addition to the κS coordination of the nucleophile ($[Z-1\times E-1]^{\bullet-}$; Scheme 3; Figure 5a). This coordination-induced ring-slippage results in a $[\text{Fe}^{\text{III}}(\eta^5\text{-C}_5\text{H}_5)(\eta^1\text{-}1,2\text{-C}_5\text{H}_4\text{-NC}(\text{S})\text{CH}_3\text{-}\kappa\text{S})(\text{CH}_3\text{C}(\text{S})=\text{N-CH}_3\text{-}\kappa\text{S})]^-$ piano stool geometry. In the $E-1^\bullet$ isomer, the sulfur substituent is incompetent to coordinate to iron(III) for steric reasons. Hence, the incoming nucleophile $[E\text{-CH}_3\text{C}(\text{S})=\text{N-CH}_3]^-$ coordinates in a chelating $\kappa\text{N},\kappa\text{S}$ fashion, resulting in a $[\text{Fe}^{\text{III}}(\eta^5\text{-C}_5\text{H}_5)(\eta^1\text{-}1,3\text{-C}_5\text{H}_4\text{-NC}(\text{S})\text{CH}_3)((\text{CH}_3\text{C}(\text{S})=\text{N-CH}_3\text{-}\kappa\text{N},\kappa\text{S}))]^-$ piano stool geometry $[E-1\times E-1]^{\bullet-}$; Scheme 3; Figure 5b). This $[\text{FeCp}(\text{C})(\text{S})(\text{N})]$ coordination also accounts for the larger g anisotropy of the EPR resonance derived from $E-1^\bullet$ ($\Delta g = 0.31$; Figure 1b, subspectrum 1) as compared to the EPR resonance of piano stool complex $[\text{FeCp}(\text{C})(\text{S})(\text{S})]$ derived from $Z-1^\bullet$ ($\Delta g = 0.21$; Figure 1b, subspectrum 2). Notably, $[Z-1\times E-1]^{\bullet-}$ features a $\eta^1\text{-}1,2\text{-C}_5\text{H}_4\text{-NC}(\text{S})\text{CH}_3$ ligand while a 1,3-substitution is favored in $[E-1\times E-1]^{\bullet-}$ according to the calculations. As a working hypothesis, the piano stool radicals $[Z-1\times E-1]^{\bullet-}/[E-1\times E-1]^{\bullet-}$ either directly transform into EPR-silent products or act as a reservoir of stabilized

open-shell species which further transform into EPR-silent products (Scheme 3). These follow-up products are probed by mass spectrometry and NMR spectroscopy.

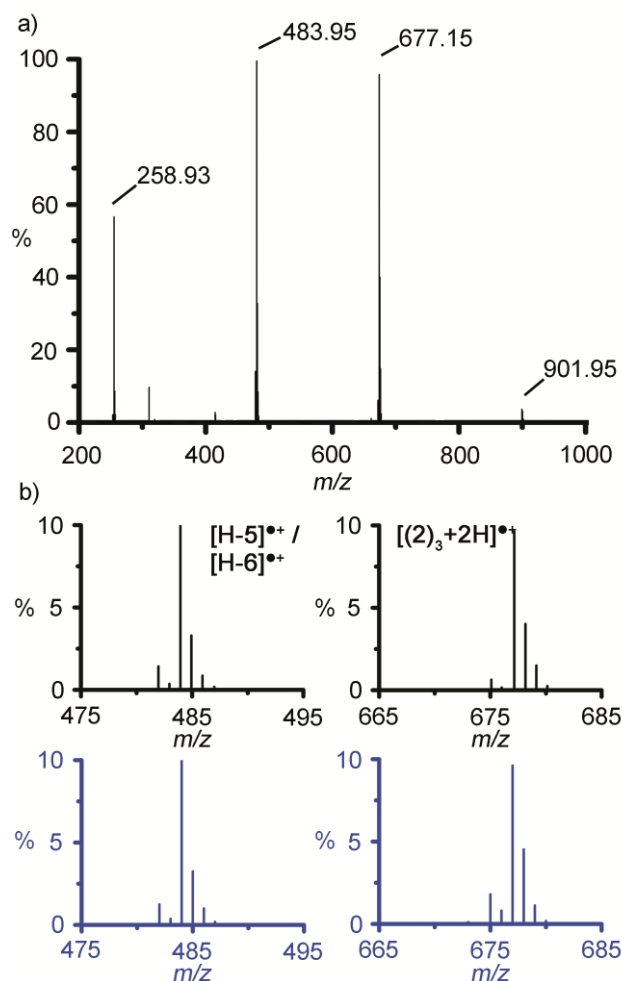


Figure 6. a) FD^+ mass spectrum of a sample prepared by method D in CH_3CN after cobaltocene reduction; b) experimental (black) and calculated (blue) isotope distributions and assignments of relevant peaks.

Treating the reaction mixture of **Z**-[H-1] and DDQ in CH_3CN after 30 min with cobaltocene $\text{Co}(\text{C}_5\text{H}_5)_2$ to reduce the paramagnetic species to diamagnetic ones gave rise to the evolution of hydrogen sulfide. The H_2S was detected by its characteristic odor as well as by precipitation of black lead sulfide PbS from the reaction of $\text{Pb}(\text{OAc})_2$ with the evolved gas. Obviously, sulfur is easily eliminated during the course of the reaction.¹⁶ Furthermore, oligomeric species lacking H_2S are observed in the FD^+ mass spectrum of the reaction mixture after reduction and chromatographic workup in addition to the peak of the starting

material **[H-1]^{•+}** at $m/z = 258.9$ (Figure 6). The peak at $m/z = 484.0$ can be assigned to species with the formula $C_{24}H_{24}Fe_2N_2S$ (**[H-5]^{•+}**/**[H-6]^{•+}**, see below), while the peaks at 677.2 and 902.0 correspond to species with the formulas $C_{36}H_{35}Fe_3N_3$ (**[(2)₃+2H]⁺**, see below) and $C_{48}H_{46}Fe_4N_4$ (**[(2)₄+2H]⁺**, see below), respectively, completely lacking sulfur (Figure 6, Scheme 3).

The (at least partial) elimination of sulfur is also confirmed by the observation of peaks with mass-to-charge ratios of 226.04 ($C_{12}H_{12}FeN$) and 243.04 ($C_{12}H_{13}FeNO$) in the ESI⁺ mass spectrum (method B, Figure 7). These peaks can be assigned to the *N*-ferrocenyl keteniminium ion **[H-2]⁺** (or its isomeric *N*-ferrocenyl nitrilium ion) and ferrocenium amide **Z-[H-3]^{•+}**, respectively (Scheme 3). These species derive from the *N*-ferrocenyl ketenimine/(*N*-ferrocenium)yl ketenimine redox couple **2/2^{•+}** by protonation (**[H-2]⁺**) and by addition of water (**Z-[H-3]^{•+}**), respectively (Scheme 3). The ferrocene/ferrocenium ketenimine redox pair **2/2^{•+}** obviously results from desulfurization of **H-1**. We suggest, that zwitterions **E-1[•]**/**Z-1[•]**, formed by deprotonation and oxidation of **E-[H-1]**/**Z-[H-1]**, or their corresponding piano stool complexes eliminate hydrosulfide to give the ferrocenium ketenimine **2^{•+}** (Scheme 3). Tentative transition states for the AgSH eliminations from piano stool complexes **[Z-1×E-1]^{•-}** and **[E-1×E-1]^{•-}** are depicted in Scheme 3. Possibly, preorganized **Ag[Z-1×E-1]^{•-}** allows for a faster **[Ag(SH)(E-1)]⁻** elimination than **Ag[Z-1×E-1]^{•-}** accounting for the rapid decay of the **[Z-1×E-1]^{•-}** EPR resonance (Figure 4). After back-slippage of the η^1 - $C_5H_4-N=C=CH_2$ rings to a η^5 coordination, the ferrocenium ketenimine **2^{•+}** is formed. This ferrocenium ion can be reduced to ketenimine **2**. Neither deprotonation, nor oxidation alone leads to the release of sulfur from **H-1** according to ESI⁺ mass spectra, hence HS⁻ elimination from the zwitterions **E-1[•]**/**Z-1[•]** (or their piano stool derivatives, see Scheme 3) is highly conceivable. Treating the organic thioamide PhNHC(S)CH₃ with oxidants and bases does not lead to detectable HS⁻ elimination or sulfur-deficient species as deduced from odor and ESI mass spectrometry, possibly due to the incompatible redox potentials.¹⁷ Hence, the redox-active ferrocenyl substituent is crucial for the observed reactivity.

The key ferrocenyl/ferrocenium ketenimines **2/2^{•+}** are certainly highly electrophilic, similar to classical ketenimines and activated keteniminium ions.³²⁻³⁷ A reactive ferrocenyl ketene Fc(H)C=C=O has been trapped by the Staudinger [2+2] cycloaddition reaction with imines to give β -lactams³⁸, and spectroscopically identified by its IR signature.³⁹ The

sterically protected ferrocenyl tri(isopropyl)silyl ketene $\text{Fc}(^i\text{Pr}_3\text{Si})\text{C}=\text{C}=\text{O}$ has been even structurally characterized.⁴⁰ The C-ferrocenyl ketenimine $\text{Fc}(\text{H})\text{C}=\text{C}=\text{NH}$ has been prepared from acetonitrile and isolated.⁴¹ To the best of our knowledge, the N-ferrocenyl ketenimine $\text{H}_2\text{C}=\text{C}=\text{NFC}$ **2** has not yet been reported. Given that reactive ferrocenyl ketenimines form, the observed peaks at mass-to-charge ratios of 677.2 and 902.0 in the FD^+ mass spectrum (Figure 6) are straightforwardly assigned to oligo ketenimines $[(\mathbf{2})_n+2\mathbf{H}]^+$ ($n = 3, 4$) with a tentative structure depicted in Scheme 3.⁴² Formally, the ketenimine **2** has oligomerized, has been hydrogenated at the end groups ($+2\text{H}^+ + 2\text{e}^-$) and is then oxidized to a ferrocenium cation in the mass spectrometer ($-\text{e}^-$) (Scheme 3). The N-ferrocenyl ketenimine cation $\mathbf{2}^{\bullet+}$ is even expected to be superelectrophilic in nature due to the cationic ferrocenium substituent.³² Indeed, the DFT calculated orbital coefficient at the central carbon atom of the ketenimine's LUMO increases upon oxidation of **2** to $\mathbf{2}^{\bullet+}$ (Supporting Information, Figure S18).³⁷

Nucleophiles are indeed present in the reaction mixture, namely the anions $\mathbf{E-1}^-/\mathbf{Z-1}^-$, simply formed by deprotonation of $\mathbf{E-[H-1]}/\mathbf{Z-[H-1]}$ (vide supra). Hence, nucleophilic attack of the ambident N/S nucleophiles $\mathbf{E-1}^-/\mathbf{Z-1}^-$ at the superelectrophilic ketenimine $\mathbf{2}^{\bullet+}$ is conceivable (Scheme 4) and should lead to neutral zwitterionic species $\mathbf{5}^\bullet$ (N attack) and $\mathbf{6}^\bullet$ (S attack) with the composition $\text{C}_{24}\text{H}_{23}\text{Fe}_2\text{N}_2\text{S}$ ($m/z = 483$). Peaks with mass-to-charge ratios $m/z = 483.95$ (FD^+ , Figure 3) and 485.06 (ESI^+ , Figure 4) are observed in the FD^+ and ESI^+ mass spectra, respectively, corresponding to protonated species $[\mathbf{H-5}]^{\bullet+}/[\mathbf{H-6}]^{\bullet+}$ and $[\mathbf{H}_2\text{-5}]^+/\mathbf{H}_2\text{-6}^+$ respectively (Scheme 4). N or S attack of $\mathbf{E-1}^-/\mathbf{Z-1}^-$ at $\mathbf{2}^{\bullet+}$ cannot be distinguished at this stage by mass spectrometry. Yet, steric arguments should favor N attack by the Z isomer and S attack by the E isomer (Scheme 4).

Preparative scale reaction (method B) yields a brown ferrocene containing product, which consists of at least two E/Z isomers of thioamides **H-5** according to ^1H and ^{13}C NMR spectroscopic assignment and FD^+ mass spectrometry, but more isomers are conceivable (Supporting Information, Figures S19-S25). These products arise from the nucleophilic attack of the amide nitrogen of $\mathbf{E/Z-1}^-$ at $\mathbf{2}^{\bullet+}$ (N attack, Scheme 4), followed by protonation and reduction of the ferrocenium fragment (Scheme 4). A single isomer **H-5** predominates, showing a characteristic ^{13}C NMR resonance for the C=S fragment at $\delta = 204.3$ ppm. No attempts were performed to separate the E/Z isomers of **H-5**.

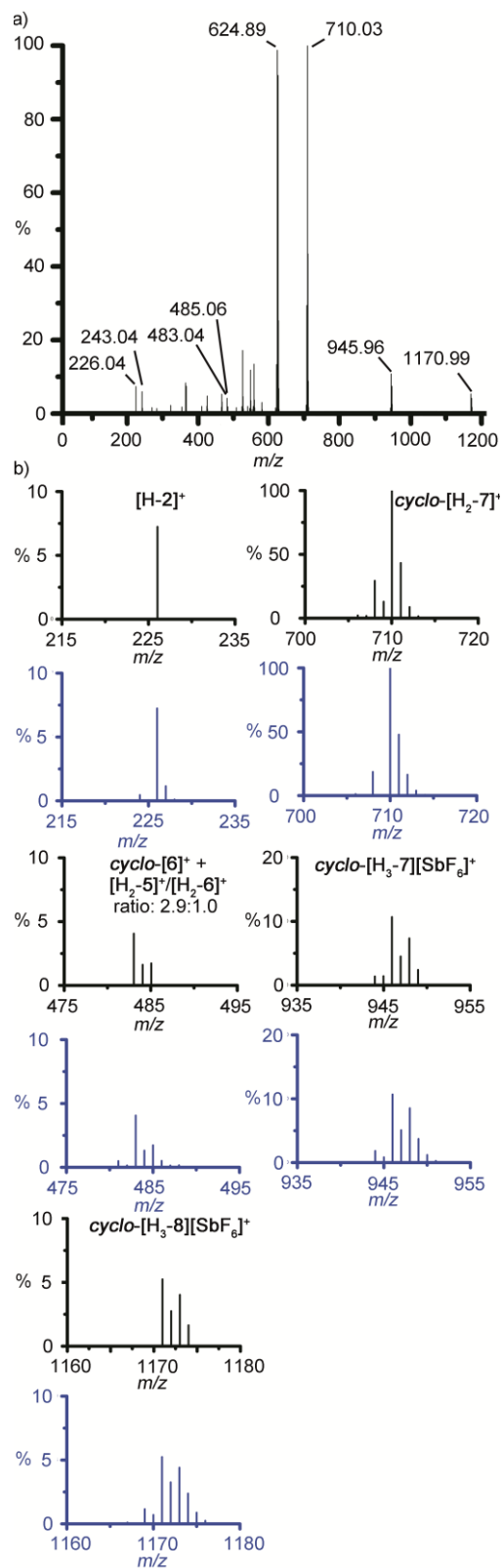


Figure 7. a) ESI⁺ mass spectrum of a sample prepared by method B in CH₂Cl₂. b) Experimental (black) and calculated (blue) isotope distributions and assignments of important peaks.

exceptional metrical parameters (Supporting Information, Table S3). The C-C and C-N distances fit to the proposed double bond characters as indicated in *cyclo*-[H₃-7]²⁺ (Scheme 4). The twofold positive charge of *cyclo*-[H₃-7]²⁺ is basically located at the ring nitrogen atom and at the terminal amidinium nitrogen atom. All ferrocenyl substituents display Fe-C distances consistent with neutral ferrocenyl substituents (Supporting Information, Table S3). The amidinium NH group engages in a non-classical NH...Fe hydrogen bond to the central ferrocene with a short Fe2...N3 distance of 3.364(5) Å forming a six-membered ring. Such non-classical bonding motifs are increasingly observed in NH containing ferrocenyl compounds with rather acidic NH groups exhibiting Fe...N distances around 3.46 Å.⁴³⁻⁴⁶

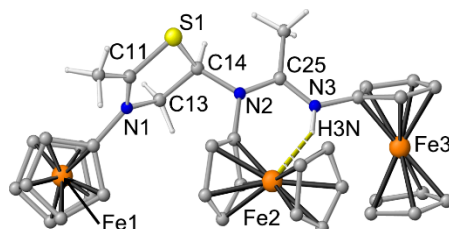


Figure 8. Molecular structure of *cyclo*-[H₃-7][SbF₆]₂ derived from single crystal XRD analysis (Cp protons and [SbF₆]⁻ counter ions omitted for clarity; atom numbering according to CIF file).

This intriguing structural motif allows tracing back the formation of the initial zwitterionic species *cyclo*-[H-6], which initiates the oligomerization of ketenimine **2** via zwitterionic *cyclo*-[H-7] and *cyclo*-[H-8] (Scheme 4). Protonation of these 4,5-dihydro-1,3-thiazolium enamides to the 4,5-dihydro-1,3-thiazolium imines *cyclo*-[H₂-7]⁺ and *cyclo*-[H₂-8]⁺ terminates the anionic oligomerization process (Scheme 4). The doubly protonated species of *cyclo*-[H-7] and *cyclo*-[H-8], namely {*cyclo*-[H₃-7][SbF₆]}⁺ and {*cyclo*-[H₃-8][SbF₆]}⁺ have been identified in the ESI⁺ mass spectra as ion pairs at $m/z = 945.96$ (calcd. 945.97) and $m/z = 1170.99$ (calcd. 1171.00) with expected isotopic distribution patterns (^{121,123}Sb), respectively (Figure 7). NMR and FD⁺ mass spectroscopic data further confirm the composition and structure of *cyclo*-[H₃-7][SbF₆]₂ (Supporting Information, Figures S27-S33).

The zwitterionic 4,5-dihydro-1,3-thiazolium heterocycle of *cyclo*-[H-6] is formed by a ring-closing reaction of **H-6** ($m/z = 484$, vide supra). To the best of our knowledge, no such

architectures have been reported before. Comparable mesoionic heterocycles are the münchnones, sydnones or montrealones.⁴⁷⁻⁵⁰ Acyclic **H-6** itself can be envisaged as the product of the nucleophilic attack of the sulfur atom of **E-1**⁻ at ketenimine **2**^{•+} after protonation and reduction (Scheme 4). Isomerization to the *E* imines **E,E-[H-6]/E,Z-[H-6]** initiates the ring closing reaction to give **cyclo-[H-6]** with a stereogenic carbon center. Chain growth by multiple additions of ketenimine **2** and termination by protonation of the enamide determine the chain lengths of the resulting oligomers (Scheme 4).

Oligomers **cyclo-[H₃-7]**²⁺ (XRD, NMR, MS) and **cyclo-[H₃-8]**²⁺ (MS, DFT) are interesting ferrocene containing, redox-active building blocks (Figure 9). Deprotonation of the amidinium NH^{•••}Fe group can possibly re-activate the active zwitterionic 4,5-dihydro-1,3-thiazolium enamide species for further anionic polymerization processes, including formation of block copolymers. These potential applications are beyond the scope of the current exploratory and mechanistic study.

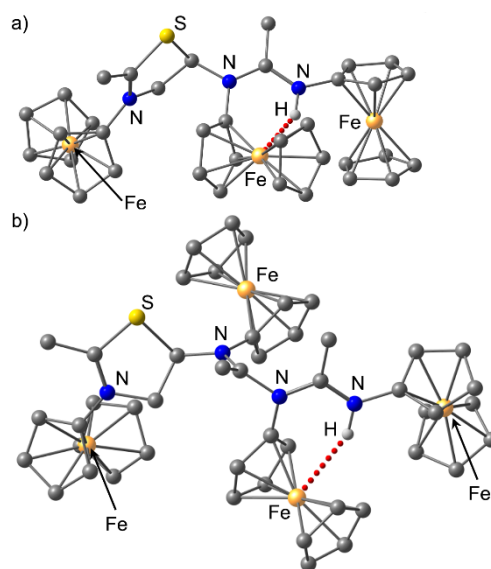


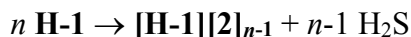
Figure 9. DFT optimized geometries of a) **cyclo-[H₃-7]**²⁺ and b) **cyclo-[H₃-8]**²⁺ (CH protons omitted for clarity).

In total, the oxidants (Ag[SbF₆], DDQ) serve only as initiators to form **2**^{•+}, yet these oxidants are not required in stoichiometric amounts. The same arguments hold for the tasks of the base: the base is only required to initially form **2**^{•+} and **1**⁻. This differs from the reported dehydrogenative formation of benzothiazoles from diaryl thioamides using

stoichiometric amounts of oxidants and base.⁵¹ The net reaction of the N attack route (Scheme 4) is:



The net reaction of the S attack route (Scheme 3) is the oligomerization of **2** with zwitterionic *cyclo*-[**H-6**] as initiator.



The formation of zwitterionic *cyclo*-[**H-6**] is conceptually similar to the preparation of münchnones (mesoionic 1,3-oxazolium-5-olates) and other mesoionic heterocycles.⁴⁷⁻⁵⁰ To the best of our knowledge, the formation of zwitterionic 4,5-dihydro-1,3-thiazolium heterocycles⁵², however, has not yet been described.

3.3.4 Conclusion

Coordination of ferrocenyl thioamide *E/Z*-[**H-1**] to Ag⁺ and subsequent electron transfer gives the ferrocenium ions *E/Z*-[**H-1**]^{•+}. Deprotonation of *E/Z*-[**H-1**] gives the anions **Z-1**⁻ and **E-1**⁻. Reaction of **E-1**⁻ with Ag[SbF₆] gives a Ag₆(**E-1**)₆ cluster and some **E-1**[•] while **Z-1**⁻ is only oxidized to **Z-1**[•]. Both zwitterions **Z-1**[•] and **E-1**[•] can be stabilized as piano stool iron(III) complexes by coordination of **E-1**⁻ but engage in further reactions to sulfur-deficient products by elimination of AgSH.

The combined action of proton and electron abstraction from ferrocenyl thioamide **H-1** leads to elimination of HS⁻ and formation of the super-electrophilic ketenimine cation **2**^{•+}. Interception of the superelectrophile **2**^{•+} by e⁻/H⁺ gives the keteniminium cation [**H-2**]⁺. Interception of **2**^{•+} by water results in formation of ferrocenium amide [**H-3**]^{•+} according to mass spectrometric studies. In addition, mass spectrometry provides evidence for oligo ketenimines [(**2**)_n+2H]⁺, likely featuring a [CN]_n backbone and ferrocenyl side chains.

Ferrocenium ketenimine **2**^{•+} is also trapped by the ambident nucleophile **1**⁻, generated from **H-1** and the base in the reaction mixture. Nucleophilic attack of the nitrogen atom of **Z-1**⁻ at **2**^{•+} and trapping by H⁺/e⁻ gives **H-5** as a mixture of *E/Z* isomers. Nucleophilic attack of the sulfur atom of **E-1**⁻ at **2**^{•+} and trapping by H⁺/e⁻ gives **H-6** as a mixture of *E/Z* isomers. Cyclization of **H-6** yields the novel zwitterionic 4,5-dihydro-1,3-thiazolium 5-substituted heterocycle *cyclo*-[**H-6**]. We coin this heterocyclic substance class “4,5-dihydro mogone imines”.⁵² The anionic substituent of *cyclo*-[**H-6**] serves as initiator for the

oligomerization of ketenimine **2** to give the oligomers *cyclo*-[**H-7**] and *cyclo*-[**H-8**]. *cyclo*-[**H3-7**]²⁺ and *cyclo*-[**H3-8**]²⁺ are structurally characterized by XRD, NMR spectroscopic and/or mass spectrometric techniques. All available spectroscopic, analytical and theoretical data are consistent with the proposed mechanistic scheme. This reactivity adds a new facet to ketenimine chemistry.⁵³

The proposed neutral and cationic *N*-ferrocenyl ketenimine intermediates **2/2**^{•+} could furthermore serve as useful monomers for ferrocene containing polymeric materials¹²⁻¹⁵ with [CN]_n backbones. Furthermore, the ability to trigger SH⁻ elimination from *E,Z*-[**H-1**] by oxidants in combination with bases could allow using *N*-ferrocenyl thioamides as structural motifs for H₂S releasing prodrugs.¹⁶

3.3.5 Experimental Section

General Procedures

All reactions were performed under an argon atmosphere unless otherwise noted. Dichloromethane and acetonitrile were dried with CaH₂, petroleum ether (b.p. 40-60 °C) and diethyl ether were dried with sodium. All solvents were distilled prior to use. All reagents were used as received from commercial suppliers (Acros, Sigma-Aldrich, ABCR). NMR spectra were recorded on a Bruker DRX 400 spectrometer at 400.31 MHz (¹H) and 100.07 MHz (¹³C{¹H}) or on a Bruker Avance III 600 at 600.134 MHz (¹H) and 150.919 MHz (¹³C{¹H}). All resonances are reported in ppm vs the solvent signal as internal standard: CD₂Cl₂ (¹H, δ 5.32 ppm; ¹³C, δ 54.0 ppm).⁵⁴ IR spectra were recorded with a BioRad Excalibur FTS 3100 spectrometer as KBr disks or by using KBr cells in CH₂Cl₂. Electrochemical experiments were carried out on a BioLogic SP-50 voltammetric analyzer by using a platinum working electrode, a platinum wire counter electrode, and a 0.01 M Ag/AgNO₃ reference electrode. The measurements were carried out at a scan rate of 100 mV s⁻¹ for cyclic voltammetry experiments and at 50 mV s⁻¹ for square wave voltammetry experiments in 0.1 M [ⁿBu₄N][B(C₆F₅)₄] as supporting electrolyte in CH₂Cl₂. Potentials are referenced against the decamethylferrocene/ decamethylferrocenium couple (*E*_{1/2} = 550 ± 5 mV vs ferrocene/ ferrocenium under our experimental conditions) and are given relative to the ferrocene/ferrocenium couple. UV/vis/near-IR spectra were recorded on a Varian Cary 5000 spectrometer by using 1.0 cm cells (Hellma, Suprasil). CW EPR spectra (X-band; ca. 9.4 GHz; ca. 20 mM) were measured on a Miniscope MS 300 at 77 K cooled by liquid

nitrogen in a finger Dewar (Magnettech GmbH, Berlin, Germany). g factors are referenced to external Mn^{2+} in ZnS ($g = 2.118, 2.066, 2.027, 1.986, 1.946, 1.906$). Simulations of EPR spectra were performed with EasySpin (v 5.0.0) for MatLab (R2015a).⁵⁵ Relative concentrations of EPR-active species (Fig. 1b, Fig. 4) were obtained by simulation and weighted combination of subspectra using EasySpin (v 5.0.0) for MatLab (R2015a).⁵⁵ ESI mass spectra were recorded on a Micromass Q-TOF-Ultima spectrometer. FD^+ mass spectra were recorded on a FD Finnigan MAT95 spectrometer or on a Thermo Scientific DFS with LIFDI upgrade (Linden CMS). Conductivities were measured with a Greisinger conductivity cell, model 6MH 3431 LFE-210 with platinum electrodes in the concentration range 10^{-3} – 10^{-4} M in CH_2Cl_2 . The equivalent conductivity Λ_e was plotted as a function of $c^{0.5}$, where c is the equivalent concentration. To determine Λ_0 , Λ_e was extrapolated to infinite dilution. $\Lambda_0 - \Lambda_e$ was plotted versus $c^{0.5}$ to obtain the Onsager plots. From this plot, the slopes of various electrolyte types can be easily compared (Supporting Information, Figures S9 and S10). Elemental analyses were performed by the microanalytical laboratory of the chemical institutes of the University of Mainz.

Density Functional Theory Calculations.

These were carried out with the ORCA 3.0.2/DFT series of programs.⁵⁶ For geometry optimizations and energy calculations, the B3LYP formulation of density functional theory was used employing the SV(P) basis set^{57,58}, the RIJCOSX approximation^{59,60}, the zeroth order regular approximation (ZORA)^{61,62}, and the KDIIS algorithm⁶³, at GRID4 and employed Atom-pairwise Dispersion Correction as reported by Grimme.⁶⁴⁻⁶⁶ No symmetry constraints were imposed on the molecules. The presence of energy minima of the ground states was checked by numerical frequency calculations. Solvent modeling was done employing the conductor like screening model (COSMO CH_2Cl_2).⁶⁷ The approximate free energies at 298 K were obtained through thermochemical analysis of the frequency calculation, using the thermal correction to Gibbs free energy as reported by ORCA 3.0.2.

Crystal Structure Determinations.

Intensity data were collected with a Bruker AXS Smart1000 CCD diffractometer with an APEX II detector and an Oxford cooling system and corrected for absorption and other effects using Mo K_α radiation ($\lambda = 0.71073 \text{ \AA}$). The diffraction frames were integrated using the SAINT package, and most were corrected for absorption with MULABS^{68,69}. The structures were solved by direct methods and refined by the full-matrix method based on

F^2 using the SHELXTL software package.^{70,71} All non-hydrogen atoms were refined anisotropically, while the positions of all hydrogen atoms were generated with appropriate geometric constraints and allowed to ride on their respective parent carbon/nitrogen atoms with fixed isotropic thermal parameters.

Crystal data for **[Cu₂(H-1)₆][BF₄]₂**: C₇₆H₈₆B₂Cl₈Cu₂F₈Fe₆N₆S₆ (2195.27); $T = 173$ K; orange needle; $0.36 \times 0.16 \times 0.12$ mm; triclinic; $P\bar{1}$; $a = 11.092(3)$ Å; $b = 15.327(4)$ Å; $c = 15.563(4)$ Å; $\alpha = 60.772(6)^\circ$; $\beta = 71.684(6)^\circ$; $\gamma = 78.348(6)^\circ$; $V = 2188.3(10)$ Å³; $Z = 1$; $F(000) = 1112$; $\xi = 1.666$ g cm⁻³; $\mu = 1.891$ mm⁻¹; Θ range 1.60 – 28.05° ; index ranges $-14 \leq h \leq 13$, $-20 \leq k \leq 20$, $-20 \leq l \leq 20$; 21797 reflections collected; 10513 independent reflections; parameters 541; maximum/minimum transmission 0.8048/0.5492; goodness of fit on F^2 0.808; largest difference peak and hole 0.959/–0.697 e Å⁻³; $R_1(I > 2\sigma) = 0.0786$; $R_1(\text{all data}) = 0.2343$; $wR_2(I > 2\sigma) = 0.1278$; $wR_2(\text{all data}) = 0.1684$.

Crystal data for **Ag₆(E-1)₆**: C₇₂H₇₂Ag₆Fe₆N₆S₆ (2196.03); $T = 173$ K; orange-red block; $0.21 \times 0.16 \times 0.01$ mm; triclinic; $P\bar{1}$; $a = 9.7540(17)$ Å; $b = 12.461(3)$ Å; $c = 16.332(3)$ Å; $\alpha = 109.710(5)^\circ$; $\beta = 106.676(4)^\circ$; $\gamma = 90.193(4)^\circ$; $V = 1779.1(6)$ Å³; $Z = 1$; $F(000) = 1080$; $\xi = 2.050$ g cm⁻³; $\mu = 3.017$ mm⁻¹; Θ range 1.75 – 27.96° ; index ranges $-12 \leq h \leq 12$, $-16 \leq k \leq 15$, $0 \leq l \leq 21$; 8515 reflections collected; 8515 independent reflections; 9 restraints; parameters 437; maximum/minimum transmission 0.7456/0.5652; goodness of fit on F^2 1.016; largest difference peak and hole 0.923/–1.126 e Å⁻³; $R_1(I > 2\sigma) = 0.0561$; $R_1(\text{all data}) = 0.1040$; $wR_2(I > 2\sigma) = 0.0973$; $wR_2(\text{all data}) = 0.1156$. The measured crystal was refined as a two-component twin with the twin law $(-1.001/0.001/0.003; -0.004/-1.000/0.000; -1.042/-0.891/1.001)$ and an occupancy factor of 0.19421.

Crystal data for **cyclo-[H₃-7][SbF₆]₂**: C₃₇H₃₉C₁₂F₁₂Fe₃N₃SSb₂ (1267.72); $T = 173$ K; brown plate; $0.180 \times 0.150 \times 0.040$ mm; triclinic; $P\bar{1}$; $a = 9.6219(8)$ Å; $b = 13.1000(11)$ Å; $c = 17.2736(15)$ Å; $\alpha = 104.403(2)^\circ$; $\beta = 92.447(2)^\circ$; $\gamma = 96.711(2)^\circ$; $V = 2088.6(3)$ Å³; $Z = 2$; $F(000) = 1240$; $\xi = 2.016$ g cm⁻³; $\mu = 2.559$ mm⁻¹; Θ range 1.761 – 28.007° ; index ranges $-12 \leq h \leq 12$, $-16 \leq k \leq 17$, $-22 \leq l \leq 22$; 24230 reflections collected; 10047 independent reflections; parameters 563; maximum/minimum transmission 1.14058/0.86244; goodness of fit on F^2 0.883; largest difference peak and hole 1.703/–1.535 e Å⁻³; $R_1(I > 2\sigma) = 0.0556$; $R_1(\text{all data}) = 0.1114$; $wR_2(I > 2\sigma) = 0.1172$; $wR_2(\text{all data}) = 0.1329$.

CCDC-1475564, 1475563, 1484852 (*cyclo*-[H₃-7], [Cu₂(H-1)₆][BF₄]₂), Ag₆(E-1)₆ contain supplementary crystallographic data for this paper. These data can be obtained free of charge from The Cambridge Crystallographic Data Centre via www.ccdc.cam.ac.uk/data_request/cif.

Deprotonation and oxidation and of *E/Z*-[H-1] with *n*-butyl lithium and Ag[SbF₆] (method A).

E/Z-[H-1] (100 mg; 0.38 mmol; 1.0 eq.) was dissolved in THF (20 ml). *n*-Butyl lithium (2.5 m in *n*-hexane; 0.15 ml; 0.38 mmol; 1.0 eq.) was added. The solvent was removed under reduced pressure. The residue was dissolved in dichloromethane (30 ml) and Ag[SbF₆] (132 mg; 0.38 mmol; 1.0 eq.) was added as a solid. The mixture was filtered through a syringe filter and the solvent was removed under reduced pressure. Re-dissolution in dichloromethane (40 ml), filtration through a syringe filter and removal of the solvent under reduced pressure yields a brown raw product.

Deprotonation and oxidation and of *E/Z*-[H-1] with lithium dimethyl amide and Ag[SbF₆] (method B).

E/Z-[H-1] (100 mg; 0.38 mmol; 1.0 eq.) was dissolved in THF (20 ml). Lithium dimethylamide (19.6 mg; 0.38 mmol; 1.0 eq.) was added. The solvent was removed under reduced pressure. The residue was dissolved in dichloromethane (30 ml) and Ag[SbF₆] (132 mg; 0.38 mmol; 1.0 eq.) was added as a solid. The mixture was filtered through a syringe filter and the solvent was removed under reduced pressure. Re-dissolution in CH₂Cl₂ (40 ml), filtration through a syringe filter and removal of the solvent under reduced pressure yields a brown raw product.

Deprotonation and oxidation and of *E/Z*-[H-1] with *tert*-butylimino-tris(dimethylamino)-phosphorane and Ag[SbF₆] (method C) for EPR spectroscopy.

E/Z-[H-1] (1 mg; 0.0037 mmol; 1.0 eq.) was dissolved in dichloromethane (300 μl) and treated with Ag[SbF₆] (1.32 mg; 0.0037 mmol; 1.0 eq.). *tert*-Butylimino-tris(dimethylamino)-phosphorane (0.94 μl; 0.0037 mmol; 1.0 eq.) was added and the sample was filtered through a syringe filter into an EPR tube. X-band EPR spectra were recorded at 77 K.

Deprotonation and oxidation and of *E/Z*-[H-1] with *tert*-butylimino-tris(dimethylamino)-phosphorane and Ag[SbF₆] (method C).

E/Z-[H-1] (100 mg; 0.38 mmol; 1.0 eq.) was dissolved in dichloromethane (20 ml) and treated with Ag[SbF₆] (132 mg; 0.38 mmol; 1.0 eq.). *Tert*-butylimino-tris(dimethylamino)-phosphorane (0.097 ml; 0.38 mmol; 1.0 eq.) was added. The mixture was filtered through a syringe filter and the solvent was removed under reduced pressure to yield a brown raw product.

Deprotonation and oxidation and of *E*-[H-1] with 2,3-dichloro-5,6-dicyano-1,4-benzoquinone (DDQ) in CH₃CN (method D) for mass spectrometry.

E-[H-1] (100 mg; 0.38 mmol; 1.0 eq.) was dissolved in acetonitrile (20 ml) and treated with 2,3-dichloro-5,6-dicyano-1,4-benzoquinone (41 mg; 0.18 mmol; 0.5 eq.). The mixture was stirred for 30 minutes and cobaltocene (73 mg; 0.38 mmol; 1.0 eq.) was added as a solid resulting in H₂S evolution. The raw product was purified by column chromatography (3×15 cm, SiO₂, ethyl acetate) giving a brown powder.

Deprotonation and oxidation and of *E*-[H-1] with 2,3-dichloro-5,6-dicyano-1,4-benzoquinone (DDQ) in CH₃CN (method D) for EPR spectroscopy.

E-[H-1] (1 mg; 0.0037 mmol; 1.0 eq.) was dissolved in acetonitrile (300 μl) and treated with 2,3-dichloro-5,6-dicyano-1,4-benzoquinone (0.41 mg; 0.0018 mmol; 0.5 eq.). X-band EPR spectra were recorded at 77 K.

Preparative synthesis of H-5 (isomer mixture).

Method B was applied, starting with *E/Z*-[H-1] (50 mg, 0.19 mmol; 1.0 eq.) The raw product was purified by column chromatography (3×30 cm, Al₂O₃ Brockmann II, CH₂Cl₂/PE 1:1) giving a yellow powder. Yield 32 % (13.2 mg, 0.03 mmol). ¹H NMR (400 MHz, CD₂Cl₂, 298 K): δ = 4.59 (ddd, 1H, H^{β1,imine}/H^{β2,imine}), 4.38 (ddd, 1H, H^{β1,imine}/H^{β2,imine}), 4.23 (ddd, 2H, H^{α1,imine}/H^{α2,imine}), 4.21 (s, 5H, H^{Cp,imine}/H^{Cp,amide}), 4.16 (ddd, 1H, H^{β1,amide}/H^{β2,amide}), 4.09 (ddd, 1H, H^{β1,amide}/H^{β2,amide}), 4.09 (ddd, 1H, H^{α1,amide}/H^{α2,amide}), 4.07 (s, 5H, H^{Cp,imine}/H^{Cp,amide}), 4.06 (ddd, 1H, H^{α1,amide}/H^{α2,amide}), 3.64 (ddd, 1H, H^{α1,amide}/H^{α2,amide}), 2.53 (s, 3H, CH₃^{imine}), 2.19 (s, 3H, CH₃^{amide}) ppm (major

isomer, 80 %); $\delta = 2.65$ (s, 3H, CH₃^{amide}), 2.38 (s, 3H, CH₃^{imine}) ppm (one minor isomer, 12 %). ¹³C{¹H} NMR (100 MHz, CD₂Cl₂, 298 K): $\delta = 204.3$ (C=S), 151.9 (C=N), 99.4 (Cⁱ, imine), 93.8 (Cⁱ, amide), 71.2 (Cp^{imine}/Cp^{amide}), 70.4 (C ^{β 1}, imine/C ^{β 2}, imine), 70.3 (Cp^{imine}/Cp^{amide}), 67.7 (C ^{α 1}, imine/C ^{α 2}, imine), 67.0 (C ^{α 1}, imine/C ^{α 2}, imine), 66.8 (C ^{β 1}, amide/C ^{β 2}, amide/C ^{α 1}, amide/C ^{α 2}, amide), 66.5 (C ^{α 1}, amide/C ^{α 2}, amide), 60.4 (C ^{β 1}, imine/C ^{β 2}, imine), 33.1 (CH₃^{amide}), 24.1 (CH₃^{imine}) ppm (major isomer); $\delta = 149.59$ (C^{imine}) ppm (one minor isomer). MS(FD⁺): m/z (%) = 484.19 ([H-5]^{•+}).

Preparative synthesis of *cyclo*-[H₃-7][SbF₆]₂.

Method A was applied. The raw product was purified by column chromatography (3×30 cm, SiO₂, CH₂Cl₂ → ethyl acetate) giving a brown powder. Yield 6 % (7.2 mg, 0.008 mmol; based on *cyclo*-[H₃-7][SbF₆]₂). The product also contains some *cyclo*-[H₃-8][SbF₆]₂. A few crystals of *cyclo*-[H₃-7][SbF₆]₂ suitable for X-Ray diffraction were obtained by evaporating a saturated dichloromethane solution of the raw product. ¹H NMR (600 MHz, CD₂Cl₂, 298 K): $\delta = 7.99$ (s, 1H, H^{NH}), 4.63 (pt, 2H, H ^{α 1/ β 1}), 4.51 (pt, 2H, H ^{α 2/ β 2}), 4.47 (pt, 2H, H ^{α 1/ β 1}), 4.46 (s, 5H, H^{Cp1/Cp2/Cp3}), 4.42 (s, 5H, H^{Cp1/Cp2/Cp3}), 4.37 (s, 5H, H^{Cp1/Cp2/Cp3}), 4.40 (pt, 2H, H ^{α 2/ β 2}), 4.34 (pt, 2H, H ^{α 3/ β 3}), 4.31 (s, 1H, H^{CH}), 4.25 (pt, 2H, H ^{α 3/ β 3}), 4.10 (s, 2H, H^{CH₂}), 2.58 (s, 2H, H^{NH-iminium-CH₃}), 2.58 (s, 2H, H^{iminium-CH₃}) ppm. ¹³C{¹H} NMR (150 MHz, CD₂Cl₂, 298 K): $\delta = 160.2$ (C^{iminium-C}), 154.8 (C^{NH-iminium-C}), 71.2 (C^{Cp1/Cp2/Cp3}), 71.1 (C^{Cp1/Cp2/Cp3}), 70.6 (C^{Cp1/Cp2/Cp3}), 70.0 (C^{CH₂}), 68.0 (C ^{α 2/ β 2}), 68.4 (C ^{α 1/ β 1}), 67.0 (C ^{α 3/ β 2}), 66.2 (C ^{α 1/ β 3}), 66.0 (C ^{α 3/ β 3}), 65.4 (C^{CH}), 64.7 (C ^{α 2/ β 2}) ppm. MS(FD⁺): m/z (%) = 707.34 (35, {*cyclo*-[H-7]-2H}^{•+}), 932.67 (100, {*cyclo*-[H-8]-2H}^{•+}).

Synthesis of [Cu₂(H-1)₆][BF₄]₂; bis- $\{\mu$ -(κ S-(*E*-[N-thioacetyl ferrocenylamine])) bis[di-(κ S-Z-[N-thioacetyl ferrocenyl-amine])-copper(I)].

Tetrakis(acetonitrile) copper(I) tetrafluoroborate (307 mg; 0.975 mmol, 3.0 eq.) and copper powder (125.0 mg; 0.375 mmol; 1.0 eq.) were suspended in CH₃CN (50 ml) and stirred at room temperature for 24 hours. *E/Z*-[H-1] (250 mg; 0.975 mmol; 1.0 eq.) was added to the suspension and the mixture was heated to reflux for one hour. The suspension was slowly cooled to room temperature and diethyl ether (200 ml) was added. A colorless precipitate formed and was filtered off. The solvent of the filtrate was removed under reduced pressure. An orange oil was obtained, which was dissolved in CH₂Cl₂ (100 ml) and precipitated by

addition of petroleum ether (bp. 40-60 °C; 100 ml). After removal of the solvent mixture under reduced pressure an orange-red powder was obtained. Single crystals were obtained from a CH₂Cl₂ solution of [Cu₂(H-1)₆][BF₄]₂. Yield. 31 % (93.5. mg, 0.51 mmol). ¹H NMR (400 MHz, CD₂Cl₂, 298 K): δ = 10.38 (s, 2H, NH of *E*-[H-1]), 10.09 (s, 4H, NH of *Z*-[H-1]), 4.94 (pt, 4H, ³J_{HH} = 1.91 Hz, H^α of *E*-[H-1]), 4.42 (pt, 8H, ³J_{HH} = 1.94 Hz, H^α of *Z*-[H-1]), 4.35 (s, 20H, CpH of *Z*-[H-1]), 4.33 (s, 10H, CpH of *E*-[H-1]), 4.25 (pt, 4H, ³J_{HH} = 1.91 Hz, H^β of *E*-[H-1]), 4.24 (pt, 8H, ³J_{HH} = 1.94 Hz, H^β of *Z*-[H-1]), 2.81 (s, 6H, CH₃ of *E*-[H-1]), 2.48 (s, 12H, CH₃ of *Z*-[H-1]) ppm. ¹³C {¹H} NMR (100 MHz, CD₂Cl₂, 298 K): δ = 200.6 (C=S of *Z*-[H-1]), 198.1 (C=S of *E*-[H-1]), 94.0 (Cⁱ of *Z*-[H-1]), 93.8 (Cⁱ of *E*-[H-1]), 70.7 (Cp of *Z*-[H-1]), 70.6 (Cp of *E*-[H-1]), 67.7 (C^β of *E*-[H-1]), 67.3 (C^β of *Z*-[H-1]), 65.7 (C^α of *Z*-[H-1]), 65.6 (C^α of *E*-[H-1]), 34.7 (CH₃ of *E*-[H-1]), 28.6 (CH₃ of *Z*-[H-1]) ppm. MS(ESI⁺): *m/z* (%) 321.93 (40) [Cu(H-1)]⁺, 580.90 (100) [Cu(H-1)₂]⁺, 839.97 (3) [Cu(H-1)₃]⁺, 1250.91 (100) [Cu₂(H-1)₄BF₄]⁺. IR (KBr): $\tilde{\nu}$ = 3281 (m, NH), 3198 (w, NH), 1548 (b, CS(I)), 1384 (b, CS(II)) cm⁻¹. IR (CH₂Cl₂): $\tilde{\nu}$ = 3361 (w, NH), 3267 (m, NH), 3209 (m, NH), 1531 (m, CS(I)) cm⁻¹. UV/vis (CH₂Cl₂): λ_{max} (ε) 256 (7430), 313 (7525), 378 (2715), 456 nm (755 M⁻¹ cm⁻¹). CV (CH₂Cl₂, vs FcH/ FcH⁺): E_{1/2} = 0.140 V (rev), 0.350 V (rev), E_p = 0.700 V (irrev). Λ_m⁰(CH₂Cl₂) = 43 S cm⁻¹ mol⁻¹. Anal. Calcd for C₇₂H₇₈Fe₆N₆S₆B₂F₈Cu₂ (1855.66)×Et₂O: C, 47.30; H, 4.50; N, 4.36; S, 9.97. Found: C, 47.43; H, 4.80; N, 4.55; S, 10.25.

Synthesis of Ag₆(E-1)₆.

E/Z-[H-1] (100 mg; 0.38 mmol; 1.0 eq.) was dissolved in dichloromethane (20 ml) and treated with Ag[SbF₆] (132 mg; 0.38 mmol; 1.0 eq.). *tert*-Butylimino-tris(dimethylamino)-phosphorane (97 μl; 0.38 mmol; 1.0 eq.) was added. The mixture was filtered through a syringe filter and the solvent slowly evaporated under inert gas conditions at standard pressure for several days giving red crystals, which were separated from the mother liquor by decantation. Yield: 3.7 % (5.2 mg, 0.0024 mmol). IR (KBr): $\tilde{\nu}$ = 1562 (m, CS(I)), 1357 (s, CS(II)) cm⁻¹.

3.3.6 Associated Content

Supporting Information

Description of the XRD and solution structure of $[\text{Cu}_2(\text{H-1})_6][\text{BF}_4]_2$ and spectra of the new compounds (PDF).

Crystal structure data for compounds $[\text{Cu}_2(\text{H-1})_6][\text{BF}_4]_2$, $\text{Ag}_6(\text{E-1})_6$ and *cyclo*- $[\text{H}_3\text{-7}][\text{SbF}_6]_2$ (cif).

Coordinates of DFT calculated compounds (xyz).

Author Information

Corresponding Author

*E-mail for K.H.: katja.heinze@uni-mainz.de.

Notes

The authors declare no competing financial interest.

3.3.7 Acknowledgement

Parts of this research were conducted using the supercomputer Mogon and advisory services offered by Johannes Gutenberg University Mainz (www.hpc.uni-mainz.de), which is a member of the AHRP and the Gauss Alliance e.V.. We thank Petra Auerbach and Dr. Mihail Mondeskhi for collecting the LIFDI mass spectra and Regine Jung-Pothmann for collection of the diffraction data. Financial support from the EU-COST Action CM1302 SIPs is gratefully acknowledged.

3.3.8 References

- [1] Heinze, K.; Schlenker, M.; *Eur. J. Inorg. Chem.* **2004**, 2974–2988.
- [2] Heinze, K.; Schlenker, M. *Eur. J. Inorg. Chem.* **2005**, 66–71.
- [3] Siebler, D.; Förster, C.; Heinze, K. *Eur. J. Inorg. Chem.* **2010**, 523–527.
- [4] Siebler, D.; Linseis, M.; Gasi, T.; Carrella, L. M.; Winter, R. F.; Förster, C.; Heinze, K. *Chem. Eur. J.* **2011**, *17*, 4540–4551.
- [5] Siebler, D.; Förster, C.; Heinze, K. *Dalton Trans.* **2011**, *40*, 3558–3575.
- [6] Kienz, T.; Förster, C.; Heinze, K. *Organometallics* **2014**, *33*, 4803–4812.
- [7] Neidlinger, A.; Kienz, T.; Heinze, K. *Organometallics* **2015**, *34*, 5310–5320.

- [8] Neidlinger, A.; Ksenofontov, V.; Heinze, K. *Organometallics* **2013**, *32*, 5955–5965.
- [9] Neidlinger, A.; Förster, C.; Heinze, K. *Eur. J. Inorg. Chem.* **2016**, 1274–1286.
- [10] Siebler, D.; Förster, C.; Gasi, T.; Heinze, K. *Organometallics* **2011**, *30*, 313–327.
- [11] Hüttinger, K.; Förster, C.; Heinze, K. *Chem. Commun.* **2014**, *50*, 4285–4288.
- [12] Pietschnig, R. *Chem. Soc. Rev.* **2016**, in press (DOI: 10.1039/c6cs00196c).
- [13] Gao, Y.; Shreeve, J. M. *J. Inorg. Organomet. Polym. Mater.* **2007**, *17*, 19–36.
- [14] Abd-El-Aziz, A.; Manners, I. *J. Inorg. Organomet. Polym. Mater.* **2005**, *15*, 157–195.
- [15] Gallei, M.; Tockner, S.; Klein, R.; Rehahn, M. *Macromol. Rapid Commun.* **2010**, *31*, 889–896.
- [16] Zheng, Y.; Yu, B.; Ji, K.; Pan, Z.; Chittavong, V.; Wang, B. *Angew. Chem.* **2016**, *128*, 4590–4594; *Angew. Chem. Int. Ed.* **2016**, *55*, 4514–4518.
- [17] Connelly, N. G.; Geiger, W. E. *Chem. Rev.* **1996**, *96*, 877–910.
- [18] Kloss, F.; Pidot, S.; Goerls, H.; Friedrich, T.; Hertweck, C. *Angew. Chem.* **2013**, *125*, 10945–10948; *Angew. Chem. Int. Ed.* **2013**, *52*, 10745–10748.
- [19] Constable, E. C.; Raithby, P. R.; *J. Chem. Soc., Dalton Trans.* **1987**, 2281–2283.
- [20] Kokkou, S. C.; Fortier, S.; Rentzeperis, P. J.; Karagiannidis, P. *Acta Cryst.* **1983**, *C39*, 178–180.
- [21] Lobana, T. S.; Castineiras, A. *Polyhedron* **2002**, *21*, 1603–1611.
- [22] Feltham, R. D.; Hayter, R. G. *J. Chem. Soc.* **1964**, 4587–459.
- [23] Su, W.; Hong, M.; Weng, J.; Liang, Y.; Zhao, Y.; Cao, R.; Thou, Z.; Chan, A. S. *C. Inorg. Chim. Acta* **2002**, *331*, 8–15.
- [24] Schwesinger, R.; Hasenfratz, C.; Schlemper, H.; Walz, L.; Peters, E.-M., Peters, K.; von Schnering, H.G. *Angew. Chem.* **1993**, *105*, 1420–1422; *Angew. Chem. Int. Ed.* **1993**, *32*, 1361–1363.
- [25] García-Vázquez, J. A.; Sousa-Pedrares, A.; Carabel, M.; Romero, J.; Sousa, A. *Polyhedron* **2005**, *24*, 2043–2054.
- [26] Sun, Q.; Chai, L.; Liu, H.; Wang, J. *Acta Cryst.* **2013**, *E69*, m50–m51.
- [27] Ashfield, L. J.; Cowley, A. R.; Dilworth, J. R.; Donnelly, P. S. *Inorg. Chem.* **2004**, *43*, 4121–4123.

- [28] Yue, C.; Yan, C.; Feng, R.; Wu, M.; Chen, L.; Jiang, F.; Hong, M. *Inorg. Chem.* **2009**, *48*, 2873–2879.
- [29] Elschenbroich, C.; Bilger, E.; Ernst, R. D.; Wilson, D. R.; Kralik, M. S. *Organometallics* **1985**, *4*, 2068–2070.
- [30] Costuas, K.; Paul, F.; Toupet, L.; Halet, J.-F.; Lapinte, C. *Organometallics* **2004**, *23*, 2053–2068.
- [31] Lohan, M.; Justaud, F.; Lang, H.; Lapinte, C. *Organometallics* **2012**, *31*, 3565–3574.
- [32] Lecomte, M.; Evano, G. *Angew. Chem.* **2016**, *128*, 4623–4627; *Angew. Chem. Int. Ed.* **2016**, *55*, 4547–4551.
- [33] Madelaine, C.; Valerio, V.; Maulide, N. *Chem. Asian J.* **2011**, *6*, 2224–2239.
- [34] Evano, G.; Coste, A.; Jouvin, K. *Angew. Chem.* **2010**, *122*, 2902–2921; *Angew. Chem. Int. Ed.* **2010**, *49*, 2840–2859.
- [35] Yasui, H.; Yorimitsu, H.; Oshima, K. *Chem. Lett.* **2008**, *37*, 40–41.
- [36] Kanemura, S.; Kondoh, A.; Yasui, H.; Yorimitsu, H.; Oshima, K. *Bull. Chem. Soc. Jpn.* **2008**, *81*, 506–514.
- [37] Ding, W.; Fang, D. *J. Org. Chem.* **2001**, *66*, 6673–6678.
- [38] Bonini, B. F.; Femoni, C.; Comes-Franchini, M.; Fochi, M.; Mazzanti, G.; Ricci, A.; Varchi, G. *Synlett* **2001**, 1092–1096.
- [39] Aguilar-Aguilar, C.; Allen, A. D.; Cabrera, E.; Federov, A. V.; Fu, N.; Henry-Riyad, H.; Kobayashi, S.; Leuninger, J.; Tidwell, T. T. *J. Org. Chem.* **2005**, *70*, 9556–9561.
- [40] Fu, N.; Allen, A. D.; Tidwell, T. T. *ARKIVOC* **2007**, *iii*, 143–150.
- [41] Dewey, F. *Tetrahedron Lett.* **1968**, 4207–4208.
- [42] Tidwell, T. T. *Ketenes II*, **2006**, John Wiley & Sons, Inc., Hoboken, New Jersey.
- [43] Förster, C.; Veit, P.; Ksenofontov, V.; Heinze, K. *Chem. Commun.* **2015**, *51*, 1514–1516.
- [44] Veit, P.; Förster, C.; Seibert, S.; Heinze, K. *Z. Anorg. Allg. Chem.* **2015**, *641*, 2083–2092.
- [45] Veit, C.; Prantl, E.; Förster, C.; Heinze, K. *Organometallics* **2016**, *35*, 249–257.
- [46] Hanauer, K.; Pham, M. T.; Förster, C.; Heinze, K. *Eur. J. Inorg. Chem.* in press (DOI: 10.1002/elic.201600918).

- [47] Reissig, H.-U.; Zimmer, R. *Angew. Chem.* **2014**, *37*, 9708-9710; *Angew. Chem. Int. Ed.* **2014**, *53*, 9708-9710.
- [48] Huisgen, R.; Gotthardt, H.; Bayer, H. O.; Schaefer, F. C. *Angew. Chem.* **1964**, *76*, 185-186; *Angew. Chem. Int. Ed.* **1964**, *3*, 136-137.
- [49] Greco, C.; V.; Nyberg, W. H.; Cheng, C. C. *J. Med. Chem.* **1962**, *5*, 861-865.
- [50] Cyr, D. J. S.; Arndtsen, B. A. *J. Am. Chem. Soc.* **2007**, *129*, 12366-12367.
- [51] Wang, H.; Wang, L.; Shang, J.; Li, X.; Wang, H.; Guia, J.; Lei, A. *Chem. Commun.* **2012**, *48*, 76-78.
- [52] In analogy to the so-called “münchnones”, “sydnones” and “montrealones” (mesoionic O,N-, O,N,N- and N,P-five-membered heterocycles) explored and exploited by research groups in Munich (München), Sydney and Montreal, we suggest the name “mogones” (Latin Mogontiacum for Mainz) for mesoionic 1,3-thiazolium-5-enolates and “4,5-dihydro mogone imines” for 4,5-dihydro-1,3-thiazolium-5-enamides such as *cyclo*-[H-6], respectively.
- [53] M. Alajarin, M. Marin-Luna, A. Vidal, *Eur. J. Org. Chem.* **2012**, 5637-5653.
- [54] Fulmer, G. R.; Miller, A. J. M.; Sherden, N. H.; Gottlieb, H. E.; Nudelman, A.; Stoltz, B. M.; Bercaw, J. E.; Goldberg, K. I. *Organometallics* **2010**, *29*, 2176-2179.
- [55] Stoll, S.; Schweiger, A. *J. Magn. Reson.* **2006**, *178*, 42-55.
- [56] Neese, F. *WIREs Comput Mol Sci*, **2012**, *2*, 73-78.
- [57] Schäfer, A.; Horn, H.; Ahlrichs, R. *J. Chem. Phys.* **1992**, *97*, 2571.
- [58] Schäfer, A.; Huber, C.; Ahlrichs, R. *J. Chem. Phys.* **1994**, *100*, 5829.
- [59] Neese, F.; Wennmohs, F.; Hansen, A.; Becker, U. *Chem. Phys.* **2009**, *356*, 98-109.
- [60] Izsák, R.; Neese, F. *J. Chem. Phys.* **2011**, *135*, 144105.
- [61] van Lenthe, E.; Baerends, E. J.; Snijders, J. G. *J. Chem. Phys.* **1993**, *99*, 4597.
- [62] van Wüllen, C. *J. Chem. Phys.* **1998**, *109*, 392.
- [63] Kollmar, C. *J. Chem. Phys.* **1996**, *105*, 8204.
- [64] Grimme, S. *J. Comput. Chem.* **2006**, *27*, 1787-1799.
- [65] Grimme, S.; Antony, J.; Ehrlich, S.; Krieg, H. *J. Chem. Phys.* **2010**, *132*, 154104.
- [66] Grimme, S.; Ehrlich, S.; Goerigk, L. *J. Comput. Chem.* **2011**, *32*, 1456-1465.

- [67] Sinnecker, S.; Rajendran, A.; Klamt, A.; Diedenhofen, M.; Neese, F. *J. Phys. Chem. A* **2006**, *110*, 2235–2245.
- [68] SMART Data Collection and SAINT-Plus Data Processing Software for the SMART System (various versions); Bruker Analytical X-Ray Instruments, Inc., Madison, WI, **2000**.
- [69] Blessing, R. H. *Acta Crystallogr., Sect. A* **1995**, *51*, 33–38.
- [70] Sheldrick, G. M. *SHELXTL*, version 5.1, Bruker AXS, Madison, WI, **1998**.
- [71] Sheldrick, G. M. *SHELXL-97*, University of Göttingen, Germany, **1997**.

4 Summary and Outlook

The successful preparation and analyses of mono and dinuclear *N*-ferrocenyl amides is presented and a comparison to parent carboxamides is made to gain insight on the direct effect of oxygen \rightarrow sulfur exchange. The synthesis reported with Lawessons reagent allows easy access to a variety of *N*-ferrocenyl thioamides. The use of the ferrocenyl carboxamides as starting materials allows variation of the substitution pattern of the thioamides through the well-established chemistry of the starting materials. Unlike the carboxamides the thioamides feature a high enough rotational barrier (75 kJ mol^{-1}) to be observed *E/Z*-isomers in solution at room temperature. Similar to carboxamides oxidation of the thioamides leads to the expected ferrocenium compounds. However, in contrast to the carboxamides, a second oxidation process at higher potentials is observed, most likely attributed to the oxidation of the electron rich sulfur atom of the thioamide unit. Dinuclear compounds are transformed into the mixed-valent compounds upon single oxidation. These mixed-valent compounds could be assigned to Robin-Day class II. Compared to the parent carboxamides the electronic coupling is almost the same for the thioamides, but the shift of the IVCT band to lower energies suggests facilitated thermal electron transfer, due to a smaller activation barrier originating from the more similar redox potentials of the ferrocenyl moieties.

The dinuclear compound featuring two thioamide units features a $\text{NH}\cdots\text{S}$ hydrogen bond in solution forming a six-membered ring in $1,2'$ -conformation, contrary to the eight-membered ring of the parent carboxamide. Upon oxidation the secondary structure changes to an eight-membered ring in $1,2'$ -conformation, according to DFT calculations. Alltogether *N*-ferrocenyl thioamides are promising building blocks for oligomers and polymers, featuring a distinct secondary structure in solution. The conformational change of the hydrogen bonding motif from an eight-membered ring of the parent carboxamides to the six-membered ring in the thioamides opens new applications as turn mimetics. Especially the conformational change from a six-membered ring to an eight-membered ring upon oxidation can attribute to research of redox triggered peptidmimetika for use in pharmaceutical applications.

Pharmaceutical applications of ferrocene have been explored in various compounds including ferrocifen, ferroquine, aminoferrocene based (pro-)drugs and anti leishmanial, antibacterial, antifungal drugs and vasorelaxants containing ferrocen. One possible mode

of action for ferrocene based (pro-)drugs centers around the oxidation of the ferrocenyl moiety to ferrocenium. In this work the formation of ferrocenyl radicals of various ferrocene derivatives under the addition of base is reported. The addition of nitrosobenzene as spin trapping agent allowed the detection of highly reactive ferrocenyl radicals and facile determination of the radical location. Aminoacetyl and thioaminoacetyl substitution of the ferrocenyl moiety lead to stabilization of the oxidized and deprotonated compounds as ferrocenium iminolate and ferrocenium thioiminolate, while the unsubstituted and alkyl substituted ferrocene derivatives undergo rapid back reaction by hydrogen abstraction from the base. These iron centered radicals do not react with nitrosobenzene, however even these stabilized ferrocene derivatives can be analyzed by the spin trapping technique, showing that the ferrocenium iminolate and thioiminolate serve as reservoir for the highly reactive carbon centered radicals. This radical reservoir may contribute to the activity of amino ferrocene based (pro-)drugs. This work clearly shows the benefit of the spin trapping technique in order to disclose the mode of action for certain (pro-)drugs. Thorough investigation may lead to new insight and development of more specifically targeting pharmaceutical compounds.

Apart from the reported radical activity for *N*-thioacetyl amino substituted ferrocene an additional reaction pathway upon oxidation and deprotonation of *N*-ferrocenyl substituted thioamides is reported in this work. A crucial factor for this additional pathway is the ability of sulfur to act as a ligand, which is shown by the formation of copper(I) and silver(I) complexes of *N*-ferrocenyl substituted thioamides and thioiminolates. This enables the ferrocenium thioiminolates to stabilize themselves as piano stool like complexes by coordination of the adjacent thioiminolate sulfur, as well as another thioiminolate functional group from a second molecule to the iron nucleus of the ferrocenium moiety. The substituted cyclopentadienyl therefore undergoes a change in hapticity from η^5 to η^1 . Finally, elimination of hydrosulfide from the molecule and backshift of the substituted cyclopentadienyl ring to η^5 hapticity leads to the formation of super electrophilic ketenimine cations. These react rapidly by either oligomerization or are attacked by a thioiminolate. The second reaction pathway leads to the formation of a novel zwitterionic 4,5-dihydro-1,3-thiazolium 5-substituted heterocycle, the “4,5-dihydro mogone imines”.

The reaction of *N*-ferrocenyl thioamides upon oxidation and deprotonation by loss of sulfur may lead to novel (pro-)drugs with a mode of action based on the release of H₂S.

The proposed ketenimine may provide interesting oligomers and polymers with a $[\text{CN}]_n$ backbone and ferrocenyl side chains. Finally, possible applications of the novel heterocyclic zwitterionic “4,5-dihydro mogone imines” cannot be foreseen and have yet to be unveiled.

5 Supporting Information

Contents

To 3.1 Impact of O→S Exchange in Ferrocenyl Amides on Structure and Redoxchemistry

Torben Kienz, Christoph Förster and Katja Heinze

Published in: *Organometallics* **2014**, *33*, 4803–4812.

[DOI: 10.1021/om500052k]

<http://pubs.acs.org/doi/abs/10.1021/om500052k>

“Adapted with permission from T. Kienz, C. Förster, K. Heinze, *Organometallics* **2014**, *33*, 4803–4812. Copyright 2014 American Chemical Society.”

To 3.2 Spin Trapping of Carbon-Centered Ferrocenyl Radicals with Nitrosobenzene

Andreas Neidlinger, Torben Kienz and Katja Heinze

Published in: *Organometallics* **2015**, *34*, 5310–5320.

[DOI: 10.1021/acs.organomet.5b00778]

<http://pubs.acs.org/doi/10.1021/acs.organomet.5b00778>

“This is an unofficial adaptation of an article that appeared in an ACS publication. ACS has not endorsed the content of this adaptation or the context of its use. Copyright 2015 American Chemical Society.”

To 3.3 Generation and Oligomerization of N-Ferrocenyl Ketenimines via Open-shell Intermediates

Torben Kienz, Christoph Förster and Katja Heinze

Submitted to: *Organometallics*

5.1 To 3.1: Impact of O→S Exchange in Ferrocenyl Amides on Structure and Redoxchemistry

Torben Kienz, Christoph Förster, and Katja Heinze

Organometallics **2014**, 33, 4803–4812.

Adapted with permission from T. Kienz, C. Förster, K. Heinze,

Organometallics **2014**, 33, 4803–4812.

Copyright 2014 American Chemical Society.

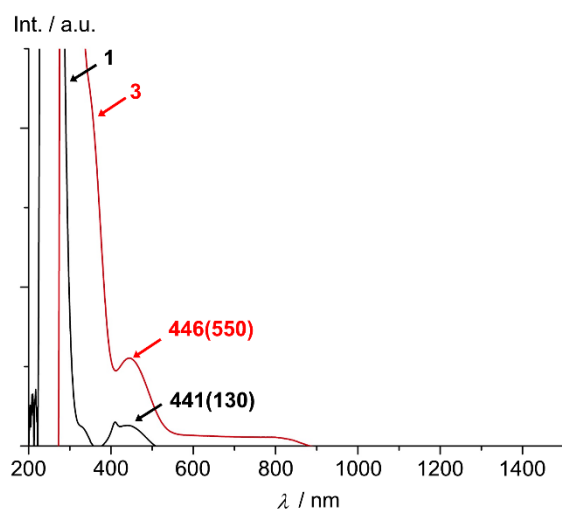


Figure S1. UV/Vis spectra of 1 and 3 in CH_2Cl_2 .

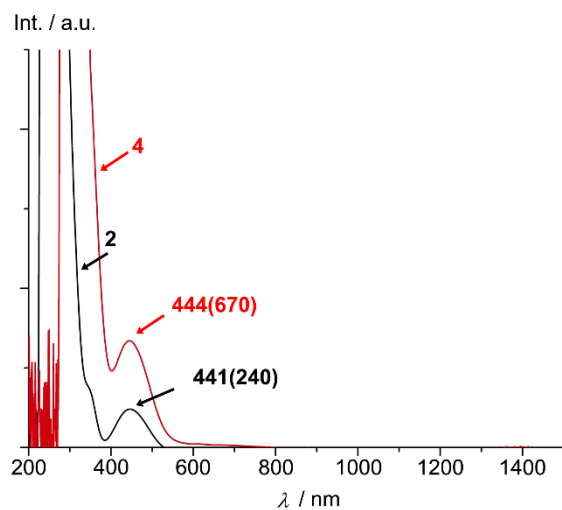


Figure S2. UV/Vis spectra of 2 and 4 in CH_2Cl_2 .

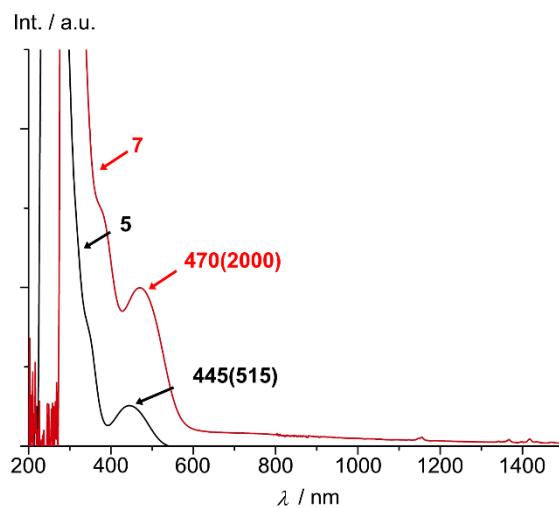


Figure S3. UV/Vis spectra of 5 and 7 in CH₂Cl₂.

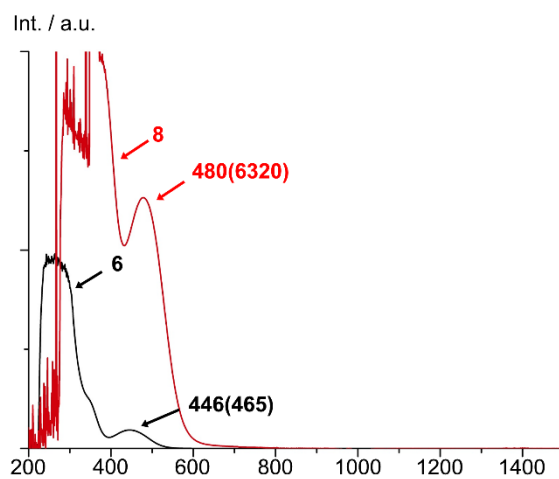


Figure S4. UV/Vis spectra of 6 and 8 in CH₂Cl₂.

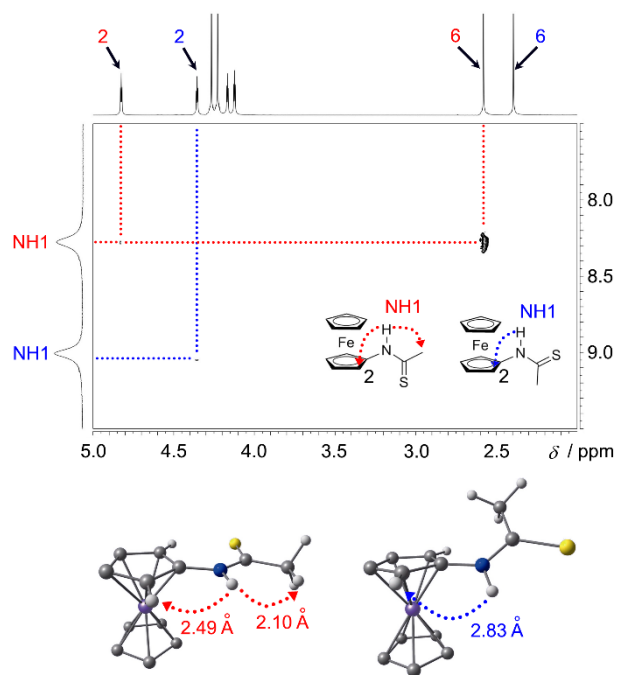


Figure S5. ^1H - ^1H NOESY of **3** in CD_2Cl_2 at room temperature.

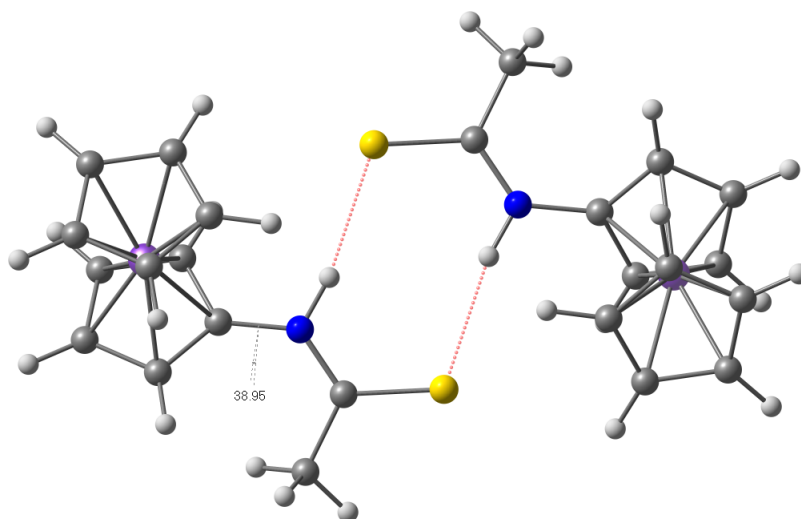


Figure S6. DFT (B3LYP, LANL2DZ, PCM CH_2Cl_2) calculated $(\text{cis-3})_2$.

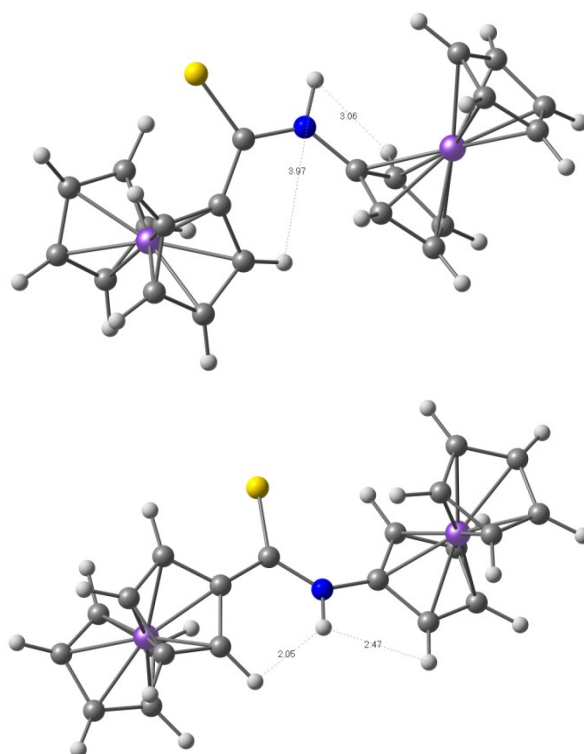


Figure S7. DFT (B3LYP, LANL2DZ, PCM CH₂Cl₂) calculated *cis*-7 and *trans*-7.

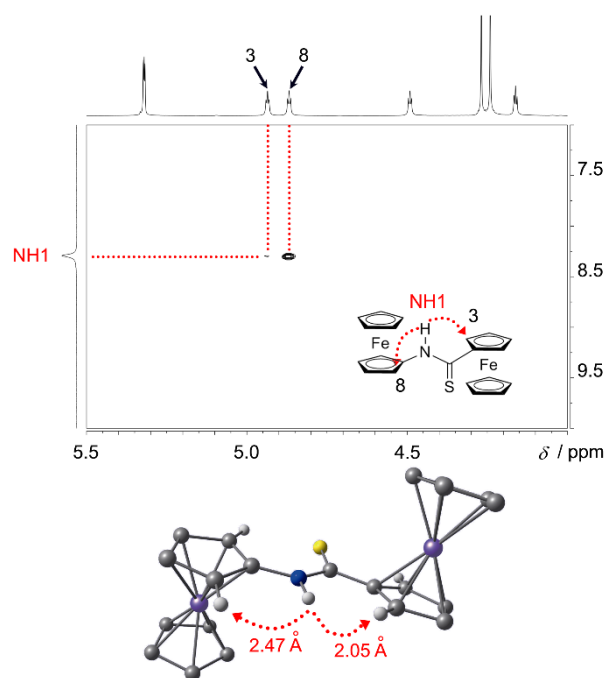


Figure S8. ¹H¹H NOESY of 7 in CD₂Cl₂ at room temperature.

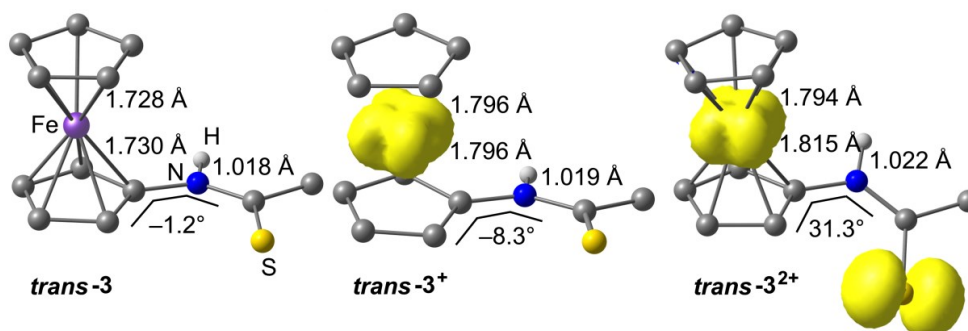


Figure S9. DFT (B3LYP, LANL2DZ, PCM CH₂Cl₂) calculated *trans-3ⁿ* ($n = 0, 1, 2$).

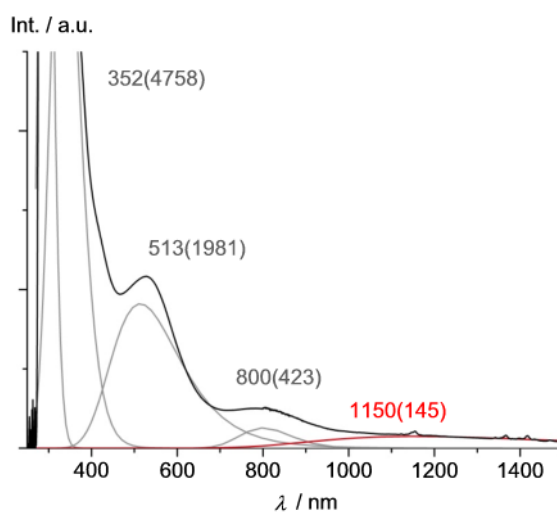


Figure S9. Gaussian band shape analysis of IVCT bands of 7⁺.

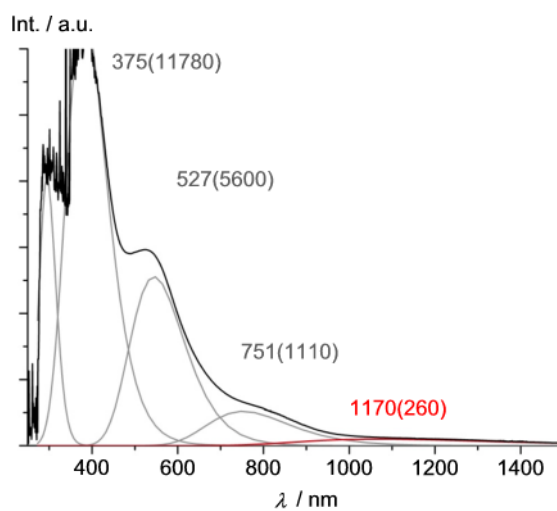


Figure S10. Gaussian band shape analysis of IVCT bands of 8⁺.

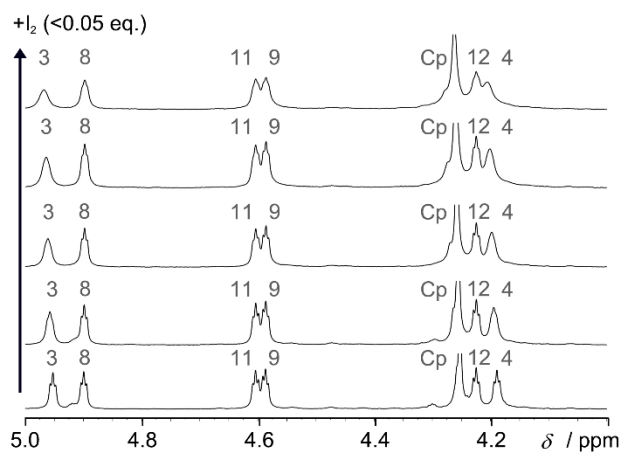


Figure S11. ^1H NMR spectra of **8** upon titration with iodine in CD_2Cl_2 .

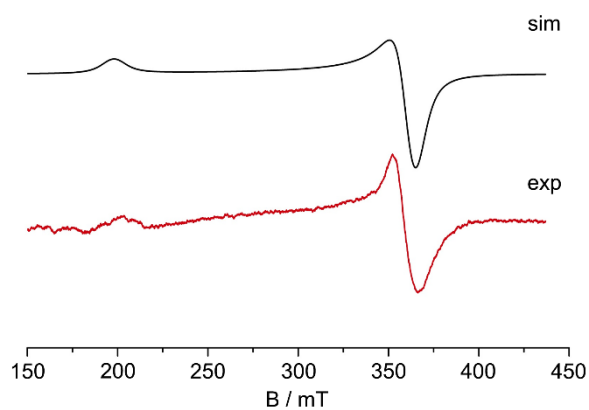


Figure S12. EPR spectrum of **3** in $\text{THF}/\text{CH}_2\text{Cl}_2$ (1:4) and simulation.

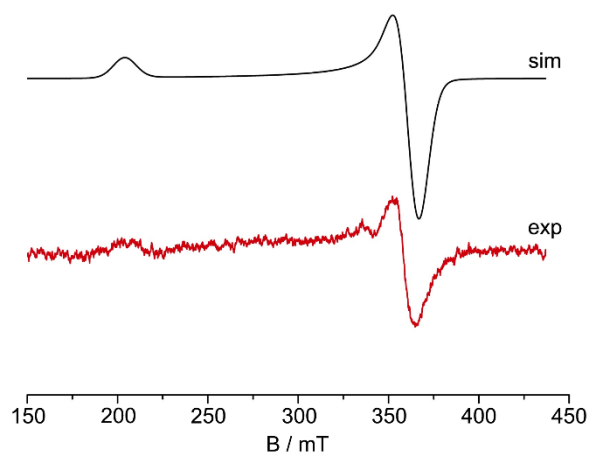


Figure S13. EPR spectra of 4 in THF/CH₂Cl₂ (1:4) and simulation.

5.2 To 3.2: Spin Trapping of Carbon-Centered Ferrocenyl Radicals with Nitrosobenzene

Andreas Neidlinger, Torben Kienz, and Katja Heinze

Organometallics **2015**, *34*, 5310–5320.

Adapted with permission from A. Neidlinger, T. Kienz, K. Heinze,

Organometallics **2015**, *34*, 5310–5320.

“This is an unofficial adaptation of an article that appeared in an ACS publication. ACS has not endorsed the content of this adaptation or the context of its use. Copyright 2015 American Chemical Society. Copyright 2014 American Chemical Society.”

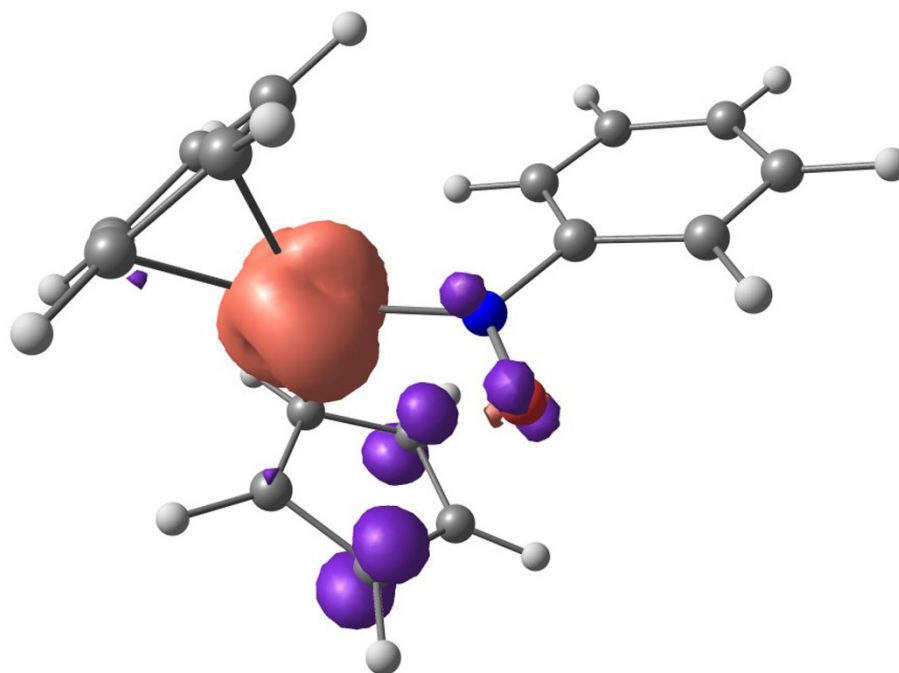


Figure S1: DFT optimized geometry with spin density (0.01 a.u. isosurface value) in CH₂Cl₂ continuum solvent for iron spin-trapped [1-PhNO]⁺.

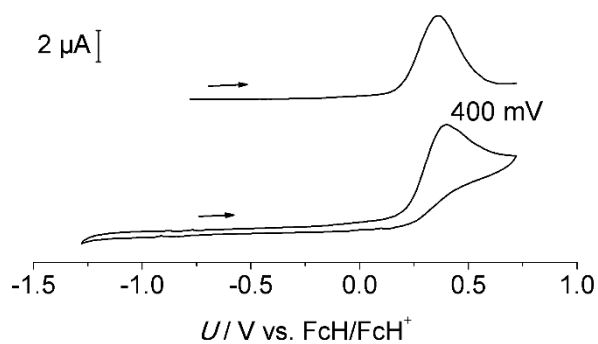


Figure S2: (top) Square wave and (bottom) cyclic voltammogram of P1'Bu in CH₂Cl₂ containing [nBu₄N][B(C₆F₅)₄] as supporting electrolyte at 298 K.

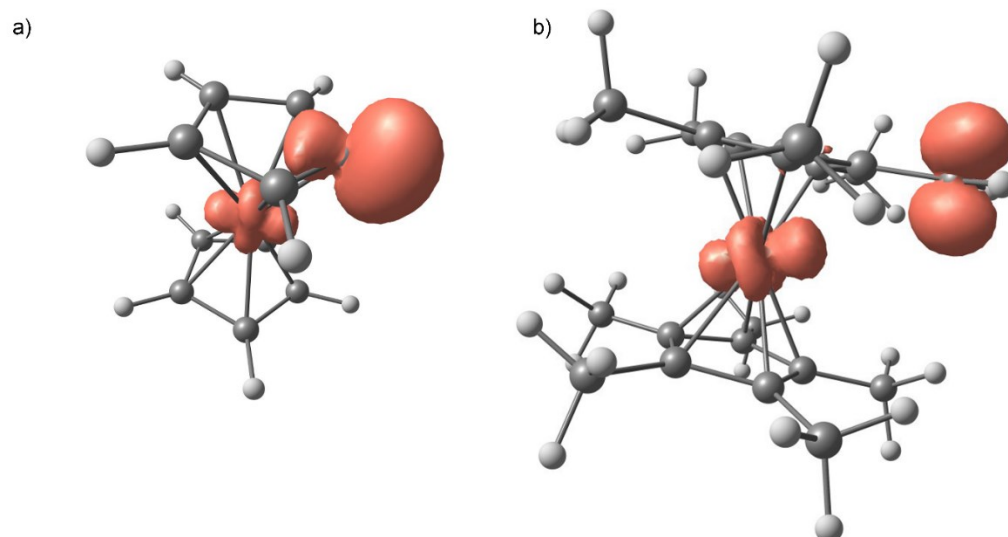


Figure S3: DFT optimized geometries with spin densities (0.01 a.u. isosurface value) in CH₂Cl₂ continuum solvent for a) ferrocenyl radical [1-H]• and b) decamethylferrocenyl radical [2-H]•.

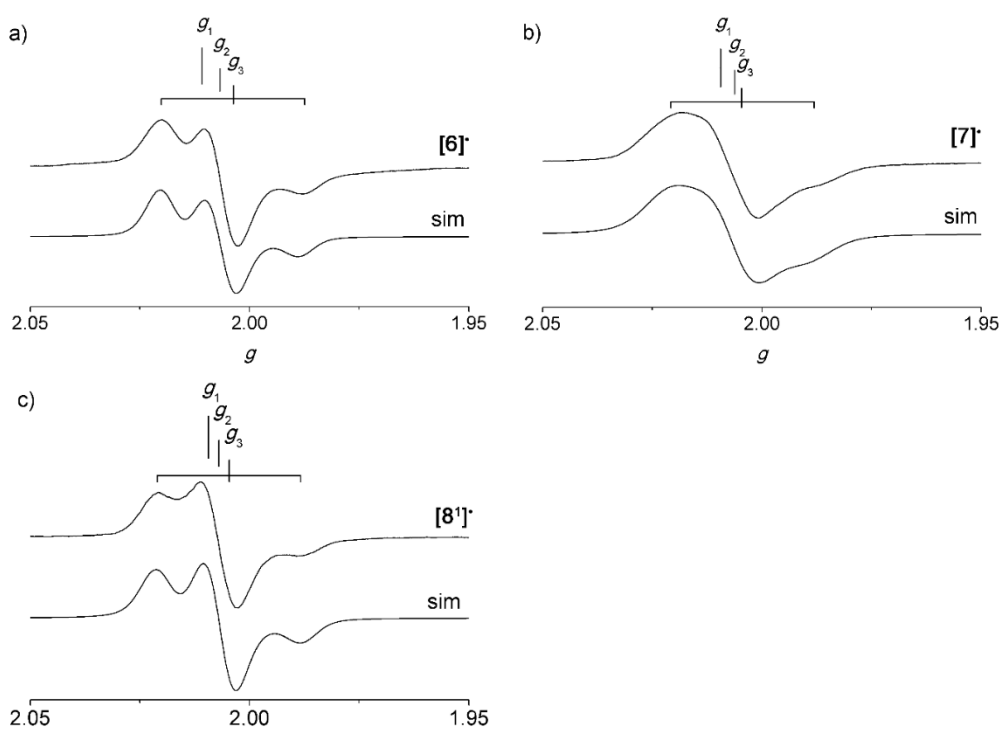


Figure S4: X-band EPR spectrum (top) and simulated spectrum (bottom) of a) [6]⁺, b) [7]⁺, and c) [8]¹⁺ (25 mM starting ferrocene in CH₂Cl₂) at the following experimental parameters: a) and b) temperature = 77 K, field = 3346.20 G, sweep = 499.77 G, sweep time = 90 s, modulation = 5000 mG, MW attenuation = 10 db and c) temperature = 77 K; field = 3346.20 G, sweep = 499.77 G, sweep time = 90 s, modulation = 1000 mG, MW attenuation = 5 db.

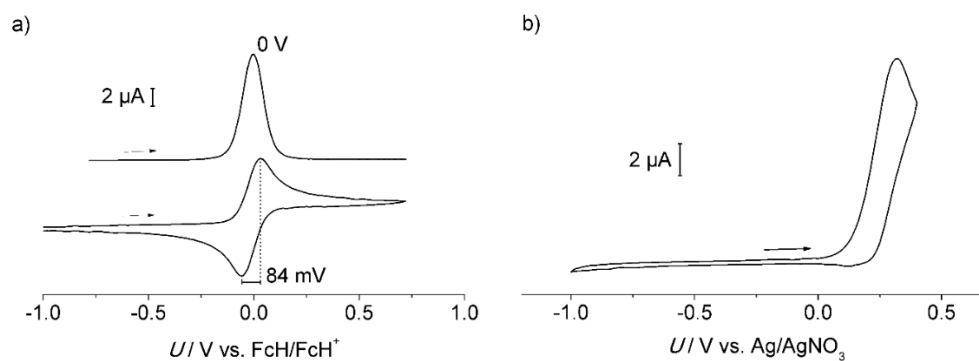


Figure S5: a) (top) Square wave and (bottom) cyclic voltammogram of 1 and b) cyclic voltammograms of a 1/P1'Bu mixture. All measurements performed in CH₂Cl₂ containing [nBu₄N][B(C₆F₅)₄] as supporting electrolyte at 298 K.

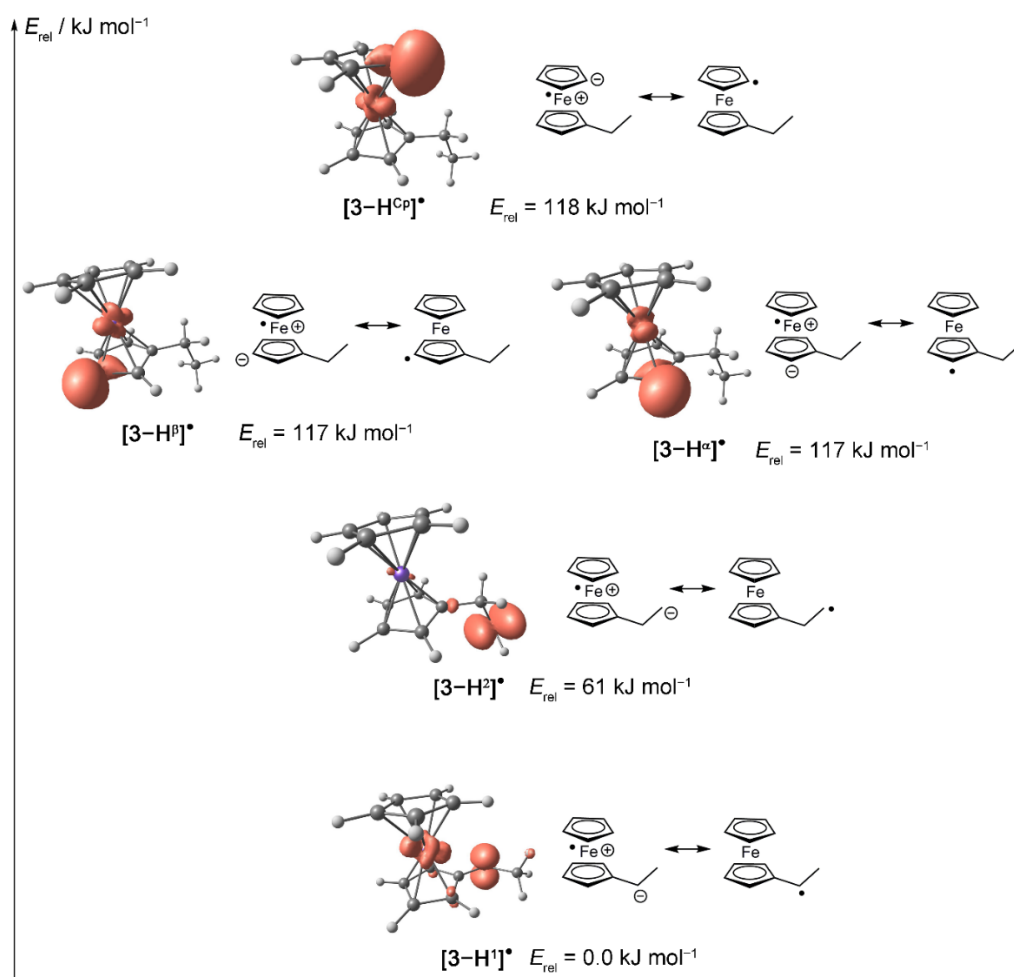


Figure S6: DFT optimized geometries with spin densities (0.01 a.u. isosurface value), Lewis structures, and energies in CH₂Cl₂ continuum solvent for radicals [3-H^x]^{*} (x = α, β, Cp, 1, 2).

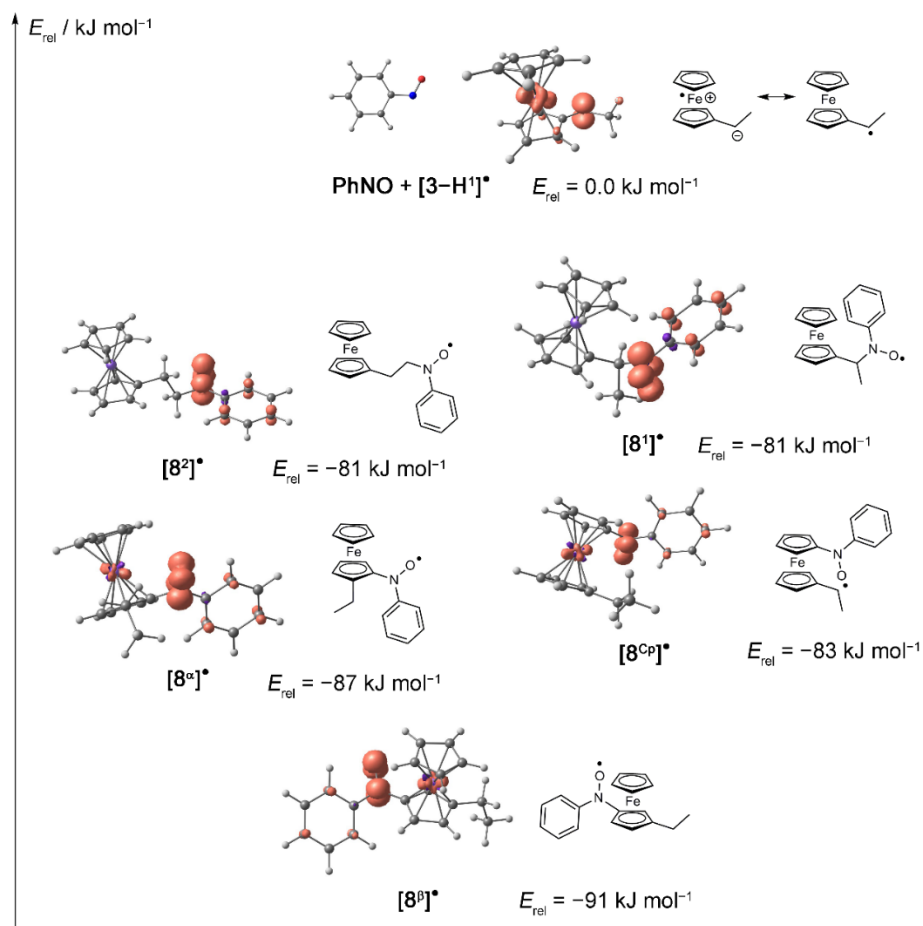


Figure S7: DFT optimized geometries with spin densities (0.01 a.u. isosurface value) and energies in CH_2Cl_2 continuum solvent as well as Lewis structures for nitroxide radicals $[8^x]^\bullet$ ($x = \alpha, \beta, \text{Cp}, 1, 2$).

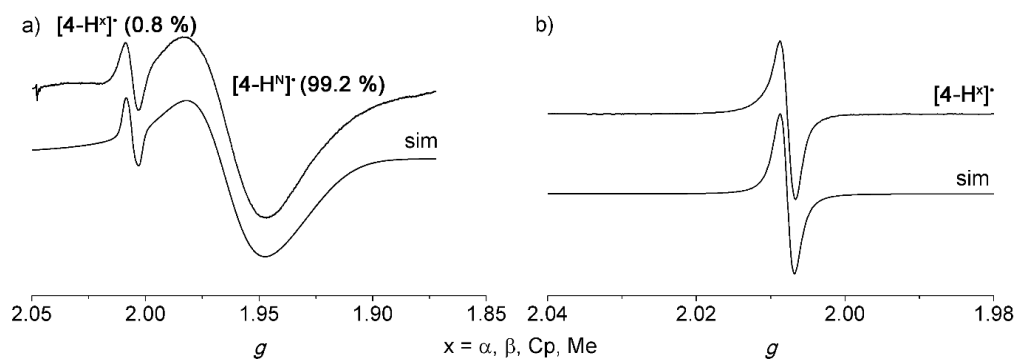


Figure S8: X-band EPR spectrum (top) and simulated spectrum (bottom) of a mixture of [4-H^N]• and [4-H^X]• ($x = \alpha, \beta, \text{Cp, Me}$) (5 mM 4⁺ + P1'Bu in CH₂Cl₂) at the following experimental parameters: a) temperature = 77 K, field = 3346.20 G, sweep = 499.77 G, sweep time = 90 s, modulation = 5000 mG, MW attenuation = 10 db and b) temperature = 298 K, field = 3346.20 G, sweep = 94.79 G, sweep time = 90 s, modulation = 1000 mG, MW attenuation = 10 db.

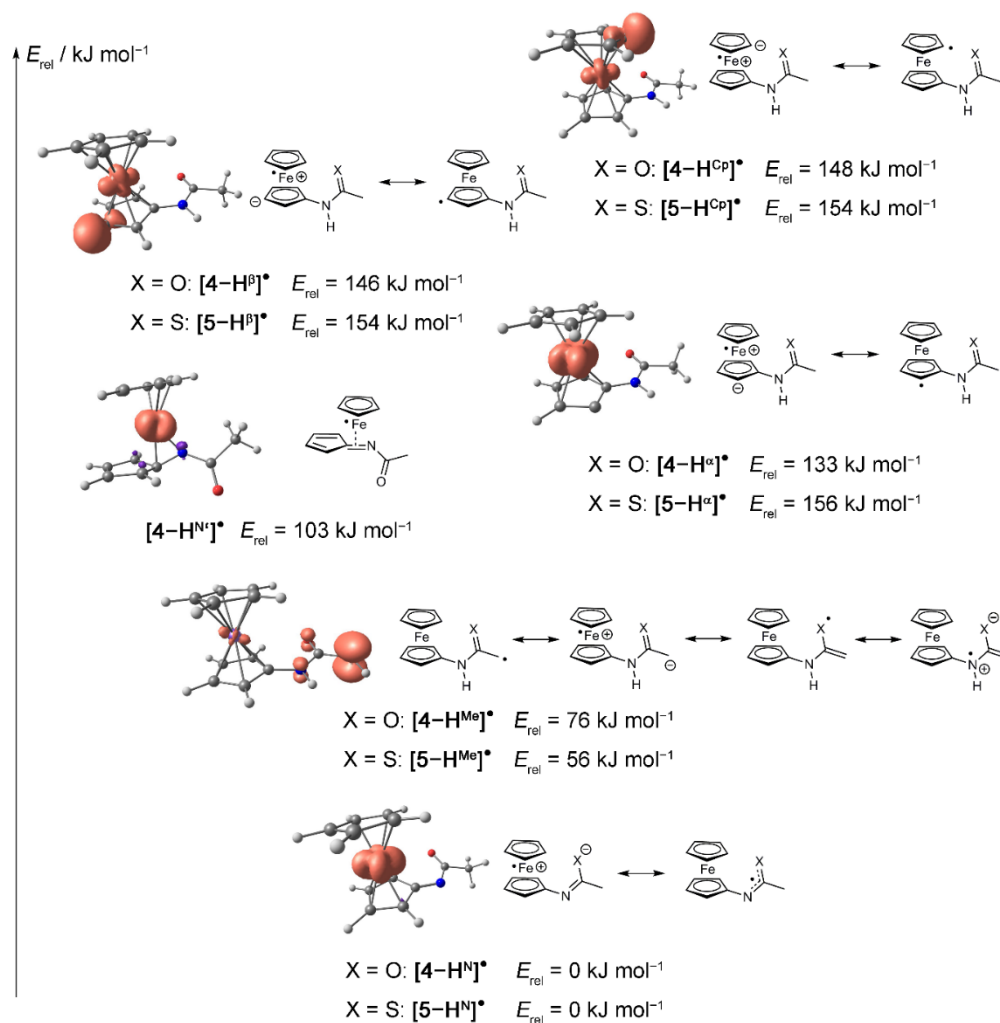


Figure S9: DFT optimized geometries with spin densities for $[4\text{-H}^x]^{\bullet}$ ($x = \alpha, \beta, \text{Cp}, \text{N}, \text{Me}$) (0.01 a.u. isosurface value) and energies in CH_2Cl_2 continuum solvent for $[4\text{-H}^x]^{\bullet}$, $[5\text{-H}^x]^{\bullet}$ ($x = \alpha, \beta, \text{Cp}, \text{N}, \text{Me}$), and $[4\text{-H}^{\text{N}}]^{\bullet}$ as well as Lewis structures.

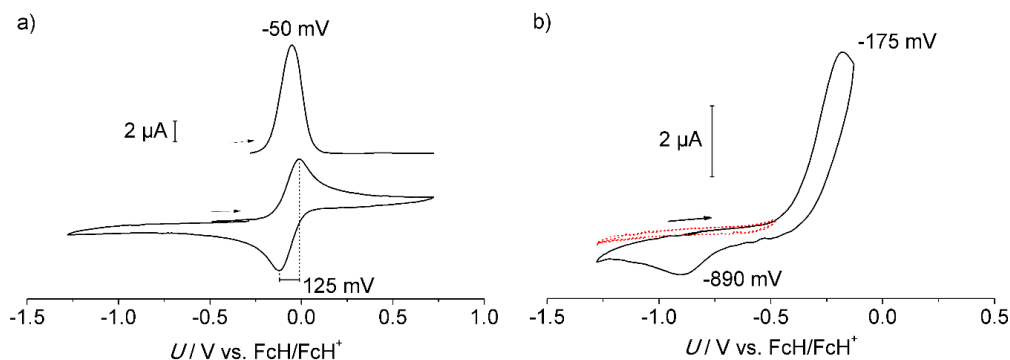


Figure S10: a) (top) Square wave and (bottom) cyclic voltammogram of 4 and b) cyclic voltammograms of a 4/P1'Bu mixture; red, dashed curve represents a scan excluding the irreversible oxidation. All measurements performed in CH₂Cl₂ containing [nBu₄N][B(C₆F₅)₄] as supporting electrolyte at 298 K.

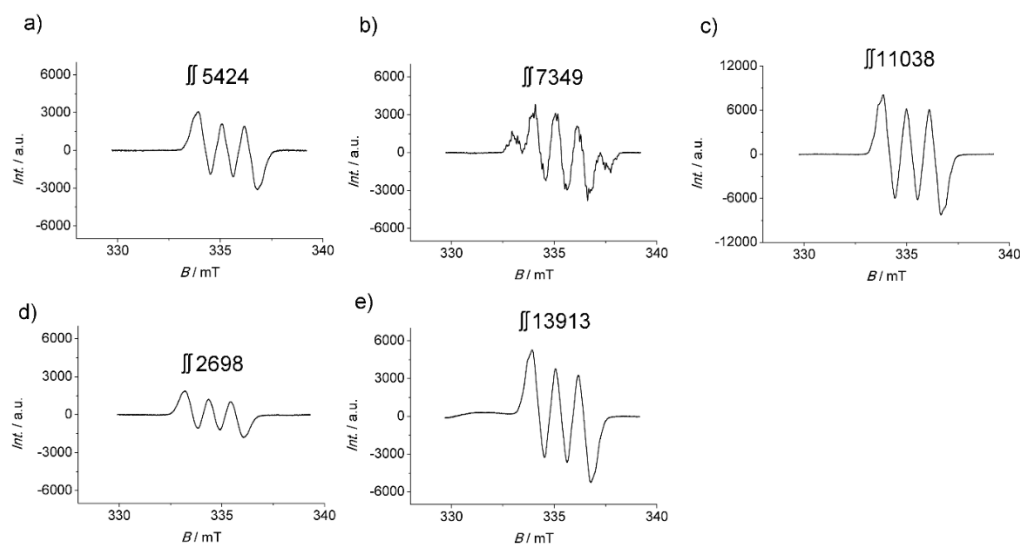


Figure S11: Experimental, baseline corrected X-band EPR spectra and values of double integration of EPR spectra of (a) [6]•, (b) [7]•, (c) [8¹]•, d) [9^x]• (x = β, Cp), and e) [10^{Cp}]• (5 mM starting ferrocene in CH₂Cl₂) recorded at the following experimental parameters: temperature = 298 K, field = 3346.20 G, sweep = 94.79 G, sweep time = 90 s, modulation = 1000 mG, MW attenuation = 10 db.

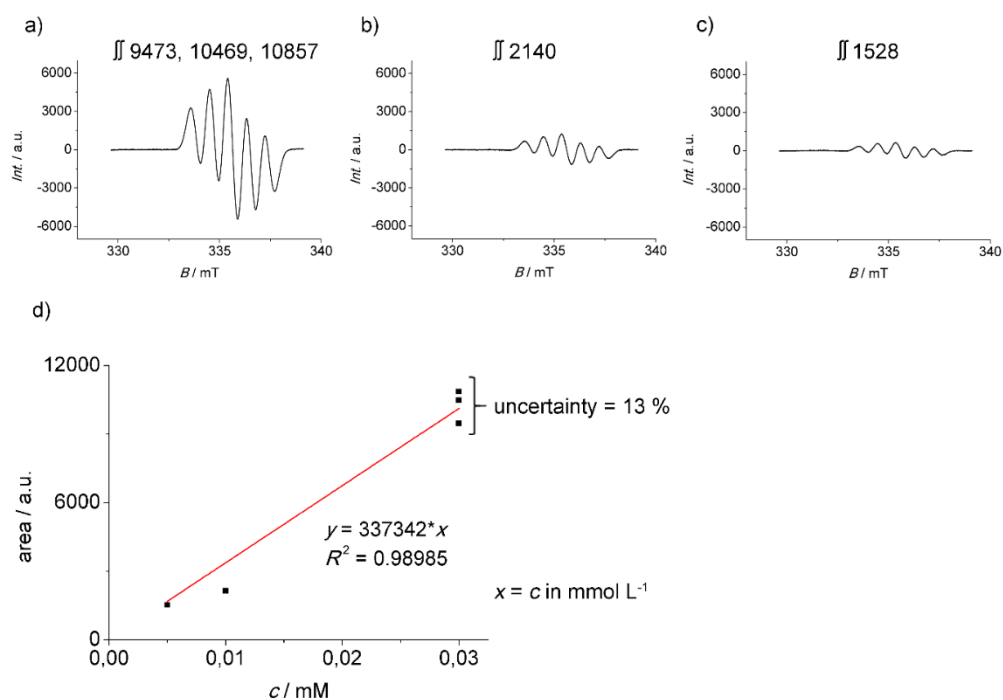


Figure S12: Experimental, baseline corrected X-band EPR spectra and values of double integration of EPR spectra of (a) 0.03 mM, (b) 0.01 mM, and (c) 0.005 mM DPPH solutions in CH_2Cl_2 recorded at the following experimental parameters: temperature = 298 K, field = 3346.20 G, sweep = 94.79 G, sweep time = 90 s, modulation = 1000 mG, MW attenuation = 10 db. (d) Linear regression of double integral values against concentration.

5.3 To 3.3: Generation and Oligomerization of *N*-Ferrocenyl Ketenimines via Open-shell Intermediates

Torben Kienz, Christoph Förster and Katja Heinze*

Discussion of XRD of [Cu₂(H-1)₆][BF₄]₂:

Copper : thioamide ratios of 1:3 have also been observed in the copper(I) complex with the biologically relevant hexathioamide closthioamide (CTA) [Cu₂(CTA)](ClO₄)₂,¹ in [Cu₂(HpyS)₆]Cl₂,² and in [Cu(HpyS)₃](NO₃)₃ (HpyS = 2(1*H*)-pyridinethione). [Cu₂(H-1)₆]²⁺ features two copper centers bridged by two κ S coordinating *E*-[H-1] ligands forming a centrosymmetric Cu₂S₂ diamond core. Four terminal κ S coordinating *Z*-[H-1] ligands complete the coordination sphere of the two distorted tetrahedrally coordinated copper(I) centers (for bond angles see Table S1). The Cu•••Cu distance amounts to 3.410 Å, which is quite long compared to dinuclear copper(I) complexes [Cu₂(HpyS)₆]²⁺ with HpyS bridging ligands sharing the same Cu₂S₂ core motif (Cu•••Cu 2.907(3) Å).² The elongation can be attributed to the six sterically demanding ferrocenyl moieties surrounding the Cu₂S₂ core. The Cu-S distances are similar to those reported for [Cu₂(HpyS)₆]²⁺ with smaller thioamide ligands (2.284(2) – 2.498(3) Å and Table S1).² Expectedly, the C=S distances increase from 1.671(2) Å in *E*-[H-1] to 1.689(8) – 1.707(8) Å in the copper(I) complex. Multiple NH•••S and NH•••F hydrogen bonds are formed in the solid state (Figure 2a). The NH group of the bridging *E*-[H-1] ligand forms a hydrogen bond to the S atom of an adjacent terminally coordinated *Z*-[H-1] ligand (Table S1, Figure 2a). An analogous NH•••S hydrogen bonding motif has been found in [Cu₂(HpyS)₆]²⁺,² while in [Cu₂Br₂(μ -HpyS)₂(PTol₃)₂]²⁺ the NH•••Br hydrogen bond from the bridging thioamides includes the coordinated bromide ligands.⁴ The NH groups of the four terminally coordinated *Z*-[H-1] ligands form hydrogen bonds to the [BF₄]⁻ counter ions (Table S1, Figure 2a). Similarly, [Cu₂(HpyS)₆]Cl₂ forms NH•••Cl hydrogen bonds to its counter ions.² As all four terminally coordinated *Z*-[H-1] ligands form hydrogen bonds to the counter ions, the anions bridge the [Cu₂(H-1)₆]²⁺ dications to give a two-dimensional polymer (Supporting Information, Figure S2).

Table S1. Selected bond lengths (Å) and bond angles (°) of [Cu₂(H-1)₆][BF₄]₂.

Cu1-S1	2.290(3)	N1•••F2	2.933(8)
Cu1-S2	2.309(2)	N1•••F4''''	3.253(9)
Cu1-S2'	2.612(2)	N3•••F1''	2.936(8)
Cu1-S3	2.305(2)	N3•••F3''	3.352(9)
S1-C11	1.689(8)	N2•••S3	3.304(7)
S2-C23	1.700(9)	Cu1•••Cu1'	3.410(2)
S3-C35	1.707(8)		
Cu1-S2-Cu1'	87.5(8)		
S1-Cu1-S2	108.26(9)	S2-Cu1-S3	121.97(9)
S1-Cu1-S2'	112.09(9)	S2'-Cu1-S3	94.92(8)
S1-Cu1-S3	121.34(9)	S2-Cu1-S2'	92.50(8)

Solution structure of [Cu₂(H-1)₆][BF₄]₂:

NMR spectra of [Cu₂(H-1)₆][BF₄]₂ in CD₂Cl₂ show two sets of resonances for coordinated **H-1** in a 2:1 ratio for the *Z* and *E* isomers, respectively (Supporting Information, Figures S3 – S8). As all terminal *Z*-[**H-1**] ligands with and without a hydrogen bond to the bridging *E*-[**H-1**] ligands appear as a single set of resonances on the NMR time scale, the NH•••S hydrogen bonds flip rapidly on the ¹H NMR time scale between the terminal C=S acceptor sites by rotation round the C=S bond of the bridging ligand (Figure 2a). Apart from the expected intraligand NOE contacts of the NH, CpH and CH₃ groups, several interligand NOE contacts are observed, most notably from the NH group of the terminal *Z*-[**1-H**] ligands to the CH₃ groups of the bridging *E*-[**H-1**] ligands. This suggests that the [Cu₂(H-1)₆]²⁺ core remains essentially intact in solution. Furthermore, EXSY signals between the NH groups of the *E* and *Z* ligands are observed suggesting chemical exchange. In principle, the bridging and terminal ligands can exchange their positions by a dissociation – isomerization - association mechanism, by a pseudorotation mechanism involving isomerization or by intra- or intermolecular proton transfer processes. As the barrier for *E/Z* isomerization of **H-1**⁵ amounts to 75 kJ mol⁻¹, the former processes should be rather slow and hence, proton transfer might account for this exchange process.

Conductivity measurements in CH₂Cl₂ suggest that the dimeric structure is retained and even the coordination of the counter ions is highly preserved. The limiting conductivity and

the slope of the Onsager plot of the formal 1:2 electrolyte $[\text{Cu}_2(\text{H-1})_6][\text{BF}_4]_2$ in CH_2Cl_2 are even below those of 1:1 electrolytes such as $[\text{Bu}_4\text{N}][\text{B}(\text{C}_6\text{F}_5)_4]$ (Supporting Information, Figures S9 and S10).⁶ This supports the view, that $[\text{Cu}_2(\text{H-1})_6][\text{BF}_4]_2$ essentially exists as hydrogen-bonded contact ion pair in CH_2Cl_2 solution. Solid state and solution IR spectra (Supporting Information, Figures S11 and S12) further corroborate the ion pair formation. As KBr disk, $[\text{Cu}_2(\text{H-1})_6][\text{BF}_4]_2$ displays absorption bands for hydrogen bonded NH groups at 3281 cm^{-1} and 3198 cm^{-1} which can be assigned to $\text{NH}\cdots\text{F}$ and $\text{NH}\cdots\text{S}$ hydrogen bonds, respectively, based on their relative intensity. In CH_2Cl_2 solution these bands are still observed at 3267 cm^{-1} and 3209 cm^{-1} , respectively. Additionally, a band at 3361 cm^{-1} appears due to the presence of two free NH groups in the neutral $[\text{Cu}_2(\text{H-1})_6][\text{BF}_4]_2$ contact ion pair. This value correlates well to the NH stretching vibration of **H-1** itself (3383 cm^{-1}).⁵

- [1] Kloss, F.; Pidot, S.; Goerls, H.; Friedrich, T.; Hertweck, C. *Angew. Chem.* **2013**, *125*, 10945–10948; *Angew. Chem. Int. Ed.* **2013**, *52*, 10745–10748.
- [2] Constable, E. C.; Raithby, P. R.; *J. Chem. Soc., Dalton Trans.* **1987**, 2281–2283.
- [3] Kokkou, S. C.; Fortier, S.; Rentzeperis, P. J.; Karagiannidis, P. *Acta Cryst.* **1983**, *C39*, 178-180.
- [4] Lobana, T. S.; Castineiras, A. *Polyhedron*, **2002**, *21*, 1603–1611.
- [5] Kienz, T.; Förster, C.; Heinze, K. *Organometallics* **2014**, *33*, 4803–4812.
- [6] Feltham, R. D.; Hayter, R. G. *J. Chem. Soc.* **1964**, 4587–459.

Table S2. Selected bond lengths (Å) and bond angles (°) of Ag₆[μ₃-(E-1)]₆.

Ag1•••Ag2	2.8863(11)	Ag1-N1	2.300(7)
Ag1•••Ag3	3.0314(10)	Ag2-N2	2.308(7)
Ag1•••Ag2'	3.5516(12)	Ag3-N3	2.325(6)
Ag1•••Ag3'	3.1023(10)	S1-C11	1.768(8)
Ag2•••Ag3	2.9446(10)	S2-C23	1.764(9)
Ag2•••Ag3'	3.2510(10)	S3-C35	1.768(8)
Ag2-S1	2.490(2)		
Ag3'-S1	2.472(2)	Ag2-S1-Ag3'	81.9(7)
Ag1-S2	2.470(2)	Ag1-S2-Ag3	75.6(6)
Ag3-S2	2.475(2)	Ag1-S3-Ag2'	88.8(7)
Ag2-S3	2.544(2)		
Ag1'-S3	2.531(2)		

Table S3 Selected bond lengths (Å) and bond angles (°) of *cyclo*-[H₃-7][SbF₆]₂.

N1-C11	1.308(7)	C13-N1-C11-S1	-5.9(7)
N1-C13	1.479(7)	Fe2•••N3	3.364(5)
N2-C25	1.347(7)	C11-N1-C13-C14	18.9(8)
N2-C14	1.478(8)	C11-N1-C6-C10	52.9(9)
N3-C25	1.298(7)	C25-N3-C27-C31	-53.7(8)
N3-C27	1.430(7)	C25-N2-C15-C19	131.7(6)

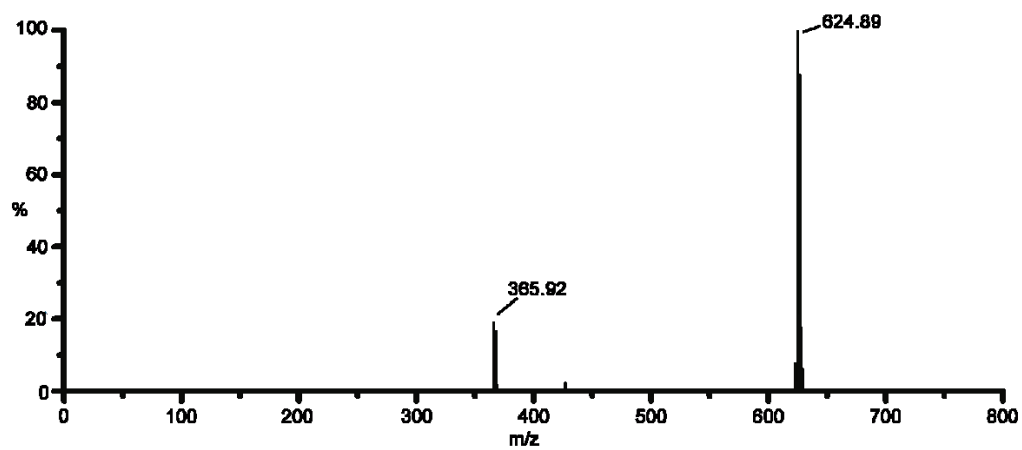


Figure S1. ESI⁺ mass spectrum of H-1 and Ag[SbF₆] in CH₃CN.

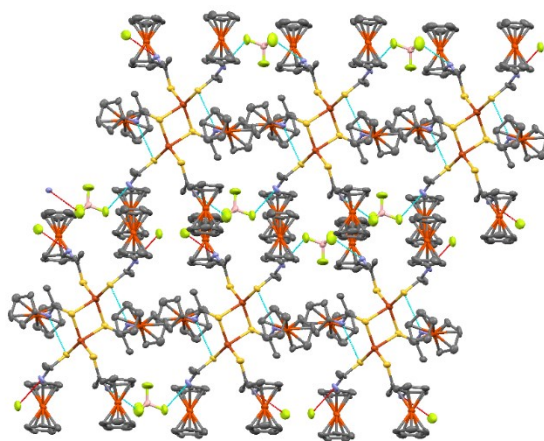


Figure S2. Thermal ellipsoid representation of [Cu₂(H-1)₆][BF₄]₂ (ellipsoids at 50% probability level) derived by single crystal XRD analysis (protons omitted for clarity).

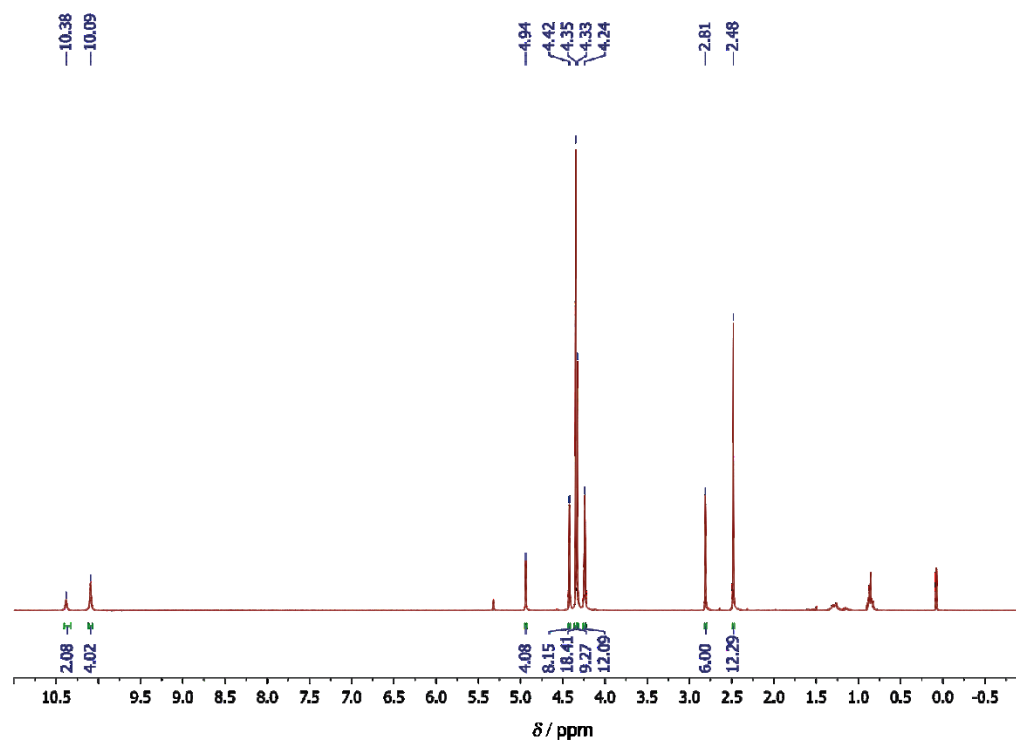


Figure S3. ^1H NMR spectrum of $[\text{Cu}_2(\text{H-1})_6][\text{BF}_4]_2$ in CD_2Cl_2 .

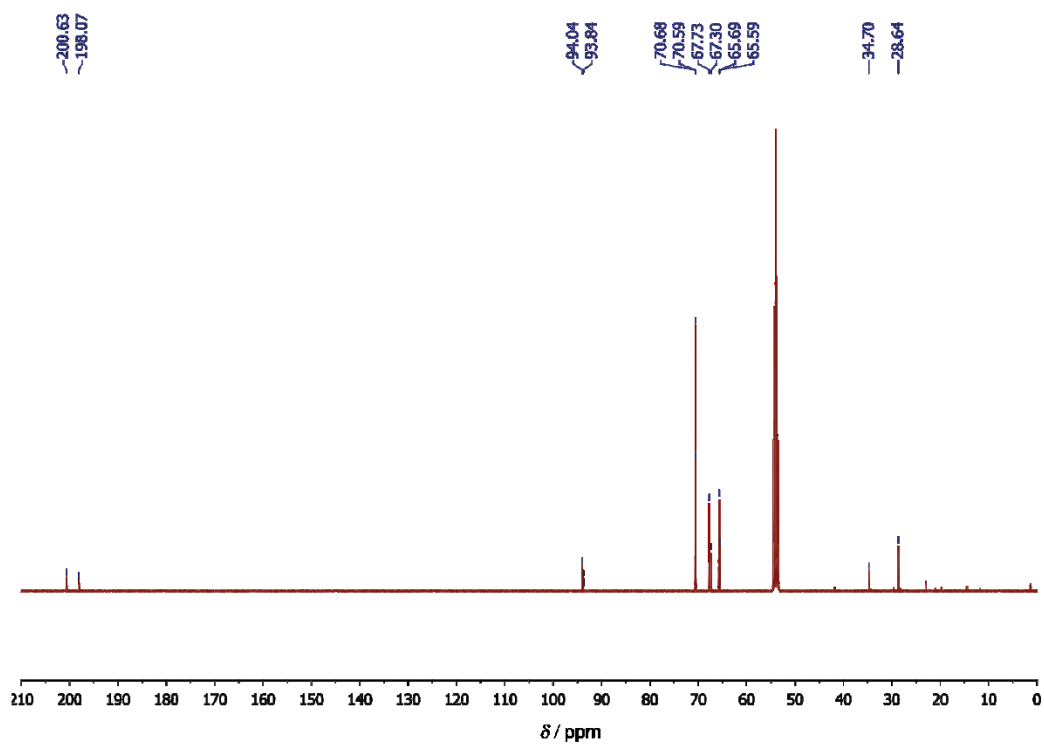


Figure S4. $^{13}\text{C}\{^1\text{H}\}$ NMR spectrum of $[\text{Cu}_2(\text{H-1})_6][\text{BF}_4]_2$ in CD_2Cl_2 .

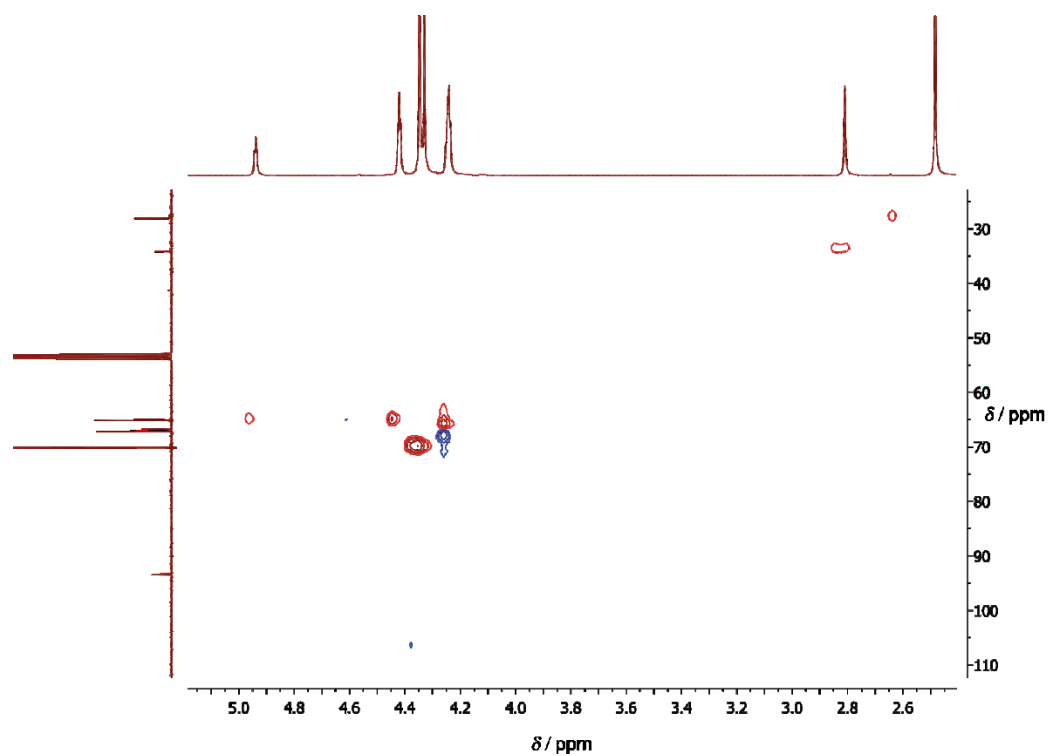


Figure S5. $^1\text{H}^{13}\text{C}$ HSQC spectrum of $[\text{Cu}_2(\text{H-1})_6][\text{BF}_4]_2$ in CD_2Cl_2 .

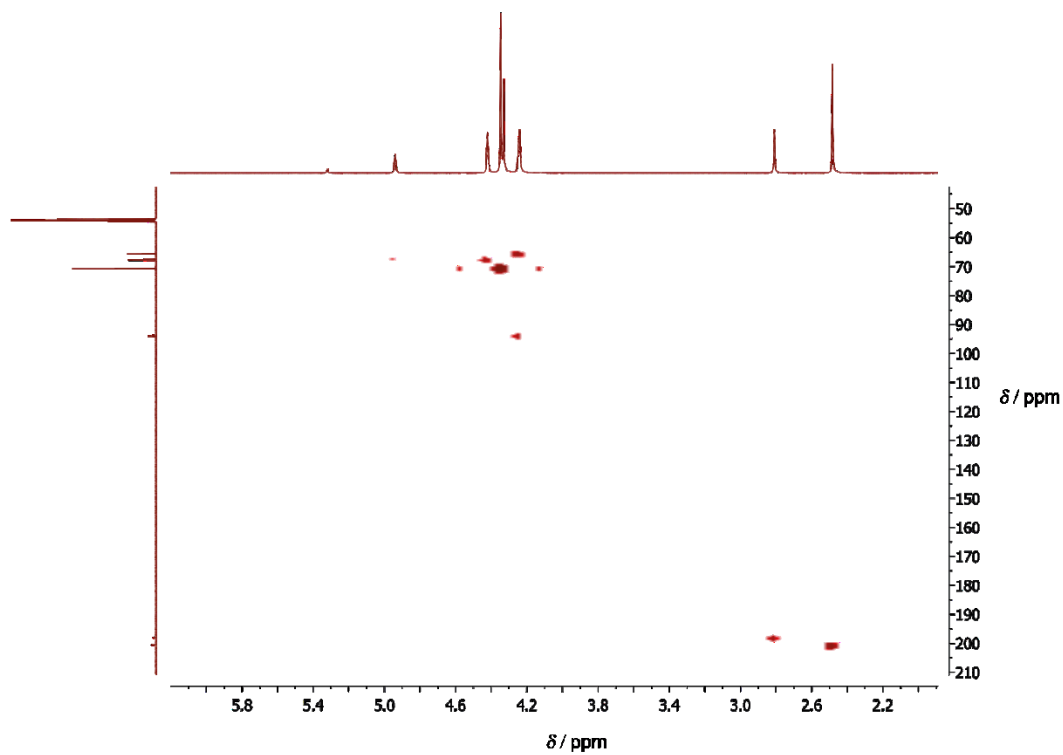


Figure S6. $^1\text{H}^{13}\text{C}$ HMBC spectrum of $[\text{Cu}_2(\text{H-1})_6][\text{BF}_4]_2$ in CD_2Cl_2 .

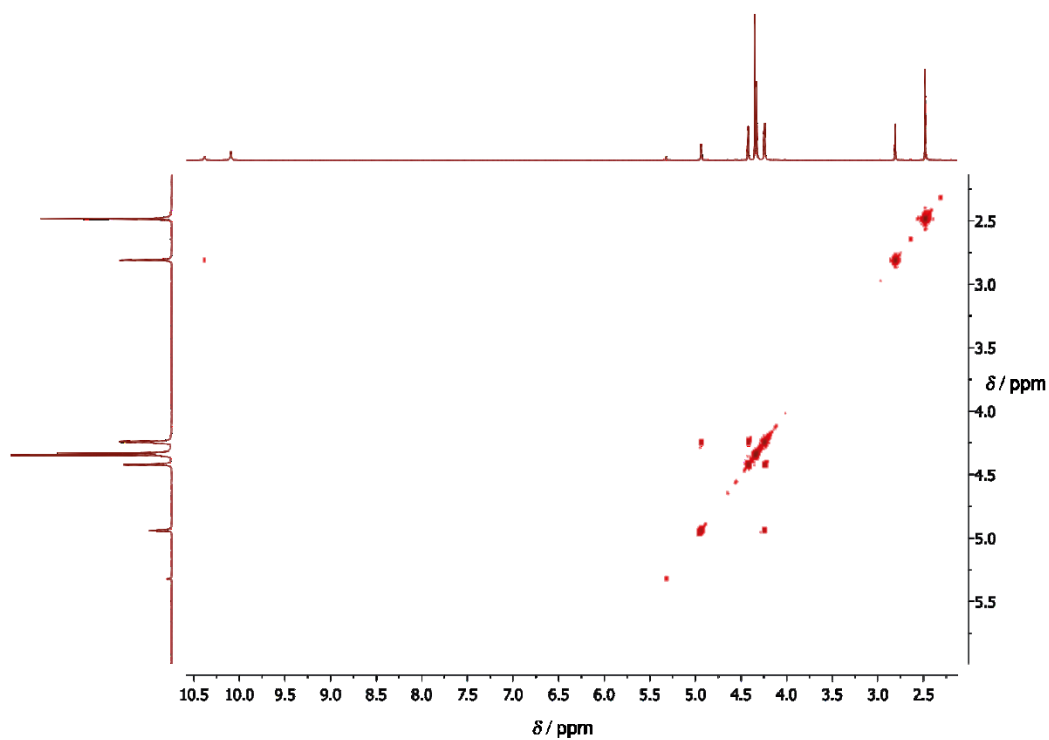


Figure S7. $^1\text{H}^1\text{H}$ COSY spectrum of $[\text{Cu}_2(\text{H-1})_6][\text{BF}_4]_2$ in CD_2Cl_2 .

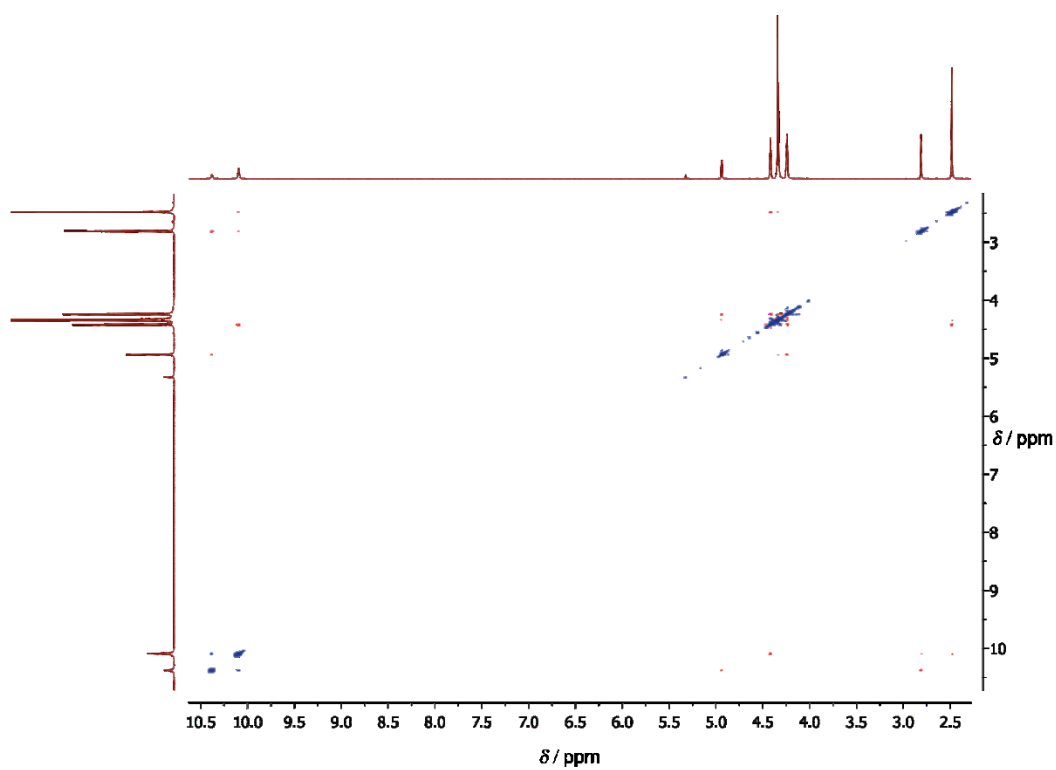


Figure S8. $^1\text{H}^1\text{H}$ NOESY spectrum of $[\text{Cu}_2(\text{H-1})_6][\text{BF}_4]_2$ in CD_2Cl_2 .

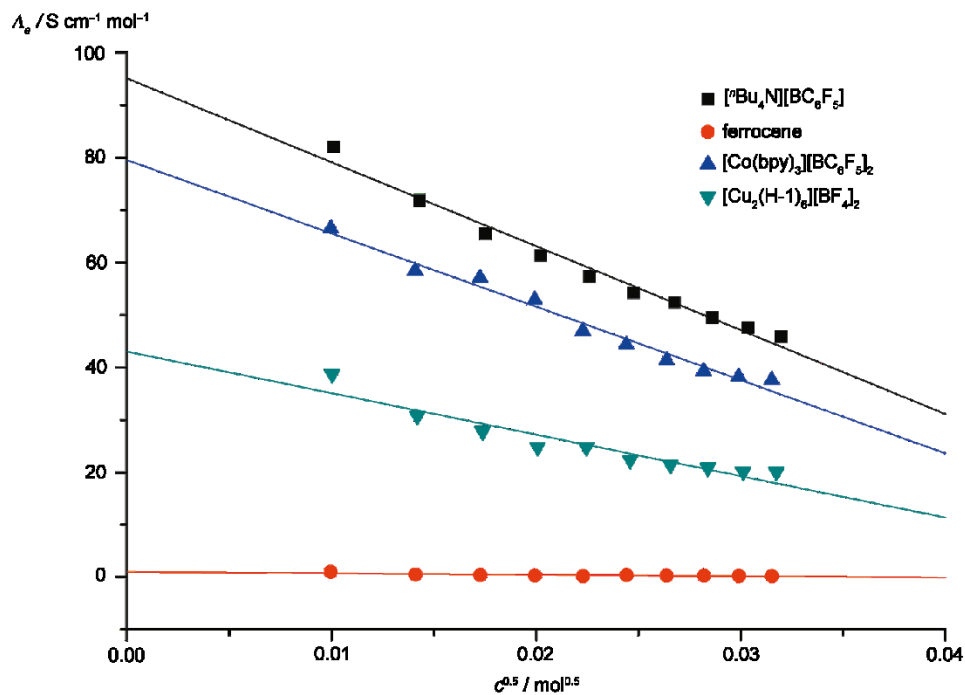


Figure S9. Equivalent conductivities of $[\text{Cu}_2(\text{H-1})_6][\text{BF}_4]_2$, ferrocene, $[\text{tBu}_4\text{N}][\text{B}(\text{C}_6\text{F}_5)_4]$ and $[\text{Co}^{\text{II}}(\text{bpy})_3][\text{B}(\text{C}_6\text{F}_5)_4]_2$ in CH_2Cl_2 .

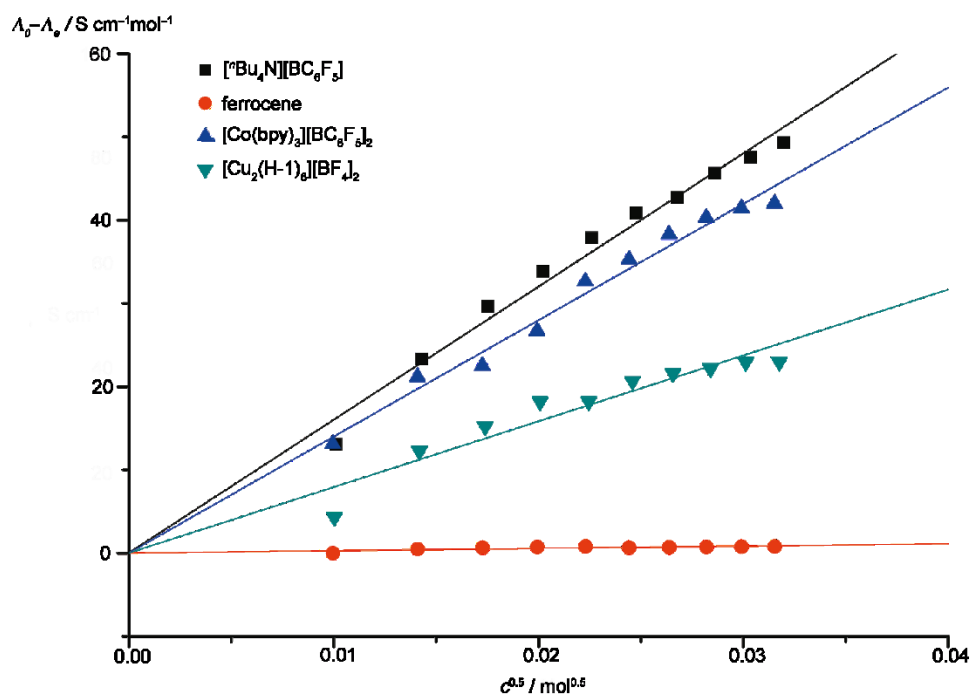


Figure S10. Onsager plots of $[\text{Cu}_2(\text{H-1})_6][\text{BF}_4]_2$, ferrocene, $[\text{tBu}_4\text{N}][\text{B}(\text{C}_6\text{F}_5)_4]$ and $[\text{Co}^{\text{II}}(\text{bpy})_3][\text{B}(\text{C}_6\text{F}_5)_4]_2$ in CH_2Cl_2 .

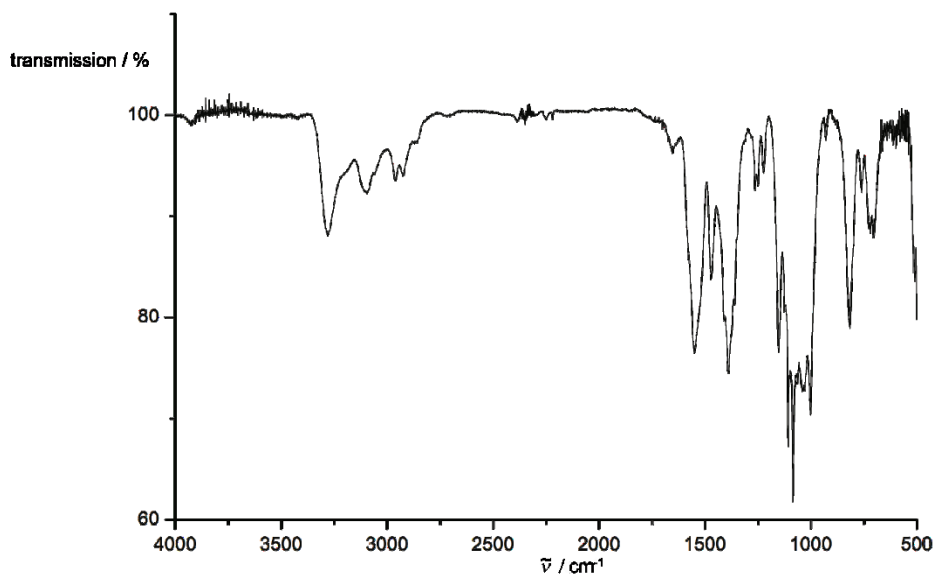


Figure S11. Infrared spectrum of $[\text{Cu}_2(\text{H-1})_6][\text{BF}_4]_2$ in KBr.

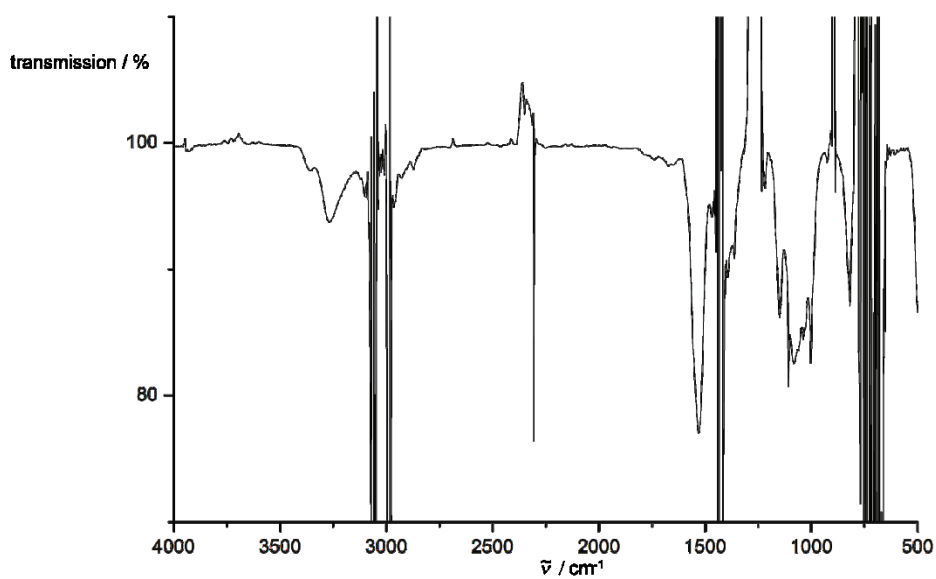


Figure S12. Infrared spectrum of $[\text{Cu}_2(\text{H-1})_6][\text{BF}_4]_2$ in CH_2Cl_2 .

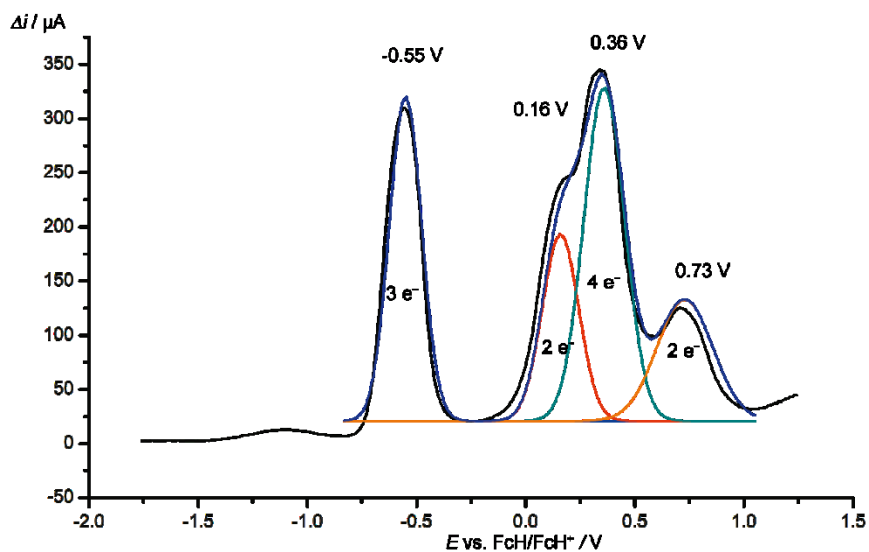


Figure S13. Square wave voltammogram of $[\text{Cu}_2(\text{H-1})_6][\text{BF}_4]_2$ at 100 mV s^{-1} with 3 eq. of decamethylferrocene in $\text{CH}_2\text{Cl}_2/[\text{nBu}_4\text{N}][\text{B}(\text{C}_6\text{F}_5)_4]$.

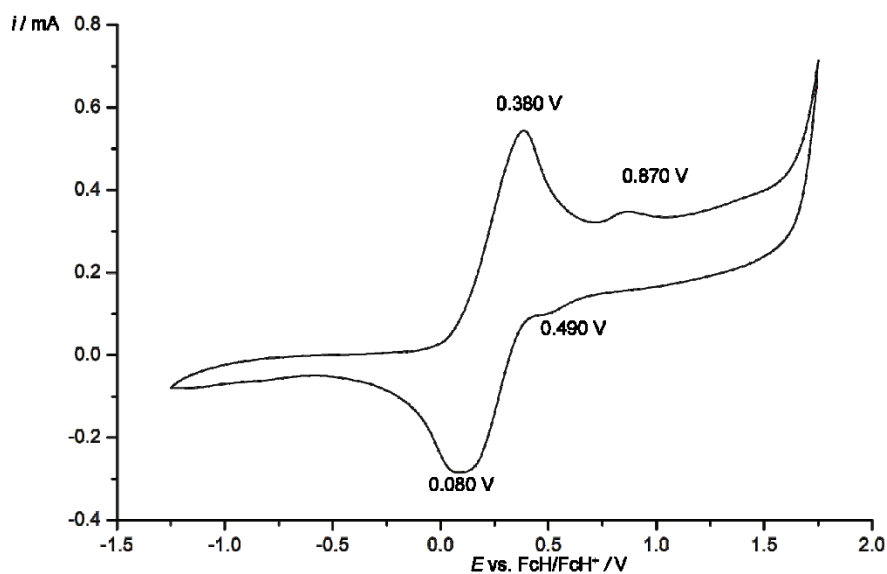


Figure S14. Cyclic voltammogram of $[\text{Cu}_2(\text{H-1})_6][\text{BF}_4]_2$ at 100 mV s^{-1} in $\text{CH}_2\text{Cl}_2/[\text{nBu}_4\text{N}][\text{B}(\text{C}_6\text{F}_5)_4]$.

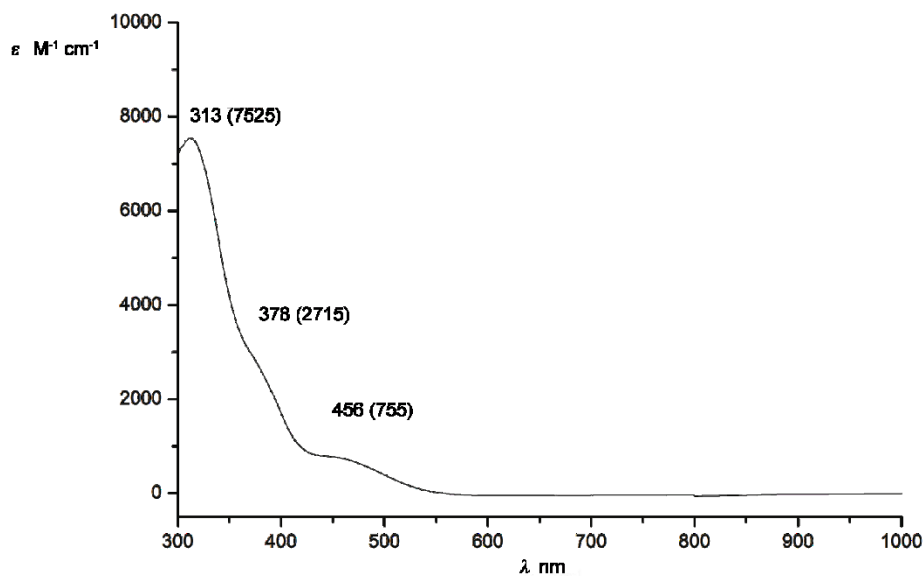


Figure S15. UV/Vis/NIR spectrum of $[\text{Cu}_2(\text{H-1})_6][\text{BF}_4]_2$ in CH_2Cl_2 .

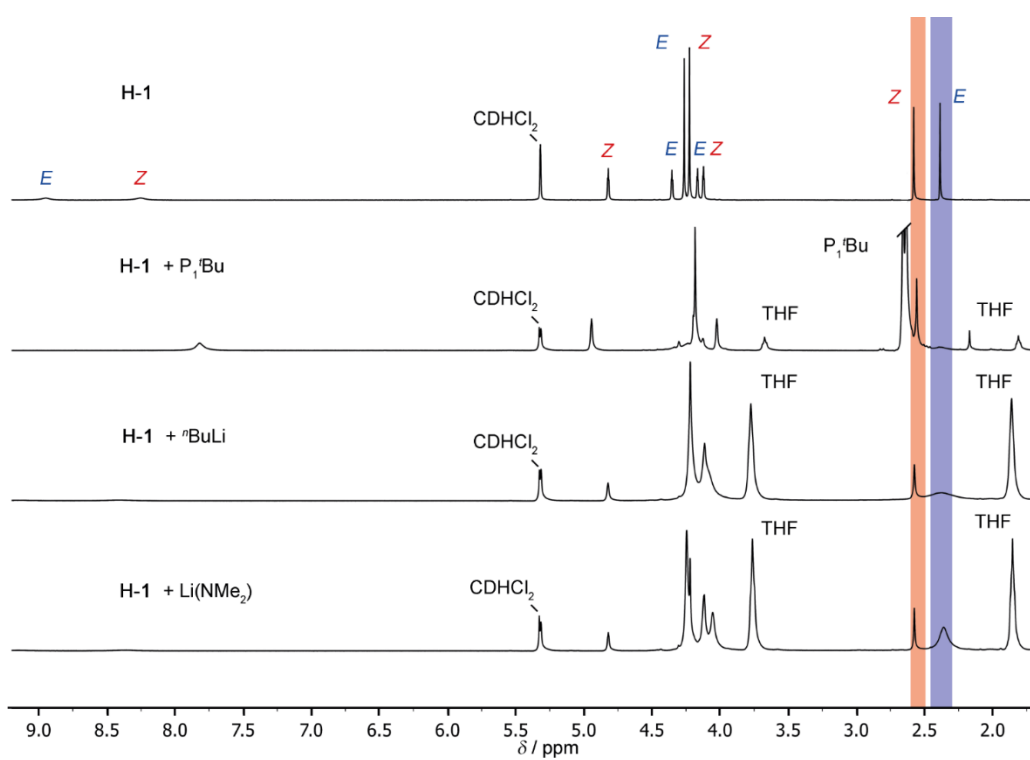


Figure S16. ^1H NMR spectra of H-1 after addition of 1 eq. $\text{P}_1'\text{Bu}$, $n\text{BuLi}$ or $\text{Li}(\text{NMe}_2)$ in THF, evaporation and dissolution in CD_2Cl_2 .

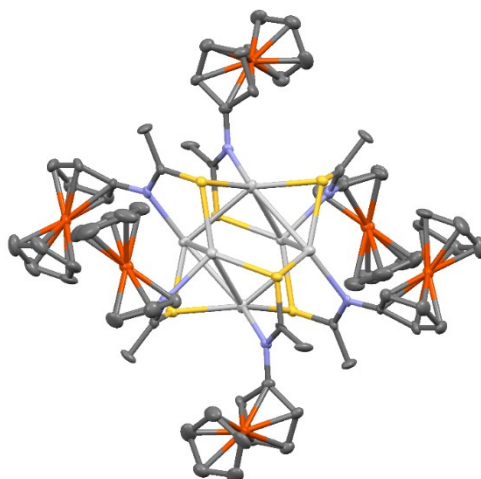


Figure S17. Thermal ellipsoid representation of $\text{Ag}_6(\text{E-1})_6$ (ellipsoids at 50% probability level) derived by single crystal XRD analysis.

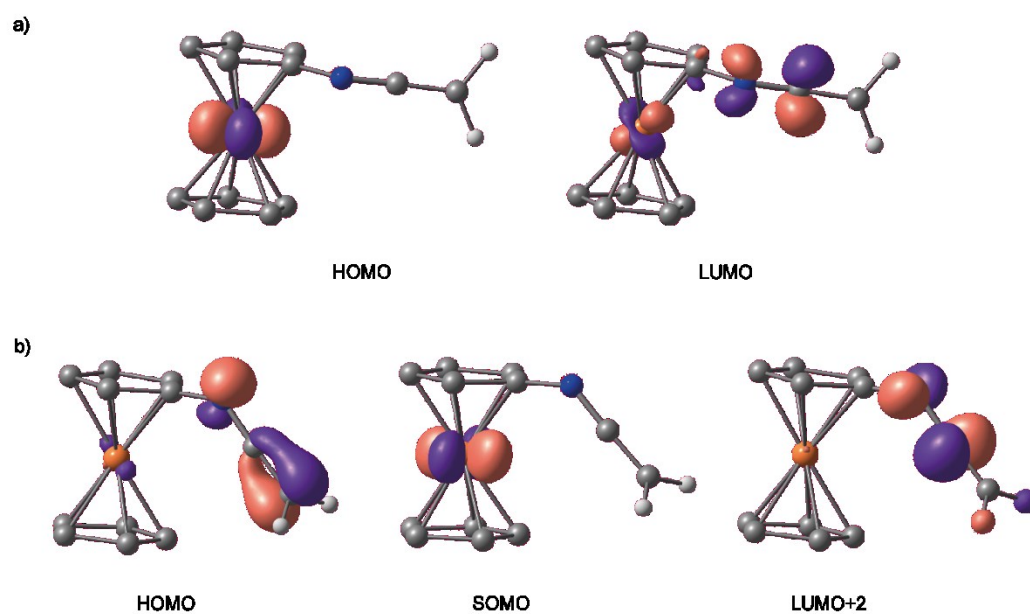


Figure S18. Frontier orbitals (DFT, B3LYP, def2-SVP, ZORA, D3) of a) *N*-ferrocenyl ketenimine 2 (HOMO and LUMO at 0.1 a.u.) and b) *N*-ferrocenyl ketenimine cation 2^{•+} (HOMO, SOMO and LUMO+2 at 0.1 a.u.). Cp protons omitted for clarity.

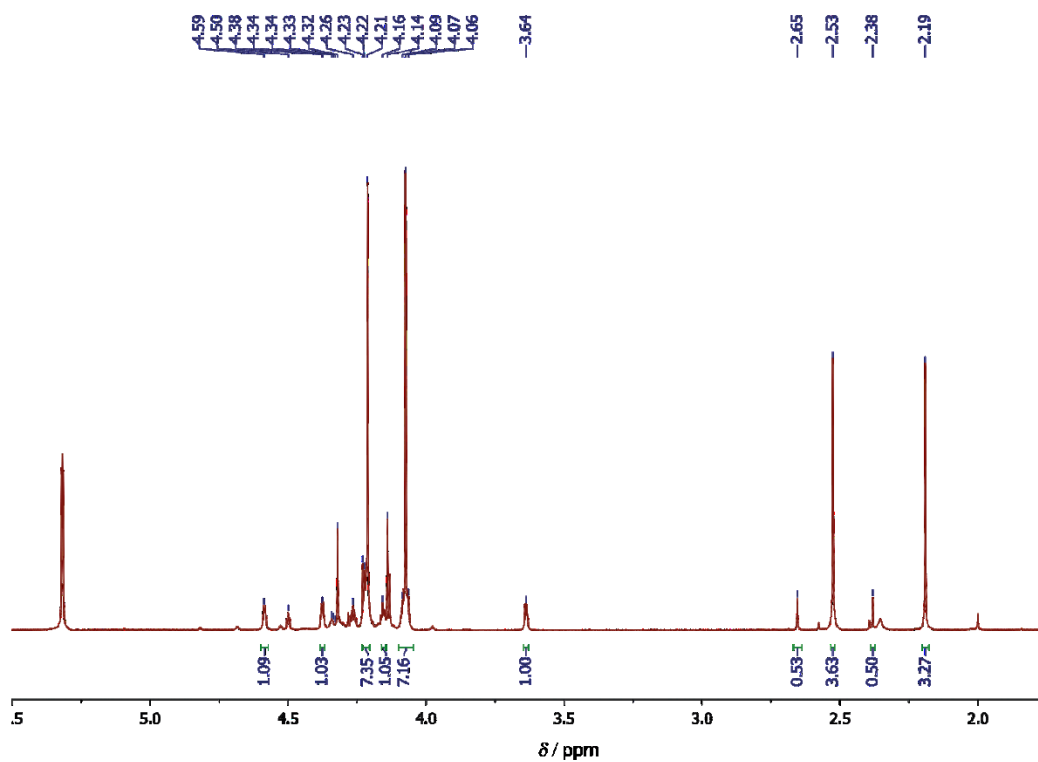


Figure S19. ^1H NMR spectrum of H-5 in CD_2Cl_2 .

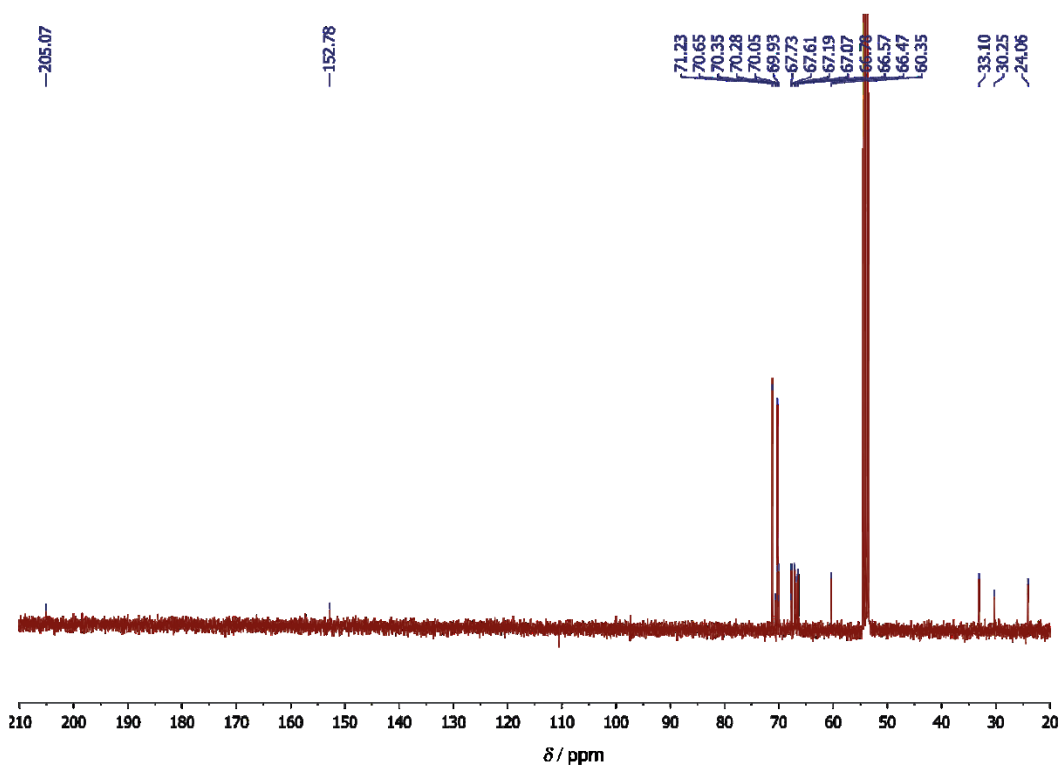


Figure S20. $^{13}\text{C}\{^1\text{H}\}$ NMR spectrum of H-5 in CD_2Cl_2 .

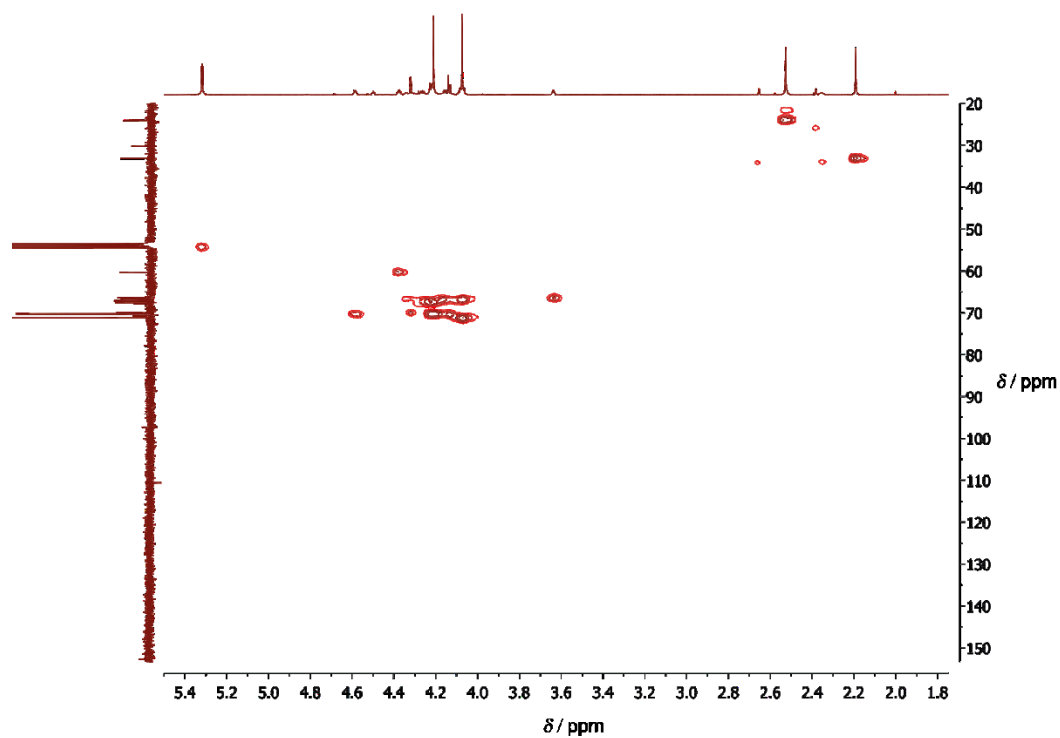


Figure S21. ^1H ^{13}C HSQC spectrum of H-5 in CD_2Cl_2 .

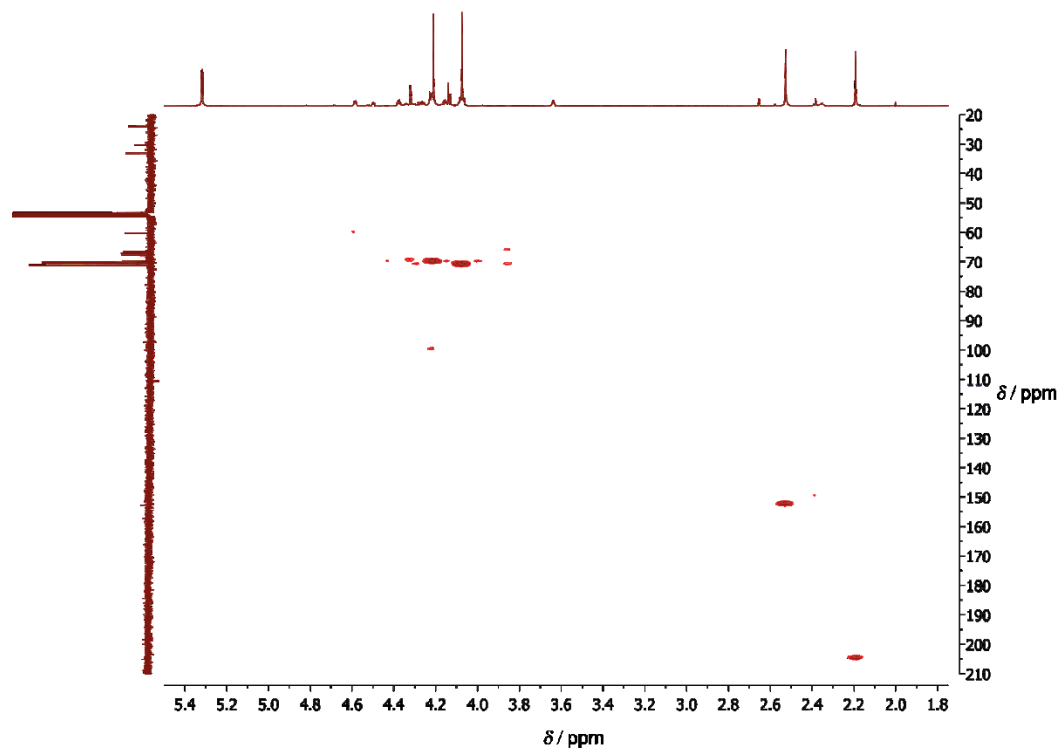


Figure S22. ^1H ^{13}C HMBC spectrum of H-5 in CD_2Cl_2 .

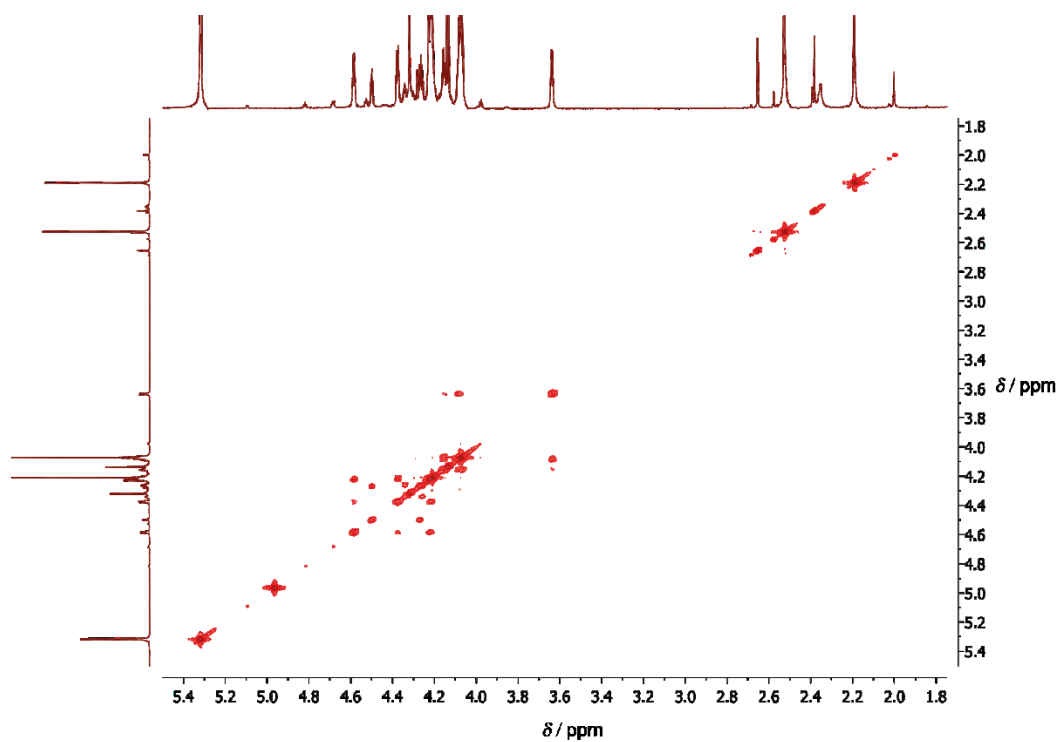


Figure S23. $^1\text{H}^1\text{H}$ COSY spectrum of H-5 in CD_2Cl_2 .

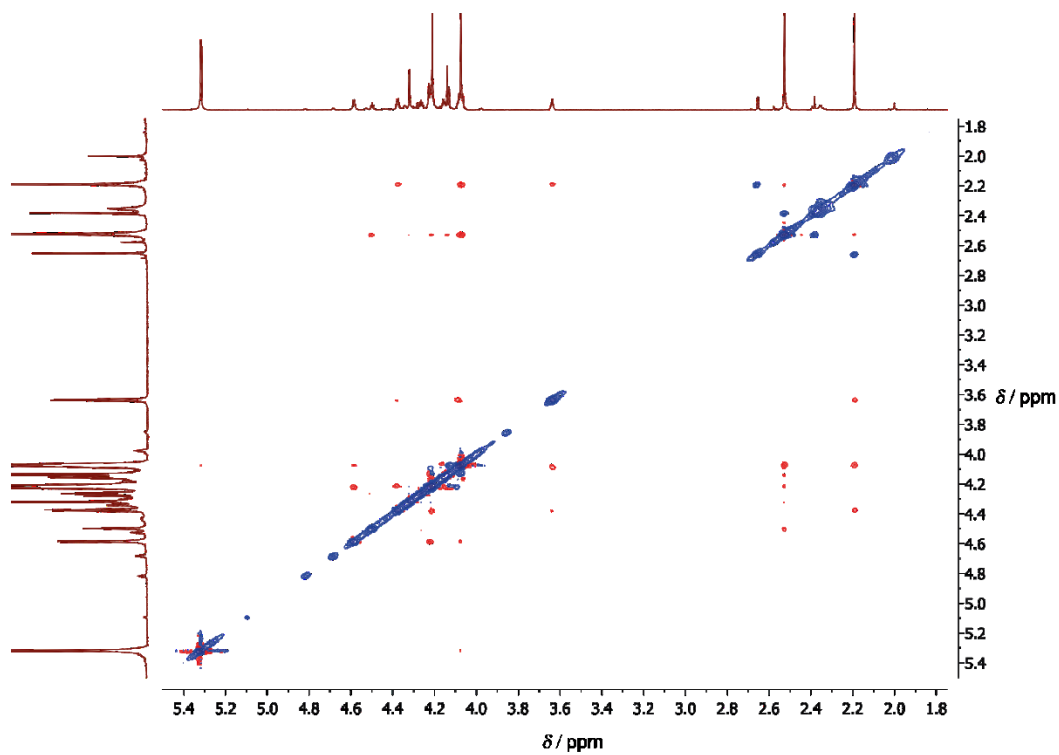


Figure S24. $^1\text{H}^1\text{H}$ NOESY spectrum of H-5 in CD_2Cl_2 .

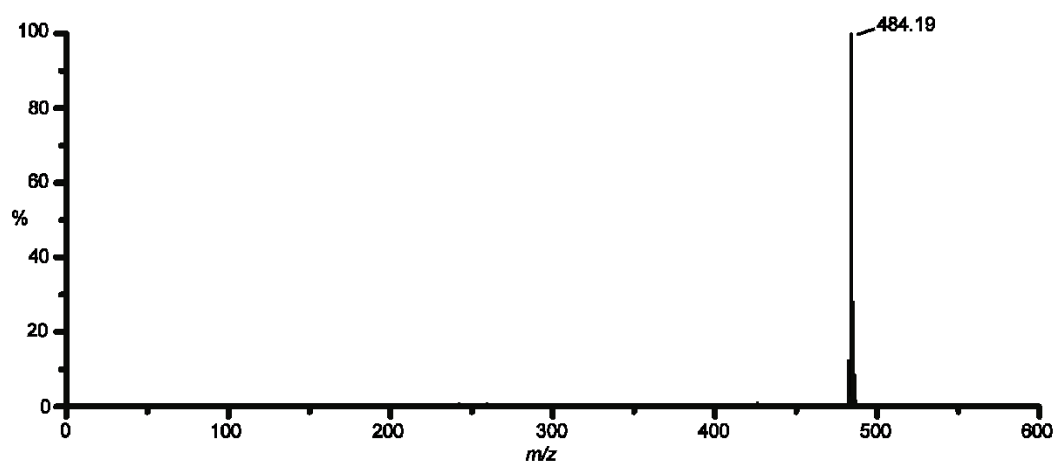


Figure S25. FD^+ mass spectrum of H-5 in CH_2Cl_2 .

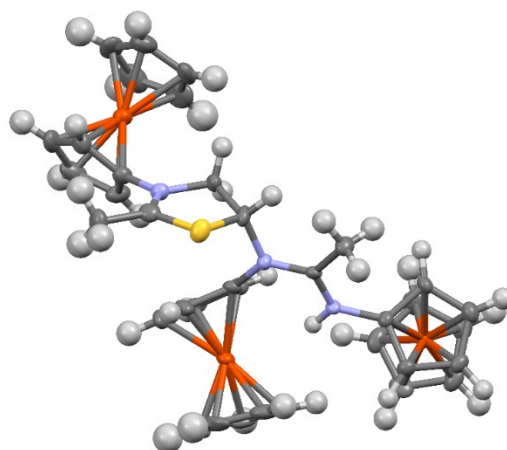


Figure S26. Thermal ellipsoid representation of *cyclo*-[H₃-7][SbF₆]₂ (ellipsoids at 50% probability level) derived by single crystal XRD analysis.

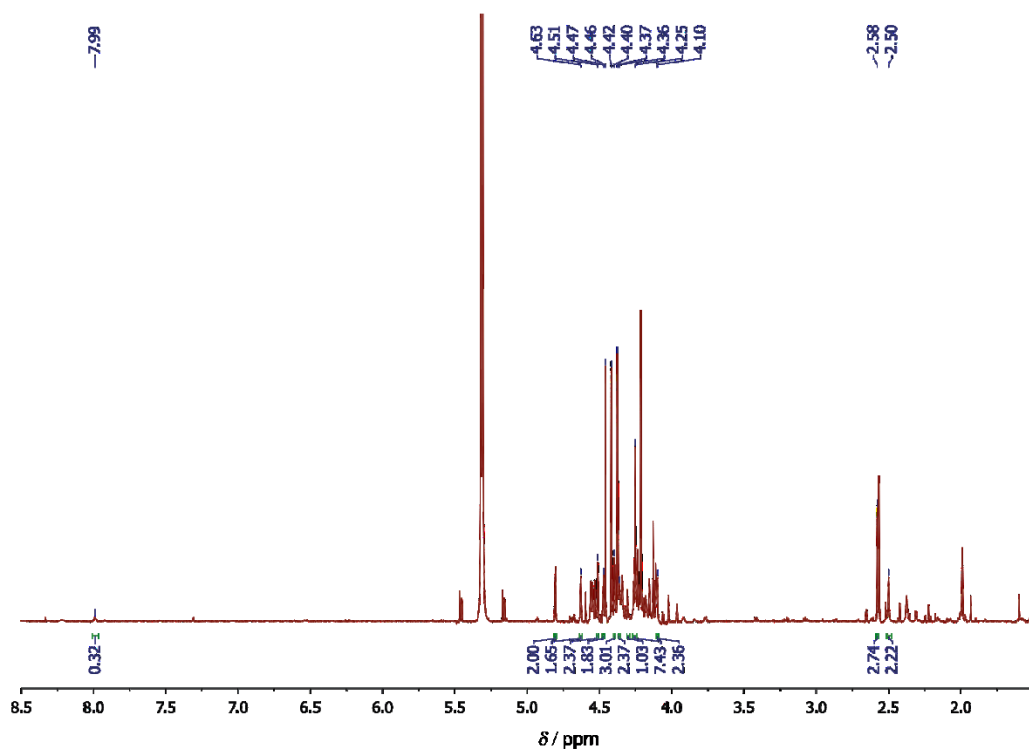


Figure S27. ^1H NMR spectrum of *cyclo*-[H₃-7][SbF₆]₂ in CD₂Cl₂.

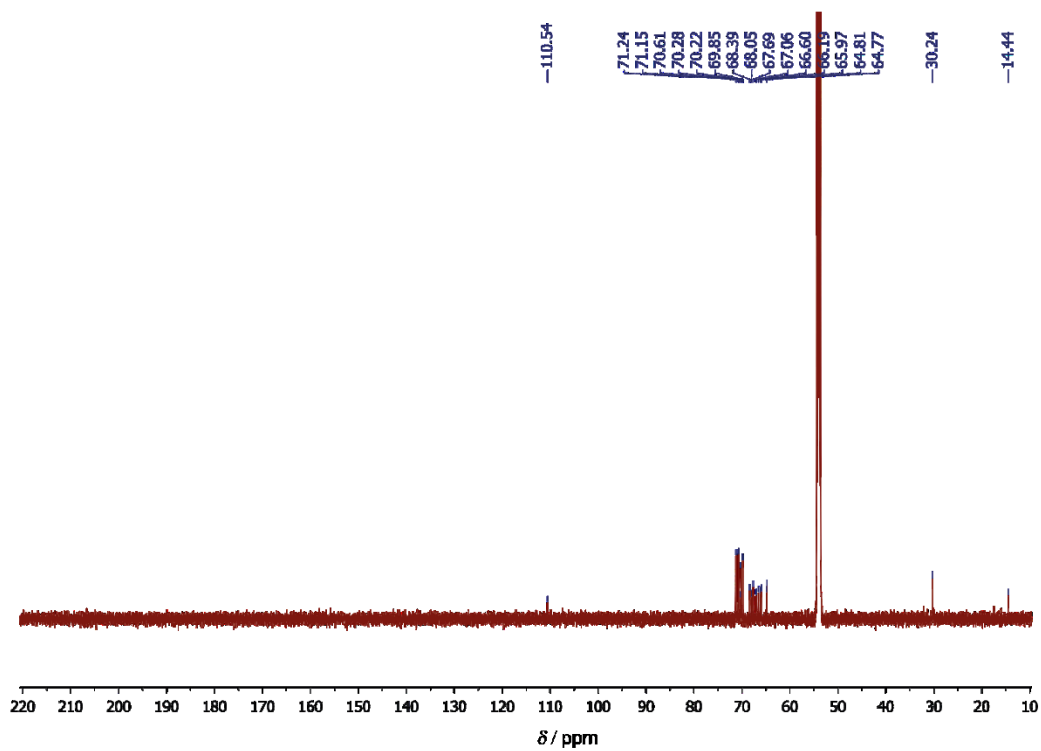


Figure S28. $^{13}\text{C}\{^1\text{H}\}$ NMR spectrum of *cyclo*-[H₃-7][SbF₆]₂ in CD₂Cl₂.

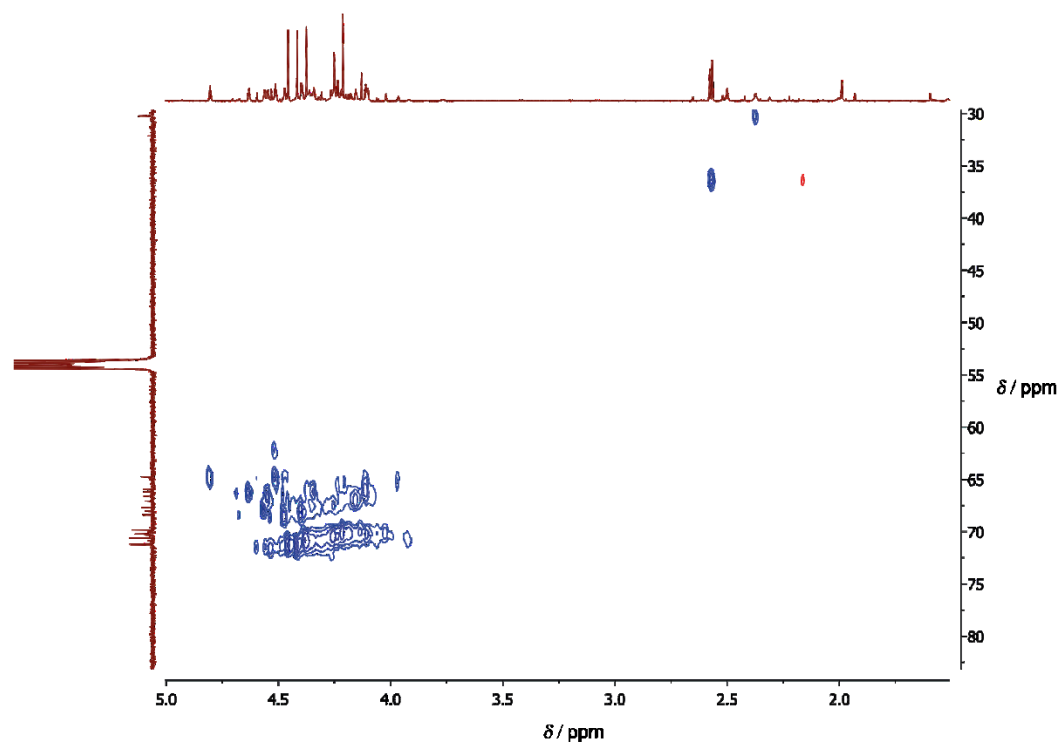


Figure S29. ^1H ^{13}C HSQC spectrum of *cyclo*-[H₃-7][SbF₆]₂ in CD₂Cl₂.

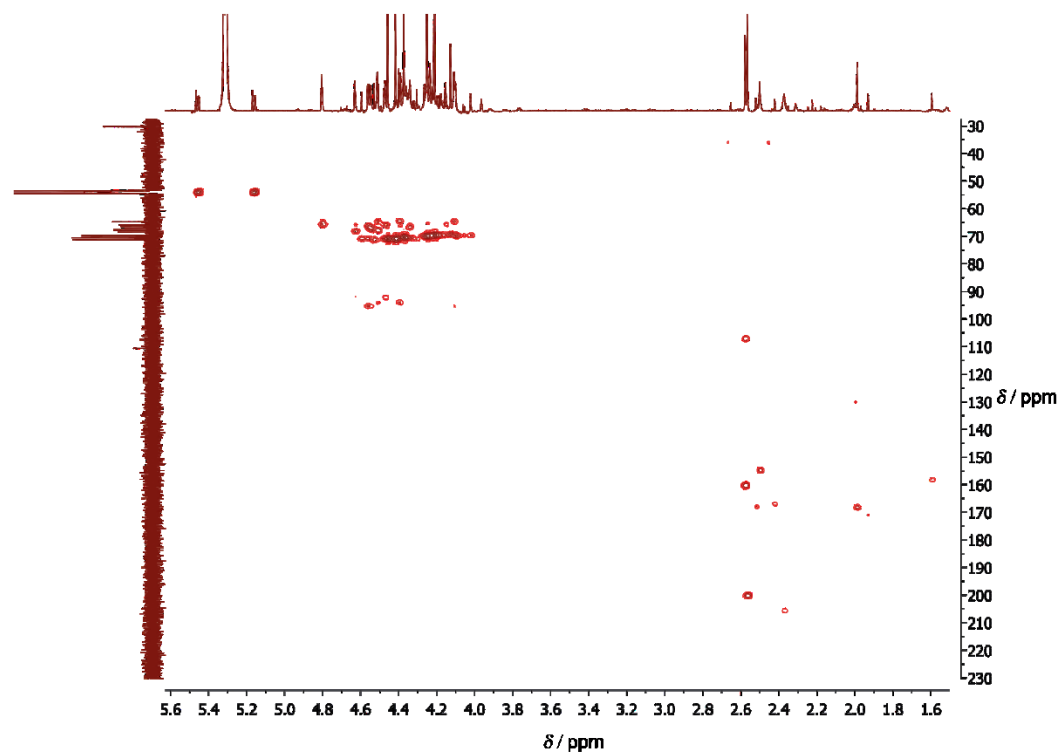


Figure S30. ^1H ^{13}C HMBC spectrum of *cyclo*-[H₃-7][SbF₆]₂ in CD₂Cl₂.

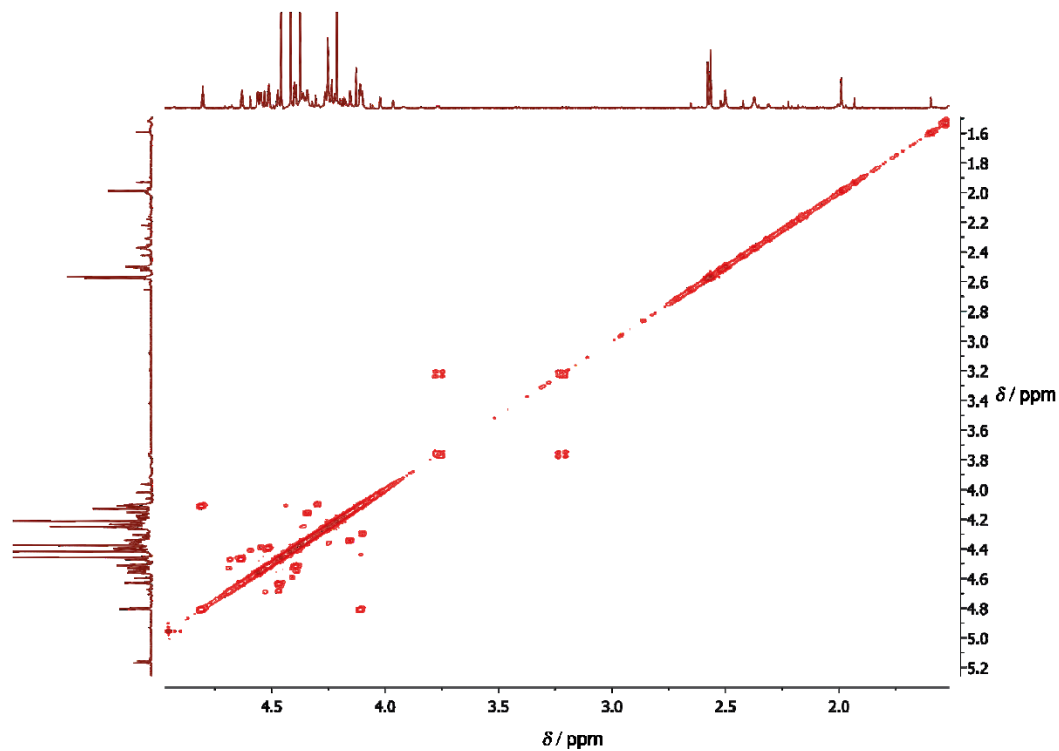


Figure S31. $^1\text{H}^1\text{H}$ COSY spectrum of *cyclo*-[H₃-7][SbF₆]₂ in CD₂Cl₂.

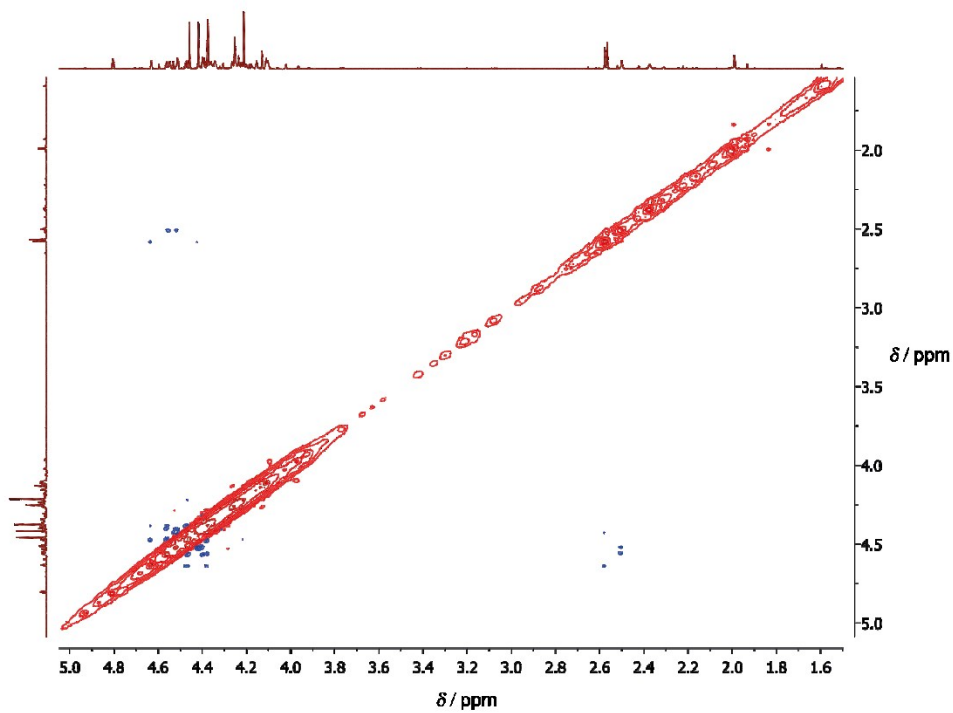


Figure S32. $^1\text{H}^1\text{H}$ NOESY spectrum of *cyclo*-[H₃-7][SbF₆]₂ in CD₂Cl₂.

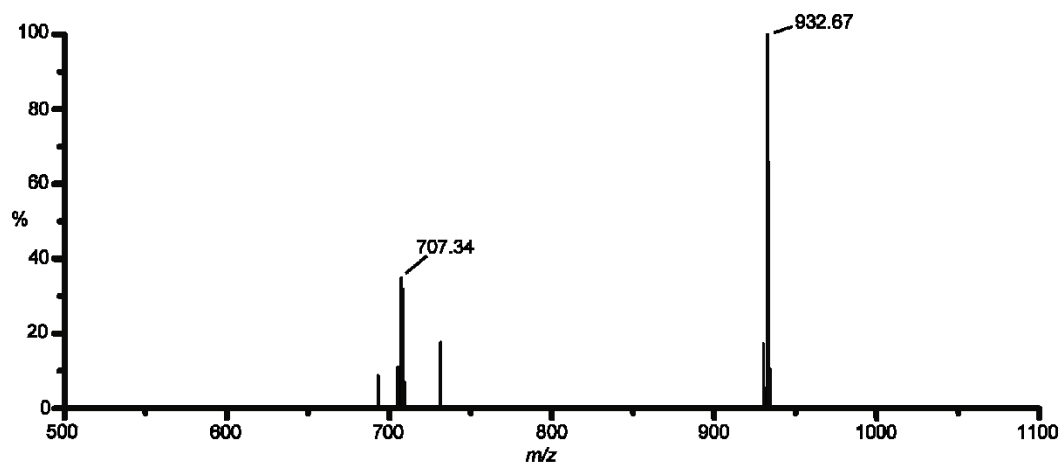


Figure S33. FD^+ mass spectrum of *cyclo*-[H₃-7][SbF₆]₂ in CH₂Cl₂.

6 Acknowledgements

Many thanks to...

- ... ___ for the opportunity to explore this subjected in depth and the scientific discussions.
- ... ___ for solving even the most complicated crystal structures.
- ... ___ aka ___ for being one of the founding members of the „ferrocene special forces“, for many helpful discussion, substance donations, for the crackling bed sheets during our conference visits and providing the right words to express myself like “Uffresche!”.
- ... ___ aka ___ for his advice under all circumstances, for giving me the insight, that molybdenum is the answer to everything, except if the answer can be beer or metal, than choose beer or metal, and the ability to keep me sane with his professionally engineered, nearly indeterminable sarcasm.
- ... ___ aka ___ for the very helpful discussions and advice and just his being there, to ensure I was never in the wrong room, and therefore keep on improving.
- ... ___ for introducing me to Bouldering; for a lot of fun times and showing me that skill surpasses strength by all means.
- ... ___ for introducing me to EPR spectroscopy, cheerful conversation and the best interpretation of an overweight elf, I have ever seen.
- ... ___ for lightening up my mood and bearing all my bad moods without choice as my office neighbor.
- ... ___ for substance donations and providing a whole lot of funny conversation.

- ... ___ aka ___, for substance donations, questioning my understanding of everything research related and forcing me to get it right and for showing me, that there are still truehearted people in the world
- ... ___ for bearing my bursts of rage, which must have threatened him to death, being my second and nearest office neighbor.
- ... ___ for her positive attitude and her ability to tie the group together.
- ... ___ for enduring my taste in music and being a real “Panzer Mensch” in case of patience.
- ... ___ for being a constant reminder to keep calm.
- ... ___ for always providing a critical point of view.
- ... ___ aka ___ for being a member of the “ferrocene special forces” and sacrificing his next years to this cause to ensure that the ferrocene chemistry is in good hands.
- ... ___ aka ___ for providing comical relief in stressful situations.
- ... ___ for his introduction to the work with our cluster and constant helpful advice for this work.
- ... ___ for doing all the things that kept our work going.
- ... all current and former members of ___, on whose results, experience and suffering this work is built on, for the great working atmosphere.
- ... my research students ___, ___, ___, ___, ___ and ___ for their help in synthesis and analytics on which parts of this work are based on.

-
- ... my bachelor student ___ for restoring my hope in the next generation of chemists due to her excellent work.
- ... ___ for constant cake donations to keep the spirit up, insightful conversations and all the laughter we permanently, entirely, nearly indefatigably shared.
- ... ___ aka ___ for keeping my spirit up, when I needed it and being there, so I did not feel alone.
- ... the ___ for having a reason to flee the canteen food and have some not work-related talk (sometimes).
- ... all my friends, who are not directly related to this work, but had to bear everything the creation of this work made me do, but still are my friends.
- ... ___ for providing distractions, when desperately needed.
- ... my whole family for their constant support to follow my dreams.
- ... ___ for NMR and LIFDI support even at the most uncivilized hours and his ability to shim faster than his own shadow.
- ... ___ for the XRD sample preparation and data collection and for getting the best reflexes out of the worst crystals
- ... ___ and ___ for mass spectrometric measurements.
- ... Chemikalienlager aka ___ for providing materials as fast as possible.
- ... the "Zentrum for Qualitätssicherung und -entwicklung" of the Johannes Gutenberg University for financial support for conference visits.

... microanalytical laboratory of the chemical institutes of the University of Mainz for the measurements of elemental analyses.

7 List of Publications

Publications

T. Kienz, C. Förster, K. Heinze: “Generation and Oligomerization of N-Ferrocenyl Ketenimines via Open-shell Intermediates”, submitted

A. Neidlinger, T. Kienz, K. Heinze: “*Spin Trapping of Carbon-Centered Ferrocenyl Radicals with Nitrosobenzene*”, *Organometallics* **2015**, *34*, 5310-4320.

[DOI: 10.1021/acs.organomet.5b00778]

T. Kienz, C. Förster, K. Heinze: „*Impact of O→S Exchange in Ferrocenyl Amides on Structure and Redoxchemistry*”, *Organometallics* **2014**, *33*, 4803-4812.

[DOI: 10.1021/om500052k]

Oral Presentations

T. Kienz, K. Heinze: “*Conformational and Electronic Effects of Oxygen→Sulfur Exchange in Ferrocene Oligopeptides*”, oral presentation at the 12th Ferrocene Colloquium, 17. – 19. February 2014, Innsbruck, Austria.

T. Kienz, K. Heinze: “*Conformational and Electronic Effects of Oxygen→Sulfur Exchange in Ferrocene Oligopeptides*”, short-oral presentation at the 11th Ferrocene Colloquium, 06. – 08. February 2013, Hannover, Germany.

Poster Presentations

T. Kienz, K. Heinze: „*Impact of O→S Exchange in Ferrocenyl Amides on Structure and Redoxchemistry*”, poster presented at “17. Vortragstagung der Wöhler-Vereinigung”, 24. – 26. September 2014, Saarbrücken, Germany.

T. Kienz, K. Heinze: „*Impact of O→S Exchange in Ferrocenyl Amides on Structure and Redoxchemistry*”, poster presented at Electrochemistry 2014, 22. – 24. September 2014, Mainz, Germany.

T. Kienz, K. Heinze: “*Conformational and Electronic Effects of Oxygen→Sulfur Exchange in Ferrocene Oligopeptides*”, poster presented at the 11th Ferrocene Colloquium, 06. – 08. February 2013, Hannover, Germany.

8 Curriculum Vitae

Torben Kienz

Date of birth 16. Oktober 1985
Place of birth Worms



Professional Experience

- 06/2011 – present **Research Associate**
Johannes Gutenberg-University Mainz
- Organization of lab courses
 - Conception of research projects
 - Communication with supplying companies
 - Training of technicians

Education

- 06/2011 – 11/2016 **Doctoral Thesis** in the group of ____
Johannes Gutenberg-University Mainz:
„Exploration of *N*-Ferrocenyl Substituted Thioamides:
Synthesis, Properties and Reactivity“
- Development of new synthetic strategies for organometallic compounds
 - Practical Experience in analysis methods (NMR spectroscopy, IR spectroscopy, UV/vis spectroscopy, fluorescence spectroscopy, EPR spectroscopy, electrochemical analyses)
 - Performance of DFT calculation for interpretation of research results (Gaussian 09, Orca)
 - Representation of the working group during international conferences by poster oral presentations
- 10/2005 – 05/2011 **Academic studies in Chemistry**
Johannes Gutenberg-University Mainz
- Inorganic Chemistry

- Organic Chemistry
- Physical Chemistry
- Macromolecular Chemistry

Diploma Thesis in the group of ____:

„Synthesis and Charakterisation of *N,N',N''*-Triaryl Substituted Guanidines“

08/1996 – 03/2005

Abitur

Eleonoren Gymnasium Worms

Skills

Languages

German:

First language

English:

Business fluent

Computing

Microsoft
Office

Excel, Powerpoint, Outlook, Word

specific
software

Chemcraft, Chemdraw, Gaussian 09,
LaTeX, Mercury, MestReNova, Orca,
Origin, Photoshop,

Mainz, 07 October 2016